Characterisation and prediction of nanofiltration charge effects.

Aljohani, Naser Hamzah

Swansea University
Prifysgol Abertawe

College of Engineering

CHARACTERISATION AND PREDICTION OF NANOFILTRATION CHARGE EFFECTS

by

Naser Hamzah Aljohani

A Thesis Submitted in Fulfilment of the Requirement

For the Degree

DOCTOR OF PHILOSOPHY

Philosophiae Doctor (Ph.D.)

June 2015

Summary

Membrane processes have many industrial applications such as desalination, water treatment, biotechnology, food industry, pharmaceutical and power generation. The advantages of membrane processes include high selectivity, low operating costs and energy consumption. Membrane charge plays an important role in the membrane separation of ionic species. Therefore, understanding the interaction between ions and membrane charge is essential to improve the performance of the separation. This interaction is a function of pH concentration and depends on membrane type.

The objective of this thesis was to investigate the role of membrane charge in separation of ionic species. Therefore the first step is to characterise membrane charge and then using the knowledge obtained along with separation data to gain insight on the mechanism governing the separation process of charged species by NF membranes. Finally correlations between membrane charge characterisation and separation process were achieved. The aim of creating such correlations is to reduce the amount of experimental work (only characterisation needed) required to evaluate the separation efficiency of a NF membrane either in a single salt system or mixtures which in turn saves time, labour work and money.

The result obtained confirms the role of membrane charge in the separation of ionic species and provides insight into the mechanism of separation in NF membranes. In fact full explanations and quantitative analysis of the role of membrane charge was achieved in this thesis.

To sum up, the knowledge obtained in this thesis is important for researchers and process engineers in industries such as desalination and water treatment plant as this helps to increase the efficiency of these plants and promote the use of membrane technology in the process industries. This can be done by right choice of membranes which fit the purpose and control of the feed parameters such as pH and concentration to maximize the efficiency.

DECLARATION

This work has not previously been accepted in substance for any degree and is not being concurrently submitted in candidature for any degree.

Signed..... ..... (*Candidate*: Naser Hamzah Aljohani)

Date.....25/09/2015.....

STATEMENT 1

This thesis is the result of my own investigations, except where otherwise stated. Other sources are acknowledged by footnotes giving explicit references. A bibliography is appended.

Signed..... (*Candidate*: Naser Hamzah Aljohani)

Date.....25/09/2015.....

Signed (*Supervisor*: Dr Darren L. Oatley-Radcliffe)

Date 25Sep2015.....

STATEMENT 2

I hereby give consent for my thesis, if accepted, to be available for photocopying and for inter-library loans **after expiry of a bar on access approved by the Swansea University.**

Signed.....25/09/2015..... (*Candidate*: Naser Hamzah Aljohani)

Date.....

Acknowledgements

I would like to thank my supervisor, Dr. Darren Oatley-Radcliffe, for the patient guidance, encouragement and advice he has provided throughout this work.

Sincere thanks are also extended to Professor Nidal Hilal for his support and encouragement.

Thank you to Dr Paul Williams for allowing me to use his laboratory and his guidance and support. I would also like to thank all the members of staff and my colleague at Swansea University who are always willing to help.

I must express my gratitude to my wife, for her continued support, encouragement and love. I owe my special thanks to my parents for all the support they have provided me over the years.

A special thanks to the Saudi Arabian Cultural Bureau that facilitated everything from the first day I arrived to the UK, until now.

Finally, I would like to take this opportunity to express my heartfelt thanks to my employer, Saline Water Conversion Corporation Saudi Arabia, for funding my PhD study and for their support and encouragement throughout my career. I am very much thankful especially for Dr.Abdullah Al-Alshaikh, late abdulaziz Al henti and Eng.Beshr Al-Nahdi for their continuous support and encouragement.

Table of Contents

Nomenclature

a_i, a	hydrodynamic (Stokes) radius of ion *i* or uncharged solute, m
a_i	activity of ion *i*, mol m^{-3}
A_k	porosity, dimensionless
c_i	concentration of ion species i, M
$c_i(0), c(0)$	concentration of ion *i* or uncharged solute at the pore entrance, mol m^{-3}
$c_i(\Delta x), c(\Delta x)$	concentration of ion *i* or uncharged solute at the pore outlet, mol m^{-3}
C_i	ionic solute bulk solution concentration, mol m^{-3}
$C_{i,f}, C_f$	bulk feed concentration, mol m^{-3}
$C_{i,p}, C_p$	permeate concentration of ion *i* or uncharged solute, mol m^{-3}
$C_{i,w}, C_w$	wall concentration of ion *i* or uncharged solute, mol m^{-3}
d	thickness of the oriented solvent layer, m
D_{eff}	effective bulk salt diffusion coefficient, $m^2\ s^{-1}$
$D_{i,p}, D_p$	pore diffusion coefficient of ion *i* or uncharged solute, $m^2\ s^{-1}$
$D_{i,\infty}, D_\infty$	bulk diffusion coefficient of ion *i* or uncharged solute, $m^2\ s^{-1}$
e	electronic charge, 1.602177 x 10^{-19} C
E_m	membrane potential, V
E_c	cell potential, V
E_c	concentration potential, V
F	Faraday constant, 96487 C mol^{-1}
i, I	electrical current, A
i	van't Hoff factor of the solute, dimensions

I	ionic strength, mol m^{-3}
j_i	ionic flux of ion *i* (pore area basis), mol m^{-2} s^{-1}
J_v	volumetric flux, m^3 m^{-2} s^{-1}
K_B	specific conductivity of the bulk electrolyte solution, Ω.
k	feed-side mass transfer coefficient, m s^{-1}
k'	mass transfer parameter, variable dimensions
k_B	Boltzmann constant, 1.38066 x 10^{-23} J K^{-1}
$K_{i,c}, K_c$	hindrance factor for convection of ion *i* or uncharged solute, dimensionless
$K_{i,d}, K_d$	hindrance factor for diffusion of ion *i* or uncharged solute, dimensionless
M	Molarity
n	number of ions in an electrolyte mixtures, dimensionless
N_A	Avagadro's number, 6.023 x10^{23} g mol
P	pressure, N m^{-2}
Pe	Peclet number uncharged solute, dimensionless
Q	volumetric crossflow, m^3s^{-1}
r_p	effective pore radius, m
r_s	solutes ionic radius, m
R, R_i, R_{real}	real rejection of salt or ion *i*, dimensionless
R	Universal Gas Constant, 8.314 J mol^{-1} K^{-1}
R_{calc}	calculated rejection, dimensionless
R_{exp}	experimental rejection, dimensionless
R_{obs}	observed rejection, dimensionless
$R_{0.1M\ KCl}$	electrical resistance of the cell filled with the high salt concentration, Ω

R_{cell}	electrical resistance of the cell filled with the working salt concentration, Ω
R_m^h	resistance across the pores when the cell is filled with the high concentration solution, Ω
R_m	resistance across the pore when the cell is filled with the measurement solution, Ω
S_y	sum of squares objective function in fitting, dimensionless
T	absolute temperature, K
u_s	solvent velocity inside pore, m s^{-1}
u_x	maximum solvent velocity inside pore, m s^{-1}
V	sample volume, L
V_{si}	solute partial molar volume, m^3 mol^{-1}
x	axial position within the pore, m
X_d	effective charge density, mol m^{-3}
Y	dimensionless group of ion *i*, dimensionless
z_i	valence of ion i, dimensionless

Greek Symbols

ΔP	applied pressure, N m^{-2}
ΔP_e	effective pressure driving force, N m^{-2}
$\Delta\pi$	osmotic pressure, N m^{-2}
ΔW_i	Born solvation energy barrier, J
Δx	membrane thickness, m
$\Delta\psi_D$	Donnan potential at the pore inlet, V
δ	thickness of the feed-side boundary film, m
$\varepsilon_{b,}$	bulk dielectric constant, dimensionless

ε_p	pore dielectric constant, dimensionless
ε_o	permittivity of free space, 8.85419×10^{-12} J^{-1} C^2 m^{-1}
ε^*	dielectric constant of the oriented water layer, dimensionless
ε_r	relative liquid permittivity (dielectric constant) , dimensionless
κ	Debye screening length, m
γ	parameter defined by Eq. (5.3), dimensionless
Λ	equivalent electrical conductance, S m^2 mol^{-1}
η	solvent viscosity within pores, N s m^{-2}
η	electrolyte viscosity, N s m^{-2}
γ_i	activity coefficient of ion *i* within pore, dimensionless
γ_i^o	bulk activity coefficient of ion *i*, dimensionless
λ	ratio of ionic or uncharged solute radius to pore radius, dimensionless
λ_s	surface conductivity, S m^{-1}
λ_o	electrolyte conductivity, S m^{-1}
$\lambda_{0.1MKCl}$	solution conductivity at high salt concentration (usually 0.1 M KCl), S m^{-1}
λ^h	conductivity of the solution at high salt concentration, S m^{-1}
λ_{pore}	conductivity in the pores, S m^{-1}
Φ_i, Φ	steric partition coefficient of ion *i* or uncharged solute, dimensionless
μ	uncharged solute chemical potential, J mol^{-1}
μ_i	electrochemical potential of ion *i*, J mol^{-1}
μ_a	apparent viscosity (the viscosity within the pores), N s m^{-2}
μ_0	bulk viscosity of the electrolyte solution, N s m^{-2}
ψ	electrical potential within the pore, V

Ψ	space charge potential within the pore, V
ψ_o	surface potential, V
ψ_d	the potential at the Stern plane, V
ζ	zeta potential, V
ξ	dimessionless zeta potential
σ_0	Charge density at the membrane surface, mol m^{-3}
σ_s	Charge density charges of the Stern-layer, mol m^{-3}
σ_d	Charge density within the diffusion layer of the electric double layer, mol m^{-3}
β	dimensionless parameter describing the electrolyte properties
v_+ , v_-	stoichiometric number of, cation or anion

Subscript

+	anion
-	cation
$\pm$	both anion and cation
1	ion 1
2	ion 2
3	ion 3
4	ion 4
(0^+)	denotes feed-membrane interface (membrane side)
(0^-)	denotes feed-membrane interface (feed side)

1.0 Introduction

Water is a key resource for sustainable development in all countries and the water demand in the world is growing by 3 to 4% annually (Ng et al. 2015). Although 70 % of the earth is covered by water, 97.41% of the water available is saline water and only 2.59% is stable for human consumption (Aljohani 2007). Furthermore, fresh water on earth is not readily available for human consumption since more than 75% of this amount is frozen in the polar ice caps, 24% is ground water. Therefore, this shortage of freshwater has encouraged the rapid development of seawater desalination technologies (Dupavillon & Gillanders 2009). The production capacities of the major countries using desalination are shown in Figure 1.1. GCC (Gulf Cooperation Council) countries have the highest growth rate for desalination capacity as they are located in hyper arid region in the world.

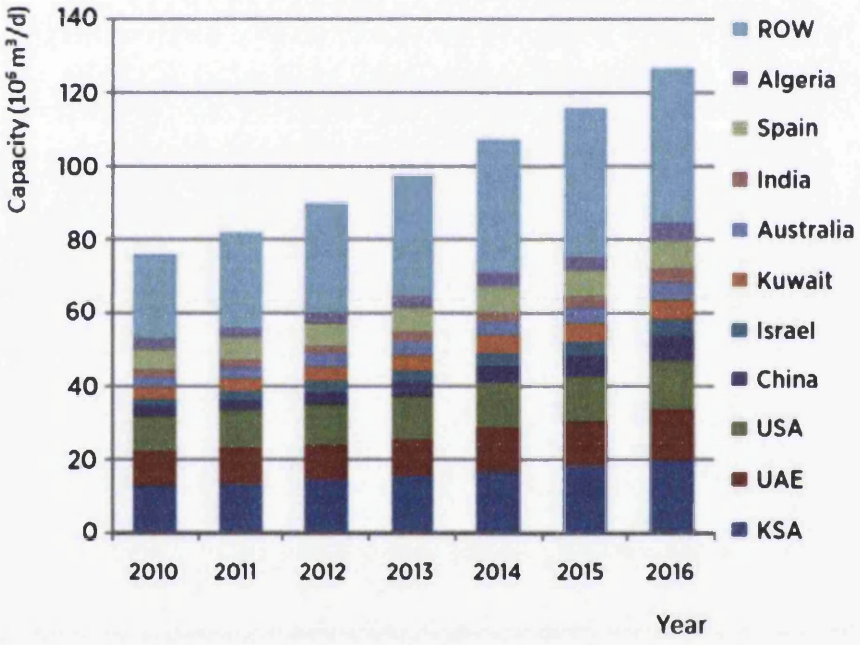

Figure 1.1: Capacities of desalination from 2010 to 2016 for all countries in the world (Ng et al. 2015).

1.1 Overview of membrane processes

The applications of membrane separation processes in industry such as seawater desalination, waste water treatment, biomedical engineering, gas separation, food and the pharmaceutical industries are growing fast. There are several reasons behind this trend namely (Merdaw et al. 2010): (1) Simplicity (2) They can be used to separate a variety of components (3) Low energy needed because there is no change in phase (4) Membrane unit operation, in most

cases, is at ambient temperature which make them a good choice for temperature-sensitive substances.

A membrane can be defined as "a permselective barrier between two homogeneous phases" (Mulder 1996). The driving force for this transportation is a pressure or a concentration difference across the membrane or electromotive force (see Table 1.1). The pressure driven processes are classified into four types: microfiltration (MF), ultrafiltration (UF), nanofiltration (NF) and reverse osmosis (RO). Figure 1.1 illustrates the main separation features of the four processes considered. The characterization of the four filtration techniques according to the International Union of Pure and Applied Chemistry [IUPAC] is as follows (Mueller et al. 2012): (1) Reverse osmosis (RO) is one of the liquid phase pressure-driven separation processes in which a selective movement of solvent against its osmotic pressure difference is caused by applied transmembrane pressure (2) Nanofiltration (NF) is characterised by its ability to separate the dissolved macromolecules and particles that are smaller than 2 nm (3) Ultrafiltration (UF) has a pore size in the range of 1–100 nm and separates the solutes that have a molecular size significantly greater than that of the solvent molecule while the solvent flows through the membrane (4) Microfiltration (MF) separates dissolved macromolecules and particles are large than 100 nm.

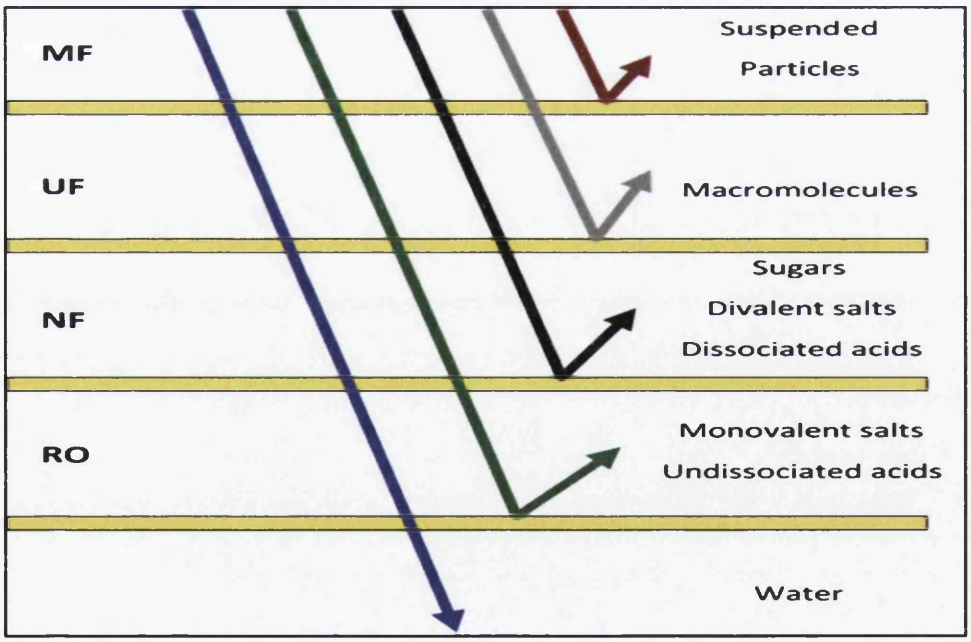

Figure 1.2: The separation features of different liquid-liquid pressure driven membrane processes (Oatley 2004).

Table 1.1: A classification of membrane processes (Mulder 1996).

Membrane Process	Feed Phase	Permeate Phase	Driving Force
Microfiltration	Liquid	Liquid	ΔP
Ultrafiltration	Liquid	Liquid	ΔP
Nanofiltration	Liquid	Liquid	ΔP
Reverse Osmosis	Liquid	Liquid	ΔP
Piezodialysis	Liquid	Liquid	ΔP
Gas Separation	Gas	Gas	Δp
Vapour Permeation	Gas	Gas	Δp
Pervaporation	Liquid	Gas	Δp
Electrodialysis	Liquid	Liquid	ΔE
Membrane Electrodialysis	Liquid	Liquid	ΔE
Dialysis	Liquid	Liquid	Δc
Diffusion Dialysis	Liquid	Liquid	Δc
Membrane Contactors	Liquid	Liquid	Δc
	Gas	Liquid	Δc / Δp
	Liquid	Gas	Δc / Δp
Thermo-osmosis	Liquid	Liquid	ΔT / Δp
Membrane Distillation	Liquid	Liquid	ΔT / Δp

1.2 Separation mechanisms of NF membranes

Nanofiltration (NF) is a pressure-driven membrane process that has separation properties between ultrafiltration (UF) and reverse osmosis (RO). The advantages of NF membranes include providing a high water flux and rejection at low operating pressure (Hilal et al. 2005). Furthermore the potential for scale formation is less than both RO and thermal desalination processes. NF membranes pore size is in the nano-scale dimension which enables them to separate small molecules (<1 kDa) and dissolved ions (Escoda et al. 2010). NF membranes separation is caused by many mechanisms such as electrostatic interactions, molecular sieving (steric hindrance), dielectric exclusion, etc. (Szymczyk et al. 2007; Afonso 2006). Neutral molecules are rejected by steric hindrance and non-electrostatic membrane–solute interactions such as Van-der-Waals forces and their transport occurrs by convection due to a

pressure difference and by diffusion due to a concentration gradient across the membrane (Childress & Elimelech 2000; Dina et al. 2001; Peeters et al. 1999; Szymczyk et al. 2007). In addition, uncharged molecules also interact with the membrane charge, mainly through polarity effects as the membrane charge directs the dipole of the natural molecules towards the membrane which reduces the rejection (Teixeira et al. 2005).

Steric hindrance and electrostatic interactions are responsible for charged compounds separation (Dina et al. 2001; Teixeira et al. 2005). In fact, the role of surface charges is more important in NF membranes than the other pressure driven membrane processes (Mänttäri et al. 2006). The ion separation resulting from the electrostatic interactions between ions and membrane surface charge is based on the Donnan exclusion mechanism and is caused when ions flow through electrically charged pores under a pressure gradient (Kukizaki 2009; Peeters et al. 1999; Teixeira et al. 2005). In this mechanism the co-ions are repulsed by the membrane surface and to satisfy the electroneutrality condition, an equivalent number of counter-ions are retained which results in salt retention.

NF membranes carry a fixed charge in aqueous solutions which originates from two sources, ionization of surface functional groups and adsorption of charged species such as ions and charged macromolecules which make them able to reject charged ions based on their valence (Escoda et al. 2010; Peeters et al. 1999). Membrane charge and separation efficiency in turn are significantly affected by the chemistry of the feed solution and the membrane material (Mazzoni & Bandini 2006; Tay et al. 2002).

1.3 Objectives of the present work

This thesis attempts to improve understanding of the role of membrane charge, particularly for nanofiltration, in the separation of ionic species. In order to achieve this goal, a reliable method is needed to characterise the membrane charge and to study the interaction between the membrane charge and the feed solutions. A variety of solution chemistries which include changes to chemical composition, concentration and the pH have been studied extensively.

First the interaction between the membrane charge and solutions containing a single salt will be examined. These single salt solutions are selected to contain the most abundant ions in drinking and sea water and the commercial membranes used are well known in industry, which makes the generated data in this thesis a valuable source for the water industry. The complexity of the solution chemistry will be enhanced by using binary salt solutions and

single salts data, to explain the interaction between the membrane charge and binary salts systems. The next stage after membrane charge characterization with different feed water chemistries will be to study the performance (rejection and flux) of the same membranes with the same solution chemistry used in the first stage. The results of both investigations will be used to gain insight about the membrane separation mechanism. Finally; the prediction of the membranes charge effects will be accomplished using a mathematical model which allows calculation of membrane charge density. This will enable the establishment of correlations such as charge density-pH and membrane charge density -zeta potential.

2.0 Literature Review

2.1 Membranes charge origin

NF membranes active layer is a hydrophilic polymeric materials such as polyamide (PA), cellulose acetate (CA), polysulfone (PS), polyethersulfone (PES), polyvinyl alcohol (PVA) which is hydrated and ionised in aqueous solutions forming charged functional groups such as amino, carboxyl and sulphonated groups (Luo & Wan 2013b). In addition to dissociation of surface functional groups, membranes acquire charge by adsorption of charged species such as ions, polyelectrolytes, ionic surfactants and macromolecules from the solutions (Schaep & Vandecasteele 2001; Teixeira et al. 2005). Polyamide is a popular group of membranes which have both weak acidic carboxyl groups (–COOH) and basic amine groups ($–NH_2$) on the surface which enable them to acquire either a positive or negative charge which depends on the pH, concentration , type of ionic species in electrolyte solutions and the ratio between acidic and basic surface groups (Kukizaki 2009; Rice et al. 2011). To illustrate, the net surface charge of polyamide membranes is positive below the isoelectric point, i.e. the pH value at which the net surface charge is zero, which is a result of the protonation of the amine functional groups and deprotonating of the carboxyl groups (Childress & Elimelech 2000). On the other hand SO_3H group which is the active layer in polysulfone and polyether-sulfone is a strong acidic group which dissociates over nearly the entire pH range (Wang et al. 2006). The dissociation reactions of the functional groups is as follow (Tra et al. 1998)

$$R\text{-}COOH = R\text{-}COO^- + H^+$$
$$R\text{-}NH_3^+ = R\text{-}NH_2 + H^+$$
$$R\text{-}SO_3H = R\text{-}SO_3^{2-} + H^+$$

Ceramic membranes are another type of membrane which are made of mineral oxides and produce charge on the surface due to the amphoteric behaviour of hydroxyl groups (MOH) in aqueous medium (Moritz et al. 2001; Zhao et al. 2005).

Adsorption of ions to the surface of the membrane can occur chemically by forming covalent bonds or physically through van der Waals forces (Hunter 1981). Furthermore, chemical adsorption can take place into the inner or compact part of the double layer and can shift the i.e.p to lower or higher pH values. However, physically adsorbed ions do not affect i.e.p but can reverse the sign of the zeta potential.

Changing of the solution pH has an effect on the membrane which in turn causes electrostatic repulsion or attraction between the membrane and solute as well as membrane hyhrophilicity (Luo & Wan 2013b). The NF membrane surface is usually negatively charged at high pH values which generates a repulsive force on multivalent anions and rejects cations to maintain electroneutrality of the solution (Ernst et al. 2000). Electrostatic repulsion not only causes higher ions rejection, but also might reduce concentration polarization and fouling (Luo & Wan 2013b) (Figure 2.1).

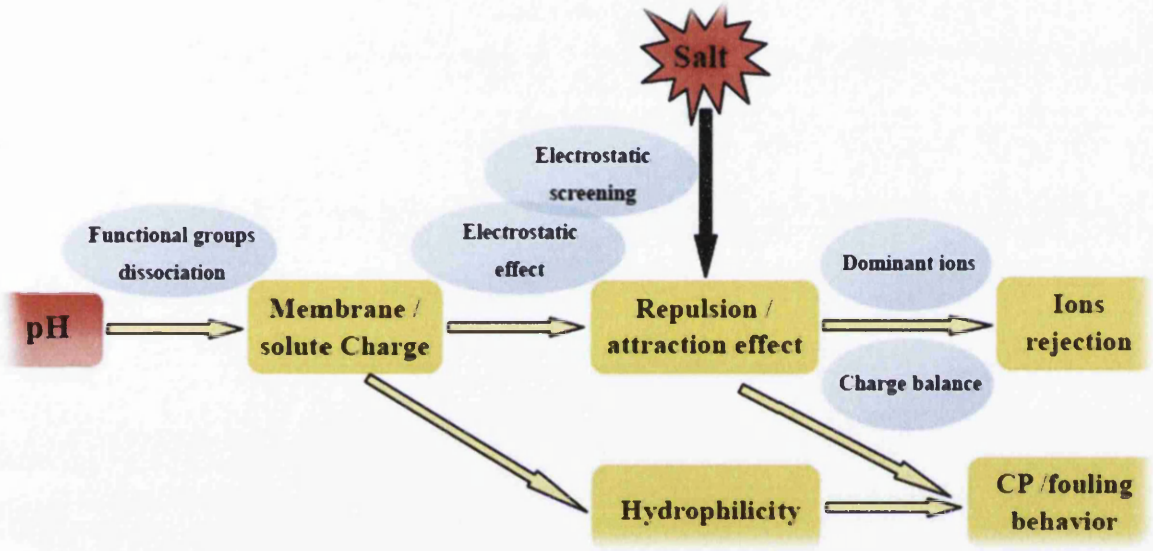

Figure 2.1: Effect of pH on ions rejection and fouling (Luo & Wan 2013b).

2.1.1 Charge distribution in the electrical double layer

When a membrane is brought into contact with an aqueous solution membrane charge forms on both the external surface and membrane pores which lead to formation of an electrical double layer due to electroneutrality (Schaep & Vandecasteele 2001), i.e. special arrangement of ions in the area adjacent to the membrane surface. Electroneutrality causes the counterions concentration to be higher near the membrane surface than that in the bulk solution to neutralize membrane charge which leads to a potential difference in the solution. The Gouy–Chapman–Stern–Grahame (GCSG) model is usually used to describe the charge distribution in the electrical double layer in which the potential decreases within the solution as a function of the distance from the surface as shown in Figure 2.2 (Wang et al. 2006). The electrical double layer (EDL) consist of two regions: (i) the immobile stern layer where ions bind at the

solid-liquid interface and the charge and potential distribution are governed by geometrical restrictions of ions, molecule size and interactions between ions, the surface and the adjoining dipoles (Hunter 1981) (ii) the diffuse layer, which is also called the Gouy-Chapman layer where the ions are free to move by thermal motion and the plane of shear separates the two layers (Möckel et al. 1998). The first layer consists of the inner Helmholtz layer (IHL) and the outer Helmholtz layer (OHL). The inner Helmholtz layer is generally dehydrated ions adsorbed chemically by forming a chemical complex or electrostatically (counter-ions) on the membrane surface while the next layer (outer Helmholtz layer) of ions, the Stern layer, is rigidly bound hydrated counter-ions (Hunter 1981). Three different potentials can be differentiated in Figure 2.2: the surface potential (Ψ_o) and surface charge density (σ_o) (i.e. the surface charge per unit area on the membrane surface is known as surface charge density), the potential at the Stern plane (Ψ_d) and the electrokinetic or zeta potential (denoted ζ) which is the potential at the surface of shear between surface and bulk solution where there is relative motion between them (Cho et al. 2012; Tay et al. 2002; Hunter 1981). As shown in Figure 2.2, the potential increases and decreases linearly from the surface to the Ψ_{OHP} and then decreases exponentially to zero in the diffuse layer (Möckel et al. 1998). Although the potential at the Stern plane is the most important potential since it governs the behaviour of the charged species, direct measurement of this potential cannot be achieved which makes the electrokinetic potential a good substitution (Peeters et al. 1999).

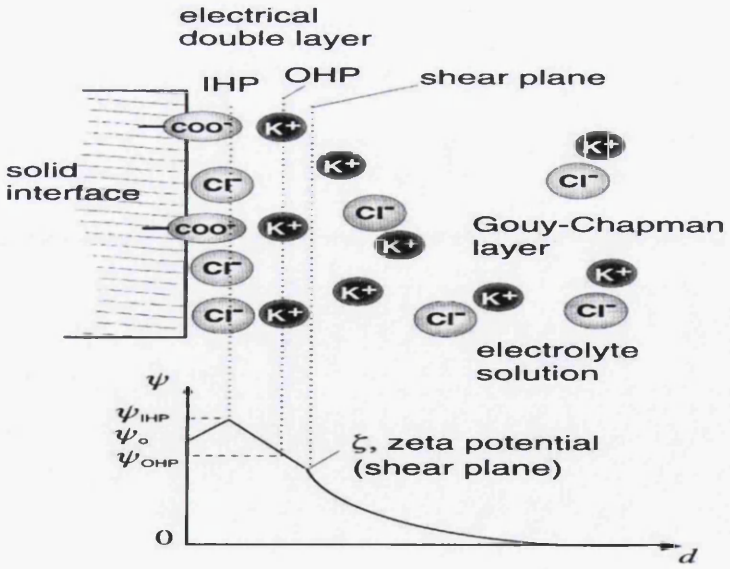

Figure 2.2: Charge distribution at a membrane –solution surface according to the GCSG model (Möckel et al. 1998).

2.2 Charge characterization methods

Studying membrane charge is essential to understand the membrane charge solution interaction which in turn helps to improve separation efficiency. These electrochemical interactions between the membrane and ions can be investigated in different ways. One of the most important methods to determine surface charge of membranes is electrokinetic techniques (see Figure 2.3), i.e. electrophoresis, streaming potential, electroosmosis and sedimentation potential (Ricq et al. 1997). The electrophoresis and streaming potential are the most popular methods while sedimentation potential is rarely used (Narong & James 2006). Electrokinetic phenomena take place when the solution containing charged species is pushed through the membrane pores or along the surface due to the application of a pressure or electric potential gradient and it occurs when an electrically charged phase moves with respect to an adjoining phase (Afonso 2006; Mart & Mart 2002).

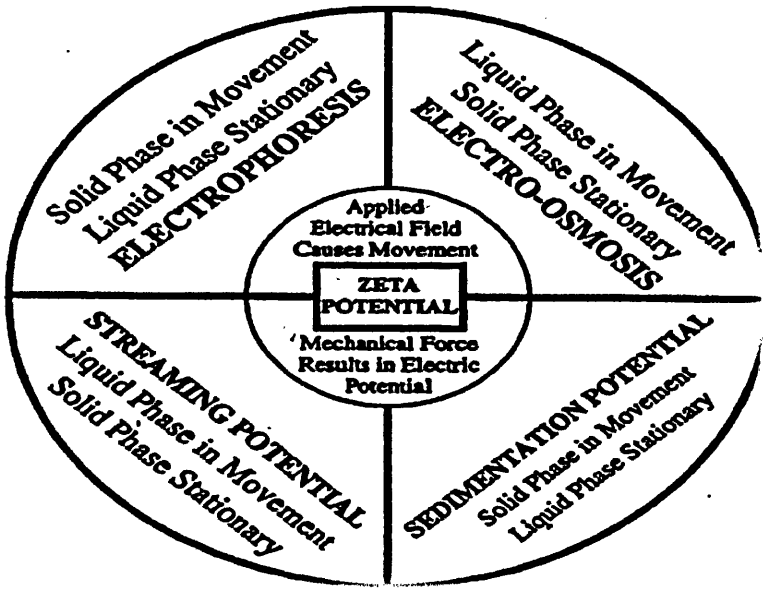

Figure 2.3: The principles of the four electrokinetic techniques (Elimelech et al. 1994).

Electrokinetic methods differ from each other in driving force, the nature of solid and liquid phases (Möckel et al. 1998). To illustrate, electroosmosis and electrophoresis methods, the driving force is electrical force which leads to a mechanical motion while the driving force in streaming current or streaming potential methods is an applied mechanical force which

produces an electric current or electric potential (Salg et al. 2013). Electrokinetic measurements have been used extensively in membrane charge studies to characterise different kinds of natural and synthetic materials such as membranes from all membranes separations spectrum, filters, textiles, hair and biomaterials and minerals etc. (Bukšek et al. 2010; Wilbert et al. 1999; Cho et al. 2012).

The other charge studying methods that are not classified as electrokinetic techniques include membrane potential measurements, separation experiments, electrical impedance measurements, electroviscous effect and measurement of the enhanced conductivity in the pores (λ_{pore}), measuring the ion adsorption on the pore surface (Huisman et al. 2000; Peeters et al. 1999).

2.2.1 Streaming potential

Since the electric potential at the membrane surface cannot be measured directly, streaming potential, which is one of the electrokinetic techniques commonly used to study the surface charge can be calculated from streaming potential or streaming current values (Ariza & Benavente 2001; Tay et al. 2002). A streaming potential is the potential difference at zero current produced by the convective flow of charge due to a pressure gradient through a charged capillary, membrane, plug or diaphragm (Peeters et al. 1999). Streaming potential depends on the constants that characterise the macroscopic behaviour of the solution and the surface–solution microscopic interactions: the solution viscosity, the ionic diffusivities, the dielectric constant, the surface charge density (or the zeta potential) and the hydrodynamic radius in units of Debye lengths (Mart & Mart 2002).

A streaming potential is generated when an electrolyte solution carrying a net charge is forced, by means of hydraulic pressure, to flow through a porous plug of material (transversal SP), across a channel formed by two plates (tangential SP), or down a capillary (Nystrom et al. 1996; Elimelech et al. 1994; Bukšek et al. 2010). The accumulation of counter charges downstream generates a streaming potential across the capillary which in turn causes a conduction current through the capillary in the reverse direction which opposes the mechanical transfer of charge, causing back-conduction by ion diffusion and electro-osmotic flow (due to the potential difference) as shown in Figure 2.4. The transfer of charges due to these two processes is called the leak current, when equilibrium condition is reached, the streaming current cancels the leak current, and the measured potential difference is the streaming potential. Datta et al. (2010) showed by using a theoretical model that an increase in the membrane charge leads to an increase in the streaming potential by improving ionic convection and reducing the streaming potential through the enhancement of ionic

conduction. In fact the former effect is dominant at low zeta potentials while the latter effect is dominant at large zeta potentials.

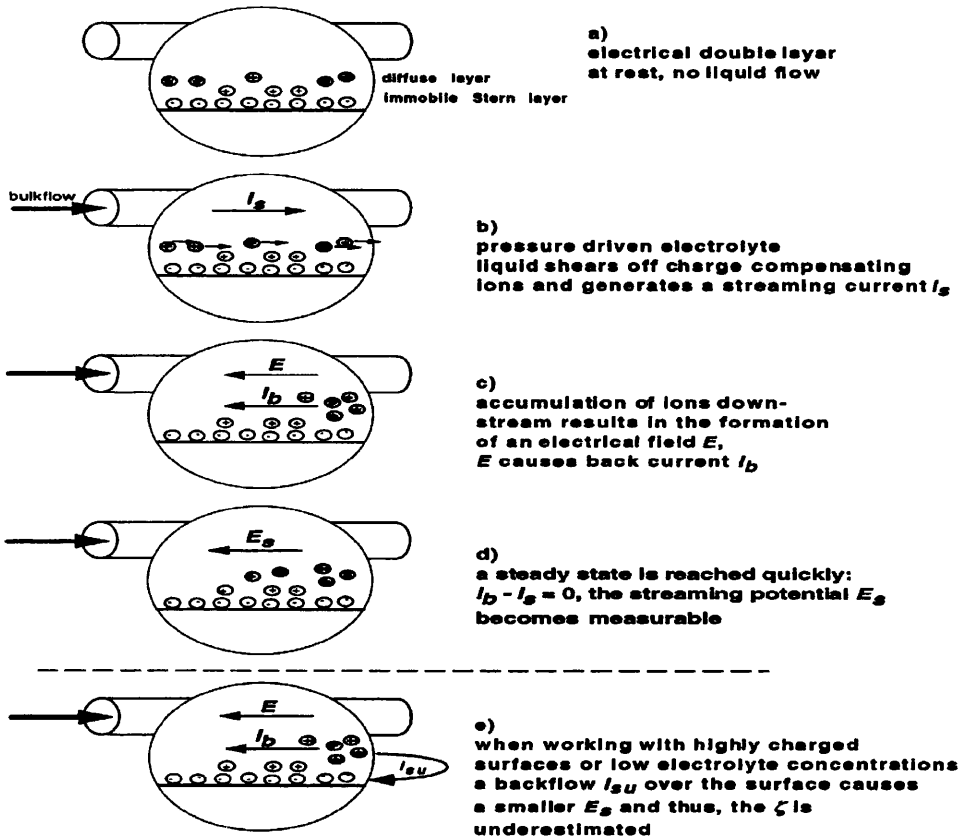

Figure 2.4: Streaming potential generation process (Möckel et al. 1998).

Streaming potential can be calculated experimentally by plotting the voltage difference across the membrane (or along the surface) (ΔE) against various pressure drops (ΔP) and a linear relation should be obtained, with the gradient of the line (streaming potential coefficient) used to calculate the zeta potential using the Helmholtz–Smoluchowski Equation (1903) (Ariza et al. 2001; Wilbert et al. 1999; Tra et al. 1998).

$$\zeta = \frac{\Delta E}{\Delta P}\frac{\eta}{\varepsilon_r \varepsilon_0} K_B \qquad [2.1]$$

where ζ is the zeta potential, $\Delta E/\Delta P$ the slope of streaming potential versus pressure (streaming coefficient), η the electrolyte viscosity, ε_r the relative liquid permittivity (dielectric constant), ε_0 the vacuum permittivity (8.854×10^{-12} C^2 J^{-1} m^{-1} or s $m^{-1}\Omega^{-1}$) and K_B the specific conductivity of the bulk electrolyte solution, Ω.

Although, the Helmholtz–Smoluchowski Equation is a well-known method to calculate zeta potential from streaming potential data, it has some limitations. The equation can be analytically solved when the surface has a low surface electrical potential (Ψ_0<25 mV) and the liquid moves on the streaming potential channel (or membrane pores) with laminar flow at a concentration high enough to prevent the electrical double layer (EDL) length overlapping (capillary radius higher than the Debye length) (Ariza & Benavente 2001). Moreover, the streaming potential channel width has to be much higher than channel height for slit-shaped cross-section channels, as that used for tangential streaming potential (TSP) measurements. In addition to that , Ding et al. (2006) found that the relation between ΔE and ΔP is not linear at very low salt concentration which makes streaming potential measurement an effective method to study the surface electrical properties of membranes at a limited range of salt concentrations. Ding et al. (2006) have performed the zeta measurements at concentrations approximately between 0.5 -8 mol m^{-3}. One possible explanation for this phenomena is that the salt is rejected by the membrane and there is not negligible electrical potential drop caused by the salt concentration difference across the membrane (Ding et al. 2006). Finally in order to have correct zeta potential values by using the Helmholtz–Smoluchowski Equation, the surface conductivity contribution has to be accounted for, this will be discussed in section 2.2.1.3.1.

The zeta potential can be determined from the measurement of the streaming potential or streaming current. Unlike streaming potential, streaming current measurements are seldom carried out through membranes due to their unknown pore structure (the calculation of the zeta potential from streaming current requires the knowledge of both the pore length and the membrane porosity) (Lanteri et al. 2012). Luxbacher (2006) compared zeta potential values obtained from streaming current and streaming potential. A significant difference was found which was explained as a result of the surface conductivity contribution.

2.2.1.1 Usage of zeta potential

The zeta potential which can be calculated from streaming potential data is an important and reliable indicator of the membranes surface charge that interacts with a solution and its knowledge can be used in different fields (Datta et al. 2010; Huisman et al. 2000; Luxbacher

2006; Lanteri et al. 2012) (i) characterization new and modified membranes to study the effect of solution chemistry (type of ions, ionic strength, pH etc.) on membrane charge properties, (ii) to confirm the attachment of surface modification agents since this modification leads to an alteration of surface charge properties (iii) to evaluate the efficiency of membranes, (iv) for better understanding of the rejection mechanisms of charged solutes and the interactions between the membrane surface and various charged foulants since both the amount of fouling and the reversibility of fouling is a function of the zeta-potentials of the feed suspension particles and of the membrane surface (Tra et al. 1998).

2.2.1.2 Transversal streaming potential

Streaming potential measurements can be performed in two different ways: by flow through the membrane pores (transversal streaming potential or filtration streaming potential (FSP)) or by flow along the top surface of the membrane (tangential streaming potential or TSP) (see Figure 2.5) and the electric potential difference is measured with a pair of reversible electrodes (Lanteri et al. 2012). Table 2.1 provides examples of journals articles which used both techniques to study the membrane charge.

Table 2.1: Examples of references used transversal streaming potential and tangential streaming potential.

Transversal streaming potential	**Tangential streaming potential**
(Szymczyk et al. 1997)	(Elimelech 1994)
(Kim et al. 1997)	(Peeters et al. 1999)
(Ricq et al. 1997)	(Childress & Elimelech 2000)
(Ricq & Pagetti 1999)	(Ariza & Benavente 2001)
(Burns & Zydney 2000)	(Ariza et al. 2001)
(Fievet et al. 2000)	(Brant et al. 2006)
(Mart & Mart 2002)	(Wang et al. 2006)
(Chun et al. 2002)	(Bukšek et al. 2010)
(Mart & Mart 2003)	(Yaroshchuk & Luxbacher 2010)
(Herbig et al. 2003)	(Lanteri et al. 2012)
(Matsumoto et al. 2003)	
(Chun & Park 2004)	
(Ding et al. 2006)	

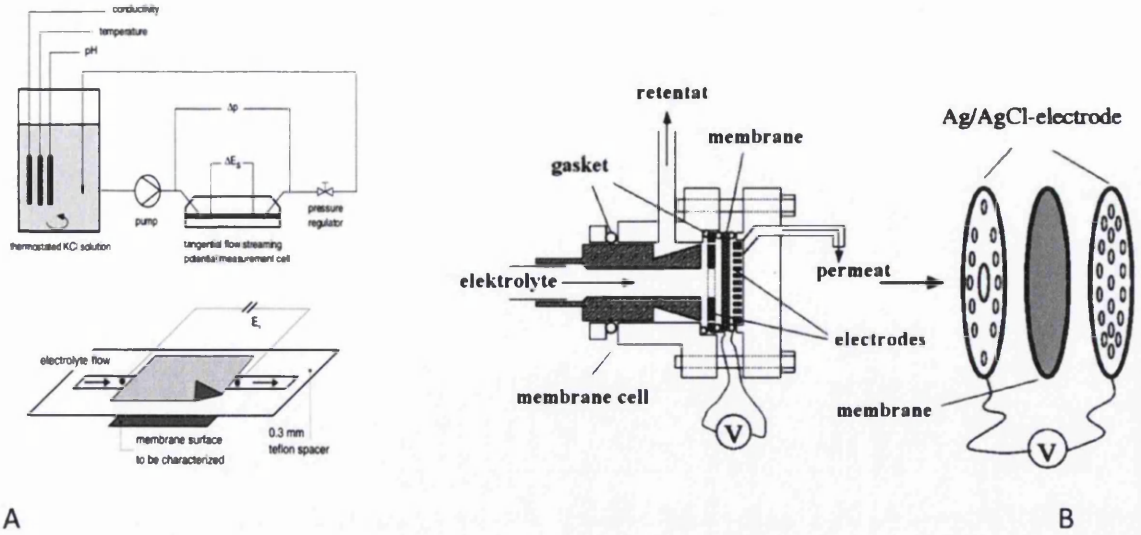

Figure 2.5: (A) Schematic representation of Electrokinetic Analyser used in measuring zeta potential by TSP technique (EKA) (Mőckel et al. 1998). (B) A set up fortransversal streaming potential (Herbig et al. 2003).

The transversal streaming potential has the advantage that the measurements and filtration process can be done at the same time which makes the measurement relatively easy and more realistic. However, this technique is not suitable for multilayer membranes (support layer (s) + skin layer) as these layers have different charge properties and noticeable contribution to the overall signal which lead to difficulties in the interpretation of the electrokinetic data and result in a global value (Ariza & Benavente 2001; Fievet et al. 2003; Herbig et al. 2003; Szymczyk et al. 2007). Moreover, the transversal streaming potential is not a good choice for the small pore size membranes due to the possibility of electric double layer overlap (Ariza & Benavente 2001; Fievet et al. 2003; Herbig et al. 2003). In fact, surface conductance and concentration polarization cause misleading conclusions about membrane surface charge especially for strongly charged pores (Fievet et al. 2000; Yaroshchuk & Luxbacher 2010).

In order to have correct zeta potential from streaming potential data the Helmholtz–Smoluchowski Equation (Equation 2.1) can be applied only when there is no overlap of the double layers inside the pores, that is , when the ratio between the pore radius and Debye length is very large, i.e. the membrane pore size is large and/or the electrolyte concentration is high, (Szymczyk et al. 1997) and overall pressure drop should take place almost entirely through the active layer (Bukšek et al. 2010). The problem of electrical double layer overlap

and the ways to avoid it will be discussed in details in section 2.2.1.2.1. TSP is alternative option to transversal streaming potential in which direct information about the membrane top layer can be provided (Fievet et al. 2003) and the difference in the zeta potential value between these two methods will be discussed in section 2.2.2.4.1.

The electrical potential measured by transversal streaming potential is sum of streaming potential and diffusion potentials (Mart & Mart 2002). Ricq et al. (1998) applied the streaming potential measurement procedure to exclude diffusion phenomena by applying an overpressure of 2 bars for 5 seconds which prevents a potential difference variation between both sides of the membrane. Fievet et al. (2000) found that the streaming potential reaches a maximum value (in absolute terms) before decreasing even if Ψ_d still increases which was explained by the author as a result of the excess conductance in the region near the pore walls.

2.2.1.2.1 Electrical double layer overlap

The difficulties in interpreting tangential streaming potential data include high surface conductivity of the membrane pores, the overlapping of the electrical double layers and the superposition of the concentration polarization phenomena (Ricq et al. 1998; Dina et al. 2001). Electrical double layer overlap takes place when the membranes pore radius is smaller than the Debye length (corresponding to the thickness of the electric double layer) which prohibits the use of Helmholtz–Smoluchowski Equation (Equation 2.1) as this equation is only valid in the absence of overlapping (Kukizaki 2009). As an example of the overlapping situation, the overlapping of the double layers will occur for a 1 mM NaCl solution (the Debye length of approximately 10 nm) for a membrane with pore radius of 5 nm. Therefore, the determination of the zeta potential might be impossible for the membranes with pore diameters less than 100 nm in monovalent salt solutions of 1 mM (Datta et al. 2010; Kukizaki 2009). On the other hand, overlapping phenomena does not existed in microfiltration membranes at ordinary electrolyte concentrations of 1 to 100 mM. According to Mart & Mart (2002) judgment of whether or not there is double layer overlap depends on the fraction of the total flow passing through pores with overlapping EDL for each concentration.

Alternatively when the EDL overlaps correction of the Helmholtz–Smoluchowski equation (Equation 2.1) using surface conductivity in the pore affects only the magnitude and not the sign of the zeta potential (Nystrom et al. 1996). Overlap of the EDL inside the membrane

pore results in a concentration gradient across the pore, and subsequently the solution conductivity at the pore region will deviate from its bulk value (Chun & Park 2004; Ernst et al. 2000) a consequence the measured Streaming potential is smaller (Ricq et al. 1997). When the EDLs overlap, the following three factors become significant (Datta et al. 2010):

1. The pressure-driven flow convects a different (less compact) distribution of charges.

2. The electrical conductivity of the solution inside the pore becomes higher than the bulk solution as the ionic distributions are affected by the charge on the pore surface. In fact if the pore is very small, the diffuse part of the double layer fills the entire pore which cause the co-ions to be significantly excluded (Fievet et al. 2000). On the other hand, the diffuse layer fills a smaller space of the pore as the pore size increases which leads to an increase in the concentration of co-ions within the pore due to the presence of the bulk solution in the pore. In fact the pore contains almost as many co-ions as counter ions and the membrane potential tends to the diffusion potential value, when the pore radius is much greater than the Debye length (κ) of the solution.

3. For a highly charged surfaces the streaming potential causes convection of ions by the electroosmotic flow which contribute to the current opposing the pressure-driven flow.

The streaming potential value in the absence of overlapping depends on the pore radius and membrane permeability (Ricq et al. 1997) and the calculated zeta potential, called the apparent zeta potential, is not equal to the true one (Datta et al. 2010). The Debby length (κ), i.e. the electrical double layer thickness, can be calculated by using Equation 2.2 (Chun & Park 2004).

$$\kappa = \sqrt{\frac{N_A e^2}{\varepsilon_0 \varepsilon_r \, k_B e^2 T} \sum_i z_i^2 \, c_i} \qquad [2.2]$$

where ε_0 is the dielectric constant of free space, ε_r is the dielectricconstant of water, k_B is Boltzmann's constant, T is the absolute temperature (K), e is the magnitude of the electron charge, N_A is Avogadro's number, c_i is the concentration of ion species i and z_i is the valence.

In aqueous medium and at 298 K, the term $\frac{N_A e^2}{\varepsilon_0 \varepsilon_r k_B e^2 T}$ is equal 5.404×10^{15} m (Ghosh n.d.). For monovalent electrolytes solutions at 25°C, the Debye length, κ (nm), is given by Equation 2.3 (Chun & Park 2004).

$$\kappa = \frac{I^{-0.5}}{3.278} \qquad [2.3]$$

where I is the ionic strength of the salt solution (M) and can be calculated from Equation 2.4

$$I = 0.5 \sum z_i^2 c_i \qquad [2.4]$$

Where c_i is the ion concentrations and z_i is the ion valence.

Many attempts have been made to obtain the true zeta potential, for example, Ricq et al. (1998) established a correction factor F attached to the Smoluchowski relationship by considering that the true zeta potential as the one calculated from electrophoresis measurements. This factor depends on both zeta potential values and the membrane pore radius, r, compared to the Debye length κ. At low $r\kappa^{-1}$ a significant correction is required, since there is double layer overlapping, whereas at high $r\kappa^{-1}$ values the correction factor tends toward 0.8, and the Helmholtz - Smoluchowski relation becomes valid. Datta et al. (2010) found that the true zeta potential is higher in magnitude (in absolute value) than the apparent zeta potential and can be predicted from the model of electric double layer overlap and streaming potential.

2.2.1.3 Tangential streaming potential

Tangential streaming potential is the second technique of the streaming potential methods that is used to measure streaming potential in which a solution flows along the top surface of the membrane. The technique was first used to characterize capillary surfaces before it was used in flat surfaces by the work of Van Wagenen and Andrade (1980) and later a

commercial machine was developed on this basis (Möckel et al. 1998; Paar n.d.). Elimelech's group (Dina et al. 2001; Elimelech et al. 1994; Childress & Elimelech 1996) performed primary experiments on the feasibility of using a streaming potential analyser to determine the zeta potential of RO membranes (B1-EKA, Brookhaven Instrument Corp., Holtsville, New Work, USA). The system that was used for streaming potential measurements is shown in Figure 2.5. The streaming channel is a well-defined slit like channel (50-300 μm width) formed by two identical membranes facing each other with Teflon spacers between them (Yaroshchuk & Luxbacher 2010; Möckel et al. 1998). The channel can be visualized as an idealized macro pore and the streaming channel geometrical dimensions cannot be used for calculation of zeta potential since it is sensitive towards the force that is used to clamp the cell halves together, as the Teflon spacer is slightly compressible (Möckel et al. 1998). In fact, the contribution of the membranes pores and support layers are excluded in TSP because of the horizontal flow direction during the potential measurements (Moritz et al. 2001; Ernst et al. 2000). There are many advantages of TSP that overcome the drawback of transversal streaming potential (Yaroshchuk & Luxbacher 2010; Moritz et al. 2001; Ariza & Benavente 2001). First, the streaming channel is relatively wide (50-300 μm) and this is enough to fulfil the conditions for the validity of the Helmholtz–Smoluchowski since there is no electric double layer overlap taking place, also the concentration polarization phenomena is not existed. Second, the zeta potential can be measured by this method for very small pore size and dense membranes where the pressure drop through the membranes are too high to investigate by transversal streaming potential measurements. Third, the method allows determination of the streaming potential of the active layer which is the most important part of the membrane and finally the simplicity of results interpretation since the contribution of the support layers is excluded. As the type of membranes is considered, TSP is now frequently used to characterize asymmetric/composite membranes or fine-porous membranes, on the other hand using this method with tubular and hollow fibers membranes is rare probably due to the fact that the tangential measuring cell for this type of membranes has been marketed only recently (Fievet et al. 2006a; Fievet 2006 et al. 2006b; Lanteri et al. 2012). Another possible explanation could be the large hydraulic diameter of the channels that prevents the establishment of a laminar flow and the use of the H–S Equation (Lanteri et al. 2012).

2.2.1.3.1 Membrane surface conductivity

The real conductivity of a membrane in contact with an electrolyte solution is the sum of the electrolyte conductivity and the surface conductivity of the membrane surface (Moritz et al.

2001). The classical Helmholtz–Smoluchowski equation (Equation 2.1) is applicable when the membrane surface conductivity is lower than the solution one, (Chun & Park 2004). However, surface conductivity becomes a problem at low electrolyte concentrations and / or at highly charged surfaces for both zeta potential measurements, i.e. TSP and transversal streaming potential (Ariza et al. 2001; Möckel et al. 1998). In these two situations the electrical resistance of the measurement liquid reaches a comparable value to that of the membrane surface (Möckel et al. 1998). Therefore, part of the back current flows over the surface which is not desirable. The surface conductivity contribution to the total conductivity is very small for a large slit channel height (the ratio of the channel half-height to the Debye length, h/κ, for non-conducting samples above about 200 (Fievet et al. 2003). Szymczyk et al. (2007) used thick spacers with a ratio of the channel half-width to the Debye length of greater than 2000 to avoid the surface conductivity contribution. The Helmholtz–Smoluchowski Equation (Equation 2.1) is applicable for weakly charged surfaces and wide pores or channels, when the surface conductivity and double layer overlapping can be neglected (Ariza et al. 2001). Modification of the classical Helmholtz–Smoluchowski equation (Equation 2.1) should be carried out, If surface conductivity (λ_s) exists the zeta potential will be obtained by (Peeters et al. 1999; Cho et al. 2012; Ariza et al. 2001):

$$\xi = \frac{\eta(\lambda_0 + \frac{2\lambda_s}{r_p})}{\varepsilon_0 \varepsilon_r} \frac{\Delta E}{\Delta P} \qquad [2.5]$$

where r_p is the pore radius (or the height of a channel) and λ_o is the electrolyte conductivity. Surface conductivity is difficult to measure (surface conductivity is measured by measuring the electroosmosis flux of membranes (Ricq et al. 1997). This problem can be solved by measuring the actual resistance of the electrolyte solution in the slit or pore and then comparing this value with the resistance that can be calculated from experiments at high concentrations (around 0.1 M monovalent electrolytes salt), where the surface conductivity is negated as follow (Ariza & Benavente 2001).

$$\lambda_0 + \frac{2\lambda_s}{r} = \frac{\lambda_{0.1MKCl} R_{0.1M\ KCl}}{R_{cell}} \qquad [2.6]$$

Where $\lambda_{0.1MKCl}$ is the solution conductivity at high salt concentration (usually 0.1 M KCl), $R_{0.1M\ KCl}$ and R_{cell} the electrical resistance of the cell filled with the high salt concentration and with the working salt concentration, respectively. This is called the Fairbrother and Mastin approximation in which it is assumed that the electrolyte solution carries most of the current and streaming potential is not dependent on the geometry of the capillary or streaming potential channel (Peeters et al. 1999; Wilbert et al. 1999). The zeta potential will be obtained by:

$$\xi = \frac{\Delta E}{\Delta P}\frac{\eta}{\varepsilon_r \varepsilon_o}\frac{\lambda_{0.1MKCl} R_{0.1M\ KCl}}{R_{cell}} \qquad [2.7]$$

Different H-S Equation versions for zeta potential calculation are shown in Figure 2.6 (Bukšek et al. 2010), where ΔI/ΔP is the slope of the streaming current versus pressure, L the length of the streaming channel, and A the cross-section of the streaming channel. The zeta potential is calculated without approximation when the geometry of the streaming channel is known by using Equations 1 and 2 in Figure 2.6. The term L/A is replaced in Equations 4 and 5 by the term $R_{Cell}\lambda_0$ for low surface conductivity solutions (concentration greater than 10^{-3} M) or by $R_{0.1M\ KCl}\lambda_{0.1M\ KCl}$ in the Fairbrother-Mastin approach (Equation 3) as discussed above (Bukšek et al. 2010; Wilbert et al. 1999).

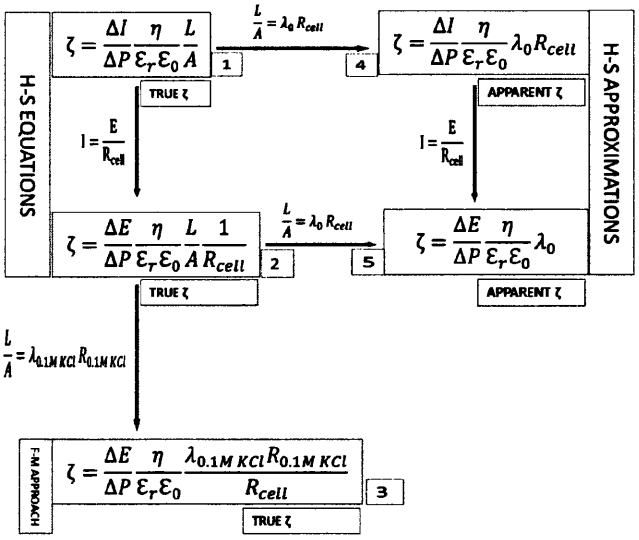

Figure 2.6: Different versions of Helmholtz–Smoluchowski equation (Bukšek et al. 2010).

Correction of the membrane surface conductivity only changes the magnitude of the zeta potential value but does not have an effect on the position of the i.e.p. or overall shape of the zeta –pH curve; therefore the surface conductivity correction is necessary in quantitative studies and not qualitative ones (Ernst et al. 2000).

Ariza et al. (2001) found big differences between apparent and actual zeta potentials with low NaCl concentrations, when surface conductivity usually presents an important contribution. Ariza & Benavente (2001) indicated that the difference between both values is higher by 50% at low concentrations ($C_i \leq 10^{-3}$ M) while at high concentrations differences are around 10%. Möckel et al. (1998) found apparent zeta potential value smaller for all materials investigated and the difference is smaller at low pH values. The authors suggest that the reason is that most of the COOH groups are not dissociated at low pH values and the resistance of the surface should be higher resulting in a smaller fraction of the back current flowing over the surface. Bukšek et al. (2010) compared correct zeta potential values without approximation (calculated from Equation 1 in Figure 2.6) and the apparent zeta potential (calculated from Equation 4 in Figure 2.6) by using two different measuring cells with a SurPASS electrokinetic analyser. The ratio between apparent and correct zeta potential for the CLC (Clamping Cell) was only 17%, whereas the difference was 90% for the AGC (Adjustable Gap Cell).

2.2.1.3.2 Membrane body conductance

Yaroshchuk & Ribitsch (2002) have theoretically called attention to membrane body conductance phenomena which may not allow the determination of the true ζ-potential by using the classical H–S formula or its versions for certain conducting materials. This is because these equations are derived with an assumption that both streaming and conduction currents flow through identical paths. The streaming current is generated dominantly inside the streaming channel and inside the porous membrane support, as a result a non-negligible amount of the conduction current is likely to flow through the channel walls (i.e. the substrate body) (Bukšek et al. 2010). In fact the conduction current in porous membranes is expected to flow wherever the electric conductivity differs from zero (Szymczyk et al. 2007). The effect of the membrane body conductance was experimentally examined by Fievet et al. (2003) who found the true ζ-potential value is determined from an extrapolation method for which a set of measurements with various channel heights is required, otherwise the zeta potential determined is lower than the true one.

The other method used to the find true zeta potential is to compute true zeta potentials directly from coupled streaming potential and total electric conductance measurements

(coupling method) (Fievet et al. 2006b; Lanteri et al. 2012; Fievet et al. 2003; Yaroshchuk & Ribitsch 2002). Wang et al. (2006) measured zeta potential with the help of a DC constant current to measure system total conduction and the experimental results showed that membrane body conductance plays a non-negligible role in the determination of zeta potential, resulting in underestimation of the zeta potentials. The zeta potential values obtained from the above mentioned extrapolation or coupling method, i.e. by taking into account the effect of the porous body conductance, have been compared to that calculated via the H–S Equation by many authors and the ratio of them was found to be in the range of 1–10 (Lanteri et al. 2012). Fievet et al. (2006b) found that the ratio of the correct potential to the apparent one for the organic membrane is a function of the pH, which is a result of a non-negligible contribution of surface conductance within the membrane pores while the effect of the membrane body for ceramic membranes is independent of the pH of solution. Luxbacher (2006) compared apparent zeta potential determined from streaming potential measurement and the zeta potential determined from streaming current measurement by using SurPASS and a significant difference in the results was found which was explained in terms of body conductance. Yaroshchuk and Luxbacher (2010) have pointed out that the membrane body conductance not only contributes to the cell electric conductance but also to the streaming current and these contributions are considerable especially in the case of membranes with large pores like MF membranes. They have also highlighted that the type of cell used may have a significant influence on measurements of the streaming current or streaming potential.

2.2.1.3.3 Electrokinetic Analyser (EKA)

The study of zeta potential of solid materials started in the 1900's (Cho et al. 2012) and the first EKA Electro Kinetic Analyser was introduced in 1990 by Anton Paar which is still in use at Yale University (New Haven, CT, USA) (Paar n.d.). Elimelech's group (Childress & Elimelech 1996; Dina et al. 2001; Elimelech et al. 1994) performed the first experiments using a streaming potential analyser to determine the zeta potential of RO membranes (B1-EKA, Brookhaven Instrument Corp., Holtsville, New Work, USA). Before that streaming potential used to be determined by a homemade setup (Teixeira et al. 2005; Peeters et al. 1999) (a full description is available in Schaep & Vandecasteele (2001). Different designs of clamping cell have been used in measuring zeta potential. Some of these cells have features not available in ordinary cells such as the ability to adjust the streaming potential channel height and measuring the zeta potential without needing to cut the membrane samples to create the streaming potential channel (Fievet et al. 2003). The most used commercial EKA in the literature are the EKA Electro Kinetic analyser (Ernst et al. 2000; Ariza et al. 2001)

and the SurPASS from Anton Paar (Yaroshchuk & Luxbacher 2010; Luxbacher 2006), zeta CAD made by CAD Instruments (Fievet et al. 2003; Egueh et al. 2010) and BI-EKA from Brookhaven Instruments (Childress & Elimelech 1996; Childress & Elimelech 2000; Bellona & Drewes 2005). In the EKA, the electrolyte solution is forced to flow through the measuring cell by means of pump or compressed gas. The cell contains well defined dimensions for a streaming channel created by using two pieces of the membrane facing each other and separated by Teflon spacers with two Ag/AgCl electrodes at each end of the channel used to measure the induced streaming potential. The streaming potential coefficient is usually determined as the average of at least ten measurement readings and the data is recorded by a computer. Möckel et al. (1998) carried out computational fluid dynamic calculations to confirm that his self-made tangential flow cell met the hydrodynamic stipulations of laminar, steady and established electrolyte flow for reproducible electrokinetic measurements (Poiseuille flow) which is required for accurate streaming potential measurements. Characteristic hydrodynamic parameters such as the Reynolds number and the hydrodynamic height of the streaming channel for the EKA Anton Paar are: $200 \leq Re \leq 400$ and h_h=200 ±10 μm (Ariza et al. 2001). So far, used the tangential technique to characterize tubular membranes and membrane hollow fibres is rare, probably due to the fact that tangential measuring cell for these type of membranes has been made only recently (Lanteri et al. 2012). However, Fievet et al. (2006a) described and tested a home-made TSP set-up for the electrokinetic characterisation of tubular membranes. Although the flow is turbulent in the streaming channel, the zeta potential could be calculated from streaming potential data. Cho et al. (2012) developed a new device to measure the zeta potential for nanofibers to avoid destroying the morphology of low modulus nanofibers by high flow rate if one of the commercial EKA's was used. Ariza and Benavente (2001) compared the streaming and zeta potentials for samples obtained from the same sheet of polysulfone membranes with two different experimental systems, namely the Anton Paar EKA and a homemade setup. The results showed some differences which the author related to the measurement itself such as kind of electrodes, potential asymmetry and influence of concentration polarization as well as the devices that are used for the measurements. Moreover, the reliability of the EKA resistance measurements was tested and high values of the cell electrical resistance at low salt concentrations was obtained ($<10^{-3}$M), which could affect electrical potential values obtained.

Until recently, zeta potential determination using electrokinetic analysers is based only on the streaming potential technique and the surface conductivity effect is cancelled by using the

Fairbrother and Mastin approach (Bukšek et al. 2010). However, the new EKA from Anton Paar (SurPASS) allows measuring the streaming current which is insensitive to the presence of any surface conductivity (Luxbacher 2006; Lanteri et al. 2012). In addition to that the machine is able to determine the exact geometry of a rectangular streaming channel (Bukšek et al. 2010). Therefore the zeta potential can be calculated by Equations 1 and 2 in Figure 2.6 without approximation as discussed in section 2.2.1.3.1.

Recently the first results obtained with the "SurPASS" for thin-film composite membranes were published in the literature (Luxbacher 2006) and the zeta potential was significantly higher than other results reported in the literature, which the author explained as a result of membrane body conductance (Bukšek et al. 2010). Zeta potential results obtained from EKA and SurPASS have been compared (Bukšek et al. 2010) and the results obtained with the EKA were more negative for the same type of membrane, and the same principle of the applied measuring cells. The results of two different measuring cells (Adjustable Gap Cell and Clamping Cell) used in the SurPASS instrument have also been compared and the obtained results showed differences in zeta potential, where the Adjustable Gap Cell gave more reproducible results. The authors explained this behaviour as a result of the design of the Clamping Cell which requires a sample size larger than necessary for zeta potential determination. Therefore the authors recommended the Adjustable Gap Cell for the zeta potential determination of flat sheet membranes.

2.2.1.3.4 Zeta potential experiment procedure and experiment reproducibility

The membranes to be used in zeta potential measurements should be cut to fit the EKA measuring cell dimension and then soaked in deionized water for at least 12 h at 25 °C (at 5 °C (Bellona & Drewes 2005) to remove preservative chemicals from the membrane surface (Moritz et al. 2001; Ariza & Benavente 2001). Using an ultrasonic bath and /or ethanol have been also used by some researchers (Tra et al. 1998; Rice et al. 2011; Mänttäri et al. 2006) and the membranes are not left to dry after this preparation. The membrane is usually soaked in the measuring solution for some time in order to establish equilibrium which is a very important step for correct measurement and this procedure can be done in the measuring cell (Hagmeyer & Gimbel 1998; Dina et al. 2001; Ariza & Benavente 2001) or in the beaker outside the machine (Wilbert et al. 1999; Childress & Elimelech 1996; Szymczyk et al. 2007; Zhao et al. 2005). The equilibration time length can vary from 30 min (Childress & Elimelech 1996), one hour (Ariza & Benavente 2001), 12h (Zhao et al. 2005; Hagmeyer &

Gimbel 1998), overnight (Szymczyk et al. 2007), 24h (Wang & Ku 2006) and more than one day (Dina et al. 2001; Wilbert et al. 1999).

Preparation of the measuring cell for zeta potential measurements is described in detail in Childress & Elimelech (1996). The measurements are not suitable to do at a pH higher than 10 to avoid precipitation of $Ca(OH)_2$ and $Mg(OH)_2$ and stripping of the Ag/AgC1 electrodes either by a high pH electrolyte or using electrolytes contains aggressive chemicals (Huisman & Tra 1999; Tra et al. 1998; Moritz et al. 2001). Acidic pH also might cause some difficulties in interpreting of the data due to the high contribution of the hydrogen ions to the conductivity of the solution (Schaep & Vandecasteele 2001). Therefore, some researchers have chosen to set a minimum pH in their experiments, the pH for which the number of the H^+ ions in solution does not represent more than 10% of the initial ionic conductivity (i.e. pH_{min} = 4 for 1mM) (Szymczyk et al. 1998). The pH values of solutions are adjusted by hydrochloric acid and sodium hydroxide (Tay et al. 2002), HC1 and KOH (Chun & Park 2004; Matsumoto et al. 2003), HCl and NaOH or $Ca(OH)_2$ (Ricq & Pagetti 1999), KOH, NaOH, H_2SO_4 and HCl (Szymczyk et al. 1997), buffer solutions (Datta et al. 2010). In general it is desirable to avoid introducing a new ion to the electrolyte during pH adjustment that may affect the measurements. Membrane storage after finishing the measurement can be done in deionized water at approximately 5°C (Brant et al. 2006; Childress & Elimelech 1996). Childress and Elimelech (1996) found that storing membranes in sodium meta-bisulfite solution might alter the membrane surface charge.

There are many factors that may cause difference in zeta potential value such as membrane storage, electrodes position, EKA operating procedure, hydrodynamic conditions or the theoretical model used for zeta potential values calculation (Ariza & Benavente 2001). Datta et al. (2010) found that streaming potential data were quite reproducible with the error being less than ±0.03 mV during a single experiment. Some researchers suggest streaming potential measurements are highly variable and accurate only within ±5 mV for polyamide membranes (Hurwitz et al. 2010). The sources of uncertainty in the zeta potential measurements are (Wilbert et al. 1999):

1. Changes of the solution properties such as temperature, pH, and conductivity which affect the viscosity and surface charge. The effect of temperature on viscosity is taken into account by EKA software, but the kinetic response of the electrode might be affected. Furthermore, shifting of pH during the measurements caused by dissolving atmospheric CO_2 into the electrolyte solution could change zeta potential readings.

2. Instrument setup and operation factors which include: changes in channel geometry, the electrodes position, rinse time, maximum pressure, pre-soaking period, and the number of cycles.

3. Differences in the membrane surface produced from handling or manufacturing the membranes which change the membrane's surface energy.

Nystrom et al. (1996) studied reproducibility of the zeta potential experiments of both streaming potential and electroosmosis and the results were reproducible within 10% error. The variation in zeta potential within the same membrane batch of the same membrane type was also investigated in literature; the difference of zeta potential values is small and in another research the same researcher (Kim et al. 1997) found the variation around 10% over the pH range 4-7. Chun et al. (2002) found that doing the measurements at several discrete pressure drops, gives more accurate and reproducible data than using a continuous pressure type and the difference in zeta potential values generated by the two procedures is less than 8%. Wilbert et al. (1999) evaluated two measurement operation procedures: the instrument's standard operating procedure, which continuously ramps the flow past the specimen and a modified procedure that periodically stepped the flow rate and required manual calculation of zeta potential from the pressure and streaming potential data. The study indicated that the kinetics of equilibration between electrolyte, electrodes, and membrane has the greatest impact on measurement uncertainty of any method used. An optimized protocol was developed for each method and the researchers recommend a long pre-soaking period to allow the membrane to become more fully hydrated, rinsing time between changes in operating conditions allows the system to reach a consistent starting point before the streaming potential is measured under new conditions and thirty minutes was found long enough for these purposes. Möckel et al. (1998) repeated the measurements at least three times with the same membrane and the results were reproducible within 10%. Elimelech et al. (1994) studied the variability in zeta potential results when two different samples of the same membrane are used: Eight of the nine measurements for the two different samples varied by less than 1 mV (about 10%) and the other measurement varied by less than 2 mV (about 20 %). The results also varied by more than 2 mV when a membrane sample was stored overnight in the measuring cell, and then used again the next day. Rice et al. (2011) found that using the same piece of membrane for multiple experiments is desirable. However, a fresh piece of a membrane should be used following any multivalent ions measurements due to strong adsorption to the membrane surface such that the rinsing process is not

sufficient to return the membrane to its original condition. Dina et al. (2001) measured zeta potential for a membrane kept for several days in the analyser. The zeta potential values showed no difference in the first two days while on the 3rd day zeta potential values are not reliable anymore. Scattering of the results was observed as the salt concentration increase which limits the concentration up to about 0.005 N for the NaCl. Childress and Elimelech (1996) found that a 30-min equilibration period is necessary for streaming potential experiment.

2.2.1.4 pH- ζ curves

pH changes leads to a displacement of the surface acid-basic equilibrium which amends the net charge of the surface and modifys the number of counter-ions in the diffuse layer, i.e. streaming potential variations varied as a result of this surface charge modification (Szymczyk et al. 1997). The magnitude of streaming potential and zeta potential decreases as the salt concentration increases due to the double-layer compression (the Debye length κ decreases) which shortens the distance between the surface of shear and the membrane surface (Ricq & Pagetti 1999; Afonso 2006). Furthermore, increased electrolyte concentration makes the solution inside the pores more conductive leading to a smaller streaming potential (Chiu & James 2007; Kukizaki 2009). pH-ζ curves are the output of zeta potential measurements which are useful to gain information about the adsorption and dissociation processes at the surface of membranes. To illustrate, the dissociation of the membranes acidic functional groups increase at higher pH values and reaches its ultimate negative value in the alkaline range where the curve levels off as indication of complete dissociation of these acidic groups (Ernst et al. 2000). On the other hand, a positive sign of the zeta potential in the acidic range is caused by either the dissociation of the alkaline surface groups and /or the adsorption of the cations such as protons, Ca^{2+} and Mg^{2+}.

The shape of pH-ζ curve and position of isoelectric point as a function of electrolyte concentration can be used to identify the type of functional groups on the membranes surface and proof for specific adsorption of anions and cations. Figure 2.7 shows pH-ζ profiles for different types of membrane materials, the dissociation of strong acidic functional groups such in the case of polyethersulfone takes place once and the membrane reaches its highest negative zeta potential at very low pH. On the other hand strong basic groups dissociate over the entire pH range and weakly basic groups have no positive charges at pH values over 8 and the surface of inorganic membranes are often positive at low pH and negative at high pH,

having i.e.p between 5 and 8. The study of the pH-ζ curve can also give information about the ratio of acidic to basic functional groups on the surface of the membranes. To illustrate if acidic and basic groups are equivalent, the membrane would be positively charged at acid pH, slightly positive at acid–neutral pH and negatively charged at basic pH while if the surface has more acidic than basic (amine groups as an example) the membrane could be negatively charged even at basic pH (Teixeira et al. 2005). Furthermore, if the net membrane surface charge is zero, the membrane behaves like a nonpolar surface to which anions such as Cl^- and OH^- can be adsorbed.

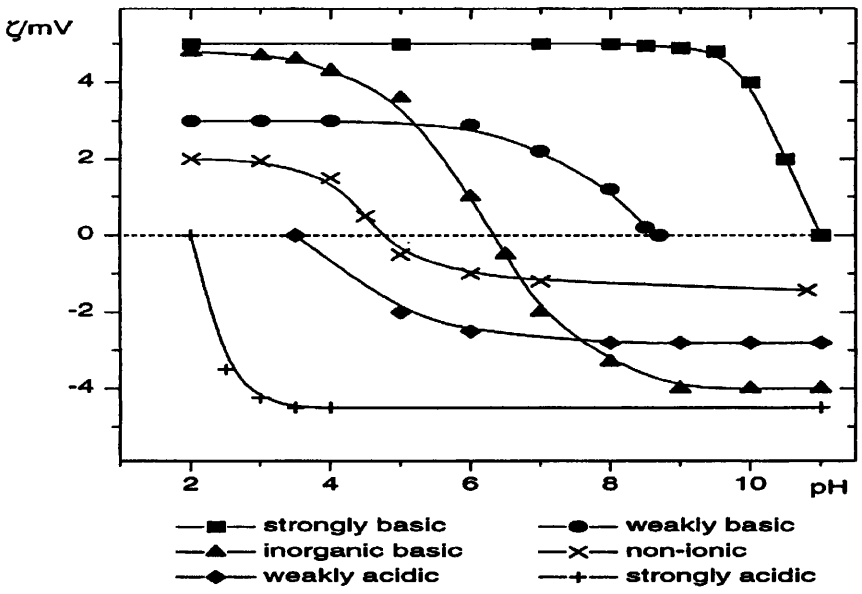

Figure 2.7: Schematic representation of the shape of zeta potential curves as a function of pH for different types of membranes materials (Möckel et al. 1998).

The effect of ions on membrane charge is different, multi-valence cations form chemical complexes with the membrane surface functional groups which make the surface more positively charged while monovalent ions (indifferent ions) form the diffuse layer (Tay et al. 2002). It is well known that the specific adsorption of ions shift the i.e.p towards higher or lower pH values for cations and anions respectively. On the other hand, if the i.e.p is independent of the ionic strength, thus indicates either the absence of specific adsorption ions or a nearly identical adsorption of both cations and anions (Mullet et al. 1997). Ca^{2+} cations are particularly attracted to the surface by penetrating into the compact layer to reach the

internal Helmholtz plane by losing a part of their hydration sphere and form a chemical complex with the membrane surface (Szymczyk et al. 1997). Specific adsorption also occurs with some multivalent anions such as sulphate anions. The specific adsorption of multivalent ions can reverse the net charge of the membrane as their concentration increases while indifferent electrolytes can only reduce the membrane surface charge to zero (Szymczyk et al. 1997). Tay et al. (2002) found the surface charge of some membranes altered more easily by the solution physico-chemistry than others. According to Elimelech et al. (1994), anions can approach more closely to nonpolar or hydrophobic surfaces because they are less hydrated than cations. In this process a surface will give a more negative zeta potential due to the presence of anions beyond the plane of shear.

Another term used in membrane charge studies is the point of zero charge (PZC) which is different from the i.e.p since the adsorption for the point of zero charge is only for potential-determining ions, H^+ and OH^-, (Kukizaki 2009). The pH (pzc) can be determined experimentally from the pH-ζ profile, and by the salt addition method (Mullet et al. 1997). Mullet et al. (1997) used two methods for determining the point of zero charge namely: membrane /or powder addition method and salt addition method in addition to surface charge and pH profiles methods. The results showed that the powder addition method was giving similar results to those usually used, i.e., the salt addition method' and potentiometric titration experiments.

2.2.2.4.1 The effect of electrolytes chemistry on zeta potential

The effect of solution chemistry on zeta potential has been studied extensively in the literature. The electrolytes which have been used in zeta potential studies include indifferent salts (NaCl and KCl), divalent cations (Ca^{2+}, Mg^{2+}), divalent anions (SO_4^{2-}), humic acids and anionic/ cationic surfactants (Childress & Elimelech 1996). Table A 2.1 (see the appendix) provides a summary of the studies that will be discussed in this section and includes the membranes used, salt solutions, charge study technique and most important findings. Elimelech et al. (1994) performed one of the pioneering studies on the effect of salts on charge of RO membranes. Ernst et al. (2000) determined the zeta-potentials of a polyethersulfone nanofiltration membrane in single salt solutions at different concentrations and pH values and results were compared with measured rejection rates of the electrolytes in the same aqueous medium. Peeters et al. (1999) measured streaming potentials of two different nanofiltration membranes with several electrolyte solutions to investigate the influence of salt type and concentration on the zeta potential. In addition to that, rejection,

kinetic surface charge density, the amounts of adsorption sites and adsorption free energy were also determined. Teixeira et al. (2005) compared zeta potential along the surface (tangential streaming potential) and through the pores (transversal streaming potential) of a commercial nanofiltration membrane with several electrolyte solutions to investigate the influence of salt type and pH on the charge of the membrane surface and in the membrane pores. Zeta potential data along with rejection and flux of single salts, mixtures and a proton have been used to examine the effect of salt type and pH on the performance of the membrane. Childress and Elimelech (2000) investigated water flux and solute rejection of a thin-film composite aromatic polyamide nanofiltration membrane and its relation to membrane surface charge. Childress and Elimelech (1996) also used streaming potential to investigate the effect of solution chemistry on the surface charge of four commercial reverse osmosis and nanofiltration membranes and studied the effect of membrane storage and equilibration time on reproducibility. Schaep and Vandecasteele (2001) used several methods to determine the charge of commercially available nanofiltration membranes, and compared them. Rice et al. (2011) studied the surface charge of three nanofiltration membranes commonly used in the dairy industry with KCl, phosphate, citrate, calcium and mixtures of them to study cancelling-out behaviour between charged species. Burns and Zydney (2000) examined the zeta potential of both standard and positively-charged polyethersulfone ultrafiltration membranes in the presence of a variety of monovalent and multivalent buffer ions and with KCl used as a background electrolyte in all the measurement. Zhao et al. (2005) studied electrical properties of alumina-based ceramic microfiltration membranes with ten different salts over a wide range of pH values (2 to 12). Mänttäri et al. (2006) studied three commercial NF membranes at different pH values. Their retention and flux were explained by the charge and the hydrophilic characteristics of the membranes. Szymczyk et al. (1997) measured the streaming potential of plane inorganic membranes during filtration with different pH, ionic strength and electrolytes. Ding et al. (2006) determined zeta potential and surface charge density of the membrane based on the Helmholtz–Smoluchowski equation and the Gouy–Chapmann theory. Deshmukh and Childress (2001) performed streaming potential measurements on RO membranes using actual membrane feed waters. Salg et al. (2013) measured the zeta potential of polyethersulfone membranes in various kinds of electrolyte. Wang and Ku (2006) studied the effect of electrolyte solution pH, fluid pressure and UV irradiation on the tangential streaming potential (TSP) and transversal streaming potential (FSP) of Degussa P-25 titanium dioxide membrane. Time dependence of TSP and different pH adjustment paths for TSP measurements were also conducted. Mart and Mart (2003)

studied the influence of the ions mobility including protons introduced to adjust the pH on zeta potentials and the isoelectric point. The author recommends to measure zeta in a high salt concentration with very similarly mobile anions and cations and then extrapolated to zero protons percentage.

2.2.2 Electrophoresis

Electrophoresis is one of the electrokinetic methods that is used to study membrane charge in which the suspended charged particles move under the influence of an applied electric field. This relative movement of particles to the liquid is a function of (Park & East 2012): zeta potential, electrical field strength, dielectric constant of medium and viscosity. The Electrophoretic Light Scattering technique (ELS) is based on Dynamic Light Scattering (DLS) and Electrophoresis and these two techniques are combined in one instrument (Systems n.d.). In DLS, Brownian motions cause particles to move in solution while ELS an applied electric field causes particle movement. Electrophoretic mobility can be measured which allow zeta potential calculation. When a dispersion is introduced to the measuring cell and the electrical field is applied to the electrodes, the charged particles will migrate towards the oppositely charged electrode with a certain velocity which is related to their zeta potential (Malvern Instruments Ltd 2012). ELS, sometimes known as the laser Doppler technique, is used to measure the velocity of particles (Kukizaki 2009). The charged particles reach a constant terminal velocity, which is proportional to the magnitude of the field, E. The proportionality constant, U, defines the electrophoretic mobility (velocity) (Systems 2006).

$$\nu = U\,E \qquad [2.8]$$

The zeta potential can be calculated and converted from the electrophoretic mobility data using Henry's equation (Chiu & James 2007).

$$U = (4\pi\varepsilon_0)\frac{\varepsilon_r\zeta}{6\pi\eta} f(\kappa^{-1}a) = \frac{2\,\varepsilon_0\varepsilon_r\zeta}{3\,\eta} f(\kappa^{-1}a) \qquad [2.9]$$

where η is liquid viscosity, f (κ^{-1} a) is Henry's function (correction factor) where κ^{-1} and a is the inverse Debye length and the particle radius respectively. For a low $\kappa^{-1}a$ ($\kappa^{-1}a$ <1) the

Henry-function in Equation 2.9 can be substituted with the value of 1 and this is called Huckel approximation (Park & East 2012; Ricq et al. 1998).

$$U = \frac{2\varepsilon_0 \varepsilon_r \zeta}{3\eta} \qquad [2.10]$$

For large $\kappa^{-1}a$ ($\kappa^{-1}a$ >100) the Henry-function approaches 1.5 (3/2) and this is called the Smoluchowski approximation.

$$U = \frac{\varepsilon_0 \varepsilon_r \zeta}{\eta} \qquad [2.11]$$

Narong and James (2006) measured electrophoretic mobility of ground particles of a ceramic (titanium dioxide–alumina layered) ultrafiltration membrane having a nominal pore size of 5 nm at three different ionic strengths of NaCl (10^{-1}, 10^{-2}, 10^{-3} M) and the pH of the oxide suspensions was adjusted in the range pH 3–10. The study found that the ζ-potential value changes with pH and is positive at low pH (< pH 3.2) and negative at higher pH. At higher concentrations of NaCl the ζ-potential is always negative, and the i.e.p. was found at about pH 3.2. Kukizaki (2009) measured the zeta potentials of SPG (Shirasu porous glass) membrane by electrophoretic measurements on the particles made by grinding the membrane with NaCl, Na_2SO_4 and $CaCl_2$ solutions of 1mM. Electrophoretic measurements showed that SPG membranes were negatively charged over the pH range of 3–10, which is a result of the dissociation of the hydroxyl groups such as silanol groups on the membrane surface in this pH range. The experimental results also showed that SPG membranes had a more negative zeta potential and lower i.e.p than ceramic membranes, due to the stronger acidity of the SPG membrane materials. Ricq et al. (1998) measured electrophoretic mobility and the streaming potential of UF and MF inorganic membranes having a filtering layer of zirconium oxide and a carbon support. It was found that isoelectric point (i.e.p.) determined by electrophoretic measurements on zirconia particles obtained by membrane scraping is different from the

i.e.p. obtained from pure zirconia powder and similar to those obtained from streaming potential measurement. The study established a correction factor F attached to the Smoluchowski equation by considering that the true zeta potential is the one that is obtained from electrophoresis measurements while the zeta potential obtained from streaming potential as an apparent zeta potential. Bellona and Drewes (2005) compared results of streaming potential and electrophoretic measurements of two commercial nanofiltration membranes at different pH values and water chemistries. It was found that streaming potential measurements give less negative results than electrophoresis. Wang and Ku (2006) found that Zeta potentials of TiO_2 membranes measured with TSP data were different from those of TiO_2 suspensions measured by electrophoresis, but the isoelectric point ($pH_{i.e.p}$) is almost same. Unlike electrophoresis, streaming potential is a non-destructive method which does not need to destroy the membrane and obtain new surface which can differ considerably from the membrane surface (Tra et al. 1998; Zhao et al. 2005; Narong & James 2006).

2.2.3 Electro-osmosis

In this elecrokinetic method, the electrolyte flow through the pores induced by electrical current applied across the membrane is measured (Huisman & Tra 1999; Tra et al. 1998; Zhao et al. 2005). For this reason many researchers have used a simple 'dipped cell' apparatus first introduced by Bowen and Clark (Bowen & Clark 1984; Szymczyk et al. 1998a; Szymczyk et al. 1998b; Nystrom et al. 1996; Mullet et al. 1997). The zeta potential can be calculated using the following equation (Zhao et al. 2005; Nystrom et al. 1996; Mullet et al. 1997):

$$J_V = \frac{I_C \varepsilon_r \varepsilon_o \zeta f}{\eta \lambda_P} \quad [2.12]$$

where J_v is the electro-osmotic flow rate, I_C the applied current and f is a function of κr. For large pores and high ionic strength, $\kappa r >> 1$ and f = 1 so Equation 2.12 is reduced to H-S equation. Szymczyk et al. (1998 a&b) compared the two electrokinetic methods of electro-osmosis and streaming potential for determination of the zeta potential of microfiltration ceramic membranes at different pH, ionic strengths and electrolytes. The authors found that

the zeta potential values from the electro-osmosis method are greater than that from the streaming potential method and the isoelectric points were very close. The results suggested this may be due to a different location of the shearing plane depending on the electrokinetic method used. Nystrom et al. (1996) also studied the electrical properties for a range of commercial membranes by electro-osmosis and streaming potential measurements under identical conditions. It was found that the apparent zeta potential determined from electro-osmosis were generally greater than those from streaming potential measurements with a greater difference at pH $\leq$ 4. In general the authors found that streaming potential measurements provide information about membrane zeta potential more simply and with less interference.

2.2.4 The electrolyte conductivity inside the pores

The electrolyte conductivity within pores can be more than the bulk conductivity due to overlapping phenomena and surface conductivity (Tra et al. 1998). Therefore, ionic conductivity measurements inside a pore can be used to characterize the electrochemical properties of membranes (Fievet et al. 2000). Electrical resistance measurements by using electrochemical impedance spectroscopy (EIS) allows the determination of the electrolyte conductivity inside pores (Mullet et al. 1997; Fievet et al. 2000; Sbaï et al. 2003). In fact, pore electrolyte conductivity represents both the mobility of ions which play an important role in transport properties across membranes and their concentrations which is a function of the surface potential (Sbaï et al. 2003). The electrolyte conductivity within pores (λ_{pore}) can be experimentally determined from electrical resistance measurements using the following equation (Fievet et al. 2000; Sbaï et al. 2003):

$$\lambda_{pore} = \frac{\lambda^{h} R_{m}^{h}}{R_{m}} \qquad [2.13]$$

where λ^{h} is the conductivity of the solution at high salt concentration (i.e. when the surface conduction effects can be neglected, which means that the conductivity in pores can be assumed to be equal to the conductivity of bulk solution), R_m^h is the resistance across the pores when the cell is filled with the high concentration solution and R_m is the resistance across the

pore when the cell is filled with the measurement solution. The term $\lambda^h R_m^h$ can be considered as the cell constant l/S where l is the length of pores. Surface potential (Ψ_o) then can be determined by using the space charge model (Fievet et al. 2000).

2.2.5 Membrane potential

The surface electrical properties of the pore of the walls can be characterized by membrane potential measurements. The membrane potential is the sum of two potentials: (i) Donnan potential caused by the partition of ions into the pores (ii) diffusion potential caused by the concentration gradient in the membrane (Ariza et al. 2001; Fievet et al. 2000). Membrane potential measurements are carried out by using the same cell used in diffusion experiments in which two solutions of the same electrolyte but at different concentration (C_1 and C_2) are separated by the membrane and the temperatures are kept constant, usually the ratio C_2/C_1 is maintained at a fixed value of 2, (Egueh et al. 2010; Szymczyk et al. 1998). The membrane potential is defined as the difference between the potential in the higher concentration solution and the potential in the solution of lower concentration and both potentials are measured by inserting two Ag/AgCl electrodes (connected to a voltmeter) directly into the bulk solutions (Ariza et al. 2001; Egueh et al. 2010; Szymczyk et al. 1998). In order to cancel the effect of the asymmetry potential, the potential difference can be measured by interchanging the electrodes in the two compartments and the average of the two values was taken (Ariza et al. 2001; Egueh et al. 2010). The membrane potential is related to the cell potential by the following relation (Egueh et al. 2010; Szymczyk, Fievet, Reggiani, et al. 1998):

$$E_m = E_{cell} - E_c \quad [2.14]$$

where E_c is the concentration potential and is given by

$$E_C = \frac{RT}{F} ln \frac{a_2}{a_1} \quad [2.15]$$

where R is the ideal gas constant, T the absolute temperature, F the Faraday constant, and a_1 and a_2 are the activities of Cl^- ions in bulk solutions 1 and 2, respectively. If KCl solution is used and with $a_1 > a_2$, the membrane potential can be calculated from the following equation:

$$E_m = \text{Ecell} - \frac{RT}{F} ln \frac{a_2}{a_1} \qquad [2.16]$$

Fievet et al. (2000) used streaming potential, membrane potential and electrolyte conductivity measurements with the space charge model to characterize the potential in the Outer Helmholtz Plane (Ψ_d) and then the accuracy and limitation of each method was estimated. The authors found that none of the three methods covers the whole range of pore sizes and potentials and the three methods together give the full picture. The authors found that the electrolyte conductivity method is the most efficient technique to study membranes with a pore radius smaller than 10 nm.

Ariza et al. (2001) used Tangential streaming potential, impedance spectroscopy, membrane potential and salt diffusion with an ultrafiltration polysulfone membrane in contact with NaCl solutions to study membrane charge. The following parameters were obtained (i) from electrokinetic results: membrane proper charge density, density of accessible sites and mean adsorption free energy (ii) from membrane potential values the obtained are: the fixed charge concentration in the bulk membrane and the cation transport number. Szymczyk et al. (1998) studied the charge of ceramic UF membranes in NaCl and $CaCl_2$ media by streaming potential and membrane potential measurements. The apparent transport numbers of cations in the membrane were obtained from cell potential measurements. Schaep and Vandecasteele (2001) characterized the membrane charge of four nanofiltration membranes by using titration, streaming potential and membrane potential. The ion-exchange capacity was determined by titration while measurements of the streaming potential provide a value for the charge density at the exterior membrane surface and finally membrane potential evaluates the total membrane charge density.

2.2.6 Electroviscous effect

This electroviscous is referred to as the phenomenon in which the viscosity of the solution is enhanced inside pores in the presence of the electrical double-layer which affects flow. This allows the comparison of the fluid behaviour in the presence and the absence of the double layer affect, i.e. high salt concentration (Sbaï et al. 2003). This can be done experimentally by measuring the water flux of the membrane at different salt concentrations and the variations in water flux can be related to zeta potential or surface charge density through electrokinetic flow theory (Huisman & Tra 1999). The advantages of this method are that there is no need to have special equipment to perform the measurement a part from an ordinary filtration unit. Another advantage is that surface conductivity does not affect the results (Tra et al. 1998), however, the membrane pore size should be known in order to calculate the zeta potential. Zeta potential is calculated using the Finite Element Electrolyte Specific Property (FEESP) model (Chiu & James 2007; Tra et al. 1998).

$$\frac{\mu_{app}}{\mu_0} = \left(1 - \frac{8\beta\left(\frac{e\,\zeta}{k_B T}\right)^2 (1-G)F}{(\kappa^{-1} r_p)^2}\right)^{-1} \qquad [2.17]$$

where μ_a is the apparent viscosity (the viscosity within the pores), μ_0 the bulk viscosity of the electrolyte solution, ζ is the zeta-potential of the capillary surface, κ^{-1} the inverse Debye constant, k_B Boltzmann constant, β dimensionless parameter describing the electrolyte properties, e electron charge, T temperture and r_p is the pore radius. G and F are dimensionless functions of the zeta potential and the pore radius that are calculated numerically. Both range smoothly from 0 to 1, as $\kappa a \rightarrow 0$ $F \rightarrow 0$ and $G \rightarrow 1$ and as $\kappa a \rightarrow \infty$ $F \rightarrow 1$ and $G \rightarrow 0$.

A pioneering study to investigate the possibility of measuring the zeta-potentials using the electroviscous effect has been performed by Tra et al. (1998) on porous membranes and the results compared with streaming potential. It was found that the electroviscous technique is a simple method to find accurate values of zeta-potential, especially for higher zeta-potentials.

However, streaming potential measurement is more suitable for the determination of the i.e.p. Huisman et al.(2000) measured the zeta potential of ultrafiltration membranes from measured electroviscous effects, salt retentions and streaming potential using three highly simplified models. It was found that all three methods give almost the same i.e.p values, but the absolute values of the zeta potentials were quite different and the results obtained from electroviscosity and salt retention measurements were smaller than those obtained from streaming potential measurements.

Sbaï et al. (2003) measured the streaming potential, electroviscous effect, pore conductivity and membrane potential for a ceramic ultrafiltration membrane at various KCl concentrations and the surface potentials from the experimental data have been calculated. It was found that surface potentials determined from the four experimental methods are in relatively good agreement although some differences occur at low ionic concentrations. The electroviscous effect was found to be negligible at low and high salt concentrations, but reaches maximum intermediate concentrations. Chiu and James (2007) investigated using the transversal streaming potential method for an asymmetric microfiltration membrane and the results obtained were compared to the electroviscous and electrophoresis. The zeta potentials obtained from each measurement show similar trends with increasing concentration and pH and i.e.p points obtained from streaming potentials, electroviscous and electrophoresis measurements were in agreement.

2.2.7 Titration

Titration is used to quantify negatively and positively charged groups on a membrane (ion exchange capacity, IEC) and charge density. In fact, direct titrations of membranes need to be developed and its quantitative information is little compared to electrokinetic techniques (Hurwitz et al. 2010). Schaep and Vandecasteele (2001) determined ion exchange capacity by immersing a membrane in a 0.1M CsCl solution where the cesium was adsorbed by the membrane surface. After that, the membrane was immersed in a 0.01M $MgCl_2$ solution where the magnesium ions exchange with cesium ions and the cesium ions are set free in the solution and measured. The number of cesium ions measured is equivalent to the number of negatively charged groups and the same procedure was used to determine the amount of positively charged groups on the membrane with NaF and Na_2SO_4. According to the author this method is more accurate than the acid–base titrations which demonstrate problems in determination of the equivalence point.

Afonso (2006) and Dina et al. (2001) determined ion exchange capacity of the top layer samples scrapped from the supports of membranes Desal G-10, Desal G-20, Celgard N30F and Celgard NF-PES-10 by acid–base titration. The value of the IEC was found in the range of the IEC of weak ion exchange membranes. Comparison of membrane charge density obtained from IEC and electrokinetic measurements showed that results from the titration are generally higher. The reason is because this technique evaluates the total amount of acidic groups, whereas the electrokinetic method only accounts for the ionised species at a given set of operating conditions. Mullet et al. (1997) measured electroosmotic rates of alumina based ceramic microfiltration membranes and surface charge densities from potentiometric titrations of a suspension obtained from ground up membrane. It was found that the surface charge density is higher than expected with respect to the low values of zeta-potentials. Chun and Park (2004) potentiometrically titrated amphoteric charge groups grafted to the pore surface of polyacrylonitrile based porous membranes having amphoteric charge groups to calculate the charge density from the end points of the titration curve. It was found that the values of the net charge density for four kinds of amphoteric charged membranes are nearly constant, which proved that the charged monomers are grafted onto the surfaces of these membranes to the same degree.

2.2.8 Contact angle

Most membranes are hydrophilic where the functional groups on their surfaces are hydrated and ionized in the aqueous solution at different degrees depending on the pH and ionic strength (Luo & Wan 2013b). In fact, studying membranes surface charge and hydrophobicity is essential for understanding water and solute transport through the membranes as well as fouling of membrane surfaces (Hurwitz et al. 2010). As an example, membrane surface charge functionality influences the membranes pore size and Donnan effect which govern water and charged solute transport through RO/NF membranes. To illustrate, the pore size of the membrane is reduced at high pH values because the negatively charged groups on the membrane pore surface adopt an extended conformation due to electrostatic repulsion between them (Teixeira et al. 2005). This expanded conformation reduces the pore size of the membrane and causes a decrease in flux and a retention increase.

There are many researches using contact angle to study membrane charge and the interaction between the membrane and membrane surface. Hurwitz et al. (2010) employed contact angle measurements to study the effect of solution chemistry on surface charge, zeta potential, wettability, and hydrophilicity of a commercial polyamide RO membrane. Surface charge density, ionization fraction, and apparent dissociation constants were determined from

contact angle titrations and converted to surface zeta potentials via the Grahame equation. Zeta potentials calculated from contact angle and streaming potential show the same trend, but are quantitatively different. It was also found that the polyamide membrane used in this study became more electron donor functionalized, more wetting, and less hydrophobic with increasing pH, salinity, and divalent cation content in the electrolyte. Brant and Childress (Brant & Childress 2004; Brant & Childress 2002a; Brant & Childress 2002b) used contact angle to characterize colloidal particle interactions with RO/NF membranes by measuring the surface energetics of several membranes and colloids using the Lifshitz–van der Waals model. A theoretical prediction of interaction energies for several membrane–colloid pairs was made using classical DLVO theory and an extended DLVO (XDLVO) approach. The predicted interaction energies were then compared with atomic force microscopy (AFM) force measurements. The results showed that the measured force curves by AFM agree with the interaction sequence predicted by the XDLVO approach for strongly hydrophilic membranes.

Rice et al. (2011) used three techniques to characterise three membranes namely contact angles, ATR-FTIR and streaming potential. The results showed that the membrane with the lowest change in zeta potential with increasing pH has the highest contact angle (lowest hydrophilic) and thus fewest dissociated functional groups, and also has the lowest water permeability, indicative of greater cross-linking. Wang et al. (2006) and Möckel et al. (1998) found that the more functional groups on the surface of the membranes the longer swelling layer which leads to a shift of shear plane toward the bulk solution and lower zeta potential plateau values were obtained. Therefore, zeta potential data can give valuable hints about the chemical nature and the hydrophilicity of membrane surfaces.

Mänttäri et al. (2006) studied the effect of changing pH on membrane structure, permeability and retention. The results showed that the effect of changing pH from 4 to 7 on zeta potential value and ions retention, increase with increasing of the degree of hydrophobicity of the membrane. In addition, flux is affected by changing pH because of some membranes become significantly more open at high pH. The changes in permeabilities and retentions were found to be reversible in the pH range studied, and in some cases, the changes were reversed very slowly. NTR 7450 which is polyethersulfone was the most hydrophobic membrane in the study while NF200 and NF270 were the most hydrophilic membranes with 30^{o} contact angle which is a result of the dissociation of carboxylic and amine groups.

2.2.9 AFM

According to Brant et al. (2006) AFM can be used to overcome some of SP measurements disadvantages such as concentration limitation of SP either at very high or low ionic strengths, differences in instrument design and the lack of a calibration standard for streaming potential analysers and the problem of membrane surfaces heterogeneity (both physically and chemically) and the charge distribution. One of the drawbacks of the technique is that it is sensitive to surface roughness, as the measured charge distribution increased with increasing surface roughness. Experimentally the interfacial interaction force between a probe and a membrane surface is measured as a function of separation distance between two surfaces (Brant et al. 2006; Bowen et al. 2002). Classical DLVO theory is used to evaluate colloid–surface chemical interactions (Brant et al. 2006). Bowen et al. (2002) developed a model for the interaction between a colloid probe and a commercial NF membrane surface using membrane zeta potential as a fitting parameter. At low ionic strength (10^{-3} M), AFM surface potential measurements were in good agreement with the zeta potential calculated. However, at higher concentration (10^{-1}M) the agreement between the zeta potential derived from the AFM data and that determined from streaming potential was poor which referred to the surface roughness. Brant et al. (2006) utilized the XDLVO approach to estimate quantitatively the zeta potential from AFM force measurements for mica and polyamide NF membranes (smooth surface). These data were then compared to the zeta potential results found with TSP data. The AFM experiments and XDLVO simulations were all performed at pH 10 to insure maximum repulsive interaction between the colloid probe and the membrane surfaces as the membrane surfaces are fully dissociated. It was found that the mean zeta potential values calculated from the AFM force curves closely agreed with those determined from streaming potential measurements.

2.2.10 Other techniques

The charge of the membrane can be partially explained by identifying the surface functional groups. Rice et al. (2011) compared the ATR-FTIR spectra for three polyamide on a polysulfone / polyester support membranes (Desal-5, SR3 and SR4) which were mostly identical because the technique detects the polysulfone support rather than the very thin polyamide layer (active layer). However, the Desal-5 membrane did not have a peak at 1740 cm^{-1}, as seen for the SR3 and SR4 membranes which might suggest that the SR3 and SR4 membranes have a higher carboxyl component than the Desal-5 membrane.

Salg et al. (2013) analysed the PES membrane surface using FTIR–ATR spectroscopy to detect the structural chemical changes originated by the phosphate ion adsorption as a function of ionic strength during the measurements of streaming potential. One characteristic peak was inspected as the evidence of the adsorption of the phosphate anion on the membrane surface, which is observed at 945.62 cm^{-1}. The variation in the intensity of the phosphate peak with the ionic strength was in agreement with the electrical double layer theory, that is, the lowest intensity of the phosphate peak was observed at 0.1 M Na_2HPO_4 where the absolute zeta potential values were also the lowest due to compression of the electrical double layer. It was also concluded that the increase in ionic strength decreased the intensity of the phosphate peak due to the decrease in the extent of specific phosphate adsorption. The highest intensity of phosphate peak was observed at 0.01 M Na_2HPO_4. Huisman and Tra (1999) developed an equation to link the absolute value of the zeta potential to salt retention of porous membranes. The equation is only valid for low zeta potentials and for symmetric electrolytes, i.e. for KCl solutions at 25°C and for $\kappa r_p > 3$.

2.3 Membrane charge density

Three kinds of surface charge densities can be distinguished: the fixed charges at the membrane surface (σ_0), the charges of the Stern-layer (σ_s), and the charges within the diffusion layer of the electric double layer (σ_d). The sum of these three charges is equal to zero (Ariza et al. 2001; Peeters et al. 1999):

$$\sigma_0 + \sigma_s + \sigma_d = 0 \qquad [2.18]$$

$$\sigma_d = -(\sigma_0 + \sigma_s) \qquad [2.19]$$

With increasing concentration, the absolute value of membrane charge density increased while the absolute value of zeta potential decreased (Ding et al. 2006; Peeters et al. 1999). Peeters et al. (1999) found that the actual charge density (σ_0) is very small compared to the adsorption charge density and the anions are the source of this adsorption. Many researchers (Ariza et al. 2001; Peeters et al. 1999; Artuğ et al. 2007) found that there is a linear relation between the membrane charge density and solution concentration (or anion concentration) which can be expressed by Freundlich isotherm

$$|\sigma| = aC_i^b \qquad [2.20]$$

where C_i is the solution concentration, a and b is the characteristic adsorption parameters obtain from the straight line of a log – log plot as (Welfoot 2001).

$$log|\sigma| = loga + b\, logC_f \qquad [2.21]$$

Molina et al. (1999) found that values of the surface charge density for the studied membranes depend on concentration and described by Langmuir's model for the big pore diameters and Freundlich's model for the smallest pore diameters. The membrane surface charge densities were calculated by some authors by using the Gouy-Chapman equation (Ding et al. 2006; Dina et al. 2001; Ariza & Benavente 2001), developed mathematical models (Tay et al. 2002) and by using a modified Donnan-Steric-Pore model (Mohammad & Takriff 2003; Hussain et al. 2008; Bowen & Welfoot 2002). Table 2.2 provide examples of the Gouy-Chapman equations used to calculate the membrane surface charge from zeta potential values.

The Donnan –Steric Pore Model (DSPM) was developed by Bowen et al. (1997) and used later in the prediction of NF performance in mixture of NaCl and dye (Bowen & Mohammad 1998b). The model is based on the extended Nernst –Planck equation with the including the effect of charge (Donnan) and steric factors to describe the transport of ions through the membrane. The three parameters needed for the model are effective pore radius (r_p), effective ratio of membrane thickness to porosity ($\Delta x/A_k$) and the effective charge density (X_d). Another development to the model by Bowen and Welfoot (2002) was to include the effect of dielectric exclusion and increasing the solution viscosity in the pore.

Table 2.2: Examples of Gouy-Chapman equations used to calculate membrane surface charge from zeta potential values.

Membrane charge density type	Equation	References
Electrokinetic charge density	$\left(\frac{2RTe\,\kappa}{z_i F}\right)\sinh\left(\frac{F\zeta}{2RT}\right)$	(Ariza et al. 2001)
Electrokinetic charge density	$\left(\frac{2\varepsilon\,\kappa\,k_B T}{Z_i e}\right)\sinh\left(\frac{z_i e\zeta}{2k_B T}\right)$	(Ariza & Benavente 2001)
Charge density in the diffuse layer	$\left(2\mathcal{E}_0\mathcal{E}_r k_B T\sum_i c_i N_A\left(exp\left(-\frac{z_i e\zeta}{k_B T}\right)-1\right)\right)^{0.5}$	(Hagmeyer & Gimbel 1999; Morão et al. 2006; Dina et al. 2001)
Electrokinetic charge Density	$\sqrt{8k_B T\varepsilon C_i}\,sinh\left(\frac{z_i e\zeta}{2k_B T}\right)$	(Han et al. 2011)
Electrokinetic charge Density	$\sigma^d=\frac{\varepsilon\,\zeta}{\kappa}$	(Schaep&Vandecasteele 2001)
Electrokinetic charge Density	$(sin\zeta)\sqrt{2C_i\varepsilon RT}\left(v_+exp\left(-\frac{z_+F\zeta}{RT}\right)+v_-exp\left(-\frac{z_-F\zeta}{RT}\right)-v_+-v_-\right)^{0.5}$	(Ding et al. 2006)

Equations terms definition: κ is the Debye length, F is faraday constant, R ideal gas constant, k_B is Boltzmann constant, e is the electron charge, z_i is the ion valence, T the absolute temperature , c_i is the concentration of ion i in the salt solution , N_A is the Avogadro constant, ε is the dielectric constant ($\varepsilon = \varepsilon_0\varepsilon_r$; ε_0 is the vacuum permittivity and ε_r is the relative dielectric constant of electrolyte), C_i is the bulk concentration , v_+ , v_- are stoichiometric number of ,cation or anion.

Ding et al. (2006) measured the zeta potential and calculated the membrane surface charge for polyethylene microfiltration membranes with five single salts and found the following sequence with absolute zeta potential: NaCl ≥ KCl > Na_2SO_4 > $MgSO_4$ > $MgCl_2$ while the membrane surface charge was: Na_2SO_4 > NaCl ≥ KCl > $MgSO_4$ > $MgCl_2$. Dina et al. (2001) provided a Freundlich isotherm relationship between the effective surface charge calculated from Gouy-Chapman equation and solution concentration. The sequence of zeta potential value found is: NaCl > Na_2SO_4 >$MgSO_4$ ≥ $MgCl_2$ while the membrane surface charge was: Na_2SO_4 > NaCl > $MgSO_4$ ≥ $MgCl_2$. Morão et al. (2006) studied the electrokinetic properties

of NF membranes in contact with KCl, K_2SO_4, potassium clavulanate and $MgSO_4$. The membrane surface charge was found follow the order: KCl, K_2SO_4 > KCA > $MgSO_4$ which shows that divalent cations lead to lower surface charge densities. The results also show that KCl rejection decreases with increasing feed concentration before it levelled off while the absolute value of membrane surface charge was shown to continually increase over the concentration range. The author explained the result was that of shielding effect of functional groups on the membrane surface as well as adsorbed anions by cations from the bulk solution facilitating the ionic transport. Bandini et al. (2005) used the Donnan Steric Pore Model and Dielectric Exclusion (DSPM&DE) to calculate membrane charge values for NaCl solution as a function of pH and with electrolyte concentration. Langmuir adsorption behaviour was observed at constant pH values and the i.e.p was found at a pH value corresponding to the pH values at which NaCl rejections are at their minimum values. Hussain et al. (2008) used the DSPM model to calculate charge density with three different radii, viz., Stokes–Einstein, Born and Pauling and each radius predicted different charge densities. Correlations were developed relating the charge density with pH. Mohammad and Takriff (2003) studied the effect of varying X_d (effective charge density) on the rejection of mixtures of NaCl: Na_2SO_4. Since the pore size is the same the pure water flux is independent on the membrane charge, however the ions rejection increases which leads to a higher osmotic pressure that causes the permeate flux to decrease.

2.4 Thesis frame works

As discussed in the literature review the studies that dealt with membrane charge used a limited number of salts, concentrations and membranes. Some of these studies used membranes that do not exist currently in the market. Furthermore, most studies investigated the single salt system and quantitative correlation between membrane charge and membrane separation has not been achieved. This thesis is a comprehensive study of the effect of membrane charge on the separation of ionic species where 6 ions make up 96.66% of the sea water composition and mixtures of them are used. In addition, the correlation between zeta potential and membrane separation has been achieved.

This thesis attempts to improve understanding of the role of membrane charge, particularly for nanofiltration, in separation of ionic species. In order to do that tangential streaming potential (TSP) which is the most common technique has been selected to study the membranes charge in this study where zeta potential obtained. A variety of solution

chemistries which include changing in chemical composition, concentration and the pH have been studied extensively. First the interaction between the membrane charge and solutions containing single salts has been examined. These single salts solutions are NaCl, KCl, Na_2SO_4, $CaCl_2$, $MgSO_4$ and $MgCl_2$ at three different concentrations 10^{-3}M, 10^{-2}M and 0.025M and between pH 3.5 to 10. Furthermore, four commercially well-known NF membranes are used in this thesis namely the Desal DK, NF270, NF99HF and NTR7450. The aim of this experimental study was to investigate the effect of electrolyte type and concentration at different pH values on the membranes charge which affects the membranes separation performance in turn. The obtained zeta potential values were used to explain the specific adsorption of ions to the membrane surface and to determine membrane isoelectric points (i.e.p) by studying the shape of the pH-zeta curves. Reproducibility, equilibration time, surface conductivity has been also studied in order to optimize the zeta potential measurement. The complexity of the solutions chemistry has been enhanced by using binary salt solutions with single salts data to explain the interaction between the membrane charge and binary salt systems. Different combinations of ions mixtures have been tested namely: Na-K, Na-Ca, Na-Mg, Ca-Mg and Cl-SO_4. The next stage after membrane charge characterization with different feed water chemistries was to study the performance (rejection and flux) of the same membranes with same solutions chemistry used in the first stage. The effect of the interaction between the membranes charge and mixtures of ions namely: Na, K, Ca, Mg, Cl, SO_4 and proton on flux and rejection have been studied and the results of both stages of the research were used to gain insight about the role of charge in membrane separation mechanisms. Finally; the prediction of membrane charge effects has been achieved by aiding of DSPM-DE model which allows calculation of the membrane charge density and establishes many correlations such as charge density-pH and membrane charge density - zeta potential.

3.0 Materials, Methods and Supporting Experiments

This chapter covers the materials and methods used in the experimental work. Zeta potential measurements (electrokinetic study) and filtration experiments have been carried out for four membranes with six different electrolytes as well as mixtures of these salts in order to comprehensively study the membrane–solution interactions. The data created from the filtration experiments have been used as inputs for a modified DSPM model in order to calculate membrane charge density (X_d). Tangential streaming potential (TSP) has been chosen to investigate the effect of changing the solution chemistry on zeta potential due to its accuracy and popularity as compared to other surface charge techniques. The electrokinetic analyser which has been used in the electrokinetic study as well as the spiral wound NF pilot plant employed to perform the filtration experiments will be described in detail. Furthermore, details will be provided of the experimental procedures used for the zeta potential measurements, filtration of salts and membrane characterization experiments, namely mass transfer study, contact angle, deionized water flux, and NaCl rejection at different pressures. The analysis methods used to determine ion concentration, solution conductivity and pH as well as contact angle measurements will be explained in detail in this chapter. Finally, the relative theory and supporting experiments will be presented to investigate the mass transfer characteristics and the experimental characterization of the nanofiltration membrane used throughout the study.

3.1 Electrokinetic study

In order to characterize membrane charge, zeta potential measurements in a single and mixtures of salts were performed. In this section, the membranes, the electrokinetic analyser and procedures used in the measurement will be described.

3.1.1 Membranes and experimental equipment

3.1.1.1 Membranes

Zeta potential measurements were performed for four commercial NF membranes, namely Desal DK, NF99HF, NF 270 and NTR7450. All the membranes' skin layer is made of polyamide except NTR7450, which is a polyether polyethersulphone. The specifications for each membrane are provided in Table 3.1. Each membrane was obtained in flat sheet format from the suppliers. NF99HF and NTR7450 were kindly donated by Alfa Laval Ltd (Surrey,

Table 3.1: Specifications of membranes.

	NTR7450	NF270	Desal DK
Manufacture	Nitto Denko	Filmtec-Dow	Osmonics-Desal
Membrane material	Sulfonated polyethersulphone (Ikeda et al. 1988)*	Polyamide on polysulphone (Luo & Wan 2013a)	Polyamide on a polysulphone layer (Mazzoni et al. 2007)
MWCO (Da)	600-800 (Schaep et al. 2001), 310 (Boussu et al. 2005)	150-200 (Luo & Wan 2013a), 120 (Merdaw et al. 2010)	150-300 (GE 2014), 225 (Bowen & Mohammad 1998a), 250 (Ben Amar et al. 2009)
Water permeability @ 25°C (L/m^2h bar)	13 (Mänttäri et al. 2006), 6.3 (Bargeman et al. 2014)	27.45 (Hilal et al. 2005), 17 (Artug 2007), 15 (Artug 2007), 12 (Mänttäri et al. 2006), 11.3±0.3 (Luo & Wan 2013a), 15 (Merdaw et al. 2010), 13.5 (Bargeman et al. 2014), 17.6 (Artuğ et al. 2007)	8,95 (Ben Amar et al. 2009), 4.788 (Chakkrit 2010), 5.4 (Religa et al. 2011)
θ (°)	69.6 ±5.9 (Boussu et al. 2005), 58 (Mänttäri et al. 2006)	30 (Luo & Wan 2013a; Mänttäri et al. 2006), <10 (Artug 2007), 51.4 (Norberg et al. 2007)	28.1± 4.8 (Petriniæ et al. 2007), 58.3 (Norberg et al. 2007)
pH	2-11 (Somicon 2014)	2-11 (DOW 2012)	1-11 (Ben Amar et al. 2009)
R_P (nm)	1.4 (Bowen & Mohammad 1998a), 0.62 (Bargeman et al. 2014), 0.81(Sabir et al. 1998)	0.71± 0.14 (Hilal et al. 2005), 0.43 (Luo & Wan 2013a), 0.5 (Argelaguet 2011)	0.58 nm at 25°C (35-2) (Ben Amar et al. 2009), 0.5 (Bowen & Mohammad 1998a), 0.45 (Bowen and Welfoot 2002)
Pressure (bar) max	40 (Somicon 2014)	41 (DOW 2012)	40 (Religa et al. 2011)
Temperature (°C) max	60 (Somicon 2014)	45 (DOW 2012)	90°C (Ben Amar et al. 2009)
Water flux (m^3/m^2 d), (L/ m^2min)	1.53 (Ikeda et al. 1988)*	150L/m^2h at 10bar, 20°C (Merdaw et al. 2010)	0.8381 at Δ P = 0.69 (Bowen & Mohammad 1998a)
NaCl rejection %	51% (Ikeda et al. 1988)*	35% at 5000 ppm, 25°C and 10 bars (Hilal et al. 2005)	50% at 25°C; 1g/L, 0.7MPa (Artug 2007)
Na_2SO_4 rejection %	92 (Ikeda et al. 1988)*	98.9% at 5000 ppm, 25°C and 10 bar 5000 (Al-Zoubi et al. 2007)	98.8% 10^{-1}M Na_2SO_4 at 9 bar, 30°C (Ben Amar et al. 2009)
$MgCl_2/CaCl_2$ rejection %	13 $MgCl_2$ (Ikeda et al. 1988)*	40-60 $CaCl_2$ at 500 ppm, 25°C and 4.8 bars (Artuğ et al. 2007)	82% $CaCl_2$ at 0.02M , 25°C and 10 bars (Mazzoni & Bandini 2006)
$MgSO_4$ rejection %	32 (Ikeda et al. 1988)*	> 97.0 at 25°C; 2g/L, 0.48MPa (Artug 2007)	98% at 1000 ppm $MgSO_4$ at 25°C and 6.9 bars (Mazzoni et al. 2007)

*Study condition: 0.5% (0.085M), 25°C, 1 MPa (10 bar).

UK, and Brussels, Belgium) and Somicon AG (Switzerland), respectively, while NF270 and Desal DK were bought from Sterlitech Corporation (USA). Membrane samples cut for measurement were soaked in deionized water for 24 hours to remove excess preservation chemicals from the surface.

3.1.1.2 Electrokinetic analyser (EKA)

The zeta potential measurements were performed using the Anton Paar Electro Kinetic Analyser (Anton Paar GmbH-Austria) as shown in Figure 3.1. The solution to be measured is placed in the external electrolyte reservoir where conductivity, temperature and pH electrode are measured (Figure 3.1B). The machine is also equipped with internal sensors for conductivity and temperature measurements. The solution is forced to flow through the measuring cell by a pump and a differential pressure sensor measures the pressure drop. The streaming potential was measured at differential pressure increments from 20 mbar to 500 mbar. Furthermore, the measurement is repeated 10 times in both directions of flow and average value calculated. The voltage is measured by two reversible Ag/AgCl electrodes inserted into the electrode connectors at each side of the cell (Figure 3.2 B). In the measuring cell, a sandwich of two membrane pieces facing each other and Teflon spacers are placed between the two cell halves and clamped using a clamping frame (Figures 3.2 C and 3.2D).

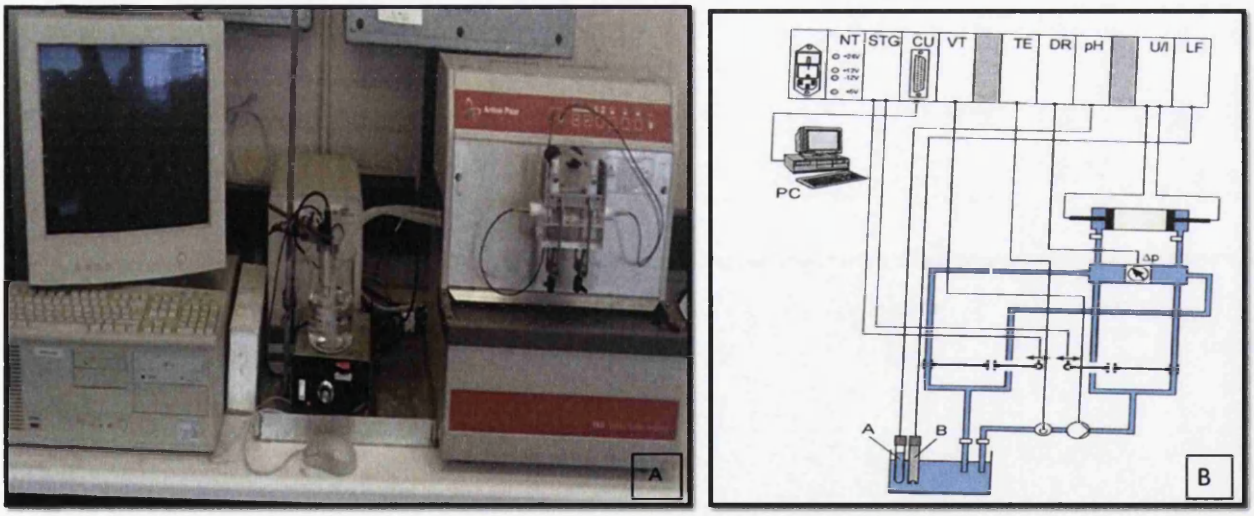

Figure 3.1: (A) The electrokinetic analyser (EKA), and (B) block diagram for the EKA, where A is the pH electrode and B, the conductivity electrode.

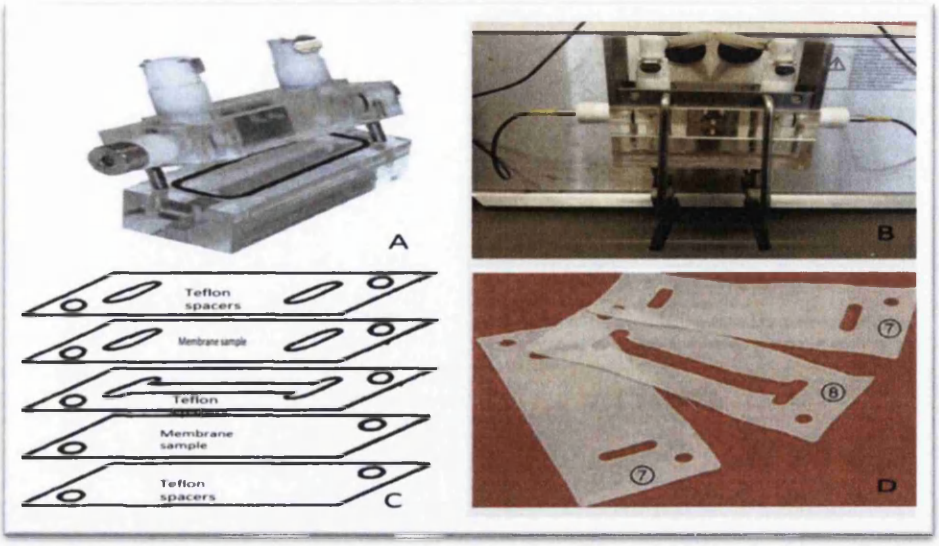

Figure 3.2: (A) Rectangular measuring cell, (B) rectangular measuring cell in the EKA, (C) the sequence of membrane samples and Teflon spacers, and (D) photos of Teflon spacers.

The size of the electrokinetic channel is 74 mm × 10 mm (Ariza & Benavente 2001). The computer is controlling the values, the pump and data recording. The zeta potential is calculated by applying the Fairbrother–Mastin method.

3.1.2 Measurement methods

The electrokinetic study for the single salt systems includes calculation of apparent zeta potential value and true zeta, which was obtained by cancelling out the surface conductivity effect. Reproducibility of the measurement as well as the time required to achieve the equilibrium (equilibration time) have been also studied. Two reproducibility experiments have been performed with KCl solution at 10^{-3}, 10^{-2} and 0.025M concentrations by comparing the zeta potential values of two membrane samples of NF99HF from different batches as well as between virgin and used membrane samples of NF270. The equilibration time study for NF270 and NF99HF took place by measuring zeta potential after the electrolyte was circulated in the EKA for 30 minutes; the measurement was repeated 24 hours later after the membrane was stored overnight in the measuring cell.

The zeta potential measurements for mixtures were performed by mixing two salts in different combinations and measuring the apparent zeta potential value of the solutions.

3.1.2.1 Determination of apparent and true zeta potential

Before the zeta potential measurements can be taken, the membrane samples must be cut and soaked in deionized water for 24 hours to remove excess preservation chemicals from the

surface. Zeta potential can be calculated by streaming potential data using the Helmholtz–Smoluchowski Equation 2.1 (Wilbert et al. 1999; Ariza et al. 2001; Tra et al. 1998).

The zeta potential calculated with Equation 2.1 is called apparent zeta potential, where no surface conductivity, which mainly affects at low ion concentrations, is taken into account. Therefore, Equation 2.1 must be modified to take this fact into account and the zeta potential that will obtained is called true zeta potential. This can be done by replacing the electrolyte solution in the EKA measuring cell with 0.1M KCl to measure cell resistance and conductivity. In this case, the surface conductivity is neglected due to the high electrical conductivity of 0.1M KCl. After that, the corrected zeta potential can be calculated according to the approach by Fairbrother and Mastin (F–M) (Equation 2.7) as discussed in Section 2.2.1.3.1 (Ricq et al. 1997; Ariza & Benavente 2001).

This approximation is called the Fairbrother–Mastin method, in which it is assumed that the electrolyte solution carries most of the current and that the streaming potential is not dependent on the geometry of the capillary or the streaming potential channel (Wilbert et al. 1999; Peeters et al. 1999).

3.1.2.2 Zeta potential measurements procedure for single salts

Six different electrolytes were used in the measurements: NaCl, KCl, Na_2SO_4, $CaCl_2$, $MgSO_4$ and $MgCl_2$ at three different concentrations, 10^{-3}M, 10^{-2}M and 0.025M, pH 3.5 to 10. H_2SO_4/NaOH were used for pH adjustment of sulphate salts, while HCl/NaOH and HCl/KOH were used for calcium/magnesium chloride and potassium chloride salts, respectively. All chemicals used in the experiments, including the pH adjustment chemicals, were analytical grade (Fisher Scientific UK) and deionized water with less than 2 μS/cm conductivity was used for preparing the solutions. The EKA pH and conductivity probes were calibrated daily by using pH4, 7 and 10 buffer solutions and with a 1413 μS/cm conductivity standard solution (Fisher Scientific UK). The measurement started with rinsing the measuring cell with the test solution to displace the deionized water in the system. After that, fresh test solution was used and the system was flushed to make sure that the solution inside the cell was well mixed and the concentration was as desired. These two steps take around 30 minutes, which allowed measuring the first zeta potential value at pH around 6. After finishing the first measurement, the pH of the test solution was adjusted with acid and the solution was recirculated for around 10 minutes before the second measurement was taken. When all measurements in the acidic region were completed, the cell was rinsed with fresh solution and rinsed again with fresh solution. After that, the pH was adjusted with base and the same procedure was followed until the last measurement (at pH 10) was taken. At the end

of all the measurements, the system was flushed again with deionized water until the conductivity reached less than 2 μS/cm, when the machine was ready for further measurements.

3.1.2.3 Zeta potential measurements procedure for mixtures

Zeta potential measurements were also performed for mixtures of two salts that have one ion in common; the two remaining ions are to be compared, which enables studying the effect of cations and anions on the membranes' charge. The ion combinations that were tested were: Na-K, Na-Ca, Na-Mg, Ca-Mg and Cl-SO_4. The total concentration of ions to be compared was 0.01M and the percentage of each ion in the solution was increased gradually from 0 to 100%. To illustrate, to compare Na-K, five solutions were tested as follows: 0%Na-100%K, 25%Na-75%K, 50%Na-50%K, 75%Na-25%K and 100%Na-0% K. The chemical composition of all the solutions to be compared is provided in Table 3.2.

Table 3.2: Chemistry of the solutions used in the mixtures in electrokinetic and filtration studies.

Ions to be compared	Solutions to be compared		Ion concentration mol/m3		
			Na	**K**	**Cl**
Na-K	1	0% Na	0	10	10
	2	25% Na	2.5	7.5	10
	3	50% Na	5	5	10
	4	75% Na	7.5	2.5	10
	5	100% Na	10	0	10
Na-Ca & Na-Mg			**Na**	**Ca/Mg**	Cl
	1	0% Na	0	10	20
	2	25% Na	2.5	7.5	17.5
	3	50% Na	5	5	15
	4	75% Na	7.5	2.5	12.5
	5	100% Na	10	0	10
Cl-SO_4			**Cl**	**SO_4**	**Na**
	1	0% Cl	0	10	20
	2	25% Cl	2.5	7.5	17.5
	3	50% Cl	5	5	15
	4	75% Cl	7.5	2.5	12.5
	5	100% Cl	10	0	10
Ca-Mg			**Ca**	**Mg**	**Cl**
	1	0% Ca	0	10	20
	2	25% Ca	2.5	7.5	20
	3	50% Ca	5	5	20
	4	75% Ca	7.5	2.5	20
	5	100% Ca	10	0	20

H_2SO_4 /NaOH were used for the pH adjustment of the sulphate salts, while HCl/NaOH and HCl/KOH were used for calcium/magnesium chloride and potassium chloride salts, respectively. At first, the natural pH of the supply water, then the pH was decreased stepwise using acids, and after the lowest pH (approximately 3.5), new solution was used for doing the measurements at the alkaline level. No surface conductivity corrections were implemented here as apparent zeta potential value is almost equal true one at this concentration (0.01M), as will be discussed later in the Results and Discussion chapter.

3.2 Filtration experiments

3.2.1 Membranes and experimental equipment

3.2.1.1 Membranes

Filtration experiments were carried out with 2.5-inch spiral wound membrane modules (Figure 3.3) purchased separately: Desal DK (GE Water & Process Technologies, UK), NF270 (Desal Supplies, Lancashire, UK) and NTR7450 (Somicon AG-Switzerland) membranes were used in these experiments. The specifications for each membrane are provided in Table 3.1 and the surface areas of the membranes were 1.6m^2, 2.6m^2 and 1.4m^2 for Desal DK, NF270 and NTR7450, respectively.

Figure 3.3: 2.5-inch spiral wound membrane modules.

3.2.1.2 NF pilot plant

A spiral wound NF membrane module enables studying a large membrane area and using large volumes of solution in order to increase accuracy and mimic industrial separations. Memtech UK Ltd supplied the NF pilot plant used in this study in which the piping,

framework and ancillary were made from 316 stainless steel and the fittings were either welded or clamp-connected with elastomer seals. The configuration of the apparatus is presented pictorially and schematically in Figure 3.4 and 3.5, respectively. The plant could be operated from an ordinary 240V, 50Hz main supply, but in order to operate the two pumps, a three-phase supply was required. The advantage of using two pumps is that it allows independent control of applied pressure and cross-flow velocity, which facilitates studies where one of these two parameters should be fixed, such as mass transfer study. For a single pump, pressure and flow are interrelated, which means that independent control of inlet feed pressure is not possible. P1 is a Wanner Hydra-Cell diaphragm pump capable of raising the feed pressure up to 60 bars at a pressure-dependent supply of up to 0.3 $m^3 h^{-1}$. Feed pressure is controlled through speed control of the motor using the inverter. P2 is a Fristam centrifugal pump that can generate flows of up to 2.5 m^3h^{-1}. The pump is designed to withstand inlet pressures of up to 60 bars and is also speed controlled via an inverter. Fine pressure adjustments are undertaken by adjustment of the needle valve, V3. The mode of operation used in the experiments was the total recirculation mode, i.e. both the concentrate and the permeate streams were recirculated into the feed tank (50L volume) so that the feed concentration was kept constant if salt was used, which was checked by measuring conductivity and by analysis of ions. In this mode, valve V2 is kept open, P2 provides a high cross-flow velocity, while P1 works as an injector pump supply for new high pressure feed from the tank into the loop. Since the flow into the loop is greater than the permeate flow rate, some material must flow through the needle valve (V3) back into the feed tank in order to satisfy a material balance and prevent accumulation within the recirculation loop.

Volumetric flows were measured on both the retentate and permeate sides of the membrane using Endress and Hauser Promag 33F flow meters, shown as FT2 and FT1, respectively. The flow meters operated on the principle of a potential being induced between a pair of electrodes as the conductive medium flows through the magnetic field. The induced potential was proportional to the flow velocity (which is converted to a volumetric flow). The detection limit of the flow meters reported by the manufacturers is 5 $\mu S\ cm^{-1}$, therefore the pure water flux measurements were measured manually using a volumetric flask and a stopwatch.

Figure 3.4: Photo of pilot-scale nanofiltration plant.

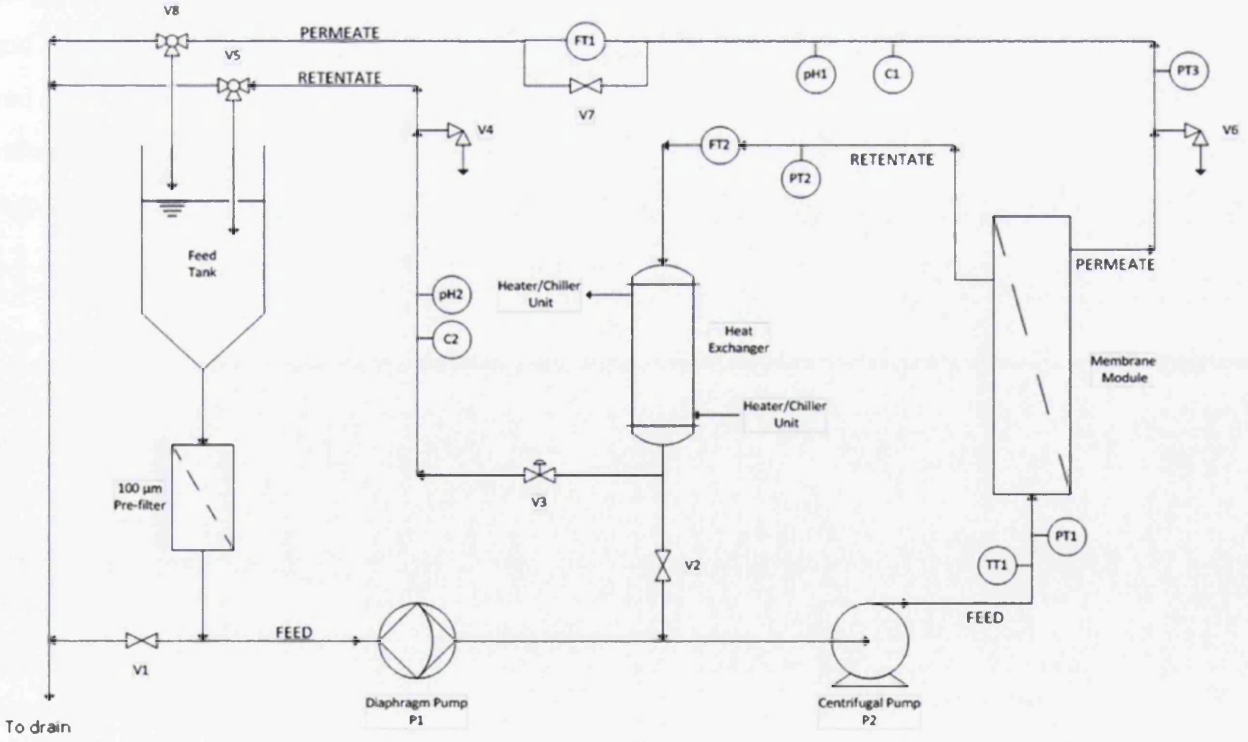

Figure 3.5: P&ID of pilot-scale nanofiltration system.

Operating pressures were measured at three points in the system, namely the module inlet (feed pressure) and the retentate and permeate lines, thus allowing the TMP to be calculated. In each case, Wika Instruments stainless steel, diaphragm-type transmitters were used and the signals fed to panel mounted displays, with the precision of the instruments being ± 0.1 bar.

Membrane flux rates are a function of temperature, therefore temperature control is vital in research experiments. The system temperature was monitored using a Thermo Data Components temperature sensor on the feed line, labelled TT1. The signal was sent to the display panel and regulated by connecting the heat exchanger to a heater chiller unit. The displayed reading was accurate to within ± 0.2°C.

Conductivity measurements are important to calculate salts rejection, to confirm that the old solution is totally replaced by the new solution and as an indicator that the pilot plant has been flushed with deionized water. Conductivity measurements were carried out on both the retentate and permeate sides of the membrane using Endress and Hauser CLS21 double electrode probes, which measure conductivity ranging from 5μS cm^{-1} to 300mS cm^{-1}. The conductivity probes were equipped with automatic temperature compensation in order to correct the measured value to the equivalent value at 25°C. The measured signal was fed to a control panel where the reading was displayed. pH is also important because the membranes' surface charge is affected by change in pH. Therefore, pH was measured in both the permeate and retentate sides. Endress and Hauser high impedance combination electrodes were used and the effect of temperature was taken into account, so the result was equivalent to the pH value at 25°C. The measured signal was fed to the control panel and displayed with a resolution of 0.01 units.

3.2.2 Experiment procedures

The membranes that were used in these experiments were new, so membrane conditioning was essential prior to any experimentation. The conditioning step was followed by the mass transfer study to determine the proper cross-flow velocity at which concentration polarization was minimum, therefore the highest concentration (0.025M NaCl) used in salts filtration experiments were chosen for this study. After that, the membranes were characterized by measuring deionized water flux and NaCl rejection and flux at different applied pressures. Finally, the filtration experiments were finished with the filtration of single and mixture solutions having the same chemistry as zeta potential measurement solutions.

The experiments were carried out in total recirculation mode, i.e. both the concentrate and the permeate streams were recirculated into the feed tank (50L volume) and at 20°C. Salt

rejection was calculated from the conductivity measurements of products and feed samples, while flux was determined from product water flow (see Section 3.2.1.2). Conductivity and pH measurements were carried out by taking samples from the NF pilot plant and measuring with bench top conductivity and pH meters. In fact, the NF pilot plant conductivity and pH probes were used as a guide only. Individual ions rejection was carried out for some of the filtration experiments which needed to analyse these ions. The procedures of conductivity and pH measurements and analysis methods for individual ions will be described in Section 3.2.3.

3.2.2.1 Water flux and NaCl rejection (characterization of membranes)

Membrane conditioning started with the wetting out of the membrane by circulating deionized water at 35°C at very low pressure; then the pressure was increased gradually to 10 bar for at least 8 hours, so that the excess chemicals attached to the membrane sheets were released and also to prevent their compaction during the permeation experiments (Dina et al. 2001; Ricq & Pagetti 1999; Teixeira et al. 2005). Then this deionized water was replaced by fresh water and kept overnight inside the pilot plant. After the conditioning step, the deionized water was replaced with fresh water and the membrane hydraulic permeability and flux was determined through the permeation of pure water at transmembrane pressures ranging from 2 to 14 bars. Also, rejection and flux of 0.01M NaCl was measured as a function of transmembrane pressures ranging from 2 to 12 bars after the mass transfer study (see Section 3.2.2.2). Additional concentration of NaCl (0.1M) was used with NTR7450 in order to calculate the dielectric constant of the membrane (see Sections 3.4 and 3.6.4).

3.2.2.2 Mass transfer study

The aim of this study is determine the cross-flow velocity at which concentration polarization is minimum, i.e. the observed and real rejection is almost equal. The mass transfer experiments were conducted at 0.025M NaCl as this is the highest concentration used in salt filtration experiments. Mass transfer study was performed for three membranes, namely Desal DK, NF270 and NTR7450 at 10 bars and different cross-flow velocities from 10 to 30 L/min and observed and real rejection were calculated. The theoretical aspects of the experiment will be discussed in Section 3.5.1 and the results in Section 3.6.1.

3.2.2.3 Single salts filtration

Salt filtration experiments were done to study the effect of pH, concentration and type of salts and ions on membrane charge, which is important for membrane performance (flux and rejection). Therefore, permeation of single solutions that were used in the electrokinetic

study, namely NaCl, KCl, Na_2SO_4, $MgSO_4$, $MgCl_2$ and $CaCl_2$ at three different concentrations 10^{-3}M, 10^{-2}M and 0.025M at 10 bars, was carried out. The temperature was kept at 20°C for pH range from 3.5 to 10 and at the cross-flow velocity determined previously from the mass transfer study. The experiments were carried out in total recirculation mode so that the feed concentration was kept constant, and this was checked by measuring conductivity and by analysis of ions. In the salts filtration experiments, samples were taken from feed and product streams to measure conductivity and individual ions. Water permeability was determined for all experiments in order to use it to calculate water flux. After any change in any parameter, i.e. pressure, pH or cross-flow velocity, the samples were taken after at least 20 minutes from that change, during which time the conductivity and pH were monitored until they reached a stable value (Mänttäri et al. 2006).

H_2SO_4/NaOH were used for pH adjustment of sulphate salts, while HCl/NaOH and HCl/KOH were used for calcium/magnesium chloride and potassium chloride salts, respectively. Beginning with natural pH, the pH was decreased stepwise using acids, and after the lowest pH (approximately 3.5), the test solution was drained and the apparatus was flushed with deionized water at a low pressure and a high flow rate and drained (Dina et al. 2001). After that, a new salt solution was prepared and the pH was increased stepwise using base until the highest pH (about pH 10) was obtained, and again, the test solution was drained and the apparatus was flushed with water to leave the equipment ready for the next use. Conductivity measurements were used as an indicator to make sure that the pilot plant was free of earlier test solutions and the flushing process was repeated, if necessary.

3.2.2.4 Mixture salts filtration

Mixtures of two salts at different combinations having the same chemistry of electrokinetic solutions (see Section 3.1.2.3 and Table 3.2) were filtered through the membranes. The filtration were carried out at 10 bars and pH from 3.5 to 10 in a total recirculation mode (50L volume is used) so that the feed concentration was kept constant if salt was used, which was checked by measuring conductivity and by analysis of ions. The temperature was kept at 20°C during the experiments. H_2SO_4/NaOH were used for pH adjustment of sulphate salts, while HCl/NaOH and HCl/KOH were used for calcium/magnesium chloride and potassium chloride salts, respectively. First natural pH was used, then the pH was decreased stepwise using acids, and after the lowest pH (approximately 3.5), the test solution was drained and the apparatus was flushed with deionized water at low pressure and high flow rate and drained (Dina et al. 2001). After that, a new salt solution was prepared and the pH was increased stepwise using base until the highest pH (about pH 10) was obtained, and again, the test

solution was drained and the apparatus was flushed with water to leave the equipment ready for the next use. Conductivity measurements were used as an indicator to make sure that the pilot plant was free of previous test solution and the flushing process was repeated, if necessary. After each change of pH, samples were taken after at least 20 minutes from that change, and during that time, the conductivity and pH were monitored until they reached a stable value (Mänttäri et al. 2006). Finally, the rejection of Na^+, K^+, Ca^{2+}, Mg^{2+}, Cl^- and SO_4^{2-} were calculated.

3.2.3 Analysis methods

The analysis methods of filtration experiments will be described in detail in this section.

3.2.3.1 Conductivity and pH measurements

Conductivity and pH measurements for retentate, product and feed tank samples were carried out with bench top conductivity and pH meters. Conductivity measurements were used to calculate salts rejection, to check the concentration of the pilot plant feed tank along with concentration analyses, to make sure that the system reached a stable condition after any change in the parameters such as pH, pressure, etc., and as an indicator during the flushing of the system. All conductivity measurements were performed at 25°C using a Russell RL060C conductivity meter and probe (Fisher Scientific, Loughborough, UK) as shown in Figure 3.6. The samples for conductivity and pH measurements were taken from product, retentate NF pilot plant sample points and directly from the feed tank. The measurements were repeated many times with a fresh sample each time to make sure that the sample was representative and to avoid dissolving of CO_2 from the atmosphere.

The pH measurements are important in investigating the behaviour of rejection when the pH is changed as the membranes' surface protonated/deprotonated with the pH. pH was measured using an IQ 150 pH meter and probe (Spectrum Technologies Inc., Illinois, USA) as shown in Figure 3.6.

Figure 3.6: (A) The Russell RL060C conductivity meter, and (B) the IQ 150 pH meter.

3.2.3.1 Analysis of ions

This section contains the analysis methods of Na^+, K^+, Ca^{2+}, Mg^{2+}, Cl^- and SO_4^{2-}. The concentration of these ions in feed and product are used to calculate their rejection separately in some filtration experiments.

3.2.3.1.1 Atomic absorption spectroscopy (AAS)

The atomic emission technique was used to analyse Na^+ and K^+ in water samples as these elements are light and they do not need energy (light) to excite their electrons other than the flame in the atomic absorption machine. Sodium and potassium were determined for product, retentate and feed tank samples for all mixtures experiments and only for 0.01M single salts by using Varian Atomic Absorption AA240FS (Varian, Inc.), shown in Figure 3.7. The AA240FS consists of an atomizer, flame, monochromator and photomultiplier detector (Figure 3.7C). The machine is a fully automated, PC-controlled, true double-beam atomic absorption spectrometer with fast sequential operation for fast multi-element determination and four lamp positions with automatic lamp selection. The AA240FS is supplied with SpectrAA Base and PRO software. Air/acetylene or nitrous-oxide/acetylene can be used in the burner. The analysed concentrations were used to calculate Na and K rejection rates as well as to check the concentration of the feed tank solution. The machine operation mode must be changed to emission instead of absorption, which can be done easily by selecting the emission option in the analysis method work-sheet (Figure 3.7D). Another difference from atomic absorption is that the emission calibration curve is not linear like in atomic absorption. The calibration curve was obtained by choosing three sodium/potassium standard solutions where the difference in concentration was fixed, e.g. 10, 20, 30 ppm or 20, 40, 60 ppm. The measurement started with estimating the concentration range of the samples so that the calibration curve would cover this range. If the concentration of samples was not in this range, dilution of the samples or change of calibration of the curve range should be made. Known concentration samples were measured with the other samples in order to ensure the accuracy of the analysis. Three calibration curves were usually required to analyse Na and K for one filtration experiment, i.e. one each for product, retentate and feed. The machine operation procedure is described step by step in this reference (San Diego Miramar College n.d.).

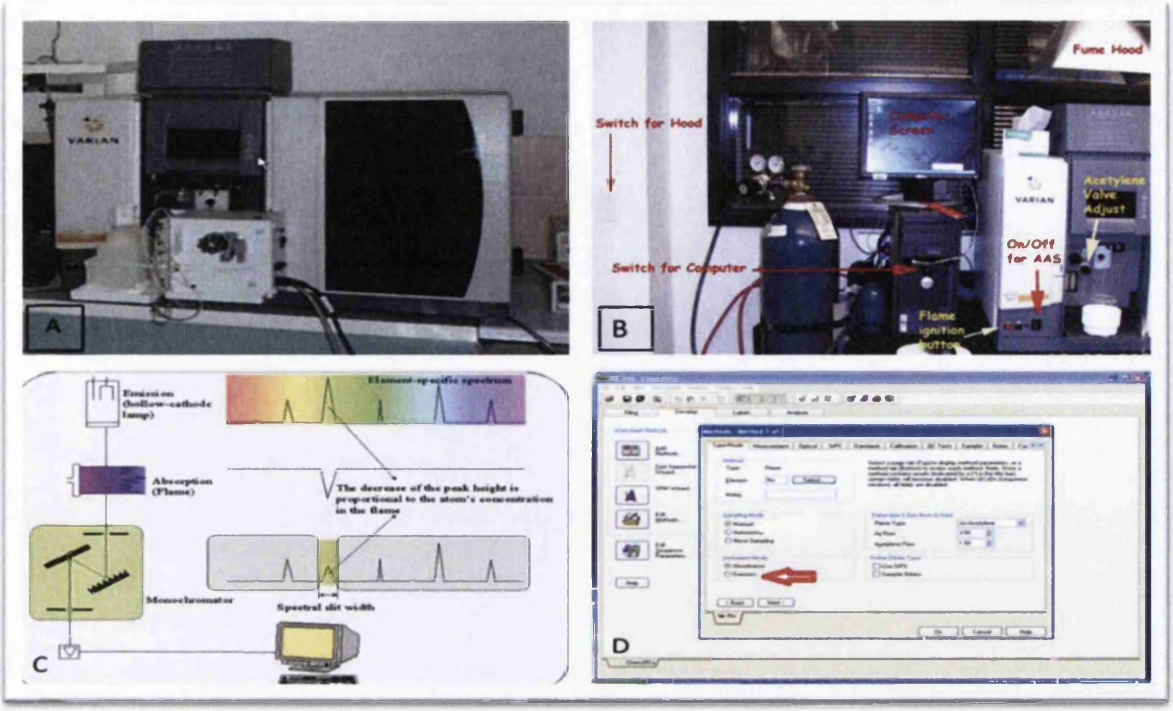

Figure 3.7: (A) A photo of the AA240FS, (B) the external components of the AA240FS, (C) the internal components of the AA240FS, and (D) the emission option in the analysis worksheet (San Diego Miramar College n.d.).

3.2.3.1.2 HACH spectrophotometer

A HACH DR 2000 spectrophotometer (Hach Company) is shown in Figure 3.8 and was used for SO_4^{2-} determination in the retentate, product and feed tank solution samples in Na_2SO_4 filtration experiments as well as for SO_4^{2-}.Cl^- mixtures filtration. The HACH spectrophotometer is a microprocessor – controlled, single beam spectrophotometer suitable for colorimetric testing in the laboratory and in the field (HACH DR2000 Manual n.d.). The HACH DR 2000 can be programmed to do more than 120 colorimetric analyses with no calibration curve required with good accuracy (which saves time). Two DR 2000 cells were filled with 25 ml of deionized water (blank) and the sample solution where the reagent was added. The instrument compared the colour of the sample to the blank and gave the concentration of the sample. SO_4^{2-} analysis was method number 680 at 450 nm in the instrument in which the SO_4^{2-} in the sample reacted with barium in the sulfaVer4 regent (supplied by HACH LANGE, Salford, UK) and formed $BaSO_4$ turbid (white) solution. The turbidity of the solution was proportional to the concentration of SO_4^{2-} in the sample and the concentration display on the screen was in ppm units.

The sulfaVer 4 also contained a stabilizing agent to maintain the precipitate in suspension. The detection range of the method is between 0 to 70 ppm; however the analysis was not used for more than 50 ppm and the samples above this concentration were diluted. The accuracy of the instrument was checked by preparing different SO_4^{2-} known concentration solutions and analysing them.

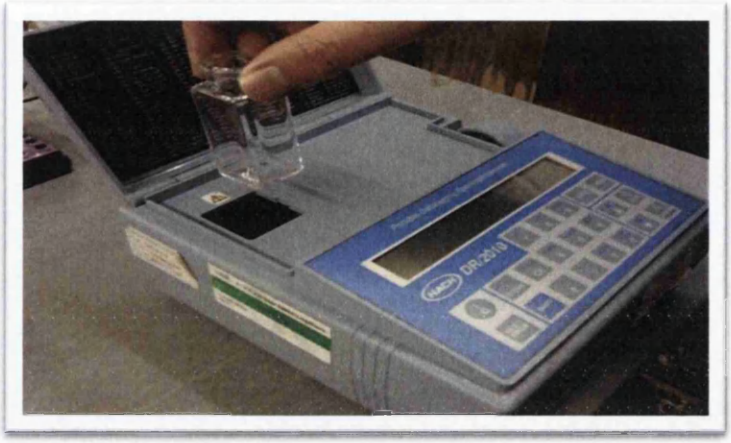

Figure 3.8: The HACH DR 2000 spectrophotometer.

3.2.3.1.3 Titration

Titration is a very old technique of analysis, but one that is still used due to its simplicity and accuracy, especially with higher concentration analytes. Two kinds of titration were used to determine Cl^-, Ca^{2+} and Mg^{2+} in the retentate, product and feed tank solution samples. Precipitation titration with AgCl was used to determine Cl^- in the NaCl and KCl filtration experiments as well as in the filtration of the SO_4^{2-}-Cl^- mixtures. On other hand, complexometric titration with EDTA was used to analyse Ca^{2+}, Mg^{2+} either in the $CaCl_2$ and $MgCl_2$ filtration experiments or when Ca was present with Mg^{2+}/Na/K. The procedures of the titration analysis were taken from the SWCC lab analysis manual (Saline Water Conversion Corporation n.d.) and the University of Canterbury (Department of Chemistry n.d.). The indicators and chemicals used in titration analysis were purchased from Fisher Scientific UK.

3.2.3.1.3.1 Determination of chloride by titration (Mohr's method)

The water sample was titrated with silver nitrate in the presence of potassium chromate as an indicator. The chloride ions in the sample were combined with the silver from the silver nitrate precipitation:

$$Ag^+_{(aq)} + Cl^-_{(aq)} \rightarrow AgCl_{(s)}$$

When all the chloride ions in the solution are consumed (the end point), the additional silver ions react with the chromate ions of the indicator to form a red-brown precipitate of silver chromate:

$$2\ Ag^{+}_{(aq)} + CrO_4^{2-}{}_{(aq)} \rightarrow Ag_2CrO_{4(s)}$$

Practically, the end point is recognised when the red colour starts to appear in the solution (Figure 3.9). Three standard solutions were prepared as follows:

(1) 0.01M $AgNO_3$ was prepared by dilution of 0.1M (Fisher Scientific) and stored in a brown bottle.

(2) 50 grams of potassium chromate indicator (Fisher Scientific) were dissolved in 100 ml deionized water.

(3) 0.01NaCl solution was prepared and treated with 0.01M $AgNO_3$ to confirm its concentration.

25 ml of the sample was pipetted into a 50 mL volumetric flask and two drops of the indicator added. The chloride ion concentration in ppm was calculated as follows:

$$Cl^{-} = \frac{(V_1)(M)\ (35453)}{V_2} * DF \qquad [3.1]$$

where V_1 is the volume of $AgNO_3$ at the end point (ml), V_2 is the volume of the sample (ml), M is the molar concentration of $AgNO_3$ (which is 0.01M in our case) and DF is the dilution factor. If no dilution has taken place, the value of DF is 1. However, if the sample is diluted, the DF is equal to the final volume after dilution divided by the initial volume, e.g. when 5 ml is taken from the sample and diluted by deionized water up to 25 ml, then DF will be 25/5 = 5.

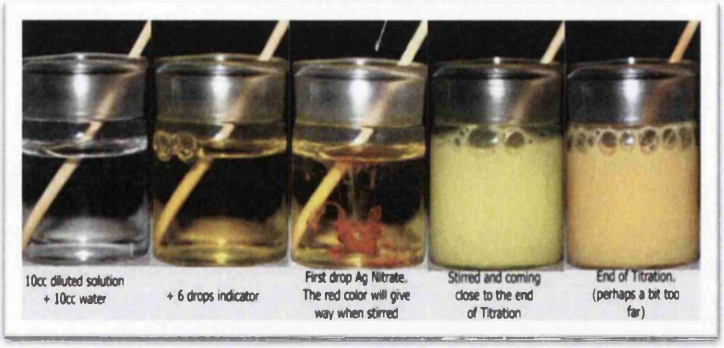

Figure 3.9: Changing of colour during Cl^- determination titration (GeoCities Chlorate Site n.d.).

3.2.3.1.3.2 Determination of Ca and Mg by titration

3.2.3.1.3.2.1 Determination of calcium

Complexometric titration is used to determine Ca^{2+} by the reaction of calcium with ethylenediaminetetraacetic acid (EDTA) to form a complex compound. A blue dye called Patton and Reeder's indicator (PR) also forms a pink/red complex with calcium ions, but calcium has more affinity towards EDTA than dye. As a result, when the indicator is added to a volumetric flask with the sample, a dye–Ca complex will form and then the solution is titrated with EDTA, whereupon the EDTA-Ca starts to replace dye–Ca complex. The endpoint is reached when the solution turns to blue (Figure 3.10), indicating that the dye–Ca complex has been completely replaced by the EDTA-Ca complex and that the dye indicator is free of calcium ion, so the dye returns to its original colour, which is blue:

$$\text{Dye-Ca (pink)} + \text{EDTA}^{4-} \rightarrow \text{dye (blue)} + [\text{Ca-EDTA}]^{2-}$$

Two standard solutions and powder of the indicator were prepared as follows:

(1) 0.02N (0.01M) EDTA was prepared by dissolving 3.723 grams ethylenediaminetetraacetic acid disodium in 1 litre deionized water and stored in a bottle.

(2) 1N NaOH solution to increase the pH.

(3) 0.2 grams of calconcarboxylic acid indicator (or Murexide) was ground with 100 grams NaCl and used as an indicator.

(4) 0.01M $CaCl_2$ was prepared from dried powder and the solution used immediately after preparation to standardize the EDTA solution.

25 ml of the sample was pipetted into a 50 mL volumetric flask with 3 ml of NaOH and around 0.2 grams of the indicator. The calconcarboxylic acid indicator changed from red or violet to the blue colour at the end point. The Ca ion concentration in ppm was calculated as follows:

$$Ca^{2+} = \frac{(V_1)(N)\ (20)(1000)}{V_2} * DF \qquad [3.2]$$

where V_1 is the EDTA volume at the end point (ml), V_2 is the volume of the sample (ml), N is the normality concentration of EDTA, which is 0.02N in our case, and DF is the dilution factor if no dilution has taken place; the value of DF is 1. However, if the sample is diluted, the DF is equal to the final volume after dilution divided by initial volume, e.g. when 5 ml is taken from the sample and diluted by deionized water up to 25 ml, then DF will be 25/5 = 5.

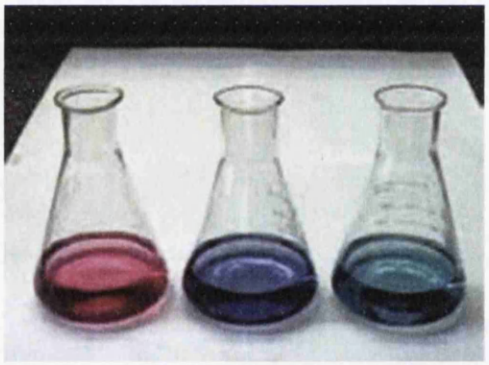

Figure 3.10: Changing of calconcarboxylic acid indicator colour during Ca^{2+} determination titration (red or violet to blue) (Chemteach n.d.).

3.2.3.1.3.2.2 Determination of magnesium

Magnesium is also analysed by complexometric titration with EDTA like calcium; however, the dye indicator is different as is the solution that is needed to increase the pH of the sample. Magnesium concentration in ppm is calculated from total and calcium hardness as follows:

$$Mg^{2+} = (\text{Total hardness} - \text{Calcium hardness}) * 0.243 \qquad [3.3]$$

If the sample contains only Mg as when $MgCl_2$ single salt is filtrated, then calcium is equal to zero and only total hardness is to be analysed. However, when Ca and Mg are present in the same sample, then total and calcium hardness tests must be performed. For total hardness analysis, three standard solutions were prepared as follows:

(1) 0.02N (0.01M) EDTA was prepared by dissolving 3.723 grams ethylenediaminetetraacetic acid disodium (Fisher Scientific) in 1 litre deionized water and stored in a bottle.
(2) Buffer solution: 1.179 grams ethylenediaminetetraacetic acid disodium and 0.644 grams $MgCl_2$ $6H_2O$ were dissolved in 50 ml deionized water (solution 1) and then a solution was prepared that contained 16.9 ml NH_4Cl and 143 ml ammonia (solution 2). After that, solutions 1 and 2 were added and diluted to 250 ml with deionized water.
(3) 0.2 grams of Eriochrom Black T (EBT) was mixed with 15 ml trimethyl amine and 5 ml ethanol.

25 ml of the sample was pipetted into a 50 mL volumetric flask with 1-2 ml of the buffer solution and two drops of the indicator. EBT is a blue dye which changes to pink when the dye forms a complex with Ca and Mg. However, Ca and Mg have more affinity towards EDTA than the dye. Therefore, Ca and Mg were chelated by EDTA, leaving the free indicator molecule and its original blue colour is restored (Figure 3.11). Total hardness was calculated as ppm $CaCO_3$ as follows:

$$Total\ hardness = \frac{(V_1)(N)\ (50)(1000)}{V_2} * DF \qquad [3.4]$$

where V1 is the EDTA volume at the end point (ml), V_2 is the volume of the sample (ml), N is the normality concentration of EDTA, which is 0.02N in our case, and DF is the dilution factor; if no dilution has taken place, the value of DF is 1.

Calcium hardness needs two standard solutions and powder of the indicator to be prepared as follows:

(1) 0.02N (0.01M) EDTA was prepared by dissolving 3.723 grams ethylenediaminetetraacetic acid disodium (Fisher Scientific) in 1 litre deionized water and stored in a bottle.

(2) 1N NaOH solution to increase the pH.

(3) 0.2 grams of Murexide was ground with 100 grams NaCl and used as an indicator.

25 ml of the sample was pipetted into a 50 mL volumetric flask with 3 ml of NaOH and around 0.2 grams of the indicator. The end point was indicated when the colour changed from pink to purple (Figure 3.11), where the Ca ion concentration as ppm $CaCO_3$ can be calculated as follows:

$$Ca - Hardness = \frac{(V_1)(N)(50)(1000)}{V_2} * DF \qquad [3.5]$$

where V1 is the EDTA volume at the end point (ml), V2 is the volume of the sample (ml), N is the normality concentration of EDTA, which is 0.02N in our case, and DF is the dilution factor; if no dilution has taken place, the value of DF is 1.

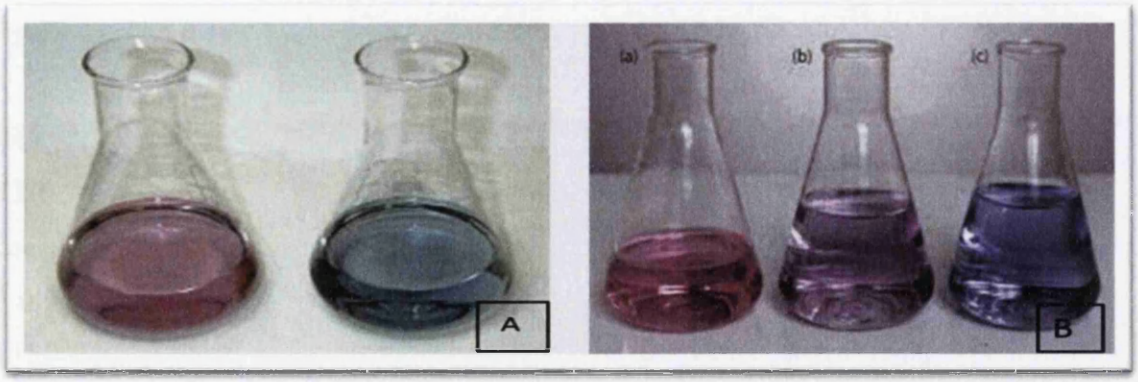

Figure 3.11: (A) Changing of Eriochrom Black T (EBT) indicator colour during total hardness titration (pink to blue), and (B) changing of Murexide indicator colour during the calcium hardness titration (pink to purple).

3.3 Contact angle

Most of the membranes' surface is made from hydrophilic materials which are hydrated and ionized in the aqueous solutions. In fact, characterization of membrane surface charge and hydrophobicity is essential for understanding water and solute transport through membranes as well as fouling of membrane surfaces (Hurwitz et al. 2010). A Fibro DAT 1100 dynamic contact angle analyser (Fibro System AB, Sweden) (Figure 3.12) was used in this study to measure hydrophobicity of the membrane surfaces. The device is equipped with a high speed video camera to monitor the side images of the drop profile as a function of time. Before doing the measurement, a sample of 6 mm width and 10 cm length was prepared and stuck to the sample holder with double sided Sellotape. A drop volume of 20 µl was chosen and the contact angle was measured as a function of time. A total of 8 droplets were placed and the contact angle was measured.

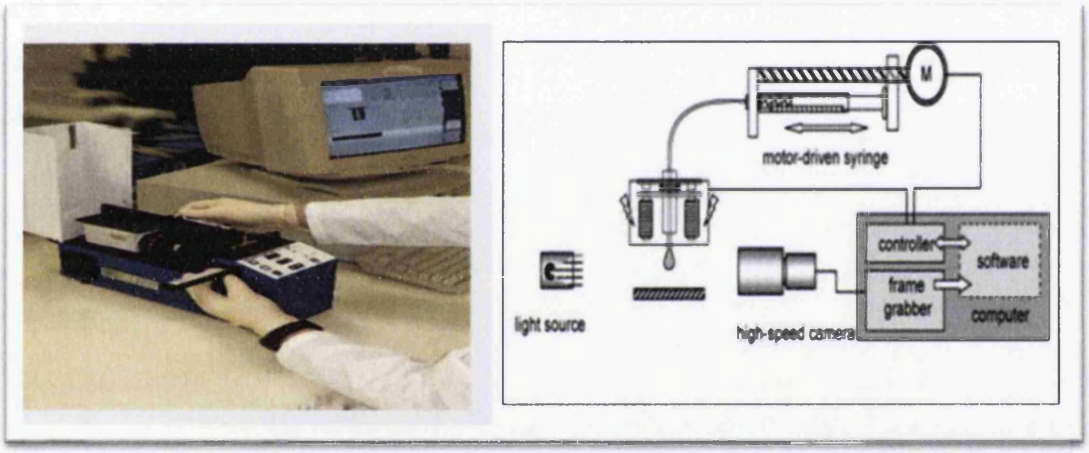

Figure 3.12: The Fibro DAT 1100 dynamic contact angle analyser (Almalek 2012).

3.4 Determination of pore size and dielectric constant of NTR7450

NTR7450 has not been studied extensively in the literature like Desal DK and NF270. Therefore, there is a lack of information about this membrane. The data generated by Williams (2015) was used here to calculate pore size of the membrane, while filtration of 0.1M NaCl at different pressures was utilized in calculating the membrane dielectric constant by using the DSPM-DE model. The theoretical aspects of this model will be discussed in Section 3.5.2.

Williams (2015) filtrated five PEGs (polyethylene glycol, molecular weight: 200, 400, 600, 1000, 1450) at feed concentration of 1 g/L through a commercially laboratory scale stirred

frontal filtration membrane cell. The PEG rejection experiments were undertaken at 300 rpm, a value optimized to reduce mass transfer and, hence, concentration polarisation effects. PEG rejection experiments were undertaken at 3, 5, 10, 20 and 30 bar with the operating temperature maintained at 25°C. The starting feed volume of 250 mL was used. Prior to starting experimentation, the membranes were pressurized for 2 hours at 30 bars with ultra-pure water. The observed and real rejection was obtained and plotted against applied pressure. The use of these data to obtain pore size as well as to calculate the dielectric constant will be discussed in Section 3.6.4.

3.5 Relevant theory

3.5.1 Description of mass transfer

An inherent feature of membrane operation is concentration polarization at the membrane surface due to local increases in the concentration of rejected solutes. The induced diffusive flow back into the feed solution will eventually attain a steady state. If flow conditions are such that a boundary layer will be established at the membrane surface, the concentration gradient will be retained within this layer (Mulder 1996). The extent of concentration polarization depends on several factors (Dresner & Johnson 1980):

(1) Competition between solute convection towards the membrane and diffusion away from the membrane.

(2) Fraction of solute rejected by the membrane.

(3) Flow regime at the membrane surface (whether laminar or turbulent).

(4) Stirrer geometry.

The rejection characteristics of a membrane are typically defined by observed rejection:

$$R_{obs} = 1 - \frac{C_p}{C_f} \qquad [3.6]$$

The quantity represents an experimental measurement of the degree of rejection of a solute by a membrane. However, in the presence of concentration polarisation, this definition of rejection is not accurate because the solute concentration at the membrane surface, C_w, is

higher than the feed concentration, C_f. The real rejection of the solute, R, which is always higher than the observed rejection, is defined as follows:

$$R = 1 - \frac{C_p}{C_w} \qquad [3.7]$$

Figure 3.13 shows a schematic diagram of the interface between the bulk feed solution and the membrane surface for a single electrolyte.

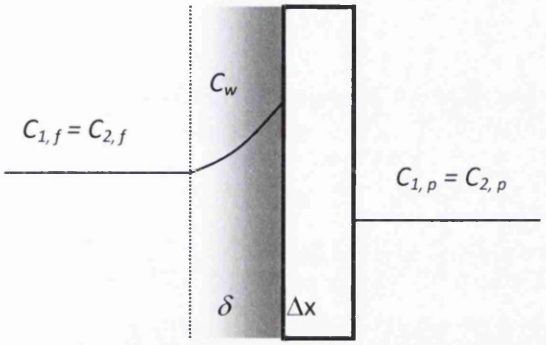

Figure 3.13: Concentration profiles within the polarized boundary layer.

However, the value of C_w is not directly measurable and so must be calculated indirectly with a suitable model for concentration polarization. Concentration polarization will be assumed to occur within a boundary film layer of thickness, δ. For a single salt such as NaCl, the cation and anion move together due to the requirement of electroneutrality and, so, there is no electromigrative transport of ions. Transport within the film layer is, in this case, due to convection and diffusion only, and so a mass balance yields:

$$j_+ = j_- = -D_{eff,\infty} \frac{dC_\pm}{dx} + C_\pm J_v \qquad [3.8]$$

where J_v is volumetric flux though the membrane and $D_{eff,\infty}$ is the effective diffusivity of the salt (Krishna & Wesselingh 1997), defined as:

$$D_{eff,\infty} = \frac{D_+ D_- (z_+ - z_-)}{z_+ D_+ - z_- D_-} \qquad [3.9]$$

Equation 3.8 is solved using the relationship $j_+ = C_p J_v$ and the boundary conditions: $C_\pm(0) = C_w$ and $C_\pm(-\delta) = C_f$ to allow C_w to be correlated to measurable parameters:

$$\frac{J_v}{k} = \ln\left(\frac{C_w - C_p}{C_f - C_p}\right) \qquad [3.10]$$

where k is the mass transfer coefficient in the polarized boundary layer, defined as:

$$\mathrm{k} = \frac{D_{eff,\infty}}{\delta} \qquad [3.11]$$

This result is equally applicable to a system of uncharged solutes, but the correction for a multicomponent electrolyte system requires the solution of the extended Nernst–Planck equation (Bowen & Mohammad 1998b). Many mass transfer correlations have been derived to predict k for simple membrane modules such as tubular and hollow-fibre membranes (Rautenbach & Albrecht 1994; Levesque 1928) and dead-end stirred cells (Opong & Zydney 1991). These correlations relate dimensionless Sherwood number to Reynolds number and Schmidt number. The mass transfer characterization for spiral wound membrane modules are complex as a detailed knowledge of the module configuration and geometry (Welfoot 2001) is needed. Therefore, it is necessary to determine the mass transfer coefficient experimentally by using the method of Nakao and Kimura (1981). Substitution of Equations 3.6 and 3.7 into Equation 3.10 and linearizing the equation gives the following expression:

$$\ln\left(\frac{1-R_{obs}}{R_{obs}}\right) = \ln\left(\frac{1-R}{R}\right) + \frac{J_v}{\mathrm{k}} \qquad [3.12]$$

k is a function of volumetric cross flow Q as follows (Welfoot 2001):

$$k = k'Q^n \quad [3.13]$$

Hence, the real rejection of a membrane is determined from the experimentally observed rejection by extrapolation to infinite Q on plotting ln $[(1 - R_{obs})/R_{obs}]$ against J_V/Q^n. The slope of the best fit line will be equal to $1/k'$.

3.5.2 Donnan-steric-pore model (DSPM)

The Donnan-steric-pore model (DSPM) was developed by Bowen et al. (1997) and used later in the prediction of NF performance in a mixture of NaCl and dye (Bowen & Mohammad 1998b). The model is based on the extended Nernst–Planck equation along with including the effect of charge (Donnan) and steric factor to describe the transport of ions through the membrane. The three parameters needed for the model are effective pore radius (r_p), effective ratio of membrane thickness to porosity ($\Delta x/A_k$), and the effective charge density (X_d). Another development has been added to the model by Bowen and Welfoot (2002) to include the effect of dielectric exclusion and increased solution viscosity in the pore (DSPM-DE). This updated model removes the dependency on $\Delta x/A_k$ by inclusion of pressure in the form of a Hagen–Poiseuille equation.

3.5.2.1 Donnan-steric-pore model transport equations

The extended Nernst–Planck equation is particularly useful for NF as consideration is given to the mechanisms of transport, namely diffusion, electrical potential and convection. The following assumptions are made when using the extended Nernst–Planck equation:

(1) The activity coefficients are assumed as unity.

(2) The effective membrane charge density is constant throughout the membrane.

(3) All ions inside the membrane are transportable.

The Donnan equilibrium is assumed at the interface between the membrane pore and bulk solution.

In terms of the diffusivity of ions, the extended Nernst–Planck equation is:

$$j_i = -\frac{c_i K_{i,d} D_{i,\infty}}{RT}\frac{d\mu}{dx} + K_{i,c} c_i V \quad [3.14]$$

where j_i is the ionic flux, c is the concentration, V is the solvent velocity and $K_{i,c}$ and $K_{i,d}$ are hindrance factors to account for the convection and diffusion in the confined NF pore.
The hindrance factors are defined as:

$$K_{i,d} = \frac{D_{i,p}}{D_{i,\infty}} \qquad K_{i,c} = \frac{u_s}{u_x} \qquad [3.15]$$

where $D_{i,p}$ is the hindered diffusivity inside the NF pore, u_s is the solute velocity and u_x is the maximum solvent velocity. Both hindrance factors are related to the ratio of solute to pore radius (λ). Therefore, Equation 3.14 becomes:

$$j_i = -\frac{c_i D_{i,p}}{RT}\frac{d\mu}{dx} + K_{i,c} c_i V \qquad [3.16]$$

The electrochemical potential is written as:

$$\mu_i = RT \ln a_i + V_{si} P + z_i F \psi + \text{constant} \qquad [3.17]$$

where R is the universal gas constant, T is the absolute temperature, V_{si} is the specific volume of the ion, P is the operating pressure, z is the ion valence, F is the Faraday constant and Ψ is the electrical potential inside the membrane.

If Equation 3.17 is differentiated, the following expression is obtained:

$$\frac{d\mu}{dx} = RT\frac{d}{dx}[\ln a_i] + V_{si}\frac{dP}{dx} + z_i F \frac{d\psi}{dx} \qquad [3.18]$$

Using the mathematical relationship $\frac{d}{dx}[\ln a] \approx \frac{1}{a}\frac{da}{dx}$ and $a_i = c_i\gamma_i$, the following equation is obtained:

$$\frac{d\mu}{dx} = \frac{RT}{c_i}\frac{dc_i}{dx} + \frac{RT}{\gamma_i}\frac{d\gamma_i}{dx} + V_{si}\frac{dP}{dx} + z_i F\frac{d\psi}{dx} \qquad [3.19]$$

Substitution of Equation 3.19 into Equation 3.16 yields the result:

$$j_i = -D_{i,p}\frac{dc_i}{dx} - \frac{c_i D_{i,p}}{\gamma_i}\frac{d\gamma_i}{dx} - \frac{c_i D_{i,p}}{RT}V_{si}\frac{dP}{dx} - \frac{c_i D_{i,p}}{RT}z_i F\frac{d\psi}{dx} + K_{i,c}c_i V \qquad [3.20]$$

Equation 3.20 represents the full extended Nernst–Planck equation and must be simplified for solution. Schlögl (1966) proposed that the contribution to ion transport of the activity coefficient (γ), is negligible. Also, Dickson (1988) and Burghoff et al. (1980) demonstrated that the effects of pressure on the chemical potential were small at low pressure ($\Delta P < 0.5$ MPa). Therefore, Equation 3.20 is simplified to:

$$j_i = -D_{i,p}\frac{dc_i}{dx} - \frac{c_i D_{i,p}}{RT}z_i F\frac{d\psi}{dx} + K_{i,c}c_i V \qquad [3.21]$$

From the definition of solute flux through the membrane, the following is obtained:

$$j_i = VC_{i,p} \qquad [3.22]$$

Substitution of Equation 3.22 into Equation 3.21 yields the result:

$$\frac{dc_i}{dx} = \frac{V}{D_{i,p}}\left[K_{i,c}c_i - C_{i,p}\right] - \frac{z_i c_i}{RT} F \frac{d\psi}{dx} \qquad [3.23]$$

This expression describes the concentration gradient of ion i across the membrane. The condition of electroneutrality in the bulk solution is expressed as:

$$\sum_{i=1}^{n} z_i C_i = 0 \qquad [3.24]$$

where C_i is the bulk concentration. Electroneutrality inside the membrane pore is expressed as:

$$\sum_{i=1}^{n} z_i c_i = -X_d \qquad [3.25]$$

where c_i is the concentration inside the membrane pore and X_d is the effective membrane charge density. If we differentiate Equation 3.25 and substitute the result into Equation 3.23, we obtain an expression for the electrochemical potential:

$$\frac{d\psi}{dx} = \frac{\sum_{i=1}^{n} \frac{z_i V}{D_{i,p}}\left[K_{i,c}c_i - C_{i,p}\right]}{\frac{F}{RT}\sum_{i=1}^{n} z_i^2 c_i} \qquad [3.26]$$

Substitution of Equation 3.26 into Equation 3.23 yields the result:

$$\frac{dc_i}{dx} = \frac{V}{D_{i,p}}\left[K_{i,c}c_i - C_{i,p}\right] - z_i c_i \left[\frac{\sum_{i=1}^{n} \frac{z_i V}{D_{i,p}}\left[K_{i,c}c_i - C_{i,p}\right]}{\sum_{i=1}^{n} z_i^2 c_i}\right] \quad [3.27]$$

Equation 3.27 forms the basis for the transport of ions through the NF pore in terms of effective pressure driving force for the DSPM model.

3.5.2.2 DSPM-DE

3.5.2.2.1 Transport equations

Eliminating the negligible effects in Equation 3.21 (in this case, the pressure term is not eliminated as was the case with the DSPM model), the following is obtained:

$$j_i = -D_{i,p}\frac{dc_i}{dx} - \frac{c_i D_{i,p}}{RT}V_{si}\frac{dP}{dx} - \frac{c_i D_{i,p}}{RT}z_i F\frac{d\psi}{dx} + K_{i,c}c_i V \quad [3.28]$$

The assumption of lamina flow through the membrane pore enables the pressure gradient to be defined from a Hagen-Poiseuille type relationship, where the pressure gradient is constant along the pore (Welfoot 2001) and is expressed as:

$$\frac{dP}{dx} = \frac{\Delta P_e}{\Delta x} = \frac{8\eta V}{r_p^2} \quad [3.29]$$

where $\Delta P_e = \Delta P - \Delta\pi$. The introduction of an osmotic pressure difference across a pore, $\Delta\pi$, is important for systems such as multivalent electrolytes at higher concentrations as the

effective pressure driving force, ΔP_e, will differ significantly from the applied pressure, ΔP. Care should be taken when using Equation 3.29, as the viscosity term, η, is not that of the bulk viscosity. Following the same treatment as in Section (3.4.2.1), the result obtained is:

$$\frac{dc_i}{dx} = \frac{V}{D_{i,p}}\left[\{K_{i,c} - Y\}c_i - C_{i,p}\right] - z_i c_i \left[\frac{\sum_{i=1}^{n} \frac{z_i V}{D_{i,p}}\left[\{K_{i,c} - Y\}c_i - C_{i,p}\right]}{\sum_{i=1}^{n} z_i^2 c_i}\right] \quad [3.30]$$

The extra term, Y, in Equation 3.30 when compared to Equation 3.27 is a dimensionless parameter and arises as a direct result of the inclusion of pressure effects on the chemical potential. The term is expressed as:

$$Y = \frac{D_{i,p}}{RT} V_{si} \frac{8\eta}{r_p^2} \quad [3.31]$$

Bowen and Welfoot (2002) showed that the effect of parameter, Y, was small.

3.5.2.2.2 Equilibrium partitioning

The solute concentrations at the feed side and permeate side of the membrane must be known in order to solve the transport equations. Again, these values are obtained from equilibrium partitioning; however, the description of the partitioning expression is significantly different in the DSPM-DE model to account for dielectric contributions. This relationship is expressed as:

$$\frac{\gamma_i c_i}{\gamma_i^o C_i} = \Phi_i \exp\left(-\frac{z_i F}{RT}\Delta\psi_D\right)\exp\left(-\frac{\Delta W_i}{k_B T}\right) \quad [3.32]$$

where ΔW_i is the ion solvation energy barrier and k_B is the Boltzmann constant. Ion solvation forces are one proposed mechanism (Oatley 2012) by which the contributions of dielectric exclusion of ions from NF membranes is possible. The solvation energy barrier is described using a (Born 1920) expression:

$$\Delta W_i = \frac{z_i^2 e^2}{8\pi\varepsilon_o a_i}\left(\frac{1}{\varepsilon_p} - \frac{1}{\varepsilon_b}\right) \quad [3.33]$$

where e is the elemental electron charge, ε_o is the permittivity of free space, ε_p is the pore dielectric constant, and ε_b is the bulk dielectric constant. The Born model requires knowledge of the pore dielectric constant. Bowen and Welfoot (2002) proposed that the solvent structure within the pores would consist of one layer of oriented water molecules at the pore wall and an inner annulus (central part) having bulk dielectric properties. The variation of average pore dielectric constant can then be calculated on a geometric basis (assuming $\varepsilon_b = 80$):

$$\varepsilon_p = 80 - 2(80 - \varepsilon^*)\left(\frac{d}{r_p}\right) + (80 - \varepsilon^*)\left(\frac{d}{r_p}\right)^2 \quad [3.34]$$

where d is the diameter of a water molecule and ε^* is the dielectric constant of the single layer of water molecules. The procedure of the DSPM solution used to calculate effective membrane charge density is presented in Figure 3.14.

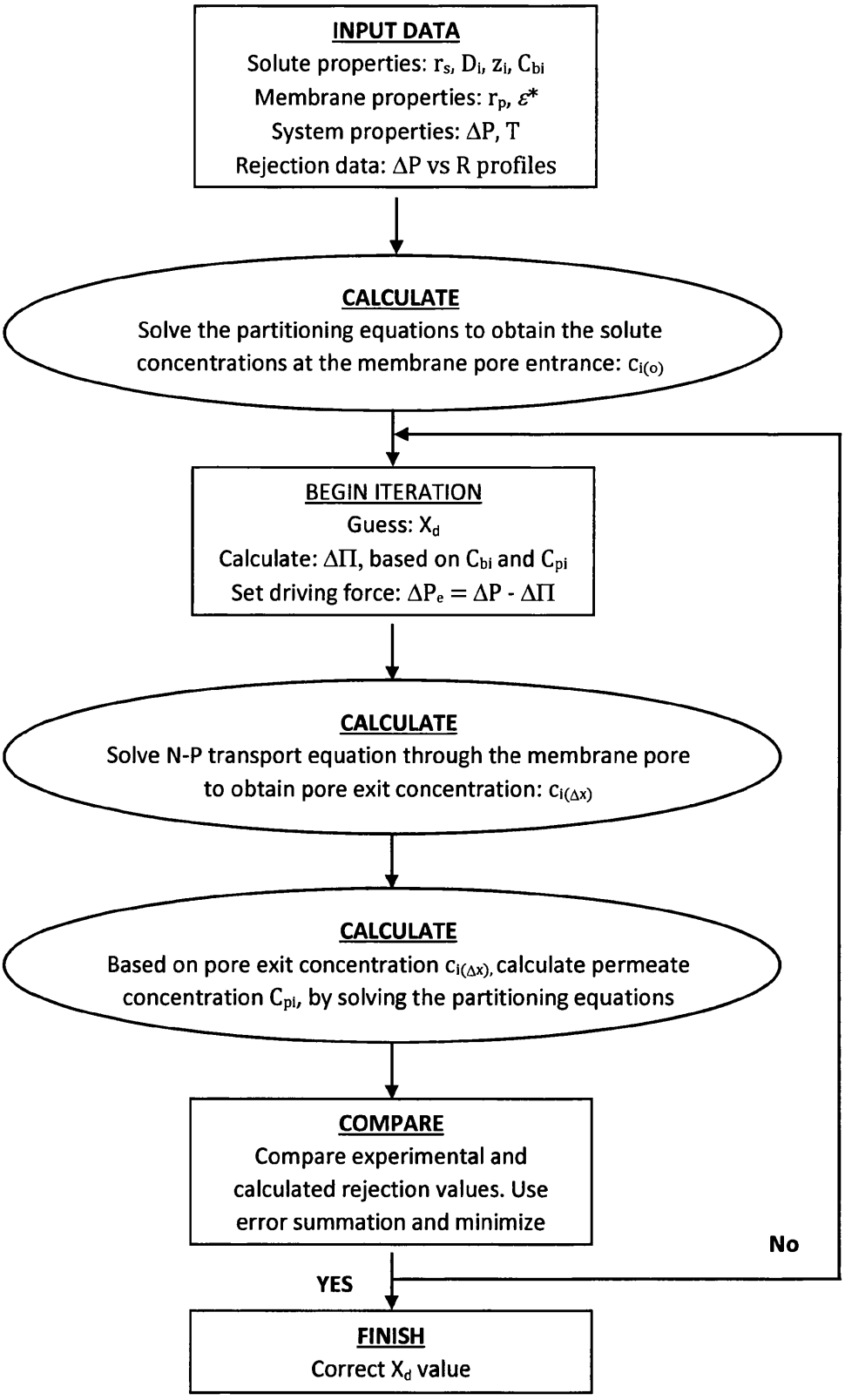

Figure 3.14: Calculation of membrane charge from rejection profiles using the Nernst–Planck equation (based on the UDSPM model, Bowen and Welfoot [2002]).

3.6 Supporting experiments

3.6.1 Mass transfer study

Concentration polarization is known to increase with increasing membrane flux and solution concentration (Oatley et al. 2012). Therefore, 0.025M NaCl has been selected to perform the mass transfer as this is the highest concentration used in filtration experiments. Figure 3.15 shows the observed rejection and water flux of 0.025M NaCl as a function of cross-flow velocity at 10 bars and natural pH (around 6) for Desal DK, NF270 and NTR7450. In order to calculate the real rejection ln $[(1-R_{obs})/R_{obs}]$ plot verses J_V/Q^n, a straight line was obtained with slope $1/k'$ and an intercept of ln [(1-R)/R] as shown in Figure 3.16. The value of n is 0.875, which is obtained from Nako and Kimura (1981). This method of studying mass transfer is called the velocity variation method (Welfoot 2001). The observed rejection as a function of cross-flow velocity shows a slight increase when the cross flow is increased, e.g. the value of the rejection at the first cross-flow velocity used and the maximum one as follows: 0.6-0.65, 0.53-0.56 and 0.56-0.59 for Desal DK, NF270 and NTR7450, respectively. Table 3.3 shows the values of calculated real and observed rejections at maximum cross-flow velocity where the observed rejection is at closest value to real rejection mass transfer coefficients were also determined. All filtration experiments were carried out at the maximum cross-flow velocity in order to make the concentration polarization at minimum.

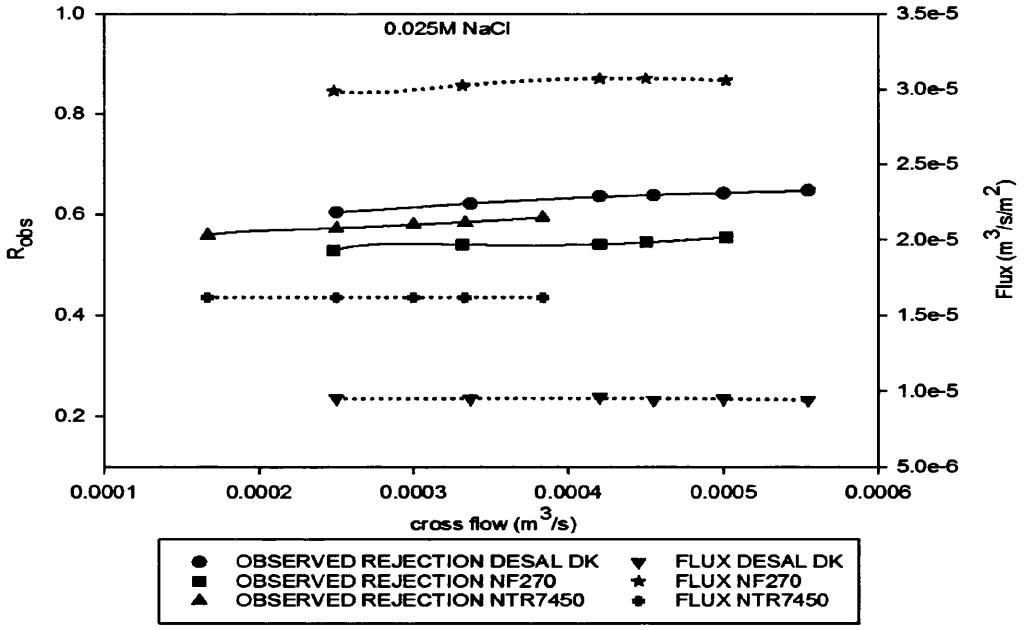

Figure 3.15: Observed rejection and flux of 0.025M as a function of cross-flow velocity.

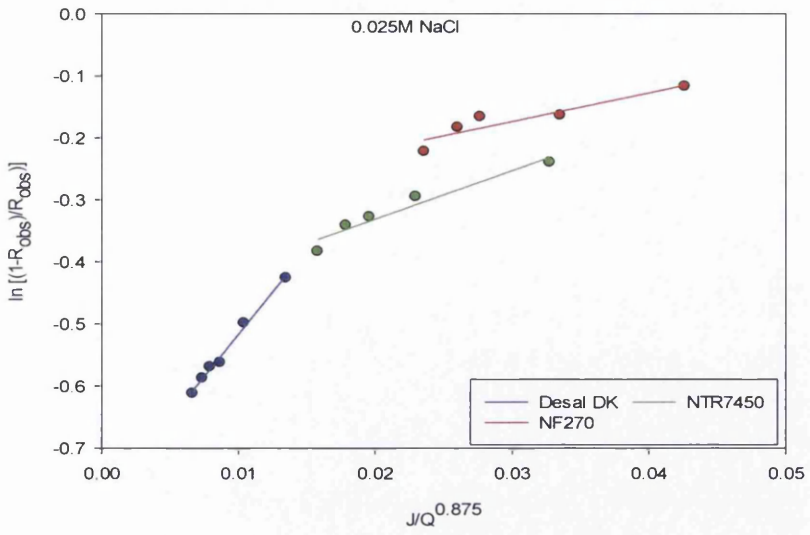

Figure 3.16: Velocity variation method analysis of the observed rejection of 0.025M NaCl.

Table 3.3: Calculated values of k', R_{real} and R_{obs} at the maximum cross-flow velocity.

Membranes	k'	R_{obs}	R_{real}	Cross-flow velocity (max) m^3/s
Desal DK	0.03689	0.648	0.687	5.55×10^{-4}
NF270	0.21638	0.555	0.577	5.0167×10^{-4}
NTR7450	0.12806	0.594	0.619	3.833×10^{-4}

3.6.2 Water flux and NaCl rejection (membranes characterization)

Table 3.1 provides a review of the three membranes' specifications taken from different references. In terms of membrane pore size, NTR7450 has the largest pores ranging between 0.62 and 1.4 nm, while Desal DK has slightly smaller pores (0.43-0.71 nm) than NF270 (0.5-0.58 nm). However, NF270 has the highest water permeability and the lowest contact angle (most hydrophilic), i.e. the permeability range is 11.3-27.45 L/m^2h bar. The second highest membrane in water permeability with permeability range between 6.3 and 13 L/m^2h bar is NTR7450, but it is the most hydrophobic surface. Desal DK has the lowest water permeability at 5.4-8.95 L/m^2h bar and its contact angle value is between the other two membranes.

Figure 3.17A shows the flux of deionized water and 0.01M NaCl of the three membranes at different pressures found in this study. As founded in the literature, NF270 has the highest flux among the membranes, followed by NTR7450. In fact, the NTR7400 series has very

high water permeability and is resistant to chemical attack (Ikeda et al. 1988). Flux linearly increases as the applied pressure increases and the deionized water flux is higher than NaCl

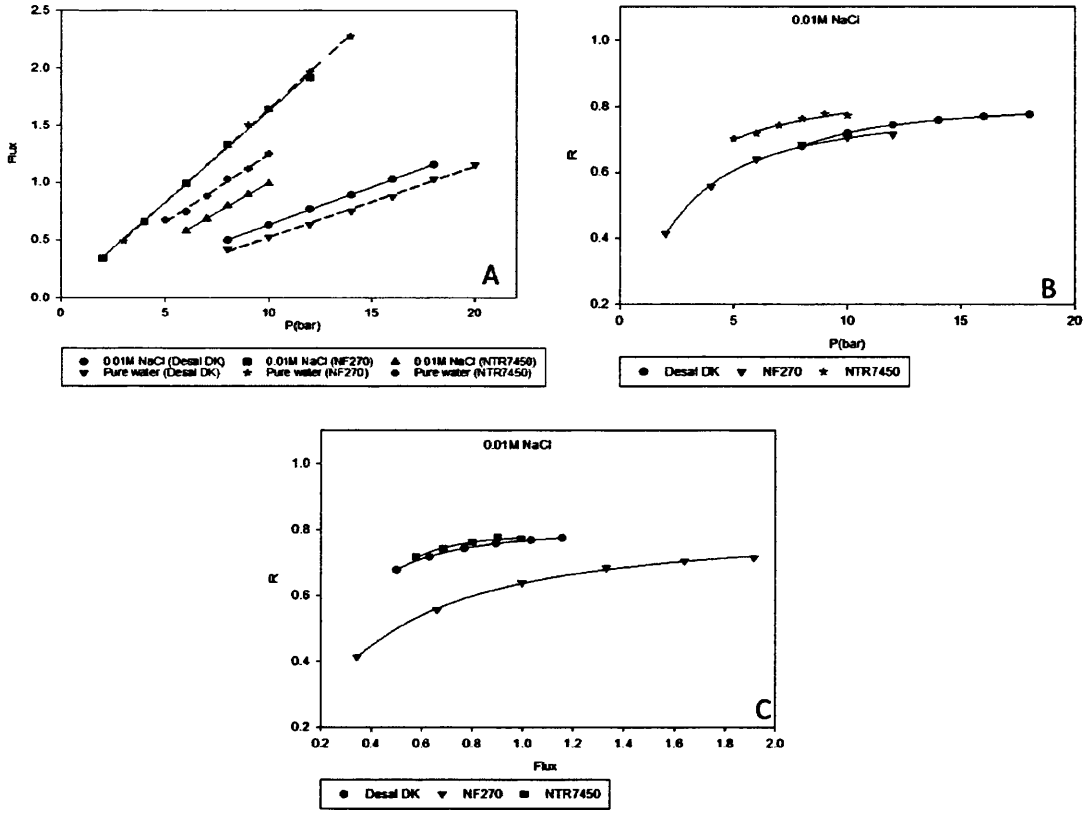

Figure 3.17: Membranes' characterization: (A) flux of deionized water and 0.01M NaCl, (B) rejection of 0.01M NaCl, and (C) flux vs. rejection for 0.01M NaCl.

solution for NTR7450. This behaviour is due to the increasing effect of the osmotic pressure difference across the membrane on the effective pressure difference, as the salt is added (Bandini et al. 2005; Ikeda et al. 1988; Mullet et al. 1997). NF270 has identical flux for deionized water and NaCl solution, while water flux is lower with Desal DK. However, flux decreases with increasing concentration for both membranes when three NaCl solution concentrations are studied, as will be discussed later in the Results section. The fact that NaCl flux is higher than deionized water flux for Desal DK was also found by Bargeman et al. (2014) for the same membrane at 10g/L (0.017M).

The mean hydraulic permeability L calculated from the slope of the plot of flux (J) versus ΔP is an image of the membrane (Artug 2007; Chakkrit 2010). The calculated hydraulic permeability from Figure 3.17 at 20^0C is 0.0556L/min m^2 bar (3.336 L/h m^2 bar), 0.1641

L/min m^2 bar (9.846 L/h m^2 bar) and 0.1264 L/min m^2 bar (7.584 L/h m^2 bar) for Desal DK, NF270 and NTR7450, respectively. Artug (2007) studied NF270, which showed the highest permeability, whilst the NF PES 10 and NF90 membranes showed the lowest ones. The order of the permeability agrees with the ones expected from the contact angle measurements, i.e. NF270 is the lowest contact angle. Furthermore, the permeate flux increased 3-4% per degree of temperature rise. Argelaguet (2011) found that the flux of NF270 was higher than that of Desal DK. The rejection of 0.01M NaCl as a function of pressure is shown in Figure 3.17B in which the rejection factor increased with increasing transmembrane pressure and reached a maximum value. The relations between permeate flux and salt rejection for the three membranes are shown in Figure 3.17C. NF270 has the lowest rejection associated with lowest flux compared to the other two membranes. Hilal et al. (2005) studied the performance of NF270 and compared it with NF90 and N30F. It was found that NF270 had the highest water permeability because it has the largest pore size and high porosity. It was also found that NF270 has lower rejection at high flux and they observed that at low concentration, the values of rejection and the permeate flux were very close, which can also be an observation in this paper (Figure 3.17C) with NF270, especially at low flux rate.

3.6.3 Membranes' surface hydrophilicity study

The membrane surface becomes hydrophilic as a result of ionization of surface functional groups, which depends on pH and the concentration of the solution (Luo & Wan 2013b). In fact, studying membranes' surface charge and hydrophobicity is essential for understanding water and solute transport through the membranes as well as fouling of membrane surfaces (Hurwitz et al. 2010). As an example, membrane surface charge functionality influences the membranes' pore size and Donnan effect, which govern water and charged solute transport through RO/NF membranes. Hydrophilicity of the membranes is measured by contact angle measurement , where a contact angle of 0° indicates a surface is completely wet, whereas a contact angle of 90° indicates no wetting (Almalek 2012). Table 3.1 provides the contact angle measurement of the three membranes taken from different references. Contact angle measurements that were done here showed that NF270 is the most hydrophilic of the three membranes, with 22°. This result agrees with Almalek (2012); Artuğ et al. (2007) could not measure NF270 as a result of the highly hydrophilic surface and they estimated contact angle as less than 10°. Desal DK and NTR7450 have contact angles at 54° and 70°, respectively. Polyethersulphone membranes like NTR7450 are more hydrophobic than polyamide membranes (Salg et al. 2013). Mänttäri et al.(2006) studied the relation between zeta potential and contact angle. It was found that the lower the membrane contact angle (more

hydrophilic membrane), the higher was the change in apparent zeta potential when pH was increased from 4 to 7. As a result, the retention of ions with more hydrophilic membranes changed more than those with hydrophobic ones when the pH was increased in the solution. In addition, some membranes became significantly more open at high pH (i.e. flux increased). The dissociation of carboxylic and amine groups on the surface of the NF200 membrane resulted in an increase in hydrophobicity, while NTR7450 showed the most hydrophobic surface.

3.6.4 NTR7450 pore size and dielectric constant determination

NTR7450 has not been studied extensively in the literature like Desal DK and NF270. There are different figures found in the literature for NTR7450 pore size, e.g. 0.81 nm (Sabir et al. 1998), 0.62 nm (Bargeman et al. 2014) and 1.4 nm (Bowen & Mohammad 1998a). The data generated by Williams (2015) has been used here to calculate pore size using the method discussed in Section 3.4. The model used to calculate pore size is the DSPM updated in which the pore size was varied and rejection calculated and compared to the experimental PEG rejection. Figure 3.18 shows all the equations required in calculating the real rejection and Figure 19 shows the flow chart of solution procedure. The result is obtained when the difference between the experimental and calculated rejection is minimum; this comparison can be done by using the least squares objective function (S_y). The results are presented in Figure 3.20, the stable PEG molecular weight is 400 as it has the minimum error (Figure 3.18A).The plot of pore size against the error (Figure 3.20C) shows that the minimum error takes place at 0.6 nm, while Figure 3.20 B compares the calculated and experimental rejections. The filtration of 0.1M NaCl solution data has been used to calculate NTR7450's dielectric constant (ε^*) by utilizing the DSPM model. The input parameters are 0.6 nm pore size and the concentration of NaCl, 100 mol/m^3. The agreement between the calculated and experimental rejection for different dielectric constants is shown in Figure 3.20 D, which indicates that 45 has the best agreement.

$$R_{real} = 1 - \frac{C_p}{C_m} = 1 - \frac{\Phi K_c}{1-[1-\Phi K_c]\exp(-Pe)}$$

$$Pe = \frac{K_c r_p^2}{8\eta D_p}\Delta P_e$$

$$\lambda = \frac{r_s}{r_p}$$

$$\Phi = (1-\lambda)^2$$

$$S_y = \sqrt{\frac{\sum_1^n \sum_1^j (R_{exp} - R_{calc})^2}{jn-1}}.$$

Figure 3.18: Equations of DSPM updated used to determine NTR7450 pore size.

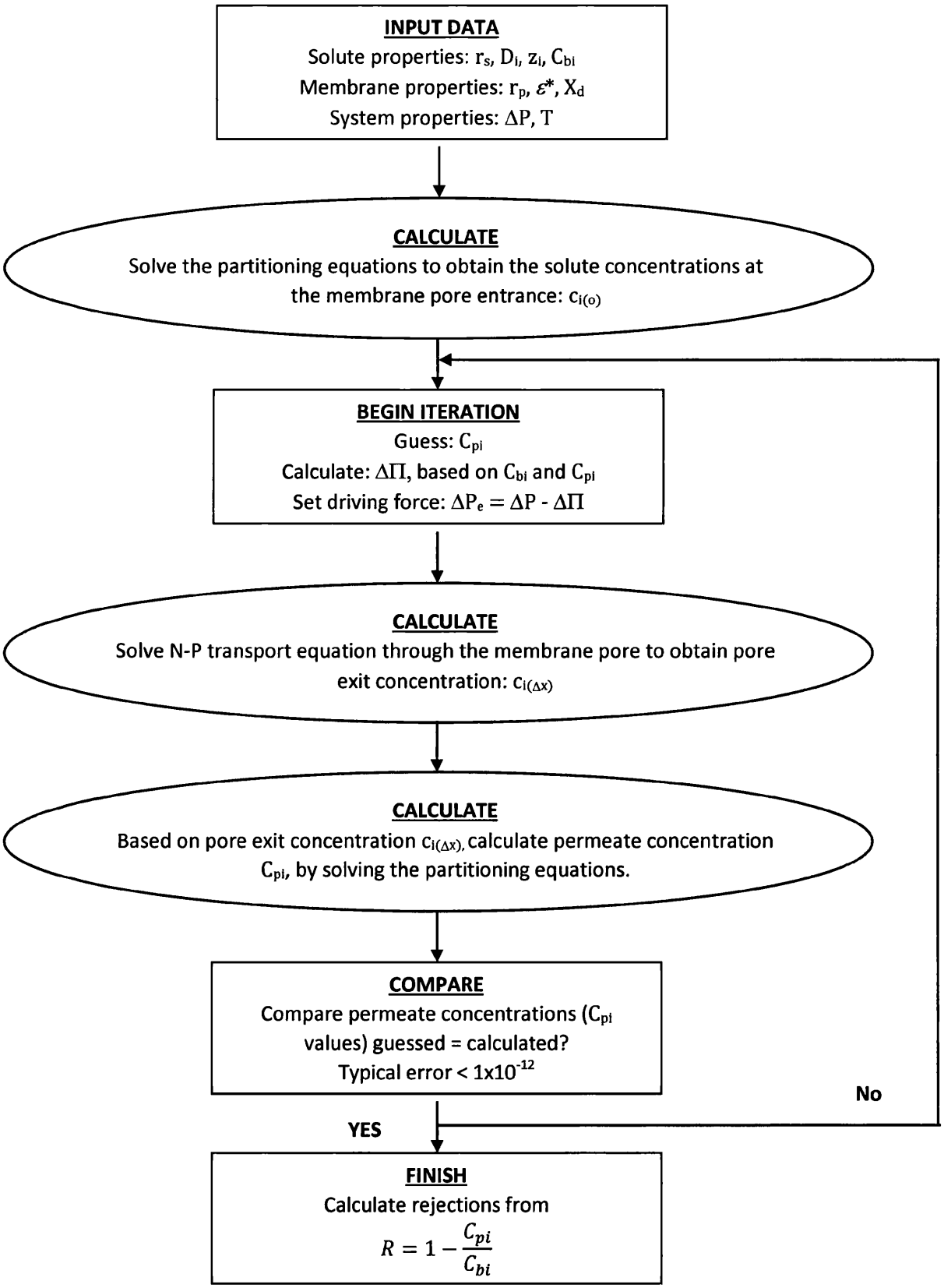

Figure 3.19: Calculation of solute rejection using the extended Nernst–Planck equation (based on the UDSPM model, Bowen and Welfoot [2002]).

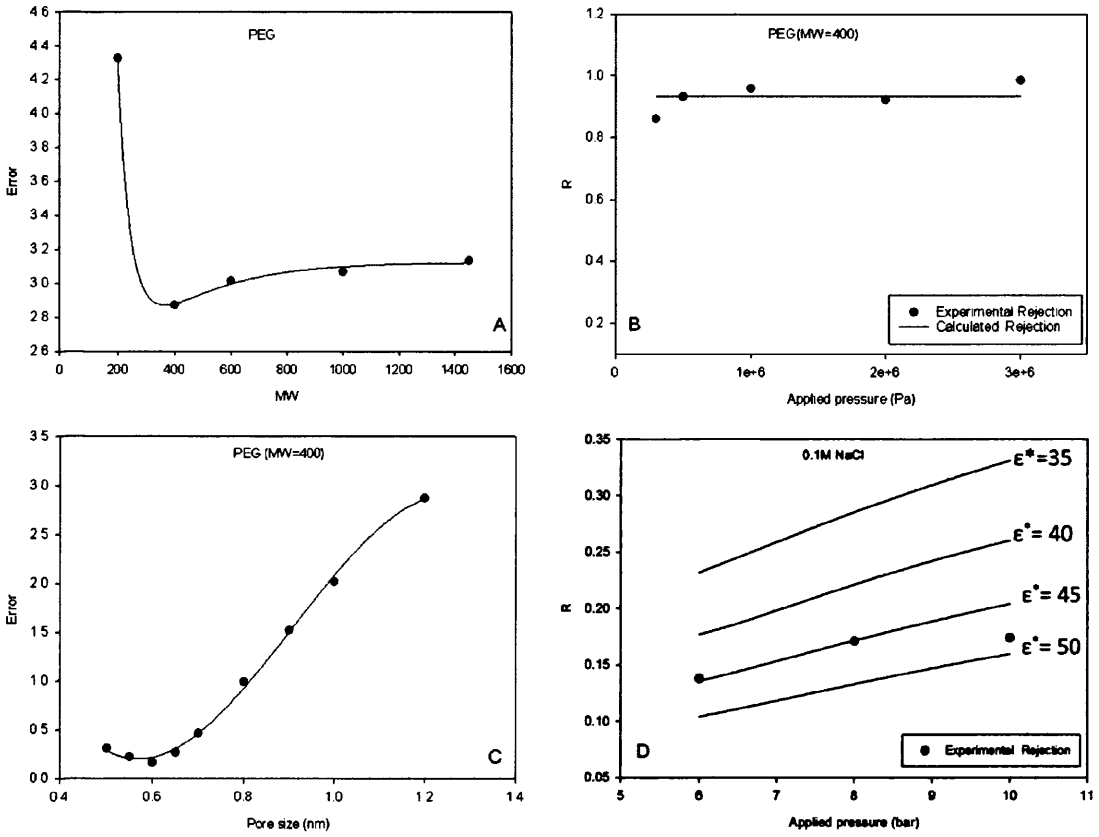

Figure 3.20: Pore size and dielectric constant curves used to determine NTR7450 pore size and dielectric constant.

3.7 Conclusion

The materials and methods used in the experimental work were discussed in this chapter. Furthermore, the relative theory of the experimental work was also provided. Finally the membranes used throughout the study were characterized and the data obtained used either as input to a modified DSPM model or to help to understand the ionic species rejection mechanism of these membranes. Table 3.4 and Figure 3.17 provide a summary of the results of Sections 3.6.2, 3.6.3 and 3.6.4.

Table 3.4: Membranes' characterization parameters.

	Desal DK	NF270	NTR7450
Pore size (nm)	0.45 (Bowen and Welfoot 2002)	0.5 (Argelaguet 2011)	0.6
Permeability at 20^0C (L/h m^2 bar)	3.336	9.846	7.584
Contact angle (°)	54	22	70
Dielectric constant	31 (Bowen and Welfoot 2002)	35 (Argelaguet 2011)	45

4.0 Charge Characterization of NF Membranes in a Single Salt System

This chapter aims to use electrokinetic measurements to study the membrane charge of nanofiltration membranes (NF) in single salt systems. This includes studying the effect of the type of electrolyte and concentration at different pH on zeta potential values. The obtained zeta potential results were used to explain the specific adsorption of certain ions to membrane surface, determine isoelectric points and study the amphoteric behaviour of the membranes under investigation. Studying this interaction between the solute and membrane charge will improve our understanding of the membrane separation mechanism, which will help to increase the efficiency of the NF process.

4.1 Introduction

NF membranes carry a fixed electric charge in an aqueous environment, which enables them to retain charged ions based on their valence (Escoda et al. 2010; Tay et al. 2002). Membrane surface charge originates from two sources: ionization of surface functional groups and adsorption of charged species such as ions and charged macromolecules. Electrokinetic properties of membranes have a large impact on the membranes' performance and fouling. NF membranes' active layer is a hydrophilic polymeric material such as polyamide (PA), cellulose acetate (CA), polysulphone (PS), polyether sulphone (PES), polyvinyl alcohol (PVA), which, when hydrated and ionized in aqueous solutions, forms charged functional ligands such as amino, carboxyl and sulphonated groups (Luo & Wan 2013b). In addition to dissociation of surface functional groups, membranes acquire charge either along the surface or on pores by adsorption of charged species such as ions, polyelectrolytes, ionic surfactants and macromolecules from the solutions (Schaep & Vandecasteele 2001; Teixeira et al. 2005). Polyamide is a popular group of membranes which have both weak acidic carboxyl groups (–COOH) and basic amine groups ($–NH_2$) on the surface, which enable them to acquire either a positive or negative charge, which depends on the pH, concentration and type of ionic species in electrolyte solutions and the ratio between acidic and basic surface groups (Kukizaki 2009; Rice et al. 2011). On other hand, the SO_3H group, which is the active layer in polysulphone and polyether sulphone, is a strongly acidic group which dissociates over nearly the entire pH range (Wang et al. 2006).

4.2 Materials and methods

All experimental procedures as well as descriptions of EKA are provided in Sections 3.1.2.2 and 3.1.1.2, respectively.

4.3 Results and discussion

4.3.1. Electrokinetic study

The effect of solutions chemistry on zeta potential has been studied extensively in the literature, in which different types of electrolytes were used. Section 2.2.2.4.1 in the Literature Review and Table A 2.1 (see the Appendix) provides a summary of these studies and the most important findings, while the ways used to analyse pH-ζ curves are mentioned in Section 2.2.1.4.

The electrokinetic study curves of the four membranes with NaCl, KCl, Na_2SO_4, $CaCl_2$, $MgCl_2$ and $MgSO_4$ at 10^{-3}M, 10^{-2}M and 0.025M are shown in Figures 4.1, 4.2, 4.3 and 4.4. Higher concentrations (10^{-1}M) were tested with Desal DK, but the obtained results were not accurate due to significant scattering; this problem of scattering was also experienced by other researchers (Dina et al. 2001). The results show that as the salts' concentration increases, the absolute zeta potential value decreases. The reason behind this phenomenon is the compression of the double layer, which leads to shortening the distance between the membrane surface and the surface of shear (Dina et al. 2001). Furthermore, counter ions can penetrate the compact layer which reduces the charge density in diffuse layers (Zhao et al. 2005). Another observation when the absolute zeta potential values for the four membranes are compared is that NF99HF and NF270 have the highest charge, followed by Desal DK, while NTR7450 has the lowest charge. Zeta potential curves obtained with Desal DK , NF270 and NF99HF in these experiments were characteristic of amphoteric surface or surfaces with both acidic and basic functional groups (Chiu & James 2007; Chun et al. 2003; Yang et al. 2003). The polyamide NF membrane shows positive surface charge below the isoelectric point, which results from the protonation of the amine functional groups ($=NH_2 \rightarrow =NH^{3+}$), and the negative charge above the isoelectric point is a result from deprotonating of the carboxyl groups ($=COOH \rightarrow =COO^-$) (Childress & Elimelech 2000). The selective adsorption of cations and anions on the membranes' surface can shift the pH of the isoelectric point (i.e.p) to the higher or lower pH values, respectively (Mullet et al. 1997; Zhao et al. 2005). Based on that, the zeta potential curves for Desal DK (Figure 4.1) shows that the i.e.p of Na_2SO_4 (Figure 4.1C) and $MgSO_4$ (Figure 4.1D) shifts from pH 4 at 10^{-3}M to pH 3 at 0.025M. This means that there is specific adsorption of SO_4^{2-} ions on the surface of Desal DK. Furthermore, moving of the i.e.p to lower values at both concentration with NaCl and KCl from 4.5 at 10^{-3}M to pH 3 at 0.025M is an indication of the selective adsorption of Cl^- on the membrane surface. Shifting of the i.e.p of $CaCl_2$ (Figure 4.1F) and $MgCl_2$ (Figure 4.1E) with increasing concentration toward lower pH value is an indication that Cl^- has more

affinity than Ca^{2+} and Mg^{2+}. However, Ca^{2+} and Mg^{2+} make the surface of the membrane more positive at higher pH, which shows that they have more affinity to the Desal DK surface than K^+ and Na^+. This can be explained by the fact that the adsorption of Ca^{2+} ions on the membranes' surfaces are favourable because of forming a chemical complex with the surface functional groups (Yang et al. 2003; Szymczyk et al. 1997). As is the case with Desal DK and NF99HF (Figure 4.3), NF270 (Figure 4.2) shows a good affinity toward Cl^- and SO_4^{2-}. However, unlike Desal DK and NF99HF, the i.e.p of $CaCl_2$ (Figure 4.2 F) and $MgCl_2$ (Figure 4.2 E) moved from pH 3.8 at 0.001M to pH 5 at 0.025M, which indicates very high adsorption of $Ca^{2+}$and Mg^{2+}. Furthermore, the i.e.p of $MgSO_4$ (Figure 4.2 D) does not change as a good indication of identical adsorption of Mg^{2+} and SO_4^{2}.

NF99HF (Figure 4.3) shows selective adsorption of SO_4^{2-} ions and the adsorption of Ca^{2+} causes increase in the i.e.p of $CaCl_2$ (Figure 4.3F) from pH 3.5 at 0.001M to pH 4 with 0.01M. However, very slight or even non-existent change of i.e.p has been noticed for KCl, NaCl and $MgSO_4$. The independent of i.e.p on the salt concentration is an indicator of either absence or identical adsorption of co and counter ions on the membrane surface. Since SO_4^{2-} adsorbs to the surface of NF99HF as mentioned at the beginning of the paragraph, the reason that makes the i.e.p not change with $MgSO_4$ (i.e.p at pH 3.4) is the adsorption of Mg^{2+}.

The zeta potential curves (Figure 4.4) for NTR7450 are typical for strongly acidic materials (Möckel et al. 1998) since the membrane did not give any isoelectric point at the range of pH 3.5 to 10 values. Therefore, the membrane is almost at its ultimate negative charge over the entire pH range studied. It was found that the membrane had very high affinity toward Cl^- and SO_4^{-2}, followed by $Ca^{2+}$and Mg^{2+}. This can be explained by the fact that anions can approach closer to hydrophobic surfaces (such as the PES membrane) (Salg et al. 2013). The results also show that NTR7450 is weakly charged as compared to the other membranes. The results were consistent with other researchers' findings (Mänttäri et al. 2006; Salg et al. 2013).

To sum up, the electrokinetic study shows that Desal DK has the following affinity sequence: $SO_4^{2-} > Cl^- > Mg^{2+}$, $Ca^{2+} > Na^+$, K^+. NF 270 shows a good affinity to Cl^- and SO_4^{-2}. However, Ca^{2+} and Mg^{2+} have higher affinity than Cl^-, so the affinity sequence is: Ca^{2+}, Mg^{2+}, $SO_4^{2-} > Cl^- > Na^+$, K and NF99HF $SO_4^{2-} > Mg^{2+}$, $Ca^{2+} > Cl^- > Na^+$, K^+.

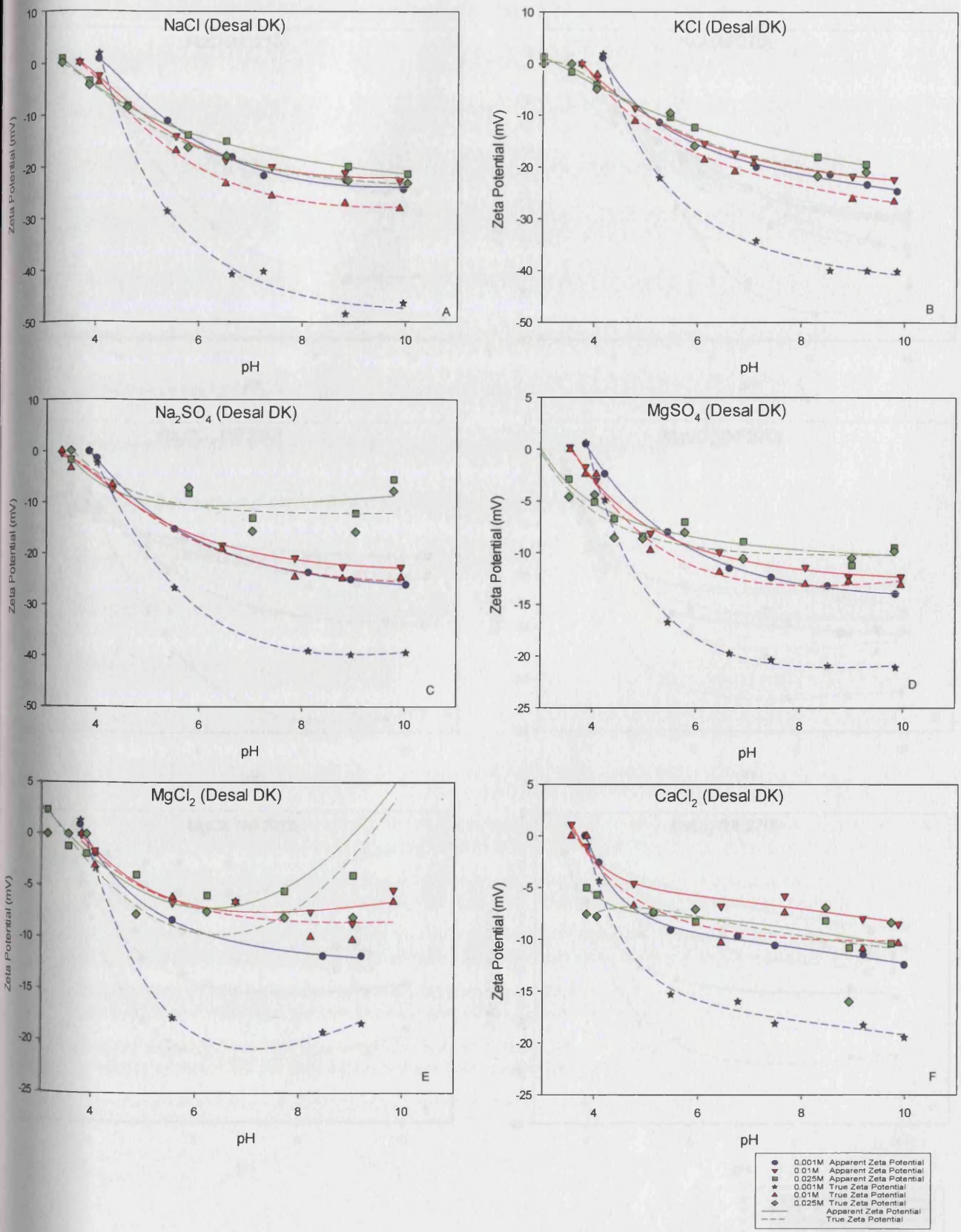

Figure 4.1: Zeta potential of Desal DK at different pH values and concentrations.

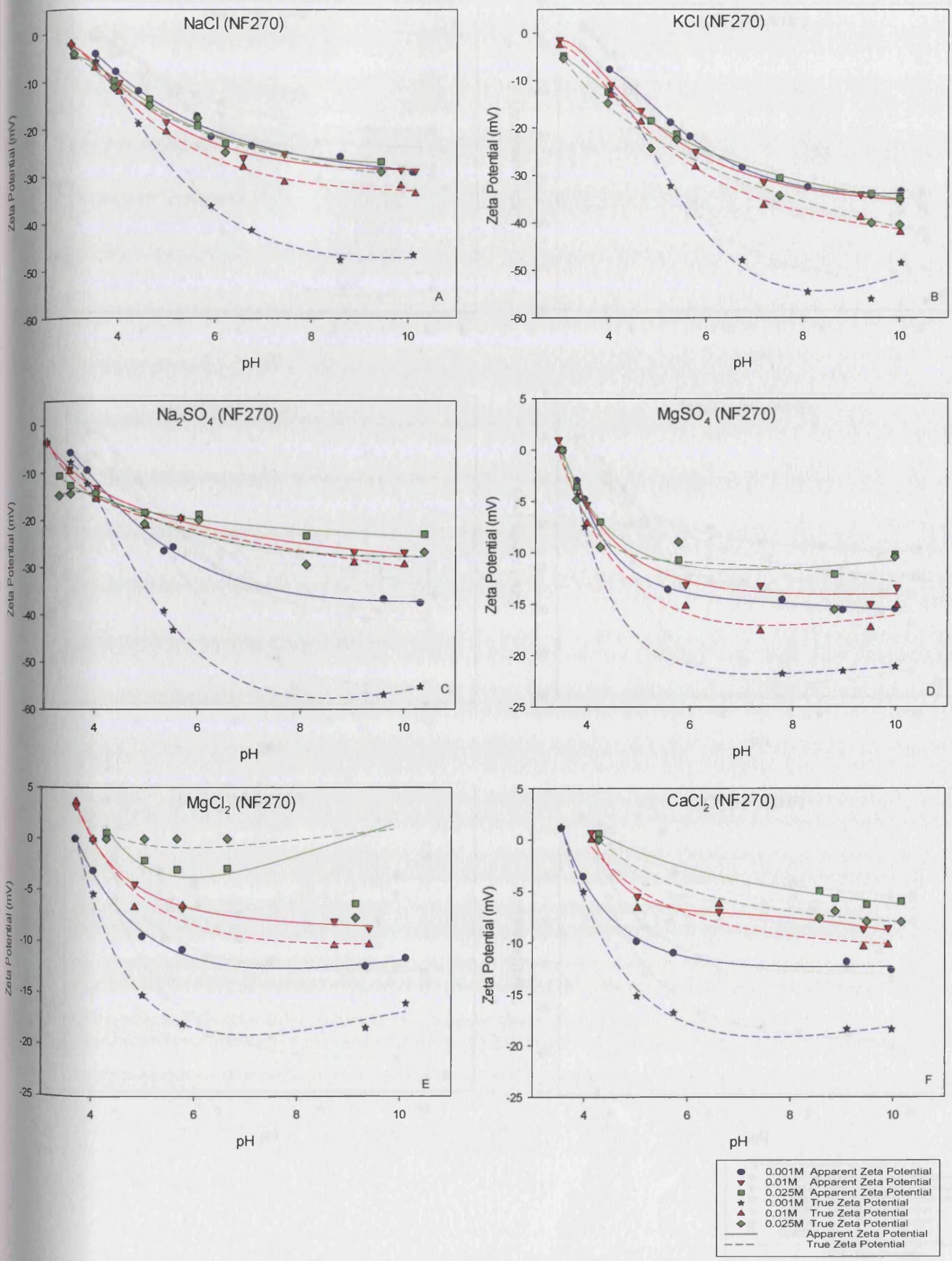

Figure 4.2: Zeta potential of NF270 at different pH values and concentrations.

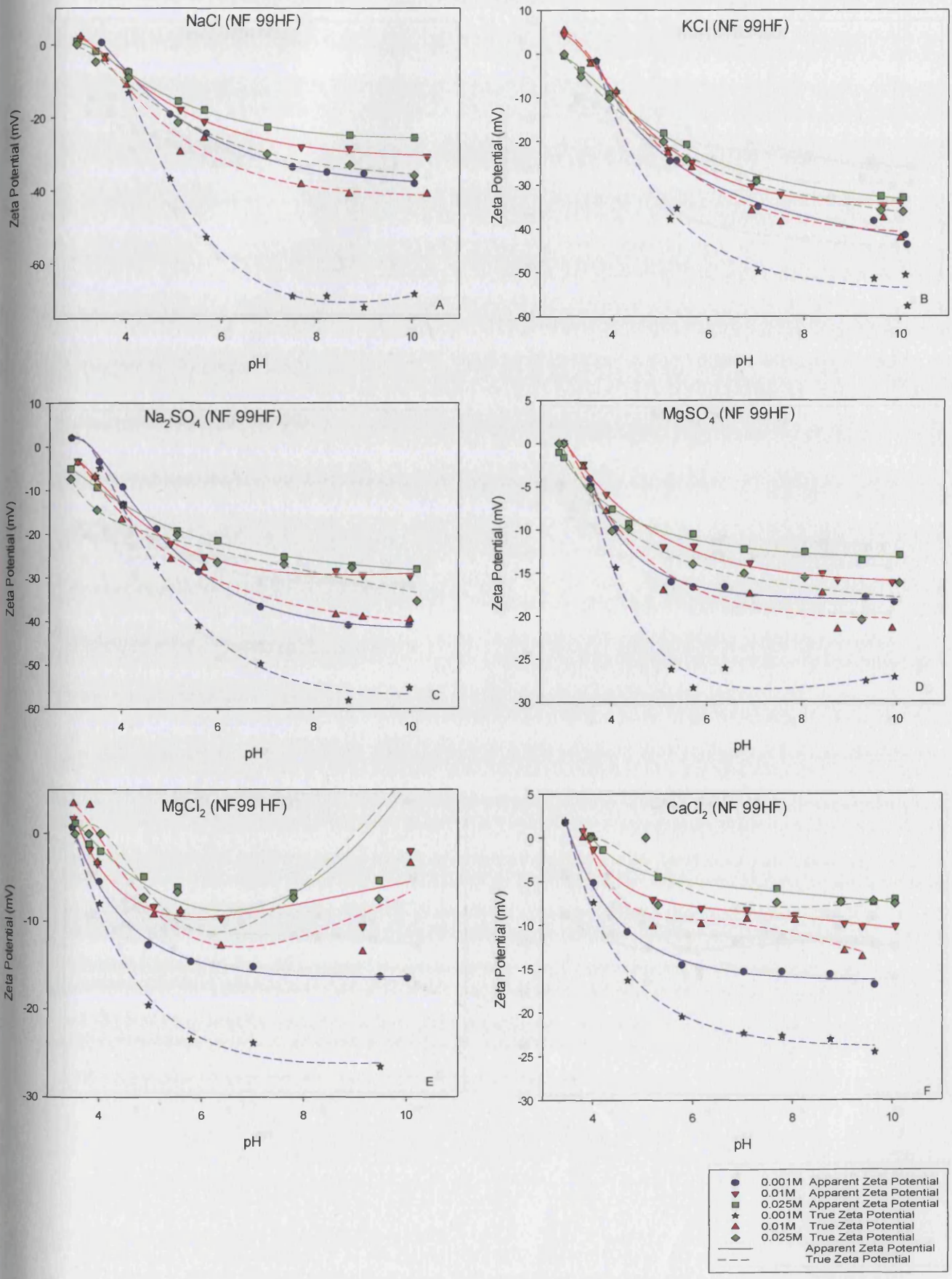

Figure 4.3: Zeta potential of NF99HF at different pH values and concentrations.

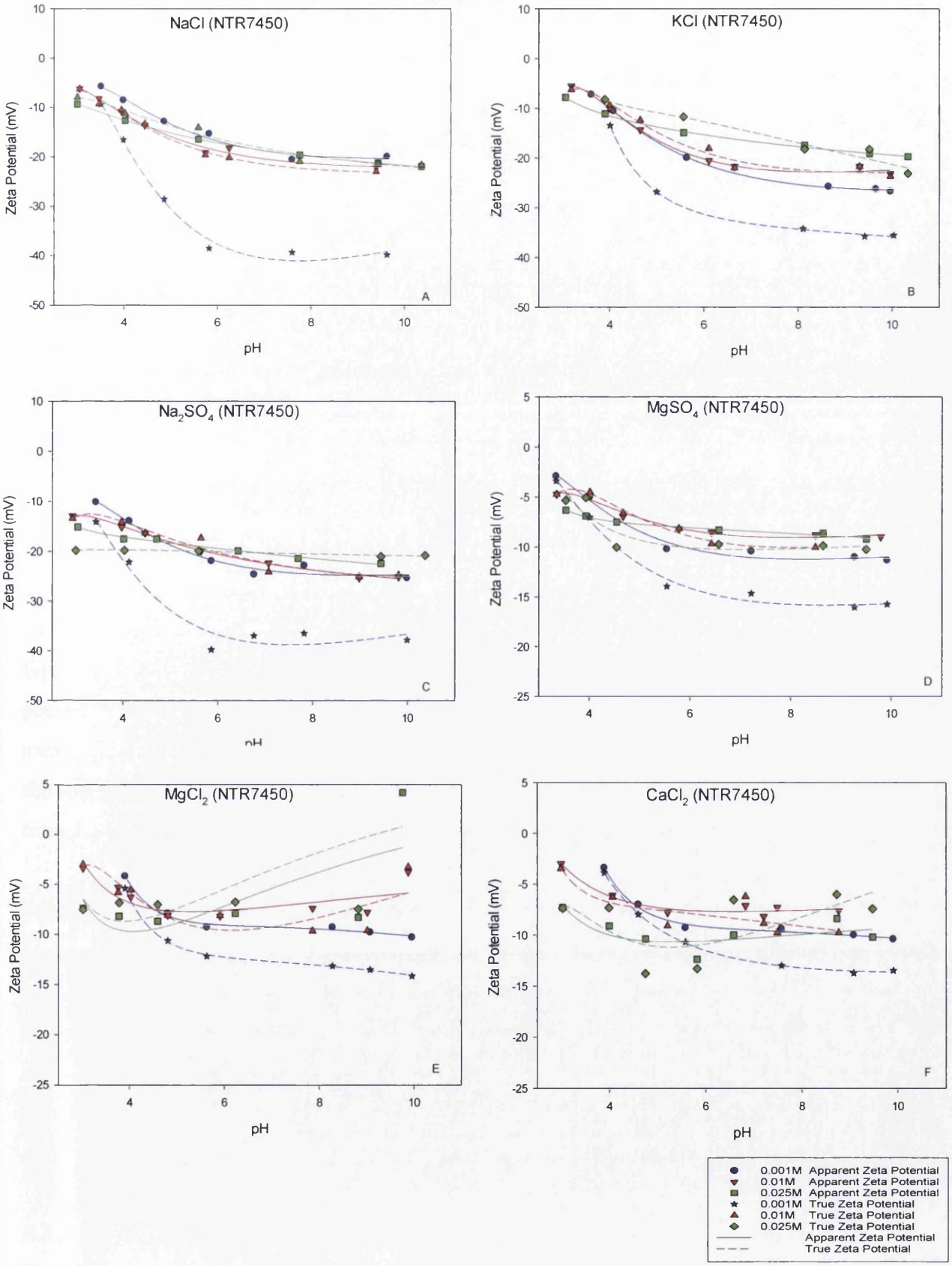

Figure 4.4: Zeta potential of NTR7450 at different pH values and concentrations.

4.3.2 Reproducibility and equilibration experiments

Reproducibility of the zeta potential experiments and the time required to establish equilibrium between solution ions and membrane surface in order to optimize the measurement are described in Section 2.2.1.3.4. Childress and Elimelech (1996) compared the streaming potential results of two different samples of the same membrane. Eight of the 9 measurements for the two different samples varied by less than 1 mV (~10%). Furthermore, the study found that new membrane samples should be used each day; the results varied by more than 2 mV when a membrane sample was reused the next day after being stored overnight in the measuring cell. The equilibration time length found in the literature varied from 30 minutes (Childress & Elimelech 1996), 1 hour (Ariza & Benavente 2001), 12 hours (Zhao et al. 2005; Hagmeyer & Gimbel 1998), overnight (Szymczyk et al. 2007), 24 hours (Wang & Ku 2006) to more than one day (Dina et al. 2001; Wilbert et al. 1999). In this study, the zeta potential values of two membrane samples of NF99HF from different batches were compared (Figure 4.5 A) and no major difference in the results was observed. Comparison between virgin and used membrane samples of NF270 was also conducted (Figure 4.5 B). The results of comparing the zeta potential values of virgin membrane and membrane that had been used to measure zeta potential for different electrolytes were in good agreement. Equilibration time was also studied for NF270 and NF99HF (Table 4.1) by measuring zeta potential after the electrolyte had been circulated in the machine for 30 minutes and the measurement was repeated after 24 hours after the membrane had been stored overnight in the measuring cell. The values of zeta potential were not subject to change during the soaking time, which showed that 30 minutes were enough to establish equilibration.

Table 4.1: Zeta potential values before and after 24 hours' soaking.

	First measurement		After 24 hours		
Membranes	pH	Zeta potential (mv)	pH	Zeta potential (mv)	Difference (mv)
NF270	5.49	-17.8	5.56	-16	1.8
NF99HF	6.45	-25.8	6.21	-25.6	0.2

4.3.3 Surface conductivity correction

The zeta potential calculated with Equation 3.1 is called apparent zeta potential, where no surface conductivity which mainly affects at low ion concentrations is taken into account.

Therefore, Equation 3.1 must be modified to take this fact into account and the zeta potential that will obtained is called true zeta potential.

The correction in surface conductivity for a given pH value at a given electrolyte only changes the magnitude of the potential value, but does not affect the position of the i.e.p and/or the shape of the zeta potential-pH curve (Ernst et al. 2000). Therefore, the need to use surface correction only appears in quantitative studies cases, not qualitative research. It is clear that the contribution of this effect is huge at low concentrations (Ariza et al. 2001). Ariza et al. (2001) have compared apparent and corrected zeta potential results and show a significant discrepancy (higher than 50%) between both values at low concentrations ($C \leq 10^{-3}$ M), while at higher concentrations, the differences are around 10%. The effect has been studied in this work (Figures 4.1 to 4.4) and the results indicate that differences are large at 10^{-3} M and start to reduce at higher concentrations (10^{-2}M, 0.025M). In fact, at 0.025M, this effect could be neglected. For example, the maximum difference with Desal DK was only 10%.

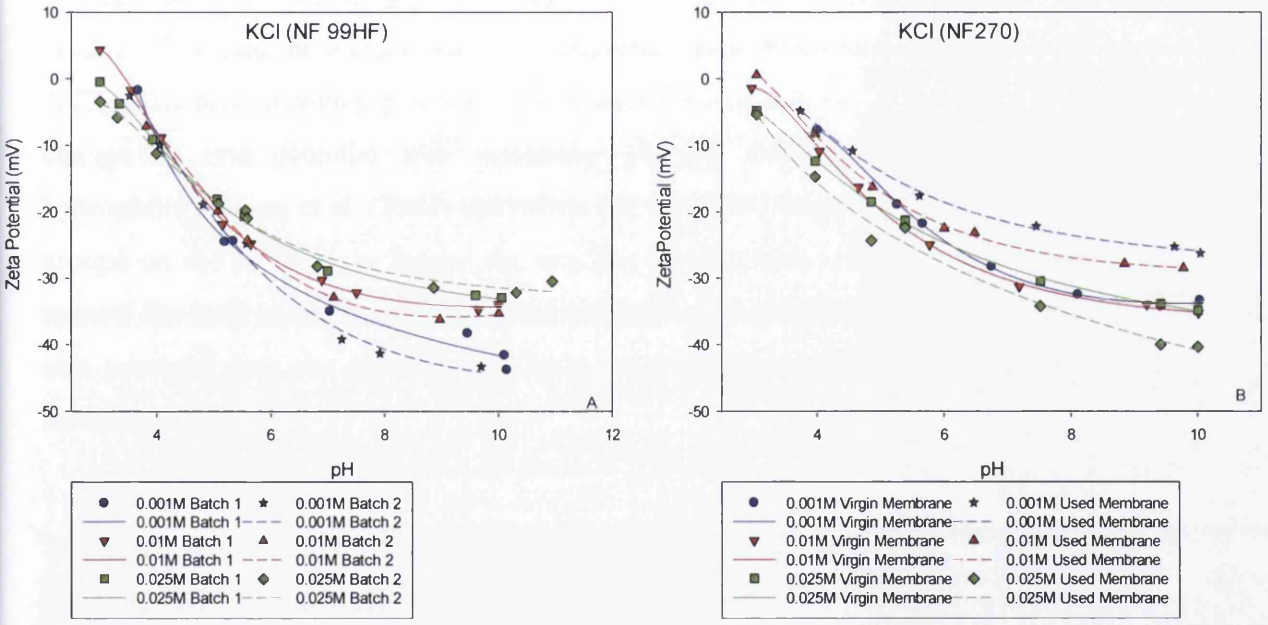

Figure 4.5: Zeta potential measurements optimization data.

4.3.4 Zeta potential and contact angle

Contact angle measurements were performed (see Section 3.5.4), which showed that NF270 is the most hydrophilic of the membranes, with 22°. This result agrees with what Almalek (2012) found, while Artuğ et al. (2007) could not measure NF270 as a result of the highly hydrophilic surface and they estimated the contact angle as less than 10°. Desal DK and

NTR7450 have contact angles of 54° and 70°, respectively. Polyethersulphone membranes like NTR7450 are more hydrophobic than polyamide membranes (Salg et al. 2013). The results of contact angle measurement shows the same trend of electrokinetic study (Section 4.3.1) in which the absolute zeta potential values of NF99HF and NF270 have the highest charge followed by Desal DK, while NTR7450 has the lowest charge. Mänttäri et al. (2006) studied the relation between zeta potential and contact angle. It was found that the lower the membrane contact angle (more hydrophilic membrane), the higher was the change in the apparent zeta potential when pH was increased from 4 to 7. The dissociation of carboxylic and amine groups on the surface of the NF200 membrane resulted in an increase in hydrophilicity, while NTR7450 showed the most hydrophobic surface. Hurwitz et al. (2010) found that zeta potentials calculated from contact angle and streaming potential show the same trend, but were quantitatively different. This study combined contact angles, acid–base surface tensions and solid–liquid interfacial free energies to show that the polyamide membrane used in this study became more electron donor functionalized, more wet and less hydrophobic with increasing pH, salinity and divalent cation content in the electrolyte. Rice et al. (2011) used three techniques to characterize three membranes, namely contact angles, ATR-FTIR and streaming potential. The results showed that the membrane with the lowest change in zeta potential with increasing pH has the highest contact angle (lowest hydrophilic). Wang et al. (2006) and Möckel et al. (1998) found that the more functional the groups on the surface, the longer the swelling layer, which leads to a shift of shear plane toward the bulk solution and lower zeta potential plateau values were obtained. Therefore, zeta potential data can give valuable hints about the chemical nature and hydrophilicity of membrane surfaces.

4.4 Conclusion

The electrokinetic study of four NF industrial polyamide membranes, namely Desal DK, NF99HF, NF270 and NTR7450 were performed with six different electrolytes, NaCl, KCl, Na_2SO_4, $CaCl_2$, $MgSO_4$ and $MgCl_2$, at three different concentrations, 10^{-3}M, 10^{-2}M and 0.025M, and different pH values. The aim of this experimental study was to investigate the effect of electrolyte type and concentration at different pH values on the membranes' charge, which affects the membranes' separation performance, in turn. The obtained zeta potential values were used to explain the specific adsorption of ions to membrane surface and to determine membrane isoelectric points (i.e.p) by studying the shape of pH-zeta curves. The results led to the conclusion that the polyamide membranes have an amphoteric surface,

while the NTR7450 (polyethersulphone) is a strongly acidic membrane: the zeta potential values decreased in negative magnitude when ionic strength was increased. The selective adsorption of ions on the membrane surfaces show that all the membranes have affinity towards SO_4^{2-}, Cl^-, Ca^{2+} and Mg^{2+} to differing extents. On the other hand, the adsorption of sodium and potassium to the surface of these nanofiltration membranes is very low. The result of this comprehensive zeta potential study shows that pH values of the isoelectric point (i.e.p) at various ionic strengths are between 3.5 and 4, except for NTR740 where no i.e.p was found. The order of absolute ζ values in general from large to small is: NaCl, KCl, Na_2SO_4 > $MgSO_4$ > $MgCl_2$, $CaCl_2$, this found sequence found by other researchers (Ding et al. 2006), while NF99HF and NF270 show higher zeta values than the other two. Reproducibility, equilibration time and surface conductivity were studied in order to optimize the zeta potential measurement. The results indicate that there is no need to use a fresh membrane every time you do new measurements. Furthermore, it was found that 30 minutes is long enough to establish equilibration (Table 4.1). The study of the effect of surface conductivity indicates that differences between apparent and corrected zeta potential are large at 10^{-3} M and start to reduce at higher concentrations (10^{-2}M, 0.025M). In fact, at 0.025M, this effect could be neglected as the difference was very small.

5.0 Charge Characterization of NF Membranes in a Ternary Salt System

In Chapter 4, tangential streaming potential (TSP) was used to assess the membrane charge and interaction between the solute and membrane charge in single salt systems. In this chapter, the complexity of the work is enhanced by mixing two salts with an ion in common and measuring the zeta potential. The aim of this is to study the effect of the type of the electrolyte and concentration for ternary ions mixtures at different pH on zeta potential values. The obtained zeta potential results were used to explain the specific adsorption of a certain ion/ions to membrane surface, determine isoelectric points and study the amphoteric behaviour of the membranes under investigation. Studying this interaction between the solute and membrane charge will improve fundamental understanding of the membrane separation mechanism in mixture solution systems, which will help to increase the efficiency of the NF process.

5.1 Relevant theory

The relevant theory required for this chapter is provided in Chapter 4.

5.2 Materials and methods

All experimental procedures as well as description of the EKA are provided in Chapter 3, Sections 3.1.2.3 and 3.1.1.2, respectively, while the chemistry of filtered solutions is available in Table 3.2.

5.3 Results and discussion

5.3.1 Effect of pH on zeta potential

The effect of pH on zeta potential for Desal DK, NF270, NF99HF and NTR7450 is shown in Figures 5.1 to 5.4. In order to do this, the zeta potential of the five ion combinations were drawn at different pH values as a function of the percentage concentration of one of the ions that was being compared. Percentage of Na was used for all mixtures that contained Na, namely Na-K, Na-Ca and Na-Mg (Figures A, B and C), while Ca and Cl percentages were used with Ca-Mg (Figures D) and Cl-SO_4 (Figures E), respectively. The difference in the manganite of membrane surface charge of the four membranes can be identified from the zeta potential of NaCl as this salt has the lowest effect on the membrane charge, i.e. NaCl has poor adsorption toward membrane surface as was seen in Chapter 4. The sequence of absolute zeta potential at pH 4 was as follows (Figure A in Figures 5.1 to 5.4): NF99HF, NF270, NTR740 > Desal DK. At pH higher than 4, the sequence of absolute zeta potential

was as follows: NF99HF, NF270 > NTR740, Desal DK. The reason for NTR7450 having high absolute zeta potential value is that polyethersulphone reaches its ultimate negative charge before polyamide membranes. The obtained order confirmed the sequence found in the single salts study in Chapter 4. Absolute zeta potential values for all membranes increased with increasing pH; however, NTR7450 showed slight change as compared to the other membranes. This can be explained by the fact that polyethersulphone reaches its ultimate negative charge at very low pH (Möckel et al. 1998).

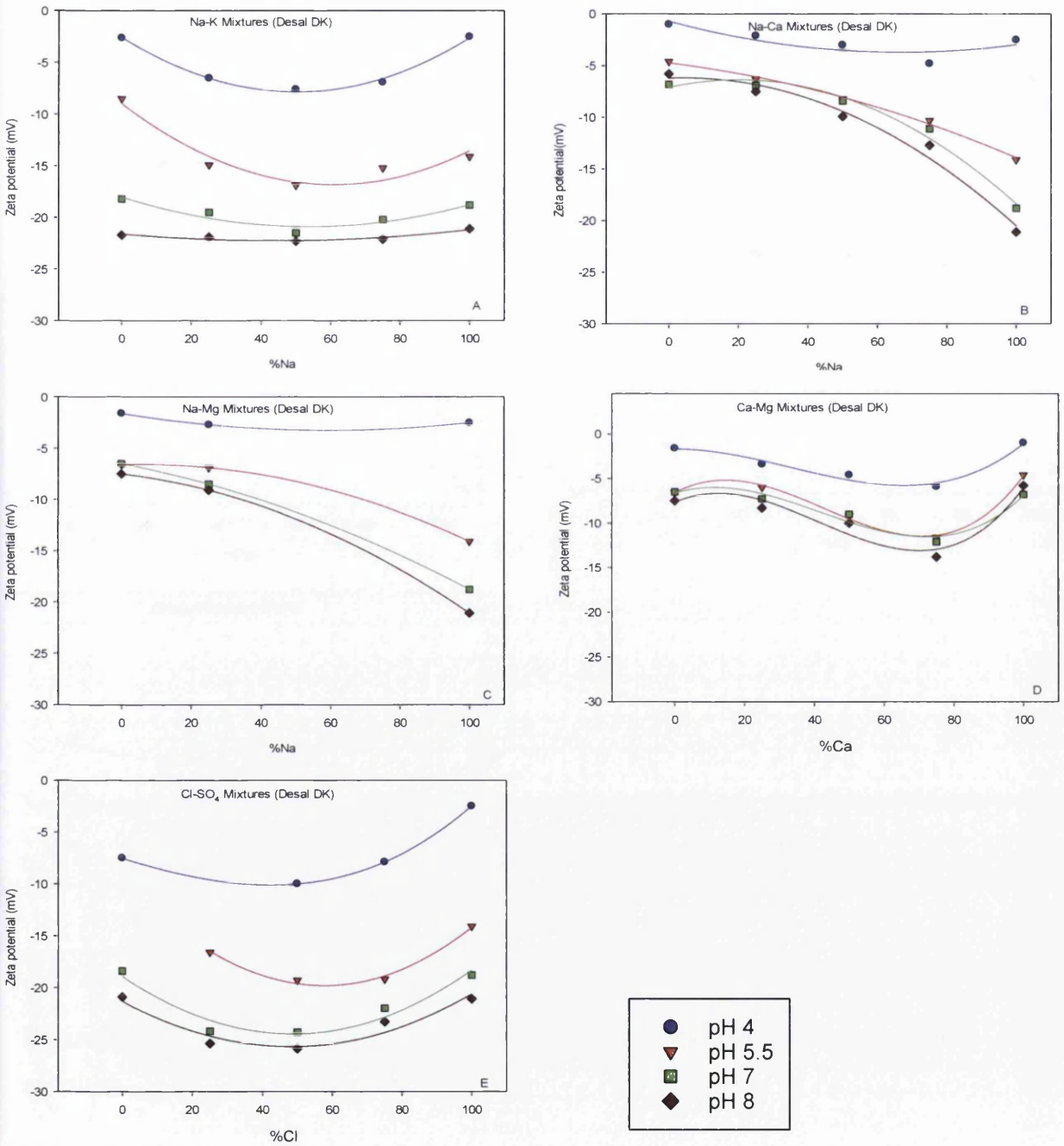

Figure 5.1: Desal DK zeta potential results as a function of pH for different ion combination solutions.

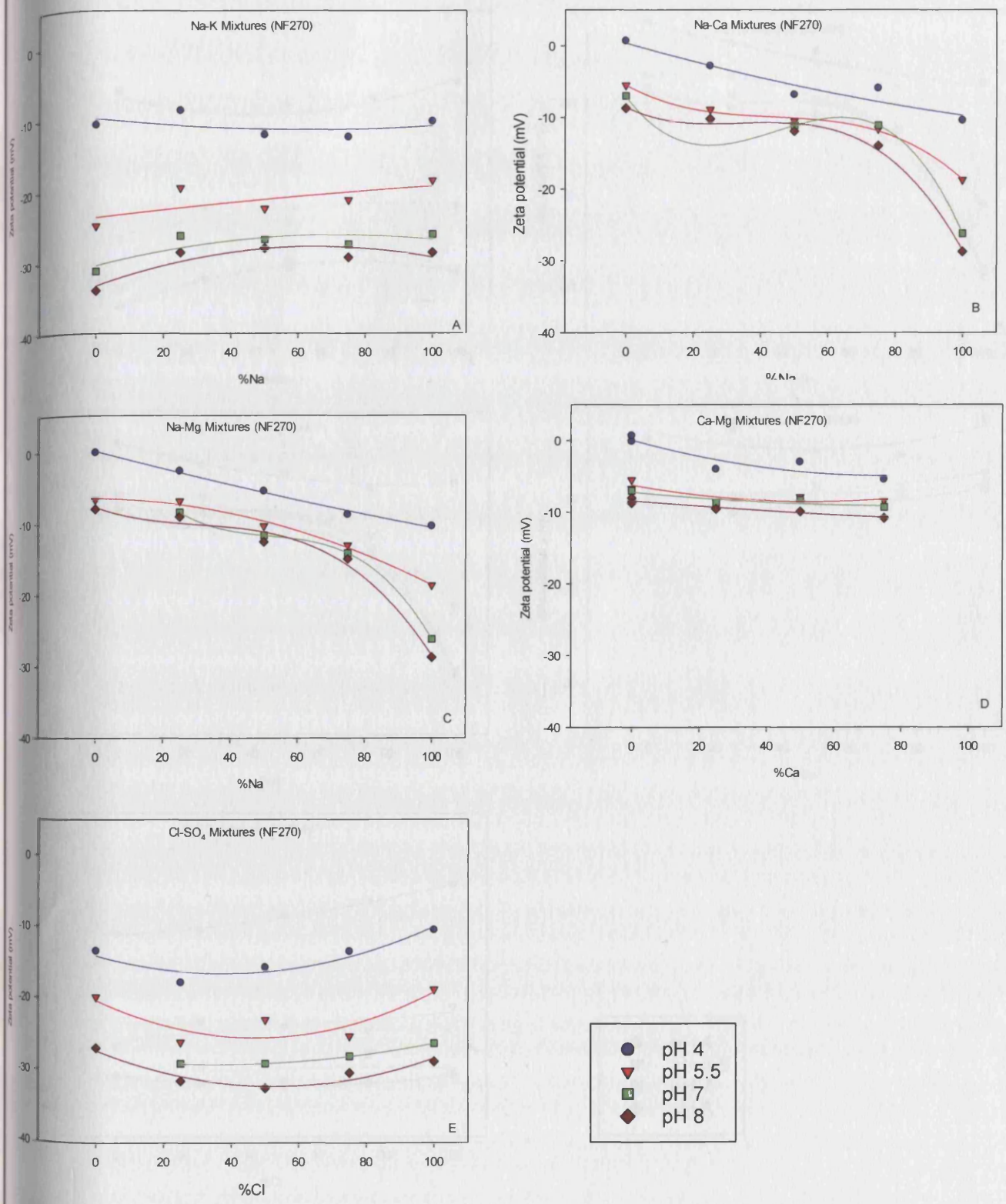

Figure 5.2: NF270 zeta potential results as a function of pH for different ion combination solutions.

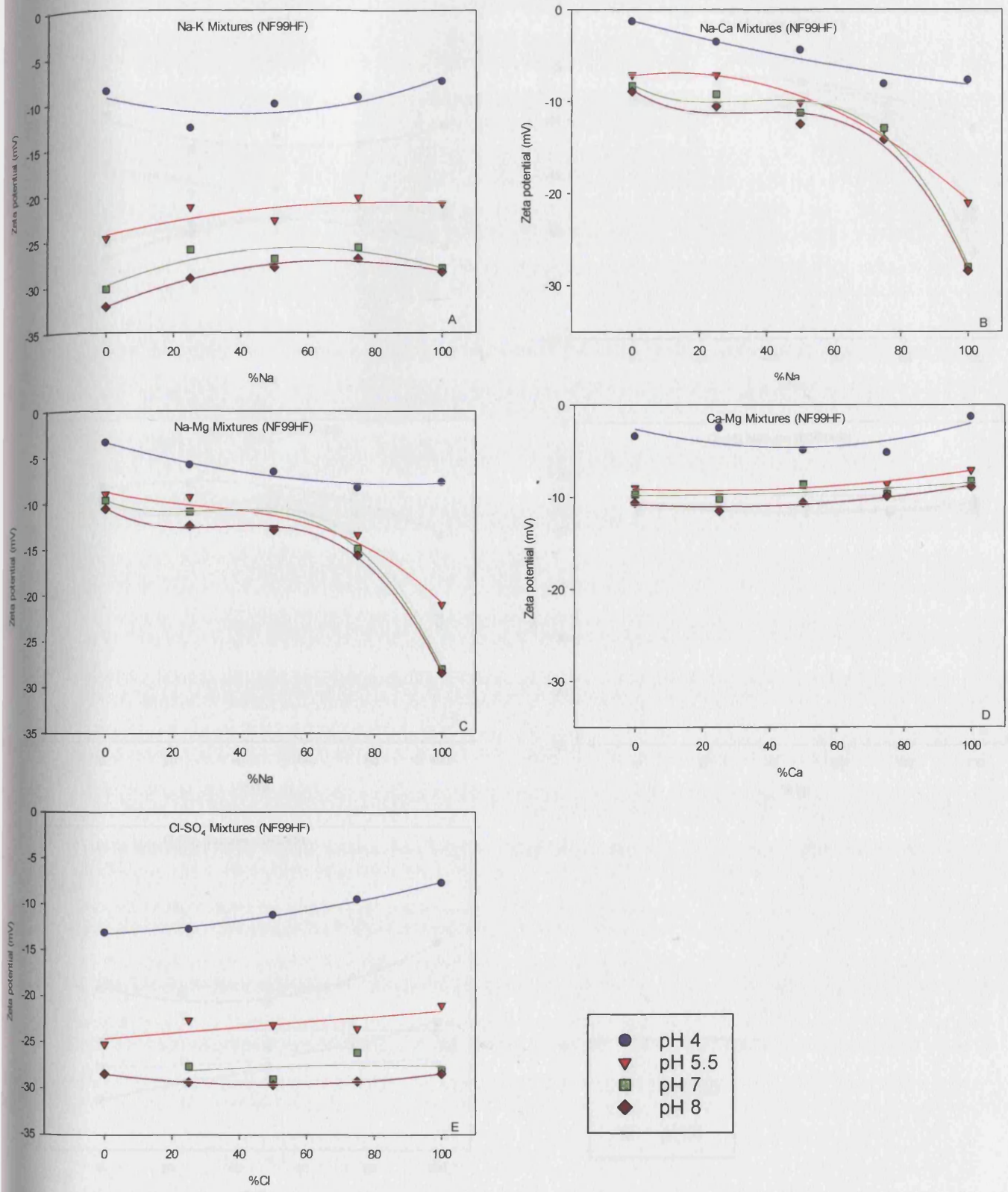

Figure 5.3: NF99HF zeta potential results as a function of pH for different ion combination solutions.

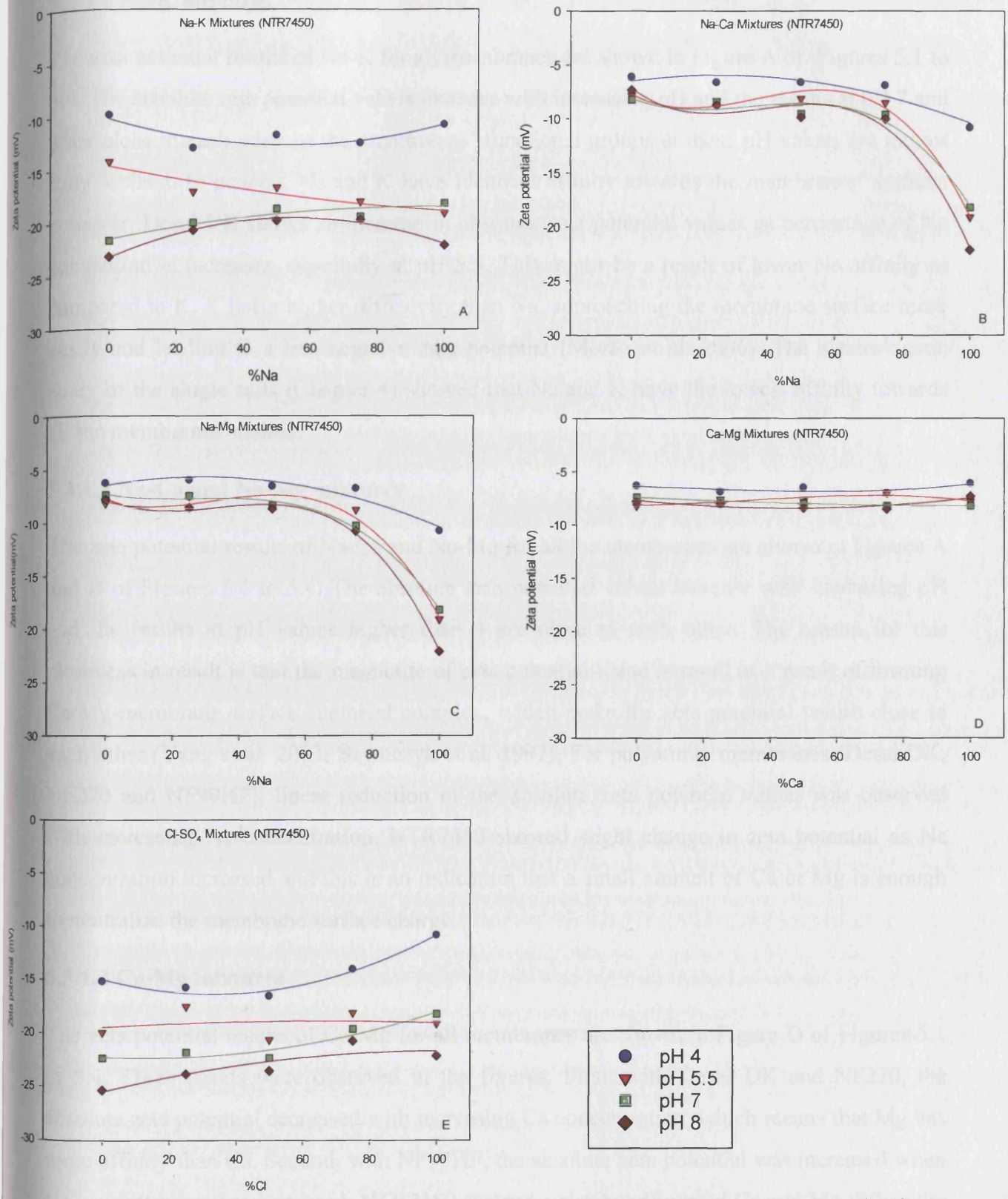

Figure 5.4: NTR7450 zeta potential results as a function of pH for different ion combination solutions.

5.3.1.1 Na-K mixtures

The zeta potential results of Na-K for all membranes are shown in Figure A of Figures 5.1 to 5.4. The absolute zeta potential values increase with increasing pH and the results at pH 7 and 8 are close to each other as the membranes' functional groups at these pH values are almost fully ionized. In general, Na and K have identical affinity towards the membranes' surface; however, Desal DK shows an increase in absolute zeta potential values as percentage of Na concentration increases, especially at pH 5.5. This might be a result of lower Na affinity as compared to K. K has a higher diffusivity than Na, approaching the membrane surface more easily and leading to a less negative zeta potential (Morão et al. 2006). The electrokinetic study of the single salts (Chapter 4) showed that Na and K have the lowest affinity towards all the membranes studied.

5.3.1.2 Na-Ca and Na-Mg mixtures

The zeta potential results of Na-Ca and Na-Mg for all the membranes are shown in Figures A and B of Figures 5.1 to 5.4. The absolute zeta potential values increase with increasing pH and the results at pH values higher than 4 are close to each other. The reason for this closeness in result is that the magnetite of zeta potential value is small as a result of forming Ca/Mg-membrane surface chemical complex, which make the zeta potential values close to each other (Yang et al. 2003; Szymczyk et al. 1997). For polyamide membranes (Desal DK, NF270 and NF99HF), linear reduction of the absolute zeta potential values was observed with increasing Na concentration. NTR7450 showed slight change in zeta potential as Na concentration increased and this is an indication that a small amount of Ca or Mg is enough to neutralize the membrane surface charge.

5.3.1.3 Ca-Mg mixtures

The zeta potential results of Ca-Mg for all membranes are shown in Figure D of Figures 5.1 to 5.4. Three trends were observed in the figures. First, with Desal DK and NF270, the absolute zeta potential decreased with increasing Ca concentration, which means that Mg has more affinity than Ca. Second, with NF99HF, the absolute zeta potential was increased when Ca concentration was increased. NTR7450 showed a similar affinity of Ca and Mg. When the absolute zeta potential of Ca-Mg mixtures for all the membranes were compared, the following sequence was obtained: Desal DK > NF270, NF99HF > NTR7450. This sequence supports the hypothesis that NF270 and NF99HF have the highest affinity toward Ca and Mg among all the membranes, as the reduction in their Na-K mixtures' absolute zeta potential is

huge, which is due to their strong affinity toward Ca and Mg. On other hand, Desal DK has the lowest surface affinity to these two ions. The zeta potential measurements of single salts (Chapter 4) showed the same trend.

5.3.1.4 Cl-SO_4 mixtures

The zeta potential results of Cl-SO_4 for all membranes are shown in Figure E of Figures 5.1 to 5.4. Sulphate shows more affinity for NF270 and NF 99HF than Desal DK and NTR7450, for Desal DK and NF270 show decrease in absolute zeta potential values with increasing Cl concentration, while NF 99HF and NTR7450 have identical affinity. However, the zeta potential measurements of single salts (Chapter 4) showed that SO_4 has the highest affinity among the other ions towards the membranes' surface.

5.3.2 Effect of cations type on zeta potential

The effect of cations type is presented in Figures 5.5 to 5.8. Three mixtures solutions were drawn as a function of Na concentration as Na ion is present in all of them, i.e. Na-K, Na-Ca and Na-Mg. Each figure represents a pH value and four pH values were selected, 4, 5.5, 7 and 8.

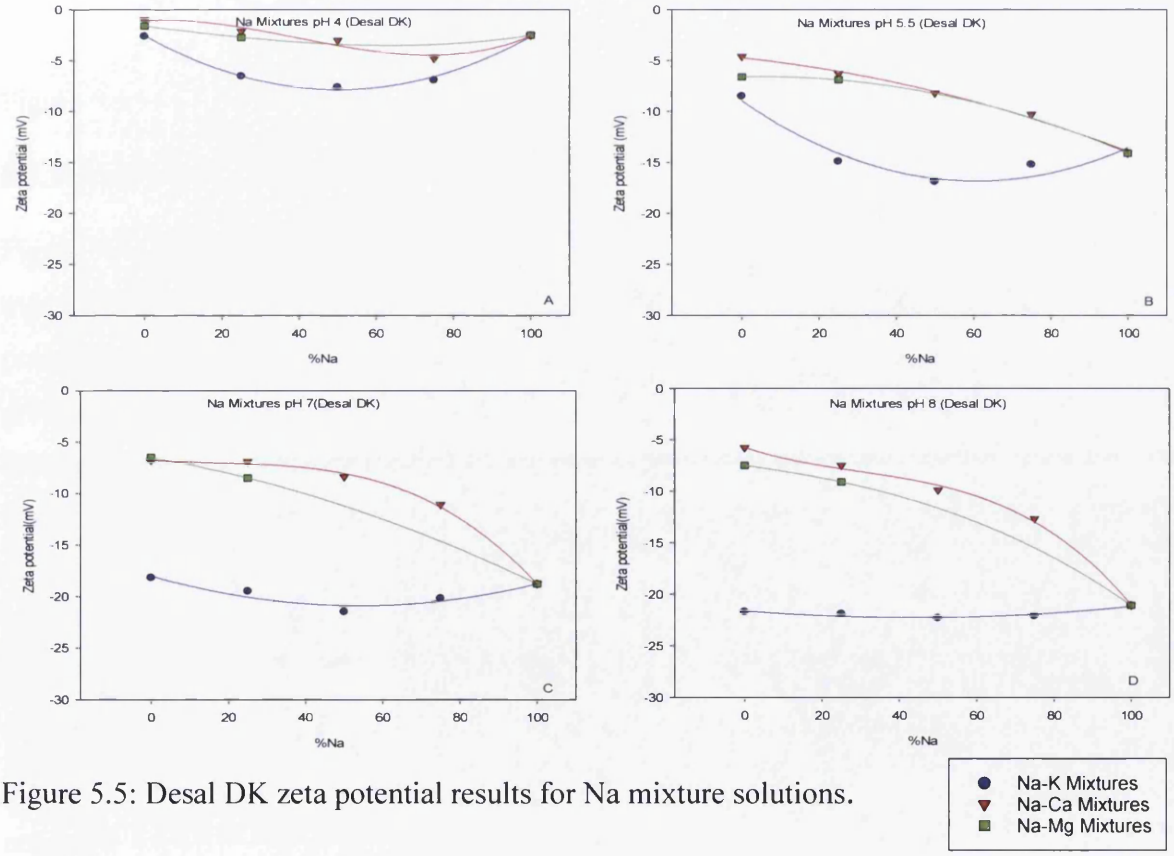

Figure 5.5: Desal DK zeta potential results for Na mixture solutions.

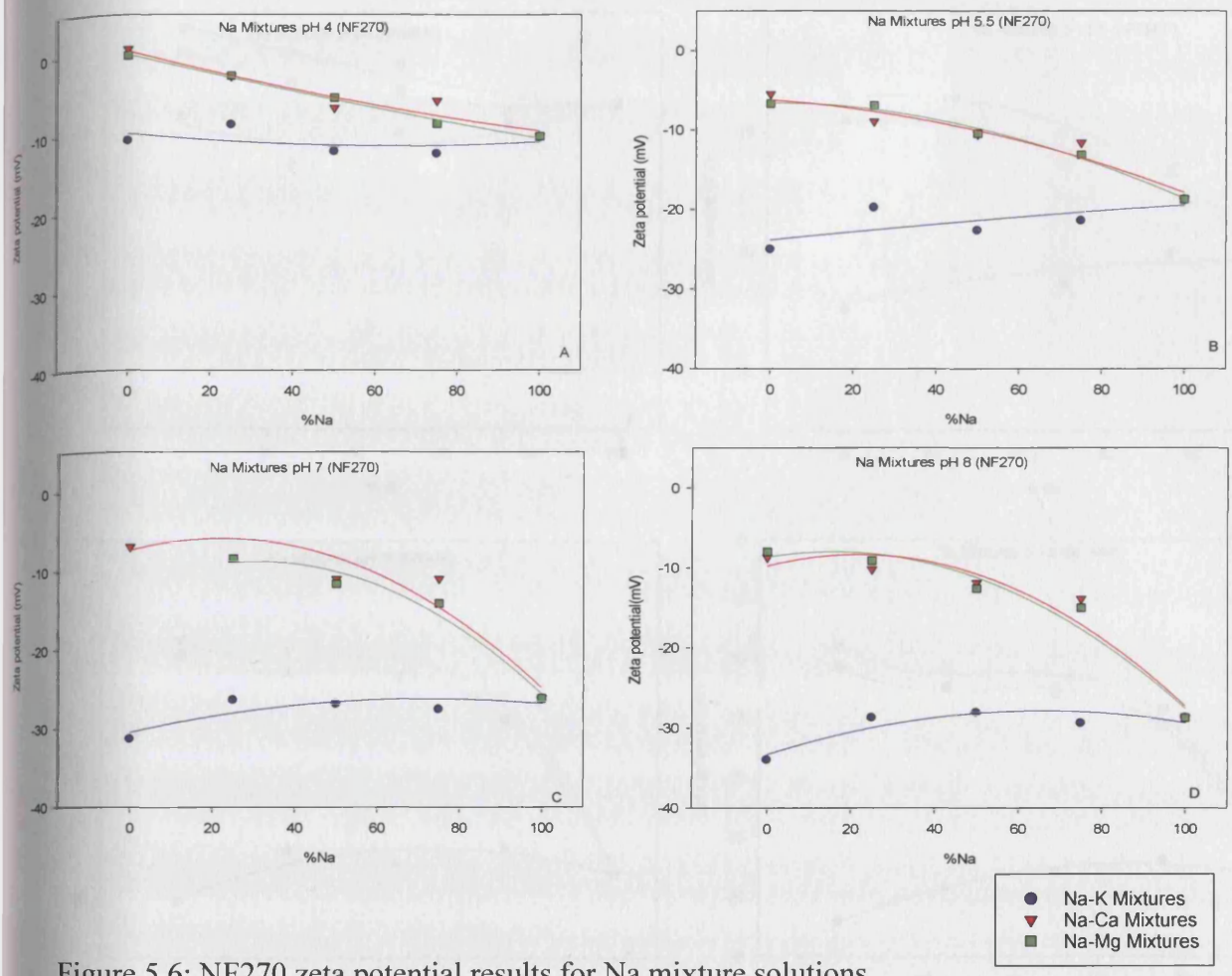

Figure 5.6: NF270 zeta potential results for Na mixture solutions.

5.3.2.1 Desal DK

Figure 5.5 shows the zeta potential values of Na-K, Na-Ca and Na-Mg for the Desal DK membrane. Replacement of K ion with Ca or Mg caused reduction in the absolute zeta potential value, which is an indication of forming a chemical complex with surface functional groups. Mg adsorbed more than Ca as its absolute zeta potential value is slightly less than that of Ca, especially at pH 4 and 5.5 as shown in Figures 5.5 A and 5.5 B. Increasing the concentration of Na in Na-K does not have any effect on the zeta potential values of the mixtures, which mean that Na and K show almost identical affinity towards the membrane surface. However, Desal DK shows increase in absolute zeta potential values as the percentage of Na concentration increases, especially at pH 5.5, as has been discussed in Section 5.3.1.1. This might be a result of lower Na affinity as compared to K. K has a higher diffusivity than Na, approaching the membrane surface more easily and leading to a less negative zeta potential. Another observation is that linear reduction of zeta potential was obtained with Mg and Ca when Na concentration was increased.

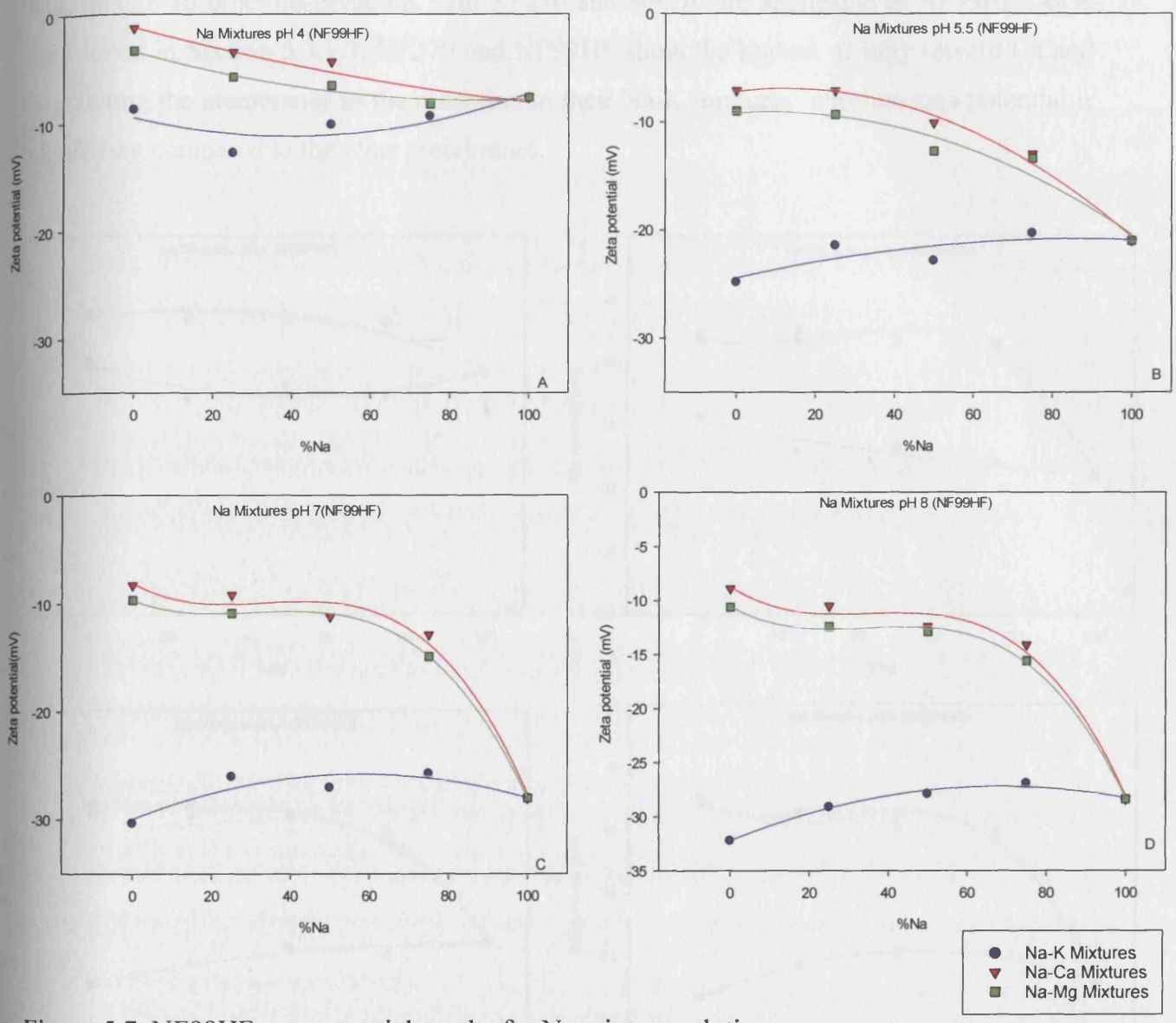

Figure 5.7: NF99HF zeta potential results for Na mixture solutions.

5.3.2.2 NF270

Figure 5.6 shows the zeta potential values of Na-K, Na-Ca and Na-Mg for the NF270 membrane. As in the case of Desal DK, Ca and Mg strongly adsorbed to the surface of NF270, while Na and K showed poor identical adsorption. Moreover, linear reduction of zeta potential was obtained with Mg and Ca when Na concentration was increased: this is applicable here as with Desal DK. However, unlike Desal DK, Ca and Mg results were almost the same as they showed identical affinity towards NF270.

5.3.2.3 NF99HF

Figure 5.7 shows the zeta potential values of Na-K, Na-Ca and Na-Mg for the NF99HF membrane. Unlike Desal DK and NF270, NF99HF has slightly more affinity toward Ca than

Mg, though all other observations with NF270 and NF270 are applicable to NF99HF. As is mentioned in Section 5.3.1.3, NF270 and NF99HF show the highest affinity toward Ca and Mg among the membranes as the reduction in their Na-K mixtures' absolute zeta potential is significant compared to the other membranes.

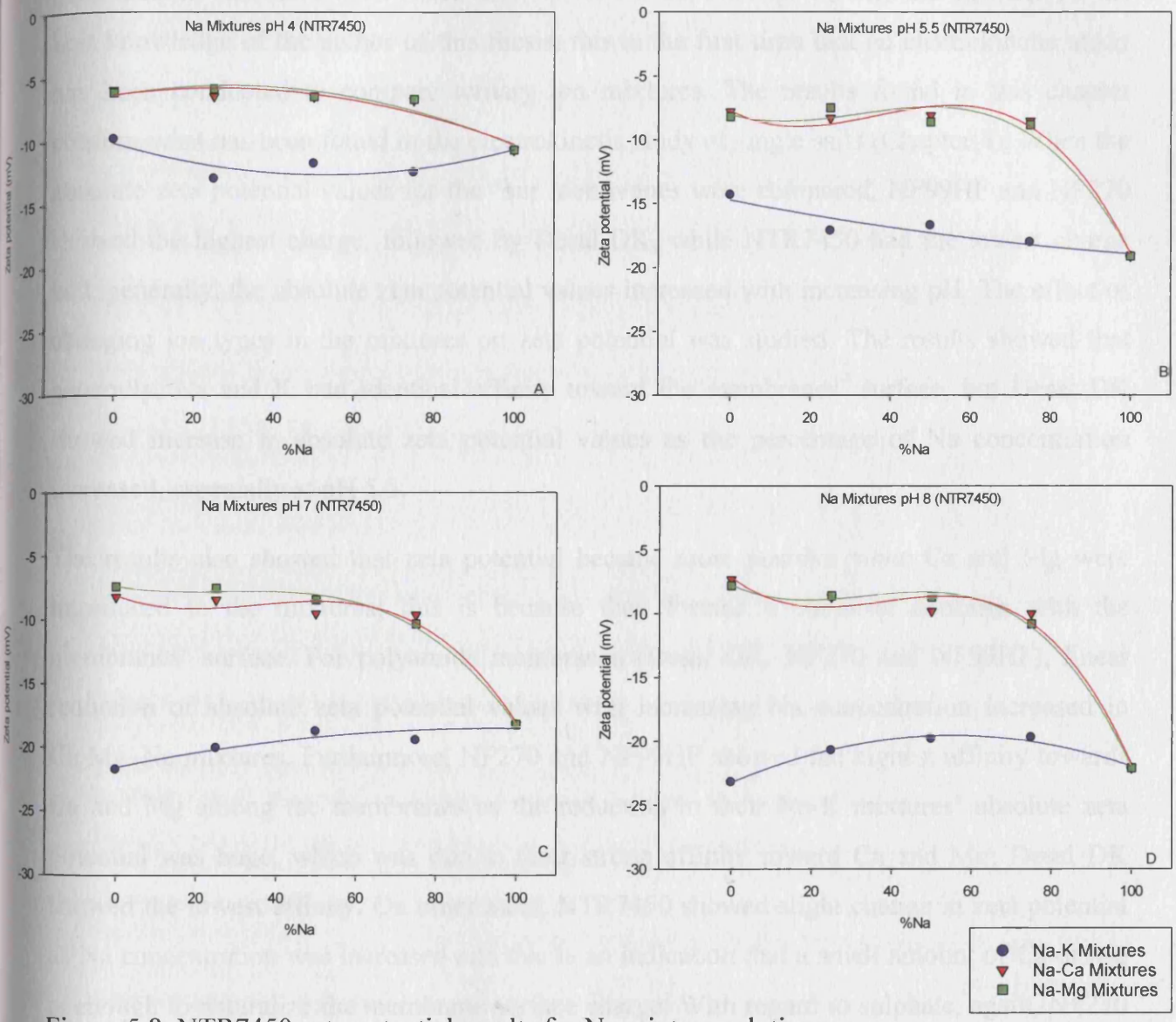

Figure 5.8: NTR7450 zeta potential results for Na mixture solutions.

5.3.2.4 NTR7450

Figure 5.8 shows the zeta potential values of Na-K, Na-Ca and Na-Mg for the NTR7450 membrane. Ca and Mg are identically adsorbed to the surface of the NTR7450 as is shown in the Figures A to D in Figure 5.8. The graph shows that absolute zeta potential decreases significantly when Na is mixed with 25% Ca or Mg. However, the zeta potential values remain constant after that even when concentration of Ca or Mg is increased.

5.4 Conclusion

Zeta potential measurements have been performed at different pH values for ternary mixtures of salts that have one ion in common, so that the other two ions can be compared, which enables studying the effect of cations and anions on the membranes' charge. The ion combinations that have been tested are: Na-K, Na-Ca, Na-Mg, Ca-Mg and Cl-SO_4. To the best knowledge of the author of this thesis, this is the first time that an electrokinetic study has been conducted to compare ternary ion mixtures. The results found in this chapter confirm what has been found in the electrokinetic study of single salts (Chapter 4). When the absolute zeta potential values for the four membranes were compared, NF99HF and NF270 showed the highest charge, followed by Desal DK, while NTR7450 had the lowest charge and, generally, the absolute zeta potential values increased with increasing pH. The effect of changing ion types in the mixtures on zeta potential was studied. The results showed that generally, Na and K had identical affinity toward the membranes' surface, but Desal DK showed increase in absolute zeta potential values as the percentage of Na concentration increased, especially at pH 5.5.

The results also showed that zeta potential became more positive when Ca and Mg were introduced to the mixtures; this is because they formed a chemical complex with the membranes' surface. For polyamide membranes (Desal DK, NF270 and NF99HF), linear reduction of absolute zeta potential values with increasing Na concentration increased in Ca/Mg–Na mixtures. Furthermore, NF270 and NF99HF showed the highest affinity towards Ca and Mg among the membranes as the reduction in their Na-K mixtures' absolute zeta potential was huge, which was due to their strong affinity toward Ca and Mg; Desal DK showed the lowest affinity. On other hand, NTR7450 showed slight change in zeta potential as Na concentration was increased and this is an indication that a small amount of Ca or Mg is enough to naturalize the membrane surface charge. With regard to sulphate, again, NF270 and NF99HF had more affinity than Desal DK and NTR7450. The high interaction (affinity) between the ions in the solution and the NF270 and NF99HF membranes might be a result of the high surface charge of these two membranes as compared to the other membranes used in this study.

6.0 Contribution of NF Membrane Charge to the Separation of Single Salts Solutions

In Chapter 4, tangential streaming potential (TSP), which is the most common technique, was used to study the membrane charge in single salts solutions and the obtained zeta potentials were used to identify the differences in the affinity of the different membranes' materials towards a specific ion/ions. Reproducibility, equilibration time and surface conductivity were also studied in order to optimize the zeta potential measurement. In this chapter, the effect of membrane charge on the performance (flux and rejection) of NF membranes in a single salt system is studied by utilizing the knowledge obtained in Chapter 4. The output of this chapter will improve fundamental understanding of the role of charge in the membrane separation mechanism and the interaction between the different ions, namely K, Ca, Mg, Cl, SO_4 and proton on flux and rejection.

6.1 Relevant theory

6.1.1 NF separation mechanism

Separation at the NF membrane surface is caused by many mechanisms such as micro hydrodynamics, electrostatic interactions (Donnan exclusion), molecular sieving (steric hindrance) and dielectric exclusion (Szymczyk et al. 2007; Afonso 2006). Electrostatic interactions and steric hindrance are responsible for charged species separation (Dina et al. 2001; Teixeira et al. 2005). In fact, the role of surface charges is more important in NF membranes than the other membrane processes (Mänttäri et al. 2006). The effect of membrane charge enables the membrane to reject ions even if the membrane pore is larger than the ionic radii (ion size) (Kukizaki 2009; Narong & James 2006; Ricq & Pagetti 1999). The ion separation resulting from the electrostatic interactions between ions and membrane surface charge is based on the Donnan exclusion mechanism, which is caused when ions flow through charged pores under a pressure gradient (Kukizaki 2009; Peeters et al. 1999; Teixeira et al. 2005). In this mechanism, the co-ions are repulsed by the membrane surface and, to satisfy the electroneutrality condition, an equivalent number of counter-ions is retained, which results in salt retention.

The charge of the membrane is significantly important to membrane performance not only because charge affects the electrostatic repulsion between charged species and the membrane surface, but also because the dissociation of membrane functional groups may affect the

"openness" of the membrane (Childress & Elimelech 2000). Additionally, pH may affect the characteristics of the molecules in the test solution: as an example, at low pH, humic functional groups will protonate, while at high pH, they will deprotonate, and this, in turn, will play a role in the interaction between the humic molecules and the membrane. A polymeric NF membrane typically consists of hydrophobic functional groups (alchyl or aromatic chains) which produce hydrophilic functional groups ($-CONH_2$, $-COOH$, $-NH_2$, $-SO_3^{2-}$, $-R_3N^+$, etc.) in aqueous solutions and these functional groups have different characteristics; the extent of hydrophilic functional groups' dissociation is indeed strongly pH dependent (Bandini & Mazzoni 2005). In fact, polymeric membranes (polyamide, polysulphone, polyethersulphone, cellulose acetate, etc.) as well as inorganic membranes (alumina, titania, etc.) show different behaviour, depending on the type of electrolyte with which they are put in contact and the feed (Mazzoni & Bandini 2006; Mazzoni et al. 2007). For many commercial nanofiltration membranes, the isoelectric point lies in the pH range of 3 to 6 (Tanninen & Nyström 2002). Thus, nanofiltration membranes are usually negatively charged in neutral or alkaline conditions and positively charged in highly acidic conditions. For example, polyamide NF membranes show positive surface charge below the isoelectric point, which results from the protonation of the amine functional groups ($=NH_2 \rightarrow =NH^{3+}$) and the negative charge above the isoelectric point would result from deprotonation of the carboxyl groups ($=COOH \rightarrow =COO^-$) (Childress & Elimelech 2000). The results of this comprehensive zeta potential study (Chapter 4) show that the pH values of the isoelectric point (i.e.p) at various ionic strengths for all membranes studied were between 3.5 and 4, except in the case of NTR740, where no i.e.p was found. Charge is very important in the membrane separation process, and that is why most studies dealing with the efficiency of membranes, including references mentioned in this section, involve a membrane charge characterization study to help in rejection and flux data analysis (see Table A 2.1).

6.1.1.1 Donnan exclusion

As mentioned above, steric hindrance and non-electrostatic membrane–solute interactions (e.g. Van-der-Waals forces) are mostly responsible for the retention of uncharged molecules, and their transport takes place by convection due to a pressure difference and by diffusion due to a concentration gradient across the membrane (Teixeira et al. 2005). In addition, neutral molecules also interact with membrane charge, mainly through polarity effects. Donnan (charge) interactions are used to explain the rejection of ion species by NF membranes. In this mechanism, ions with the same charge sign as that of the membrane (the

co-ions) are excluded and cannot pass through the membrane, and to satisfy the electroneutrality condition, an equivalent number of counter-ions is retained, which results in salt retention, while the ions with the opposite charge sign as that of the membrane (counter-ions) are able to pass through the membrane in principle (Peeters et al. 1999; Teixeira et al. 2005). Therefore, rejection increases with the valence of the ions, so that multivalent co-ions are rejected by the membrane, while monovalent co-ions permeate through the membrane to maintain electroneutrality (Durham et al. 2003). The composition of associated counter-ions also determines the rejection characteristics of the membrane based on Donnan exclusion, wherein higher counter-ion valence leads to lower rejection. The salts rejection sequence of the membranes that are governed by the Donnan exclusion mechanism is as follows (Artuğ et al. 2007; Oatley 2004; Welfoot 2001):

$$Na_2SO_4 > MgSO_4 = NaCl > CaCl_2$$

This sequence is for negative charged membranes, while for positive membranes, it is vice versa. Another type of rejection sequence which does not follow the Donnan exclusion mechanism is as follows (Oatley 2004; Welfoot 2001):

$$Na_2SO_4 > CaCl_2 > NaCl$$

This sequence indicates that the rejection mechanism is a combination of the Donnan and steric effects (Artuğ et al. 2007). Welfoot (2001) believe that this sequence is due to the coupling of the Donnan and dielectric mechanisms.

6.1.2 Water flux

Three factors can be used to explain flux behaviour (1) pore size, (2) electroviscous effect, and (3) osmotic pressure at the membrane surface (Childress & Elimelech 2000; Teixeira et al. 2005).

6.1.2.1 Pore size

Teixeira et al. (2005) found that the pore size of the membrane was reduced at high pH values because the negatively charged groups on the membrane pore surface adopted an extended conformation due to the electrostatic repulsion between them. This expanded conformation reduced the pore size of the membrane and caused a decrease in flux and an increase in retention. This effect is particularly important for KCl because the zeta potential varies significantly through the pores, but this is not the case with divalent salts, where the membrane is less negative. Furthermore, the effect of these phenomena is very low at i.e.p and natural pH compared to higher pH values where the negative charge is more.

Mänttäri et al.(2006) found that in the NF200 and NF270 membranes, at acidic pH, the ion rejection decreased, whereas uncharged glucose was retained due to its size. In an alkaline solution, the results showed that the membranes became more negative and the ions were retained better. However, the negative charge of the polymer chains in the three-dimensional network of the surface started to repel each other and made the skin layer more open. This led to flux increasing and the glucose molecules were enabled to utilize the free space between polymer chains and pass through the membrane. For highly charged membranes, rejection and flux increase at alkaline pH, while for weakly charged membranes like NTR7450 or NF-PES-10, this is not the case. On other hand, Childress & Elimelech (2000) found the flux of the NF55 membrane was relatively constant over the entire pH range, with the exception of a slight peak at pH 5, where it is expected that the NF55 membrane pores are uncharged. Childress (2000) explained that peak in flux was the result of several mechanisms, including (1) increased pore size due to conformational changes of the cross-linked membrane polymer structure, (2) increased apparent water permeability due to decreased electroviscous effect, and (3) increased net driving pressure due to decreased osmotic pressure at the membrane surface.

Childress and Elimelech (2000) explained the reduction of the pore size of the membrane at higher pH values, saying the charged groups adopted an extended chain conformation due to electrostatic repulsion between them. This expanded conformation reduced the pore size (or pore volume) of the membrane and, therefore, caused decreased flux and increased salt rejection. This explanation is opposite to the pore narrowing effect at alkaline pH that is mentioned above. The pore size changing effect of the membranes takes place at both high and low pH. To illustrate, carboxylic and amine groups of the membranes are ionized at

alkaline and acidic pH, respectively. On the other hand, at the pore isoelectric point, the pore size will not be changed. Durham et al. (2003) found that flux reduced at low pH and explained it as the result of the replacement of water molecules on membrane surface by protons which cause the membrane to shrink, reducing pore size and retarding the flow across the membrane.

6.1.2.2 Osmotic pressure

The osmotic pressure can be calculated using Morse Equation (Edward et al. 2014):

$$\pi = iMRT \qquad [6.1]$$

where π is the osmotic pressure, i is van't Hoff factor of the solute, M is molar concentration, R is the universal gas constant and T is the absolute temperature.

The osmotic pressure near the membrane surface increases at high pH because of the high retentions along with the concentration polarization effect, which results in increase of the osmotic pressure (Teixeira et al. 2005). This leads to a decrease in net driving pressure, which causes a decrease in water flux (operating pressure was kept constant). This effect is particularly important for divalent salts, highly rejected by the membrane. Mazzoni et al. (2007) found that in the case of NaCl solutions, the effect is almost neglected. In the case of $CaCl_2$ solutions, on the other hand, the effective driving force is greatly decreased by the osmotic contribution, above all at $CaCl_2$ concentrations higher than 50 mol/m^3.

6.1.2.3 Electroviscous effect

The electroviscous effect is a physical phenomenon that occurs when an electrolyte solution is pressed through a narrow capillary or pore with charged surfaces (Childress & Elimelech 2000). The electroviscous effect is least pronounced at the isoelectric point where double-layer effects are negligible. At low pore surface charge, the solution appears to exhibit a reduced viscosity when its flow rate is compared with the flow at high pore surface charge. Accordingly, flux would be at a maximum when the capillary is uncharged, or in other words, at the membrane pore isoelectric point.

6.2 Materials and methods

The filtration of single salts started after the membrane characterization experiments (Sections 3.2.2.1 and 3.6.2) and the mass transfer study (Sections 3.2.2.2 and 3.6.1). The full

experiential procedure of single salt filtration is explained in Section 3.2.2.3, while Section 3.2.1 gives the specification of the membranes used and describes the NF pilot plant.

6.3 Results and discussion

6.3.1 Effect of pH, concentration and type of salt on rejection

The results of salt rejection, flux, individual ions rejection and proton rejection for NaCl, KCl, Na_2SO_4, $CaCl_2$, $MgCl_2$ and $MgSO_4$ at 10^{-3}M, 10^{-2}M and 0.025M by Desal DK, NF270 and NTR7450 are shown in Figures 6.1 to 6.6. Table 6.1 gives the physical properties of the solutes used in this study.

Table 6.1: Molecular weight, diffusivity and ionic radius for solutes used in this study (Oatley 2004; Mohammed 1998).

Species	Valence	MW Da	$D_{eff,\infty}$ x10^9 m^2 s^{-1}	r_s nm
Cl	-1	35.5	2.030	0.121
H	+1	1	9.311	0.026
Ca	+2	40.1	0.791	0.310
Mg	+2	24.3	0.72	0.350
Na	+1	23	1.333	0.184
K	+1	39.1	1.957	0.125
SO_4	-2	96	1.062	0.231

The Desal DK and NF270 rejection decreased with increasing concentration for NaCl, KCl, Na_2SO_4 and $MgSO_4$ and increased in the case of $MgCl_2$ and $CaCl_2$. On other hand, NTR7450's performance (rejection and flux) decreased with increasing concentration for all the salts studied. The salt rejections usually decreased with the increasing concentration because of the shield effect (charge screening) of the cations on the membrane charged groups (Dina et al. 2001). The other possible explanation is that the thickness of the electric double layer (Debye length) decreases with increase in the ionic strength of the feed solution

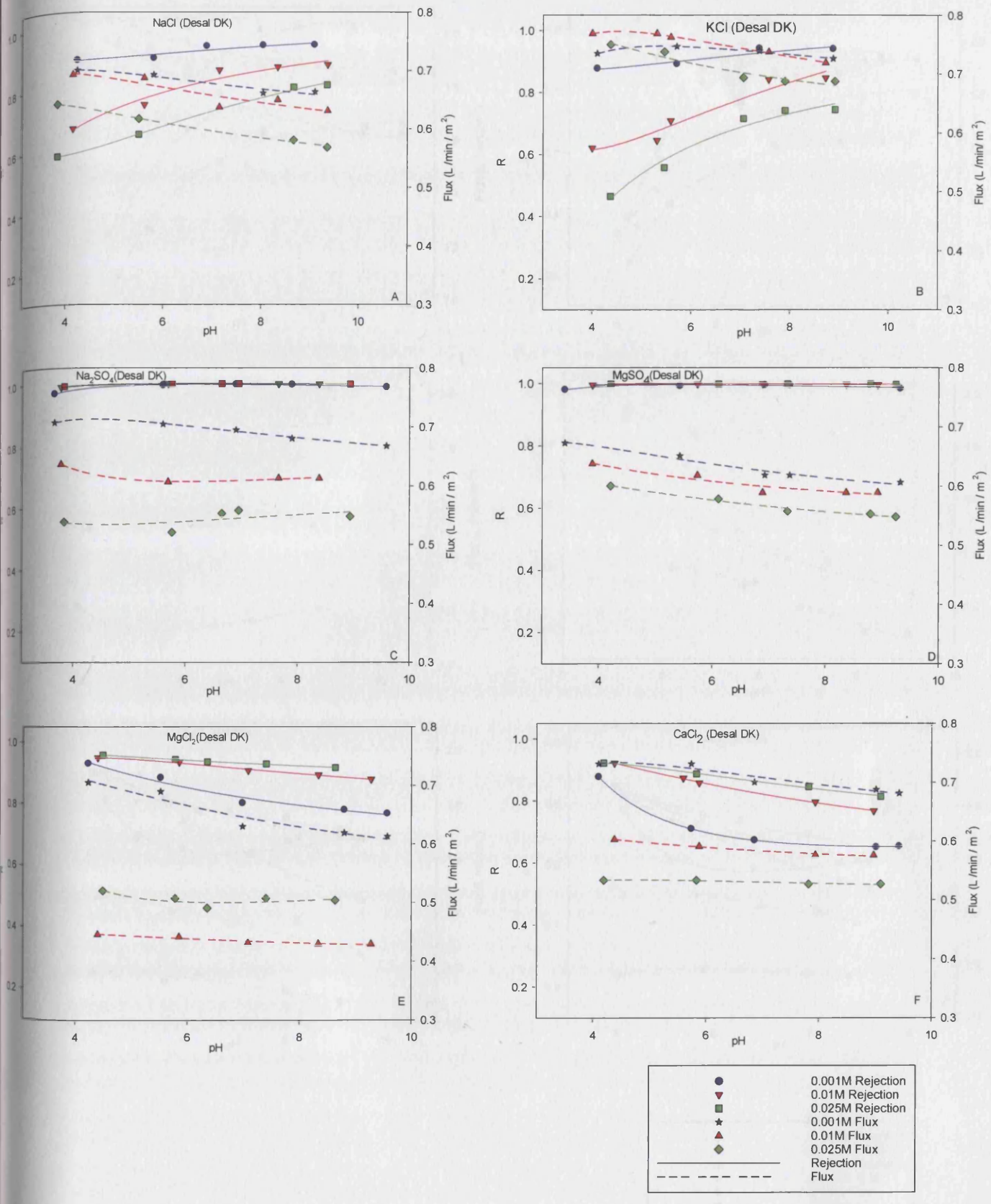

Figure 6.1: Performance of Desal DK with different salts.

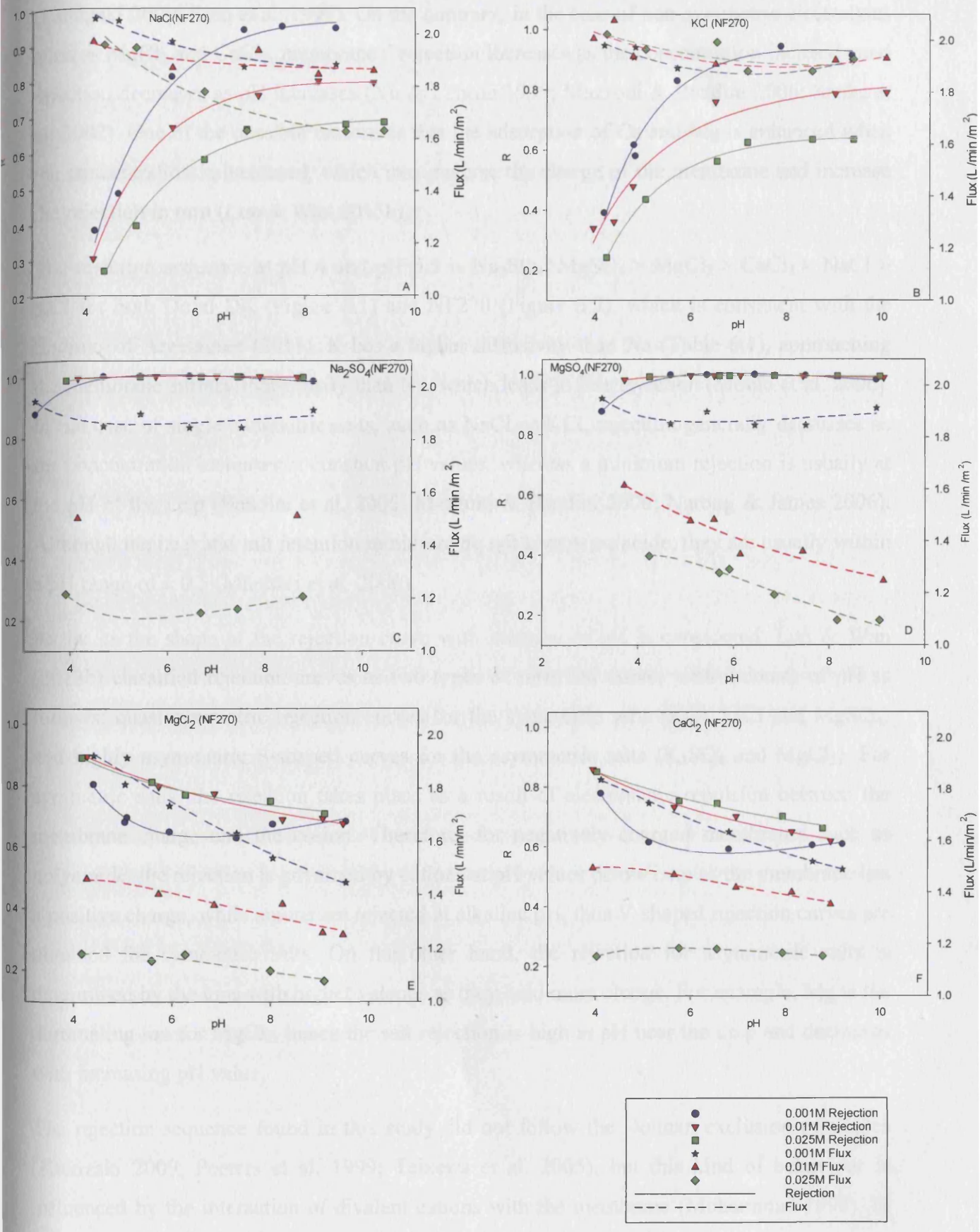

Figure 6.2: Performance of NF270 with different salts.

(Kukizaki 2009; Ricq et al. 1997). On the contrary, in the case of non-symmetric electrolytes such as $MgCl_2$ and $CaCl_2$, membranes' rejection increases as the concentration increases and rejection decreases as pH increases (Xu & Lebrun 1999; Mazzoni & Bandini 2006; Szoke et al. 2002). One of the possible reasons is that the adsorption of Ca and Mg is enhanced when the concentration is increased, which may reverse the charge of the membrane and increase the rejection in turn (Luo & Wan 2013b).

The rejection sequence at pH 4 and pH 5.5 is Na_2SO_4, $MgSO_4$ > $MgCl_2$ > $CaCl_2$ > NaCl > KCl for both Desal DK (Figure 6.1) and NF270 (Figure 6.2), which is consistent with the findings of Argelaguet (2011). K has a higher diffusivity than Na (Table 6.1), approaching the membrane surface more easily than Na, which leads to less rejection (Morão et al. 2006). In the case of single symmetric salts, such as NaCl or KCl, rejection generally decreases as the concentration increases at constant pH values, whereas a minimum rejection is usually at the pH of the i.e.p (Bandini et al. 2005; Mazzoni & Bandini 2006; Narong & James 2006). Although the i.e.p and salt retention minimum do not always coincide, they are usually within a pH range of ± 0.5 (Mänttäri et al. 2006).

As far as the shape of the rejection curve with increase of pH is considered, Luo & Wan (2013b) classified rejection curves as two types of retention curves with increase of pH as follows: quasi-symmetric rejection curves for the symmetric salts (KCl, LiCl and $MgSO_4$) and highly asymmetric S-shaped curves for the asymmetric salts (K_2SO_4 and $MgCl_2$). For symmetric salts, the rejection takes place as a result of electrostatic repulsion between the membrane charge and the co-ion. Therefore, for negatively charged membranes such as polyamide, the rejection is governed by cations at pH values below i.e.p as the membrane has a positive charge, while anions are rejected at alkaline pH, thus V-shaped rejection curves are obtained for symmetric salts. On the other hand, the rejection for asymmetric salts is determined by the ions with higher valence as they hold more charge. For example, Mg is the dominating ion for $MgCl_2$, hence the salt rejection is high at pH near the i.e.p and decreases with increasing pH value.

The rejection sequence found in this study did not follow the Donnan exclusion principles (Kukizaki 2009; Peeters et al. 1999; Teixeira et al. 2005), but this kind of behaviour is influenced by the interaction of divalent cations with the membrane (Mohammad 1998). In fact, the rejection sequence is a match with the electrokinetic affinity sequence in which SO_4^{2-} has the highest affinity and the rejection of Na_2SO_4 and $MgSO_4$ was found to be the

highest among the other salts. SO_4^{2-} ions can be chemically adsorbed on the surface through a hydrogen bond after overcoming repulsion force (Kukizaki 2009). Therefore, the rejection for these two salts increases with increasing pH, which is an indication of increasing repulsive force between negative membrane charge and SO_4^{2-} ions, and to satisfy the electroneutrality condition, an equivalent number of associated cations is retained, which results in salt retention (Peeters et al. 1999; Teixeira et al. 2005).

It has been found also in the electrokinetic study that the membrane shows affinity toward $Ca^{2+}$and Mg^{2+} as these ions form chemical complexes with surface functional groups (Szymczyk et al. 1997; Yang et al. 2003) and rejection increases as the concentration increases and decreases as the feed pH increases. The enhanced rejection of divalent cations confirms that acidic conditions induce a positive charge on the membrane, causing Donnan exclusion of multivalent cations (Durham et al. 2003).

The rejection sequence of NTR7450 (Figure 6.3) is: Na_2SO_4 > NaCl > KCl > $MgSO_4$ > $MgCl_2$ > $CaCl_2$. The same rejection sequence with NTR7450, which follows the Donnan exclusion mechanism, has been observed by other researchers (Schaep & Vandecasteele 2001; Xu et al. 2011). Sabir et al. (1998) studied the rejection of NF40 (polyamide membrane) and NTR7450 and found that NF40 did not follow the Donnan exclusion mechanism like NTR7450. In this mechanism, co-ions with the same charge sign as that of the membrane are excluded and cannot pass the membrane, and to satisfy the electroneutrality condition, an equivalent number of counter-ions is retained, which results in salt retention; however, the ions with the opposite charge sign as that of the membrane (counter-ions) are able to pass through the membrane in principle (Peeters et al. 1999; Teixeira et al. 2005). SO_4^{2-}, followed by Cl^-, has the most affinity to the membrane surface (as shown in the electrokinetic study), and at the same time, both of them are co-ions. Therefore, the rejection of SO_4^{2-} followed by Cl^- is the highest among other ions (Figures A and C in Figures 6.3 and 6.6), while monovalent sodium permeates through the membrane to maintain electroneutrality. NTR7450 showed some affinity toward $Ca^{2+}$and Mg^{2+} because these are counter ions which cause reduction in membrane negative charge, which causes decline in sulphate rejection from 97% in Na_2SO_4 to 53% with $MgSO_4$ (Figures C and D in Figures 6.3 and 6.6). Furthermore, Cl^- rejection in the NaCl solution is 79%, reduced to 20% and 16% with $MgCl_2$ and $CaCl_2$, respectively. Ca^{2+} rejection (50%) is higher than Mg^{2+} rejection (20%), while Cl^- rejections are 20% and 17% for $MgCl_2$ and $CaCl_2$, respectively.

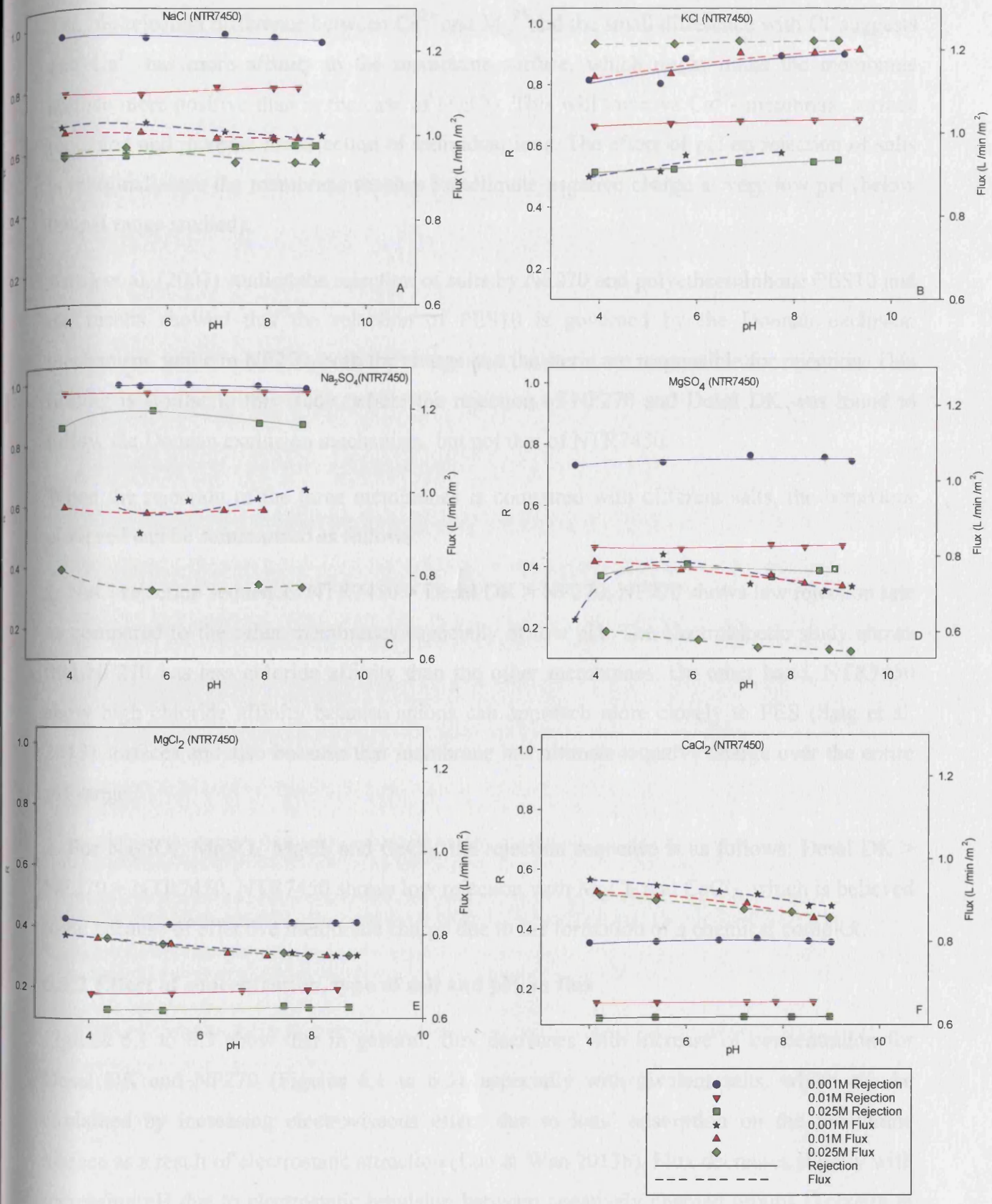

Figure 6.3: Performance of NTR7450 with different salts.

The big rejection difference between Ca^{2+} and Mg^{2+} and the small difference with Cl^- suggests that Ca^{2+} has more affinity to the membrane surface, which might make the membrane surface more positive than in the case of $MgCl_2$. This will improve Ca^{2+}- membrane surface repulsion and increase the rejection of individual ions. The effect of pH on rejection of salts is marginal since the membrane reaches its ultimate negative charge at very low pH (below the pH range studied).

Artuğ et al. (2007) studied the rejection of salts by NF270 and polyethersulphone PES10 and the results showed that the rejection of PES10 is governed by the Donnan exclusion mechanism, while in NF270, both the charge and the steric are responsible for rejection. This finding is similar to this study, where the rejection of NF270 and Desal DK was found to follow the Donnan exclusion mechanism, but not that of NTR7450.

When the rejection of the three membranes is compared with different salts, the behaviour observed can be summarized as follows:

1. NaCl rejection sequence: NTR7450 > Desal DK > NF270. NF270 shows low rejection rate as compared to the other membranes especially at low pH. The electrokinetic study shows that NF270 has less chloride affinity than the other membranes. On other hand, NTR7450 show high chloride affinity because anions can approach more closely to PES (Salg et al. 2013) surfaces and also because that membrane has ultimate negative charge over the entire pH range.

2. For Na_2SO_4, $MgSO_4$, $MgCl_2$ and $CaCl_2$, the rejection sequence is as follows: Desal DK > NF270 > NTR7450. NTR7450 shows low rejection with $MgCl_2$ and $CaCl_2$, which is believed to be because of effective membrane charge due to the formation of a chemical complex.

6.3.2 Effect of concentration, type of salt and pH on flux

Figures 6.1 to 6.3 show that in general, flux decreases with increase of concentration for Desal DK and NF270 (Figures 6.1 to 6.3), especially with divalent salts, which can be explained by increasing electroviscous effect due to ions' adsorption on the membrane surface as a result of electrostatic attraction (Luo & Wan 2013b). Flux decreases slightly with increasing pH due to electrostatic repulsion between negatively charged groups (Teixeira et al. 2005). Teixeira et al. (2005) found flux decrease was higher for divalent salts than for monovalent salt and there is no significant difference between $CaCl_2$ and $MgSO_4$, which can be explained by several mechanisms: membrane pore size, electroviscous effect and osmotic

pressure gradient. Decreasing water flux due to increased osmotic pressure near the membrane surface is particularly important for the divalent salts which are highly rejected by the membranes.

Mazzoni et al. (2007) found that in the case of NaCl solutions, the effect is quite negligible. In the case of $CaCl_2$ solutions, on the other hand, the effective driving force is greatly decreased by the osmotic contribution. The flux sequence for Desal DK (Figure 6.1) is as follows: KCl > NaCl, Na_2SO_4, $CaCl_2$ > $MgSO_4$ > $MgCl_2$; for NF270 (Figure 6.2), it is: KCl > NaCl > Na_2SO_4 > $MgSO_4$ > $CaCl_2$ > $MgCl_2$. The difference between the two sequences is that the $CaCl_2$ flux is lower with NF270 than with Desal DK, which may be a result of the higher affinity of Ca^{2+} toward NF270 as has been found in the electrokinetic study. NTR7450 flux decreased with increasing concentration (Figure 6.3) and it is clear that NaCl, KCl and Na_2SO_4 have higher flux than $MgSO_4$, $MgCl_2$ and $CaCl_2$. Furthermore, the flux of the group of salts with higher flux is more stable when pH increases, while there is decline in flux in the second group. However, the flux curves show some peaks especially for NaCl and 0.025M Na_2SO_4 and these peaks take place at pH 5. Ikeda et al. (1988) studied the rejection and flux of the NTR7400 series and found that flux depends on the kind of salts and the impact of that on the degree of membrane hydration. The flux sequence is: KCl > NaCl > Na_2SO_4 > $CaCl_2$ > $MgSO_4$, $MgCl_2$. KCl flux in all cases is the highest, and in one case (NTR7450), flux increased with increasing concentration, which happened only with this salt and this membrane.

6.3.3 Proton rejection

pH values of the solutions are adjusted with 0.1 M KOH, NaOH, H_2SO_4 and HCl solutions. Many researchers have chosen to take the pH at which the number of the H^+ ions in solution does not represent more than 10% of the initial ionic strength as minimal pH (i.e. pH_{min} = 4 for 10^{-3}M) (Szymczyk, Fievet, Reggiani et al. 1998; Szymczyk et al. 1997). Proton rejection curves are shown in Figures 6.4 to 6.6 along with individual ion rejection. Proton concentration is very high at low pH, while it is very low at higher pH values. On inspecting Figures 6.4 to 6.6, it can be seen that the rejection is positive at very low pH (high H^+) and negative at natural pH. This indicates that proton rejection is a function of concentration and increases with H^+ concentration. Negative retention of H^+ ions for different electrolytes have been referred to by many other researchers (Mazzoni et al. 2007; Ricq & Pagetti 1999; Childress & Elimelech 2000). This is an indication that there is significant proton passage th-

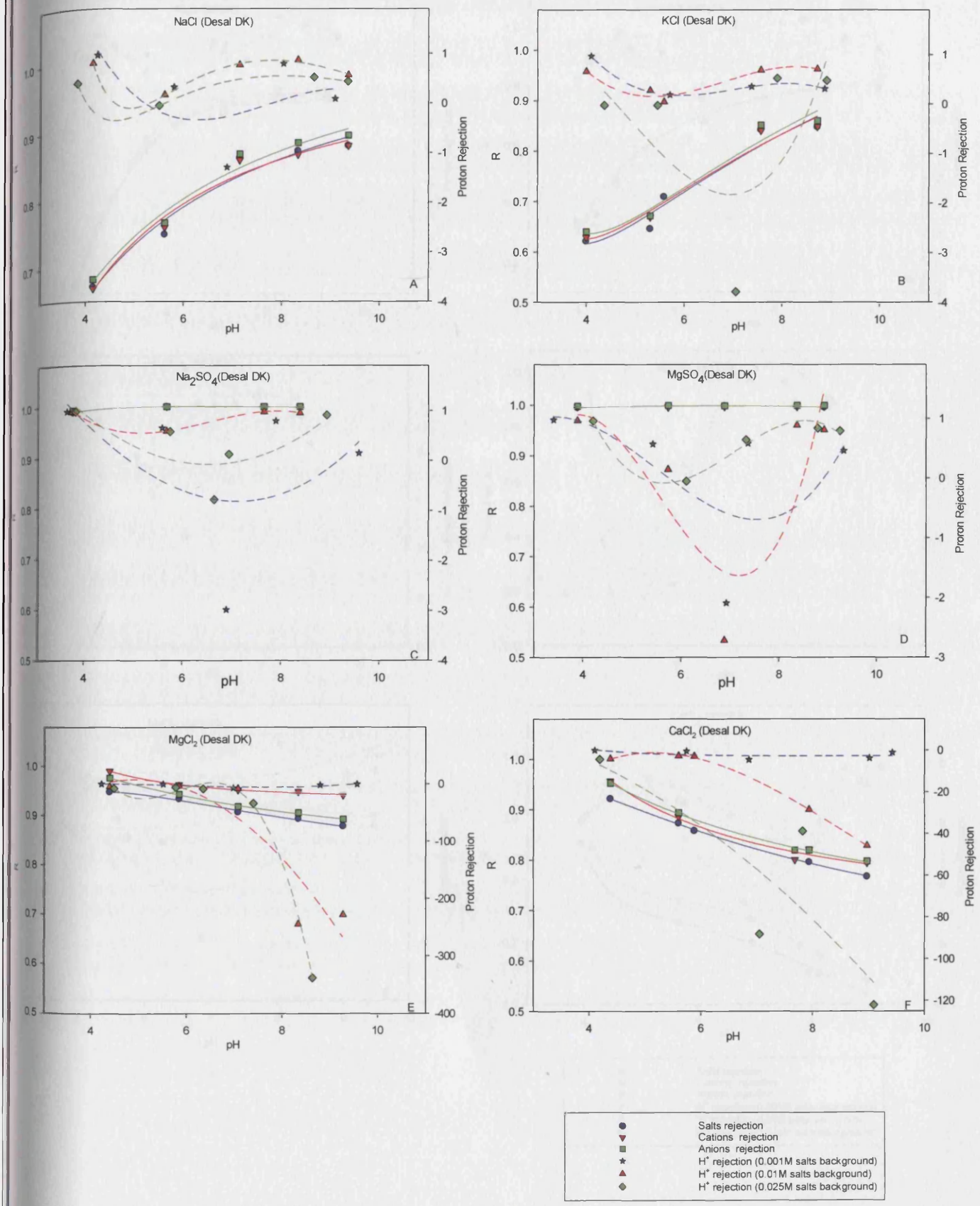

Figure 6.4: Individual ion and proton rejection in Desal DK.

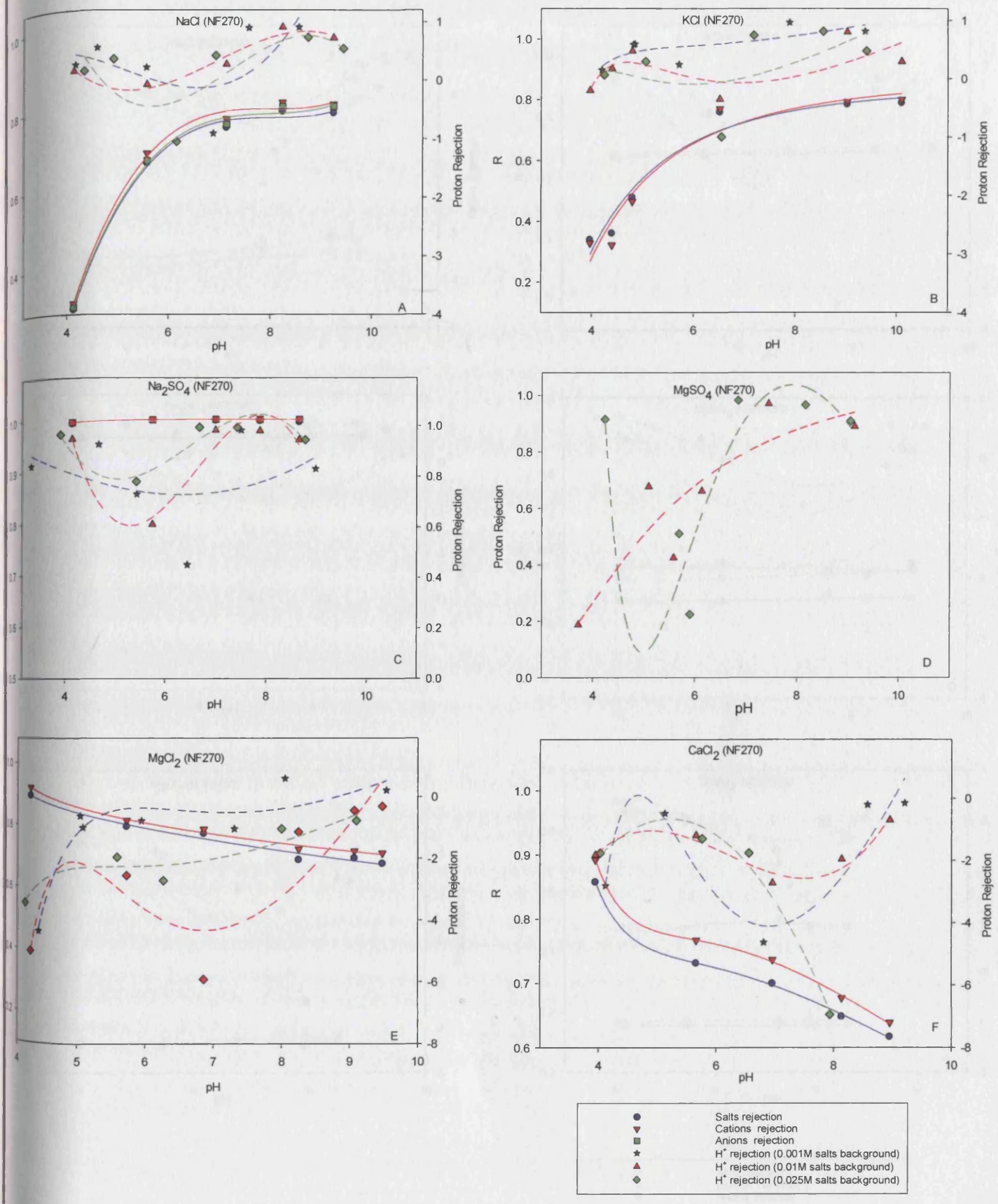

Figure 6.5: Individual ion and proton rejection in NF270.

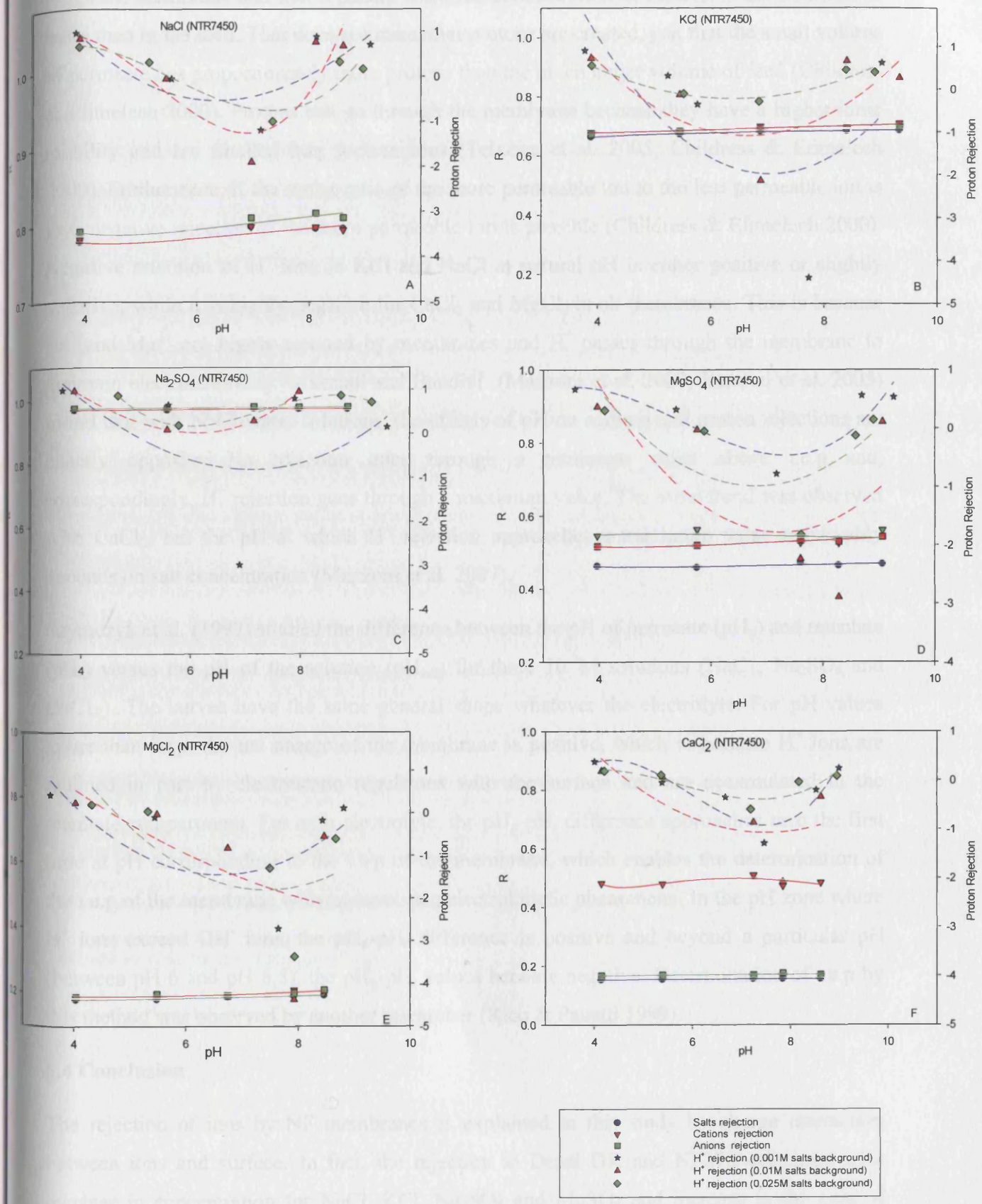

Figure 6.6: Individual ion and proton rejection in NTR7450

rough the membrane and that it occurs when the concentration of protons in the permeate is more than in the feed. That does not mean that protons are created, just that the small volume of permeate has proportionately more protons than the much larger volume of feed (Childress & Elimelech 2000). Protons can go through the membrane because they have a higher ionic mobility and are smaller than sodium ions (Teixeira et al. 2005; Childress & Elimelech 2000). Furthermore, if the molar ratio of the more permeable ion to the less permeable ion is low, negative rejection of the more permeable ion is possible (Childress & Elimelech 2000). Negative retention of H^+ ions in KCl and NaCl at natural pH is either positive or slightly negative, while it is highly negative for $CaCl_2$ and $MgCl_2$ in all membranes. This is because $Ca^{2+}$and Mg^{2+} are highly rejected by membranes and H^+ passes through the membrane to maintain electroneutrality. Mazzoni and Bandini (Mazzoni et al. 2007; Bandini et al. 2005) found that with NaCl-water solutions, the effects of pH on sodium and proton rejections are exactly opposite: Na rejection goes through a minimum value above i.e.p and, correspondingly, H^+ rejection goes through a maximum value. The same trend was observed with $CaCl_2$, but the pH at which H^+ rejection approaches a maximum value remarkably depends on salt concentration (Mazzoni et al. 2007).

Szymczyk et al. (1997) studied the difference between the pH of permeate (pH_p) and retentate (pH_r) versus the pH of the solution (pH_{sol}) for three 10^{-3}M solutions (NaC1, Na_2SO_4 and $CaC1_2$). The curves have the same general shape whatever the electrolyte. For pH values lower than i.e.p, the net charge of the membrane is positive, which is because H^+ ions are retained in part by electrostatic repulsions with the surface and are accumulated in the retentate compartment. For each electrolyte, the pH_p-pH_r difference approaches zero the first time at pH corresponding to the i.e.p of the membrane, which enables the determination of the i.e.p of the membrane without involving electrokinetic phenomena. In the pH zone where H^+ ions exceed OH^- ions, the pH_p-pH_r difference is positive and beyond a particular pH (between pH 6 and pH 6.5), the pH_p-pH_r values become negative. Determination of i.e.p by this method was observed by another researcher (Ricq & Pagetti 1999).

6.4 Conclusion

The rejection of ions by NF membranes is explained in this study by charge interaction between ions and surface. In fact, the rejection in Desal DK and NF270 decreased with increase in concentration for NaCl, KCl, Na_2SO_4 and $MgSO_4$ and increase in the case of $MgCl_2$ and $CaCl_2$. On other hand, the performance of NTR7450 (rejection and flux)

decreased with increasing concentration for all the salts studied. The rejection mechanism does not follow the Donnan exclusion principles for Desal DK and NF270, but it is applicable in NTR7450 rejection. SO_4^{2-} rejection is the highest with all membranes as a result of the repulsion force between negative membrane charge and SO_4^{2-} ions. In the case of NaCl, NTR7450 shows the highest rejection, while NF270 shows the lowest rejection rate as compared to other membranes, especially at low pH. However, NTR7450's performance with other salts is the lowest, which is an indication of the high affinity of Cl^- ions towards the membrane surface. Dina et al. (2001) studied the rejection and zeta potential for Desal G-10 and Desal G-10, which are polyamide membranes, and the results showed that the electrokinetic phenomenon is determined mainly by the cation valence, i.e. zeta potential for the salts that contain multivalent cations are lower than that for monovalent ones, while the separation performance is determined mainly by the anion valence, i.e. rejection for the salts that contain multivalent anions are higher than that for monovalent ones.

Flux behaviour explanation is not straightforward because there are a number of factors to be taken into account, i.e. electroviscosity, osmotic pressure, pore size and the effect of pH on the membrane structure. Generally, KCl flux in all cases is the highest and the flux decreases with increasing concentration, especially with divalent salts, which can be explained by the increasing electroviscous effect due to ions' adsorption on the membrane surface as result of electrostatic attraction. Proton rejection has been studied and shows that the rejection is positive at very low pH (high H^+) and negative at natural pH. This indicates that proton rejection is a function of concentration and increases with H^+ concentration.

7.0 Contribution of NF Membrane Charge to the Separation of Ternary Salts Solutions

This chapter is a continuation of the study of the charge effect on NF membranes' separation. In Chapter 4, the NF membranes' charge was characterized by using the streaming potential technique with six different salts and at three different concentrations. The obtained zeta potentials were used to identify the differences in the affinity of different membrane materials towards specific ion/ions. The effect of membrane charge on the performance of NF membranes in a single salt system was studied in Chapter 6 by utilizing the knowledge obtained in Chapter 4. The complexity of the studying solution has been increased in Chapters 5 and 7 by mixing two salts with one ion in common and studying the effect of the resulting solution chemistry on zeta potential (Chapter 5) and membrane performance (Chapter 7).

7.1 Relevant theory

7.1.1 Introduction

The performance of membranes (flux and rejection) is greatly affected by three major solute–membrane interactions: steric exclusion (sieving), Donnan (charge) interactions and solute–membrane affinity (i.e. hydrophobic attraction, hydrogen bonding, dielectric effects, etc.) (van der Bruggen 2009; Mazzoni & Bandini 2006; Szymczyk et al. 2007). The main mechanism responsible for the rejection of the salt is the electrostatic interactions between ions and the membrane surface (Narong & James 2006), which enable the membrane to reject the ions even when the membrane pore is larger than the ionic radii (ion size) (Kukizaki 2009; Narong & James 2006; Ricq & Pagetti 1999). More details about the impact of membrane charge on the performance of membranes are provided in Chapter 6.

7.1.2 Rejection of ions in mixtures

Rejection of $CaCl_2$ is usually lower as compared to KCl and this corresponds to the increase in the order of cation charge density, i.e. the attraction forces on the cations become progressively stronger (Teixeira et al. 2005). On the other hand, the higher $MgSO_4$ retentions as compared to KCl correspond to increase in the anion charge density, i.e. the anion repulsion forces become stronger. When the electrolyte mixture of KCl and $CaCl_2$ is used, both flux and retention decrease as compared to values obtained with single solutions due to the increase of the electrolyte concentration responsible for higher ionic strength and the stronger attraction forces of the cations. However, the curve shape is very similar to the one

found for single $CaCl_2$, which emphasizes the importance of the Ca^{2+} adsorption onto the membrane surface on the membrane's overall performance. Ricq and Pagetti (1999) found that the presence of NaCl in the solution has no effect on the membrane selectivity. Chloride and calcium transmission in the mixture correspond to those observed during $CaCl_2$ filtration:

$$\text{Chloride transmission } (NaCl+CaCl_2) = \text{chloride transmission } (CaCl_2)$$
$$\text{Calcium transmission } (NaCl+CaCl_2) = \text{calcium transmission } (CaCl_2)$$

On the other hand, calcium presence has a great influence on sodium transmission. Actually, the sodium transmission measured during the mixture filtration is equal to the calcium transmission measured during calcium chloride filtration. In fact, the transmission of Na is lower in the mixture than in the NaCl solution despite the higher ionic strength of the mixture and this is because the mobility of Ca is higher than that of Na, which slows down the Na transmission.

Durham et al. (2003) studied the effect of anion composition on calcium rejection. It was found that rejection was consistent with the Donnan exclusion principles. At neutral and high pH, the rejection characteristics were determined by anion composition. Therefore, the addition of citric acid improved the rejection of calcium from 60% to 80%. The large negatively charged citric anions were repulsed by the membrane and a greater proportion of the calcium was retained to maintain electroneutrality. However, the presence of citric anions did not affect flux at neutral pH. In the absence of citrate, there were no large anions retained and the small permeable chloride ions moved through the membrane, encouraging permeation of calcium ions to maintain electroneutrality.

Mänttäri et al. (2006) found the retention of ions with more hydrophilic membranes changed more than hydrophobic ones when the pH was increased in the feed solution. Tanninen and Nyström (2002) found that the addition of nitric acid led to a sharp increase in the Na^+ retention mostly because of two things: an increase in H^+ concentration (H^+ permeates more easily than the Na^+ ion) and the positive charge of the membrane due to the decrease in pH, increasing the rejection of all cations. In addition, the Na^+ retention decreased with an increase of the Mg^{2+} concentration in the feed. Nitric acid permeated freely and concentrated in the permeate when the metals were retained.

7.2 Materials and methods

A full description of the filtration procedure is provided in Section 3.2.2.4, while Section 3.2.1 gives the specifications of the membranes used and describes the NF pilot plant.

7.3 Results and discussion

Three kinds of drawings are used in this chapter to illustrate the effect of pH and ions' concentration on the rejection for each membrane. The first type is shown in Figures 7.1, 7.3 and 7.5, where the rejection of Na, K, Ca and Mg are drawn as a function of sodium percentage concentration in the sodium mixtures solution (Na-K, Na-Ca and Na-Mg) at a particular pH (pH 4, 5.5, 7 and 8). The second type is shown in Figures 7.2, 7.4 and 7.6 in which the effect of pH was investigated on each mixture combination as a function of percentage concentration of one of the ions that form the mixture. Figures 7.7, 7.8 and 7.9 represent the third kind of drawings in which the overall rejection is calculated from conductivity data and drawn as a function of pH.

7.3.1 Na mixtures (Na-K, Na-Ca and Na-Mg)

7.3.1.1 Desal DK and NF270

Desal DK and NF270 are polyamide membranes (Table 3.1) having positive surface charge below the isoelectric point, which results from the protonation of the amine functional, and negative charge above the isoelectric point, which results from deprotonation of the carboxyl groups (Childress & Elimelech 2000). Figures 7.1, 7.2, 7.3 and 7.4 show that Ca, Mg, K and Na rejection increased with increase in their concentrations in the solution. Ca and Mg had higher rejection values as compared to Na and K for both membranes and Na and K had the same rejection values.

Mazzoni and Bandini (2006) found that calcium rejection increased as the concentration increased and decreased as the feed pH increased. However, as the salt concentration increased, calcium rejection went through a maximum value. Ca^{2+} and Mg^{2+} formed a chemical complex with surface functional groups (Szymczyk et al. 1997; Yang et al. 2003) and rejection increased as the concentration increased and decreased as the feed pH increased. The results also showed that when Ca or Mg ions were introduced into the solution, the rejection of Na was dramatically reduced as compared to the Na rejection in the Na-K mixture.

Magnesium rejection was higher than Ca for both membranes and higher in Desal DK than in NF270. The rejection of Mg and Ca decreased with increasing pH, while rejection of K and Na increased. This was caused as a result of the Donnan exclusion of multivalent cations at low pH in which divalent calcium and magnesium were retained, while monovalent sodium and potassium permeated through the membrane to maintain electroneutrality (Durham et al. 2003). On the other hand, at neutral and high pH, the rejection characteristics were determined by anion composition. When inspecting Figure 7.1, it can be seen that Ca and Mg

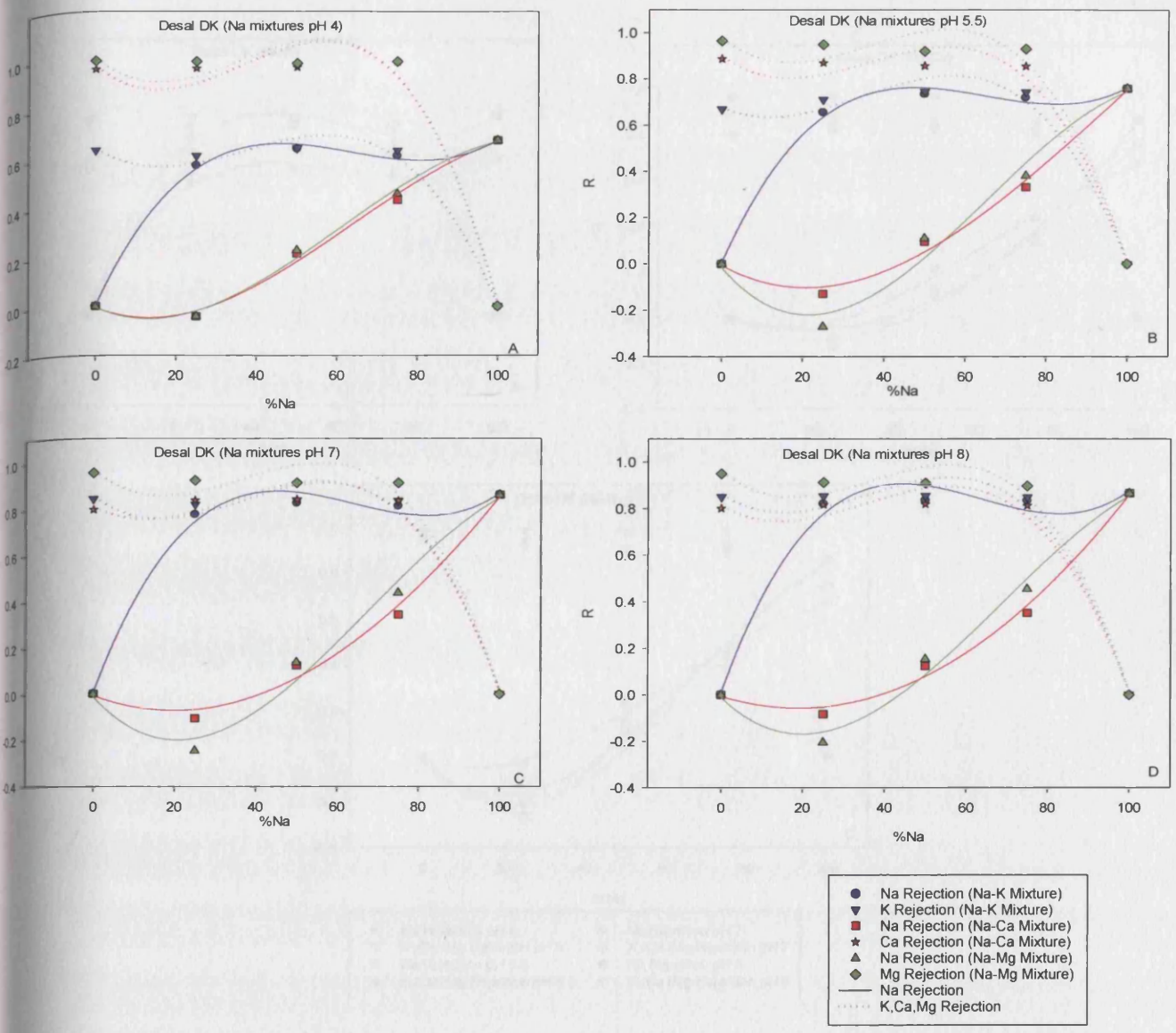

Figure 7.1: Desal DK rejection of Na, K, Ca and Mg in Na mixture solutions as a function of % Na concentration.

rejection is high at pH 4 and very close to each other, and with increasing pH, rejection starts to reduce, while Na and K rejection is low and increases with increasing pH. At pH 7, K and Ca rejection are almost same, and at pH 8, the rejection of K is slightly higher than that of Ca. Amount of change in rejection with increasing pH is smaller for Desal DK than NF270 (Figures 7.2 and 7.4) and the amount of change in magnesium rejection for both membranes is the smallest among the other ions. Na and K rejection for NF270 is very low as compared to Desal DK at pH 4, which is an indication of low affinity towards Na at low pH. However, rejection increases sharply at higher pH and reaches close to that for Desal DK: this is due to Cl rejection when the membrane is negatively charged. Rejection of Na shows negative rejec-

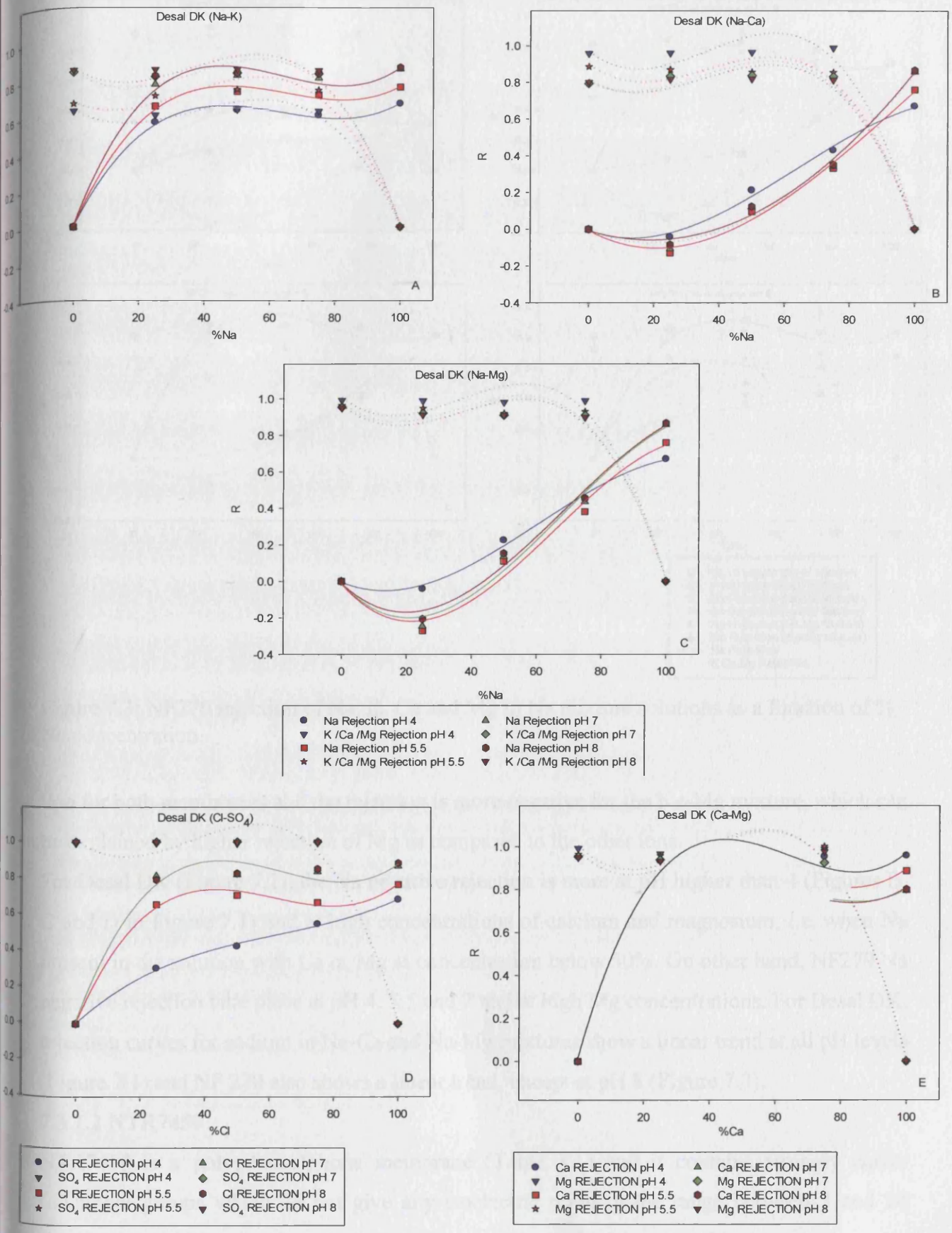

Figure 7.2: Desal DK rejection of Na mixture, Cl-SO_4 mixture and Ca-Mg mixture solutions as a function of pH and % Na, Cl and Ca concentrations, respectively.

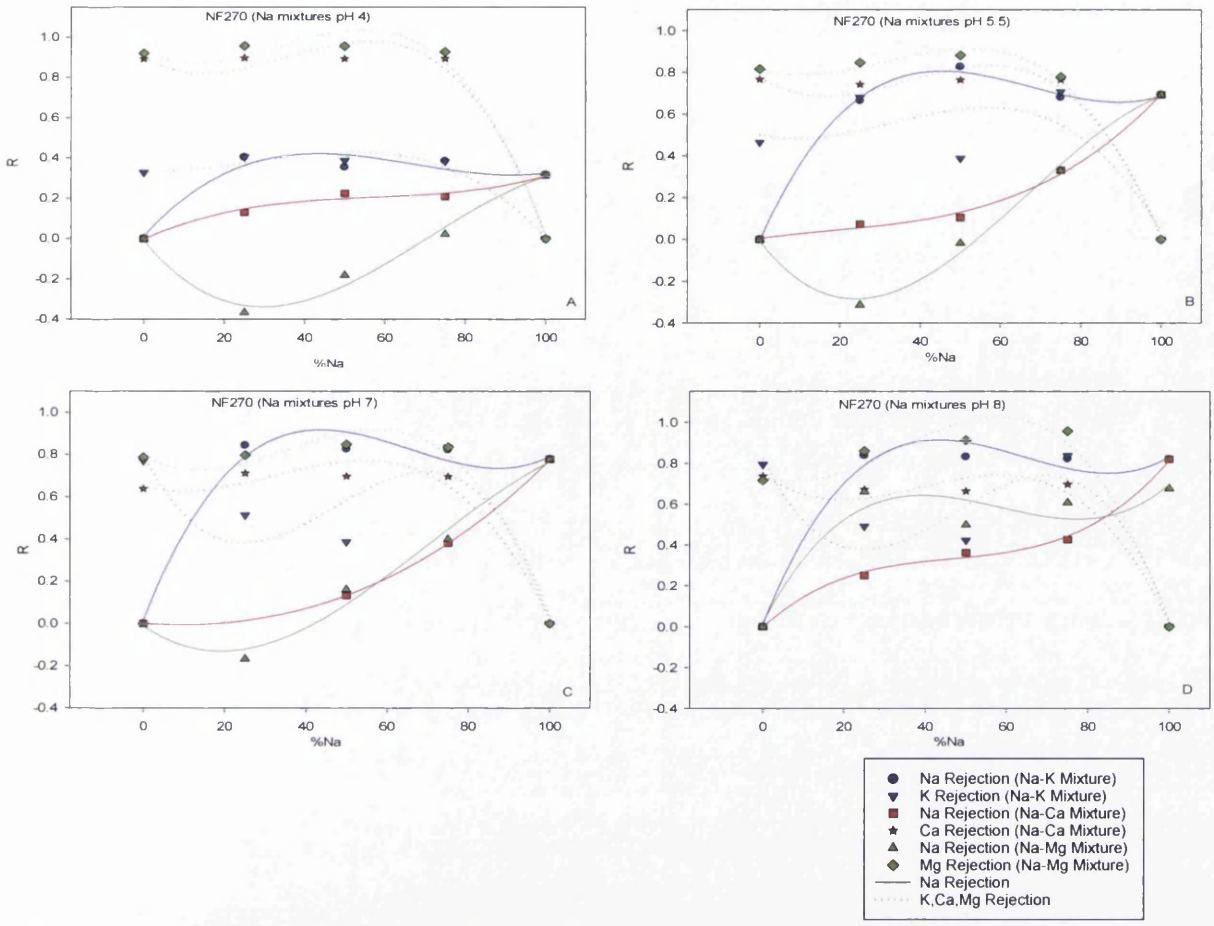

Figure 7.3: NF270 rejection of Na, K, Ca and Mg in Na mixture solutions as a function of % Na concentration.

tion for both membranes and the rejection is more negative for the Na-Mg mixture, which can be explained by higher rejection of Mg as compared to the other ions.

For Desal DK (Figure 7.1), the Na negative rejection is more at pH higher than 4 (Figures B, C and D in Figure 7.1) and at high concentrations of calcium and magnesium, i.e. when Na present in the solution with Ca or Mg at concentration below 50%. On other hand, NF270 Na negative rejection take place at pH 4, 5.5 and 7 and at high Mg concentrations. For Desal DK, rejection curves for sodium in Na-Ca and Na-Mg mixtures show a linear trend at all pH levels (Figure 7.1) and NF 270 also shows a linear trend, except at pH 8 (Figure 7.3).

7.3.1.2 NTR7450

NTR7450 is a polyethersulphone membrane (Table 3.1) and it contains strongly acidic functional groups which do not give any isoelectric point in the range between 3 and 10 (Möckel et al. 1998), i.e. the membrane's negative charge is ultimate at this range.

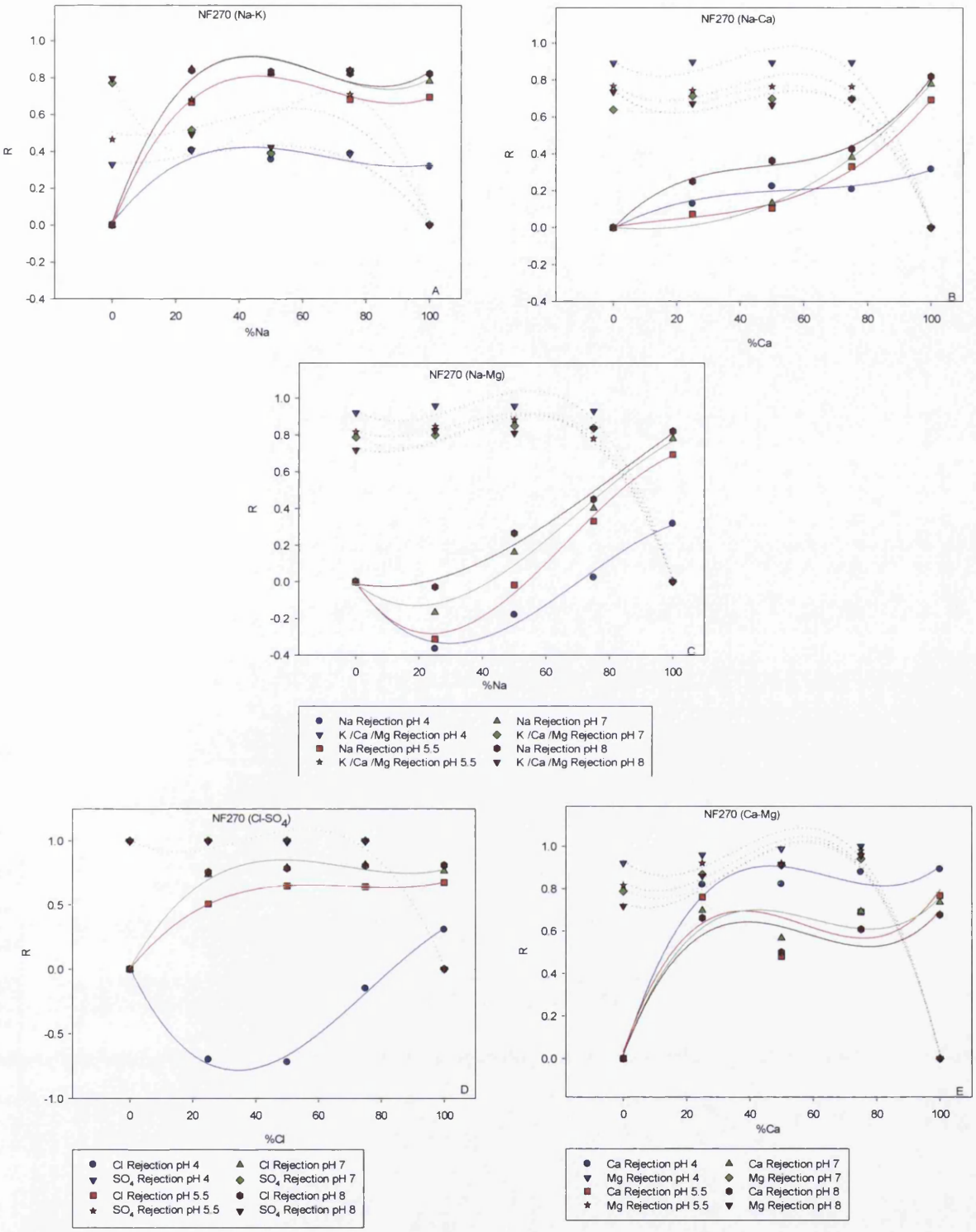

Figure 7.4: NF270 rejection of Na mixture, Cl-SO_4 mixture and Ca-Mg mixture solutions as a function of pH and % Na, Cl and Ca concentrations, respectively.

Figures 7.5 and 7.6 show that Ca, Mg, K and Na rejection increase generally with increase in their concentrations in solution. Unlike Desal DK and NF270, Ca and Mg (Figure 7.5 and Figures A, B and C in Figure 7.6) have lower rejection values as compared to Na/K and Na and K have the same rejection values as are shown in Figure 7.5. Also, Ca rejection is higher than that for Mg (in Desal DK and NF270, Mg is more rejected than Ca). Ca rejection (Figure 7.5) decreases with decrease in its percentage and reaches lowest point at around 80% Ca-20% Na (rejection around 5%) and then the rejection increases again to reach the peak at 20%Ca-80%Na (rejection around 60%). The peak locations and rejection values are almost the same in all the graphs in Figure 7.6 and these phenomena were not observed in the Desal DK and NF270 membranes.

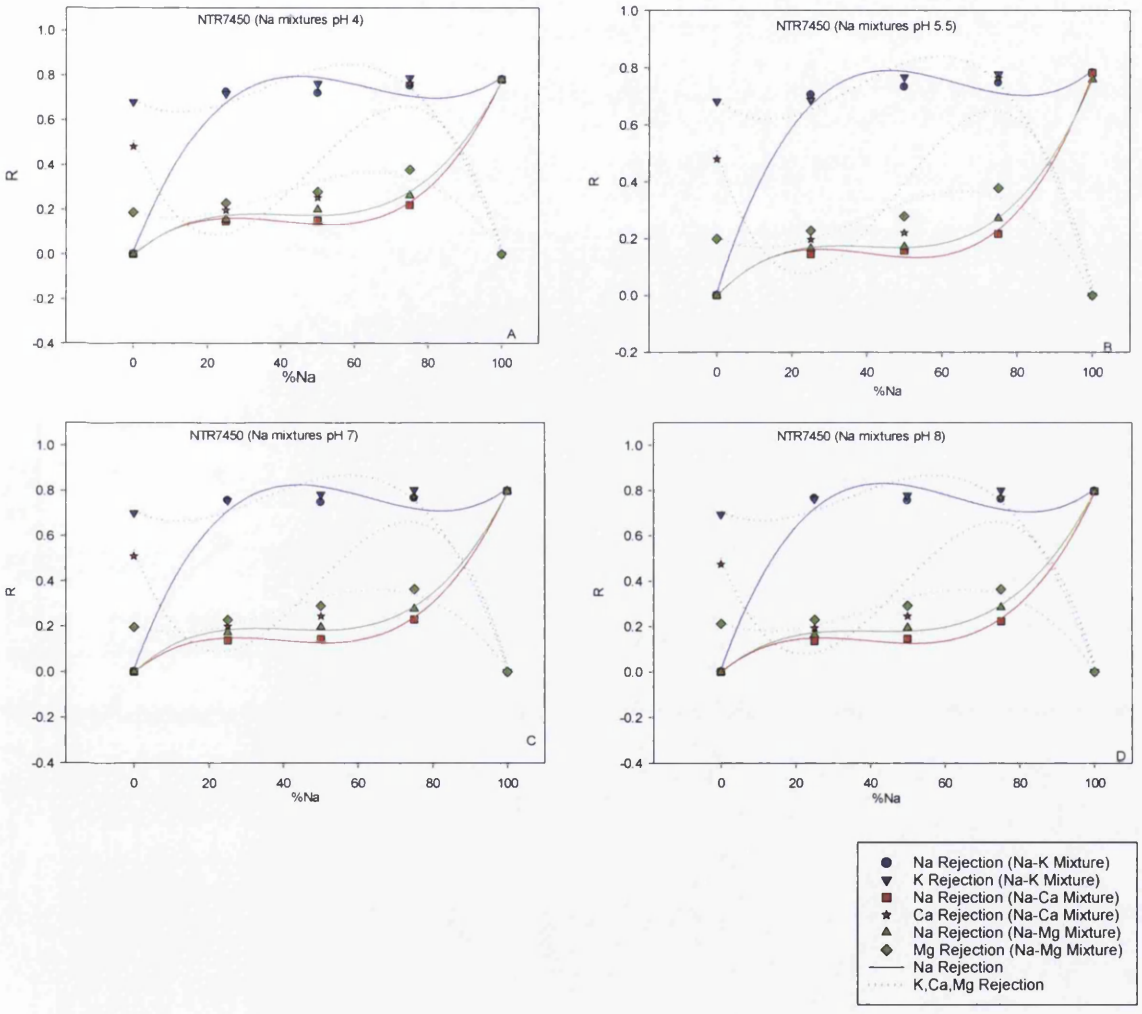

Figure 7.5: NTR7450 rejection of Na, K, Ca and Mg in Na solution mixtures as a function of % Na concentration.

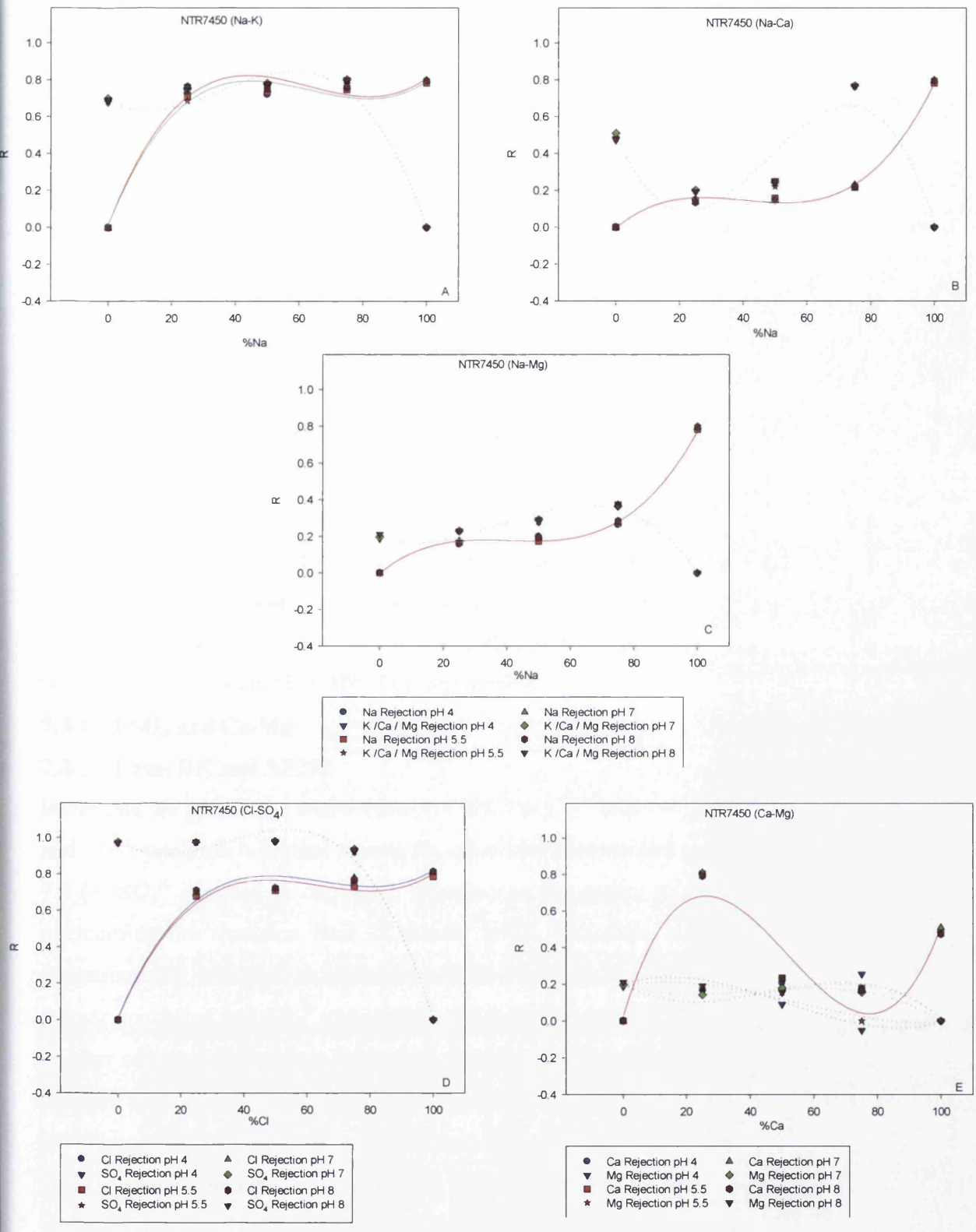

Figure 7.6: NTR7450 rejection of Na mixture, Cl-SO_4 mixture and Ca-Mg mixture solutions as a function of pH and % Na, Cl and Ca concentrations, respectively.

The NTR7450 membrane shows high Na rejection at pH 4 and 5 as compared to the other membranes (Figure 7.6 A). The reason for this is that the charge of NTR7450 is negative over the entire pH range, which means Cl is responsible for the rejection, while Na is retained to maintain electroneutrality. In fact, anions can approach more closely to hydrophobic surfaces (such as PES membrane) (Salg et al. 2013).

Na and K rejection values are close to each other and rejection increases with increase in their concentration percentages in the solutions and no linear relation or Na negative rejection was observed as in the case of the other membranes.

Another difference between NTR7450 and the other membranes is that the rejection is constant over the pH range (4 to 8) since the membrane is at its ultimate negative charge. The presence of Ca and Mg reduce the Na rejection (Figures A, B and C in Figure 7.6). The Na rejection is equal to Ca at three concentrations, namely 18%, 38% and 88% Na. Mg also reduces the Na rejection by the same value and the Na rejection curve is almost same. However, the Mg rejection curve shows less fluctuation than Ca and the only point at which both rejections are equal is at 80% Na concentration.

7.3.2 Cl-SO_4 and Ca-Mg

7.3.2.1 Desal DK and NF270

Increasing the percentage concentration of SO_4^{2-} and Cl^- in the solution increase the rejection and SO_4^{2-} rejection is highest among the other ions (cations and anions) (Figures 7.2 D and 7.4 D). SO_4^{2-} ions can be chemically adsorbed on the surface through hydrogen bonds after overcoming the repulsion force (Kukizaki 2009). Therefore, the rejection increases with increasing pH, which is an indication of the increasing repulsive force between negative membrane charge and SO_4^{2-} ions, and to satisfy the electroneutrality condition, an equivalent number of associated cations is retained, which results in salt retention (Peeters et al. 1999; Teixeira et al. 2005). Furthermore, Cl^- rejection in Cl-SO_4 mixtures increases with increasing pH (Figures 7.2 D and 7.4 D) and the Cl rejection values are close to Na and K rejection in Na-K mixtures(Figures 7.2 A and 7.4 A). The only exception is at pH 4, where the membrane surface charge is almost positive so that the Na ion (not Cl) is responsible for the rejection. At this pH, Cl rejection is lower than Na and K rejection in K and Na solutions and this may be the result of increase in the Na ions' concentration in Cl-SO_4 mixtures as compared to Na-K mixtures, i.e. the molar ratio of sodium Na_2SO_4 is double that of NaCl. For NF270 (Figure 7.4 D), negative rejection has been observed as the membrane's Na rejection is poor as

compared to Desal DK (Figure 7.2 D). The rejection becomes more positive as the concentration of chloride increases, as observed by Mohammad and Takriff (2003), who explain it as the result of Cl^- washing out at higher SO_4^{2-} concentration. The rejection of Cl^- and SO_4^{2-} are equal at 87%, 90% and 93% for pH 7, 8, 5.5 and 4, respectively. Mg rejection is more than Ca rejection for both membranes (Figures 7.2 E and 7.4 E) and Desal DK rejects Ca and Mg ions more than NF270. From all of the above, it is clear that the rejection sequence is SO_4 > Mg > Ca > Na, Cl, which is consistent with the findings of Argelaguet (2011).

7.3.2.2 NTR7450

An increase in the percentage of SO_4^{2-} and Cl^- in the solution increases the rejection and SO_4^{2-} rejection is the highest rejection among the ions (cations and anions) (Figure 7.6 D). The rejection of both ions is not affected by pH changes and rejection is slightly lower than rejection in KCl and NaCl solutions (Figures A and B in Figure 6.3) as a result of the increase in the Na ions' concentration, i.e. the molar ratio of sodium in Na_2SO_4 is double that in NaCl. Negative Cl^- rejection has not been observed as with NF270 and the rejection of Cl and SO_4 are equal at 80%.

Unlike Desal DK and NF270, Ca is rejected more than Mg by the NTR7450 membrane (Figure 7.6 E). Change of ions rejection with pH low for Ca while Mg rejection show two patterns, the first one is from 0% to 40% Ca concentration, where the rejection increases with increasing pH, and the other is above 40% Ca, in which the rejection decreases with increasing pH. The rejection sequence of NTR7450 is: SO_4 > Na, K > Ca > Mg. The same rejection sequence with NTR7450, which follows the Donnan exclusion mechanism, has been observed by other researchers, too (Schaep & Vandecasteele 2001; Xu et al. 2011).

7.3.3 Overall rejection

7.3.3.1 Na-K mixtures

There is slight decrease and increase in rejection when K is introduced to the solution with Desal DK (Figure 7.7 A) and NF270 (Figure 7.8 A), respectively. However, as it has been seen, the rejection of individual ions (Na and K) is almost identical (Figures 7.2 A and 7.4 A). The overall rejection varies between 60% and 85% with increasing pH for 25%, 50% and 75% Na solutions, which is almost the same as the rejection figures for individual K and Na, though the pure NaCl solution gives slightly higher values. NTR7450 rejection also decreased when K is introduced into solution (Figure 7.9 A) and the overall rejection is almost stable over the entire pH range.

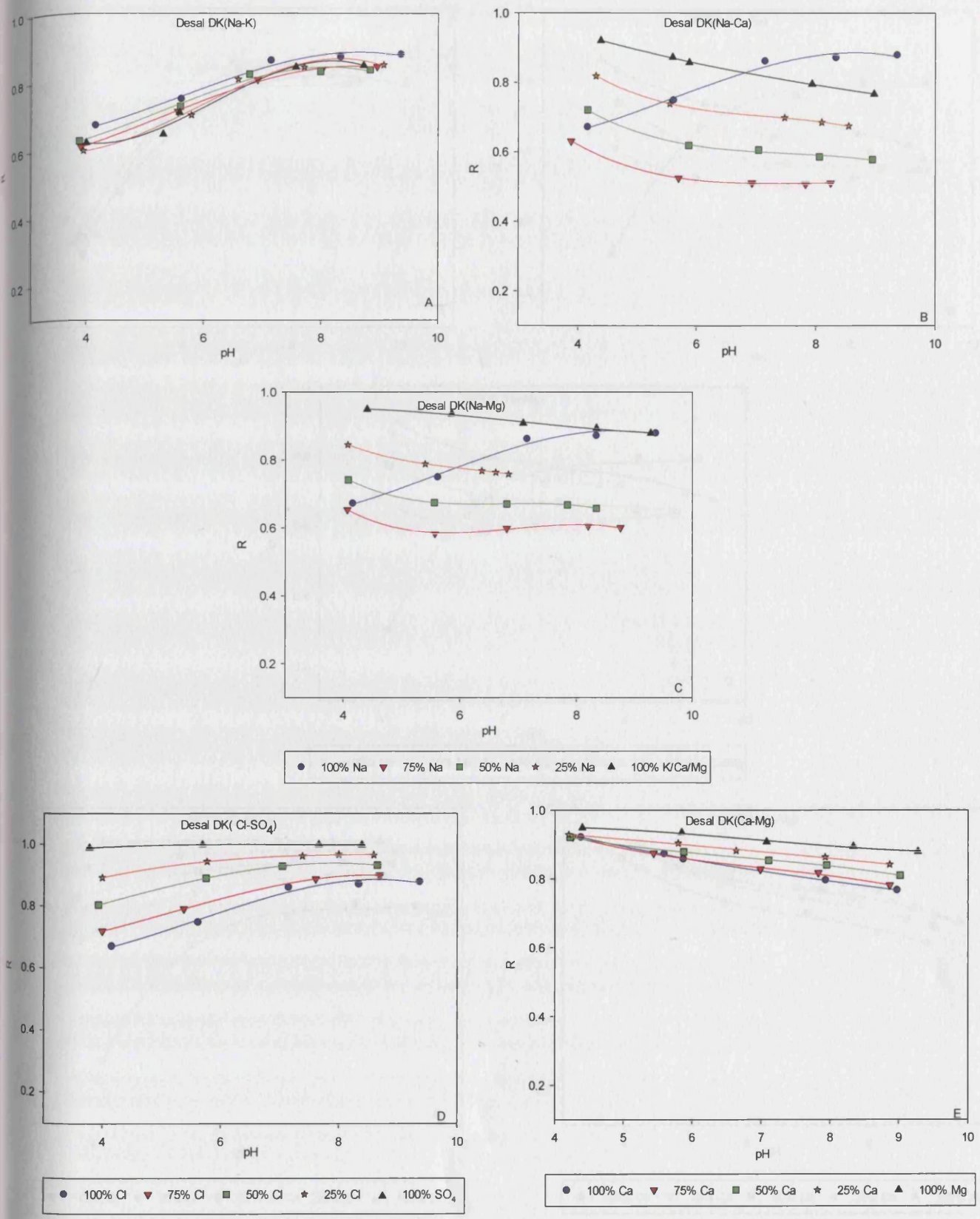

Figure 7.7: Desal DK overall rejection.

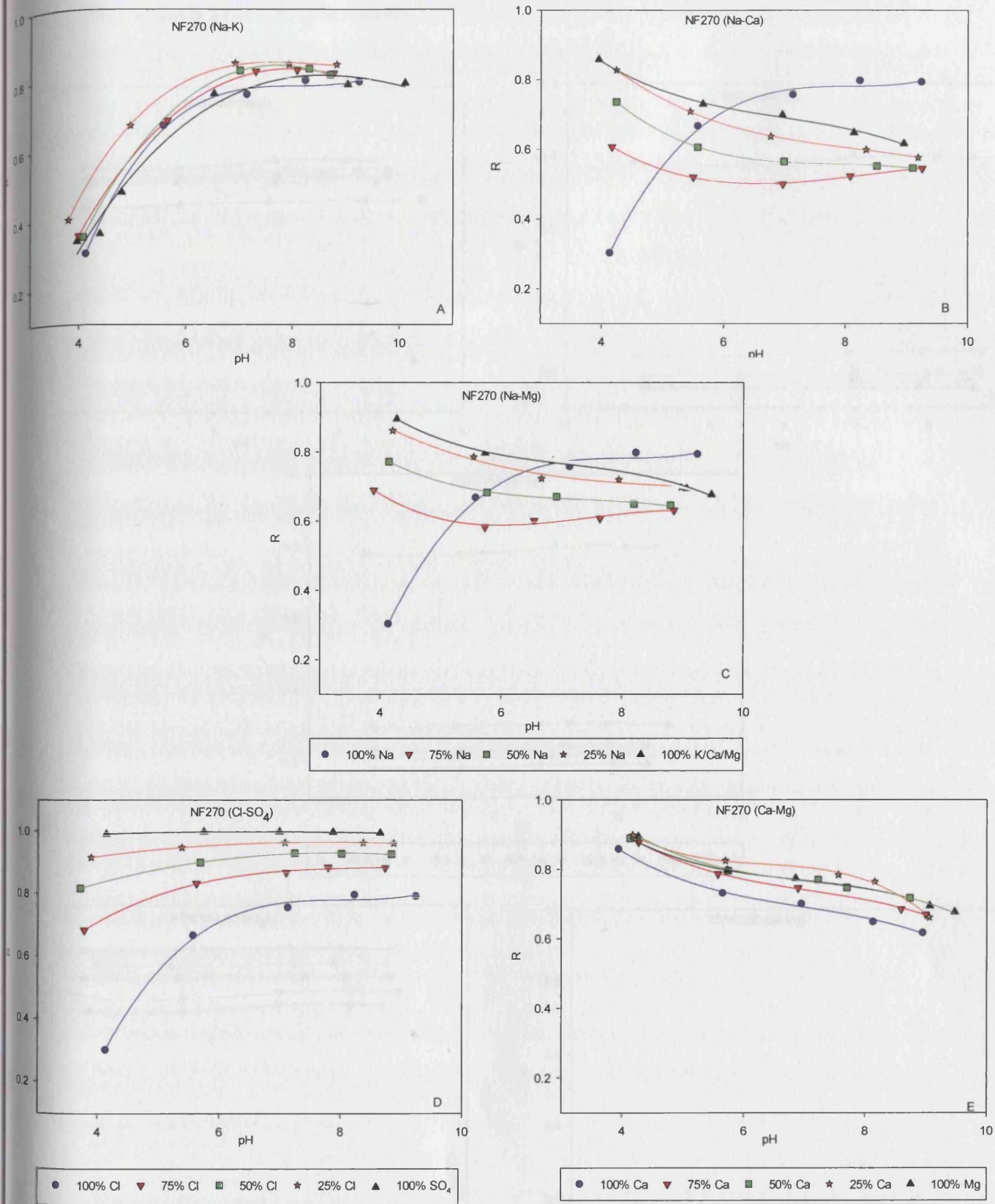

Figure 7.8: NF270 overall rejection.

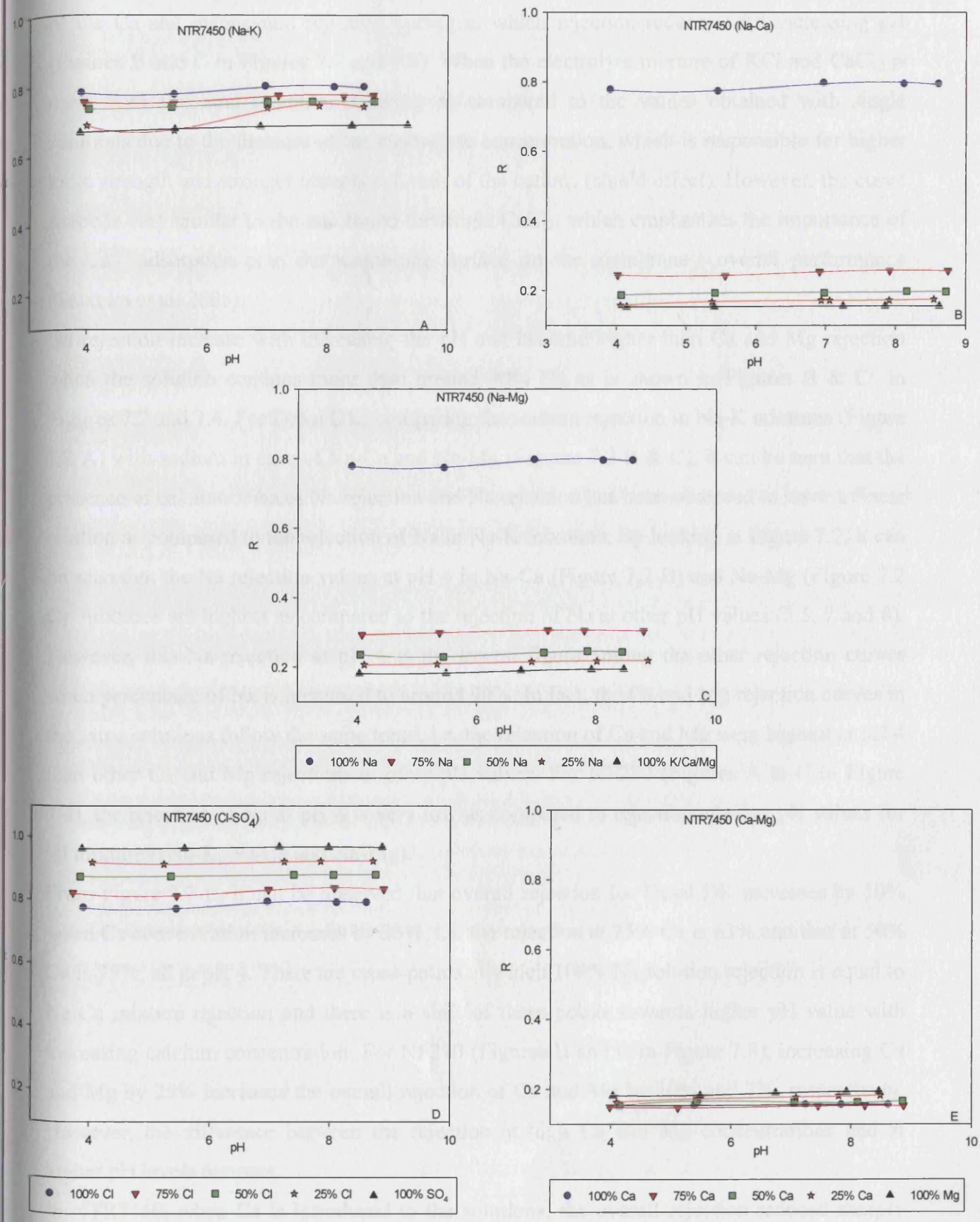

Figure 7.9: NTR7450 overall rejection.

7.3.3.2 Na-Ca and Na-Mg mixtures

When Ca and Mg are introduced to the solutions, the overall rejection curves take the shape of the Ca and magnesium rejection curves in which rejection reduces with increasing pH (Figures B and C in Figures 7.7 and 7.8). When the electrolyte mixture of KCl and $CaCl_2$ is used, both flux and retention decrease as compared to the values obtained with single solutions due to the increase of the electrolyte concentration, which is responsible for higher ionic strength and stronger attraction forces of the cations (shield effect). However, the curve shape is very similar to the one found for single $CaCl_2$, which emphasizes the importance of the Ca^{2+} adsorption onto the membrane surface on the membrane's overall performance (Teixeira et al. 2005).

Na rejection increase with increasing the pH and become higher than Ca and Mg rejection when the solution contains more than around 90% Na as is shown in Figures B & C in Figures 7.2 and 7.4. For Desal DK, comparing the sodium rejection in Na-K mixtures (Figure 7.2 A) with sodium in case of Na-Ca and Na-Mg (Figures 7.2 B & C), it can be seen that the presence of calcium reduces Na rejection and Na rejection has been observed to show a linear relation as compared to the rejection of Na in Na-K mixtures. By looking at Figure 7.2, it can be seen that the Na rejection values at pH 4 in Na-Ca (Figure 7.2 B) and Na-Mg (Figure 7.2 C) mixtures are highest as compared to the rejection of Na at other pH values (5.5, 7 and 8). However, this Na rejection at pH 4 is the lowest figure among the other rejection curves when percentage of Na is increased to around 90%. In fact, the Ca and Mg rejection curves in the same solutions follow the same trend, i.e. the rejection of Ca and Mg were highest at pH 4 than other Ca and Mg rejections at other pH values. For NF270 (Figures A to C in Figure 7.4), the rejection of Na at pH 4 is very low as compared to rejection at other pH values for all mixtures (Na-K, Na-Ca and Na-Mg).

From Figure 7.7 B, it can be observed that overall rejection for Desal DK increases by 10% when Ca concentration increases by 25%, i.e. the rejection at 25% Ca is 63% and that at 50% Ca is 75%, all at pH 4. There are cross-points at which 100% Na solution rejection is equal to Na-Ca mixture rejection and there is a shift of these points towards higher pH value with increasing calcium concentration. For NF270 (Figures B and C in Figure 7.8), increasing Ca and Mg by 25% increases the overall rejection of Ca and Mg by 10% and 7%, respectively. However, the difference between the rejection at high Ca and Mg concentrations and at higher pH levels narrows.

In NTR7450, when Ca is introduced to the solutions, the overall rejection reduced sharply from 80% to 20% (Figure 7.9 B), which is caused by a reduction of effective membrane

charge and then the rejection decreases slightly with increase in the percentage of Ca. The rejection curves' shape is almost a straight line, which is an indication that the rejection does not depend on change of pH over the pH range studied, as mentioned previously.

7.3.3.3 Cl-SO_4

An increase in SO_4 concentration by 25% increases the overall rejection of Desal DK by 7% at lower pH and 5% at higher pH. In fact, 25% of SO_4 is enough to make the overall rejection of the solution higher than that of the 100% Cl solution over the entire pH scale (Figure 7.7 D). For individual ions, in Figure 7.2 D, the percentage point of Cl at which the rejection of Cl and SO_4 are equal are 80%, 85% and 90% at pH 7, 8, 5.5 and 4, respectively. For NF270 and NTR7450 (Figures 7.8 D and 7.9 D), an increase in SO_4 concentration by 25% leads to an increase in the overall rejection by 10% and 5%, respectively.

7.3.3.4 Ca-Mg

An increase in the percentage of Mg leads to an increase in the overall rejection for both Desal DK and NF270 (Figures 7.7 E and 7.8 E). However, at lower pH, rejections become closer to each other. The rejection decreases almost linearly with increasing pH. In NTR7450 (Figure 7.9 E), an increase in the percentage of Mg leads to a slight increase in overall rejection.

7.4 Conclusion

Rejection of ions by NF membranes affected by charge interaction between the ions and the surface. Desal DK and NF270 show high Ca and Mg rejection, while NTR7450's Na rejection at pH 4 and 5 is high as compared to the other membranes. Another difference between NTR7450 and the other membranes is that the rejection is constant over the pH range studied. The overall rejection of the mixtures was also calculated from conductivity data in this study and then drawn as a function of pH. The results showed that when Ca and Mg were introduced into the solutions, the overall rejection curves took the shape of the Ca and Mg rejection curves in which the rejection was reduced with increase in pH. For Desal DK, comparing the sodium rejection in Na-K mixtures with sodium in case of Na-Ca and Na-Mg, it was seen that the presence of calcium reduced Na rejection; also, a linear relation of Na rejection was observed as compared to the rejection of Na in Na-K mixtures. In NTR7450, when Ca was introduced into the solutions, the overall rejection reduced sharply, but the rejection curves' shape was an almost straight line, which was an indication that the rejection does not depend on change of pH over the pH range. Increasing SO_4 concentration increased the overall rejection for the three membranes. In Ca-Mg mixtures, increasing Mg

concentration led to an increase in the overall rejection for both the Desal DK and NF270 membranes.

8.0 Membrane Charge Prediction

The characterization of membranes charge in a single salt system and mixture of salts solution was described in earlier chapters. The aim of that was to gain insights into how the ion species interacted with membrane charge and how this affected the separation process. The rejection data that were generated in previous chapters will be used in this chapter to calculate effective membrane charge density (X_d). The calculated membrane charge density will be correlated with pH, zeta potential and concentration for both single and mixtures salt systems.

8.1 Relevant theory

NF membranes' active layer is a hydrophilic polymeric material such as polyamide (PA), cellulose acetate (CA), polysulphone (PS), polyethersulphone (PES), polyvinyl alcohol (PVA), which, when hydrated and ionized in aqueous solutions, form charged functional groups such as amino, carboxyl and sulphonated groups (Luo & Wan 2013b). In addition to dissociation of surface functional groups, membranes acquire charge either along the surface or on pores by adsorption of charged species such as ions, polyelectrolytes, ionic surfactants and macromolecules from the solutions (Schaep &Vandecasteele 2001; Teixeira et al. 2005).

When a membrane is brought into contact with an aqueous solution, the membrane charge is formed on both the external surface and the membrane pores, which lead to forming the electrical double layer (Figure 2.2) due to electroneutrality (Schaep & Vandecasteele 2001), i.e. a special arrangement of ions in the area adjacent to the membrane surface (see Section 2.1.1). Three different potentials can be differentiated in Figure 2.2: the surface potential, Ψ_o, and surface charge density, σ_o (i.e. the surface charge per unit area on the membrane surface is known as surface charge density); the potential at the Stern plane (Ψ_d); and the electrokinetic or zeta potential which is the potential at the surface of shear between the surface and the bulk solution where there is relative motion between them (Cho et al. 2012; Tay et al. 2002; Hunter 1981). As shown in Figure 2.2, the potential increases and decreases linearly from the surface to Ψ_{OHP} and then decreases exponentially to zero in the diffuse layer (Möckel et al. 1998). Although the potential at the stern plane is most important because it governs the behaviour of the charged species, direct measurement of this potential cannot be achieved, which make the electrokinetic potential a good substitute (Peeters et al. 1999).

Three kinds of surface charge densities can be distinguished: (1) the fixed charges at the membrane surface (σ_0), (2) the charges of the Stern-layer (σ_s), (3) and the charges within the

diffusion layer of the electric double layer (σ_d) (Ariza et al. 2001; Peeters et al. 1999). With increasing concentration, the absolute value of the membrane charge density increases, while the absolute value of the zeta potential decreases (Ding et al. 2006; Peeters et al. 1999). Peeters et al. (1999) found that the actual charge density (σ_0) was very small as compared to the adsorption charge density and the anions were the source of this adsorption.

Ding et al. (2006) measured zeta potential and calculated membrane surface charge for polyethylene microfiltration membrane with five single salts and found the following sequence with absolute zeta potential: NaCl $\geq$ KCl > Na_2SO_4 > $MgSO_4$ > $MgCl_2$; the membrane surface charge was: Na_2SO_4 > NaCl $\geq$ KCl > $MgSO_4$ > $MgCl_2$. Dina et al. (2001) provided a Freundlich isotherm relationship between the effective surface charge calculated from the Gouy–Chapman equation and solution concentration. The sequence of zeta potential value found was: NaCl > Na_2SO_4 > $MgSO_4$ $\geq$ $MgCl_2$; the membrane surface charge was: Na_2SO_4 > NaCl > $MgSO_4$ $\geq$ $MgCl_2$. Morão et al. (2006) studied the electrokinetic properties of NF membranes in contact with KCl, K_2SO_4, potassium clavulanate and $MgSO_4$. The membrane surface charge was found in the following order: KCl, K_2SO_4 > KCA > $MgSO_4$; this showed that divalent cations led to lower surface charge densities. The results also showed that KCl rejection decreased with increase in the feed concentration before it levelled off, while the absolute value of membrane surface charge showed a continual increase over the concentration range. Morão et al. (2006) explained that this was a result of the shielding effect of functional groups on the membrane surface as well as adsorbed anions by cations from the bulk solution facilitating the ionic transport.

8.2 Methods

In this chapter, rejection data that were generated in Chapters 6 and 7 were used as inputs in the DSPM model to calculate membrane charge density (X_d). The calculated membrane charge density was then correlated with pH, concentration and zeta potential for both single (Chapter 4) and mixture salt systems (Chapter 5).

8.3 Results and discussion

8.3.1 Single salt system

8.3.1.1 NaCl and KCl

8.3.1.1.1 Effect of pH on membrane charge density

Figure 8.1 correlates the X_d value of Desal DK, NF270 and NTR7450 with pH for NaCl and KCl at three different concentrations, 0.001M, 0.01M and 0.025M. The absolute value of X_d increases with increasing pH value for Desal DK and NF270 (Figures A to D in Figure 8.1).

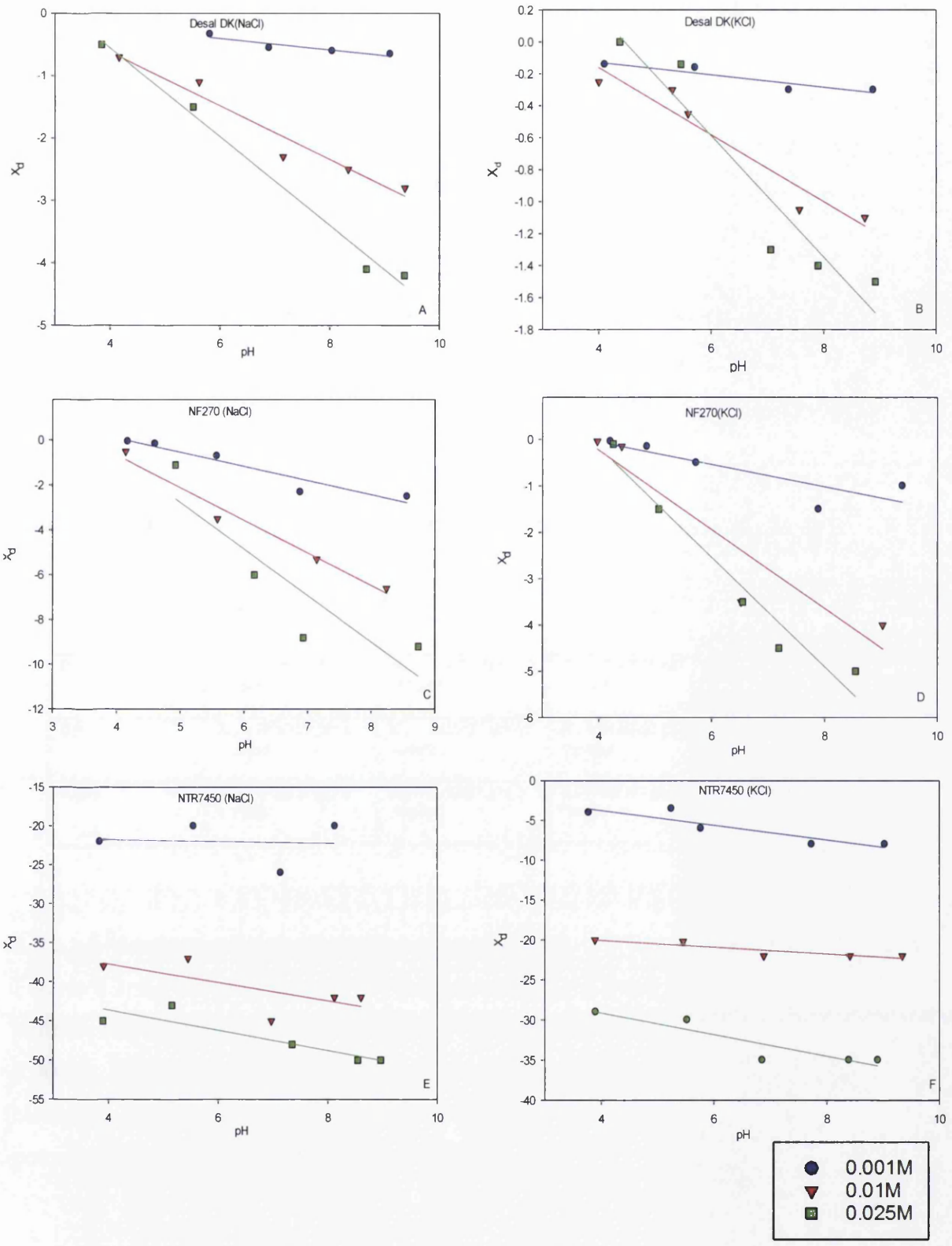

Figure 8.1: Variation of X_d value of Desal DK, NF270 and NTR7450 with pH.

X_d is almost stable in the case of NTR7450 over the entire pH range (Figures 8.1 E and 8.1 F). These findings are consistent with the results found in Chapters 4 and 6. To illustrate, in Chapter 4, the absolute zeta potential value of Desal DK and NF270 increased with increase in the pH as a result of increasing membrane charge due to enhancement of membrane functional groups' dissociation. Furthermore, the rejection of NaCl and KCl increased as well with increase in pH (Chapter 6). On the other hand, the electrokinetic study (Chapter 4) showed that the NTR7450 membrane did not give any isoelectric point in the range of pH 3.5 to 10 values, which is an indication that the membrane is almost at its ultimate negative charge over the entire pH range studied, which causes the effect of pH on rejection of salts to be marginal. The equations obtained from Figure 8.1, which correlate X_d with pH are provided in Table 8.1.

Table 8.1: Correlation equations for X_d with pH for NaCl and KCl.

	Desal DK		NF270	
Concentration (M)	NaCl	KCl	NaCl	KCl
0.001	X_d = -0.0915pH + 0.1504	X_d = -0.039 pH + 0.0291	X_d = -0.6301 pH + 2.6126	X_d = -0.2408 pH + 0.9053
0.01	X_d = -0.4317 pH + 1.1105	X_d = -0.2105 pH + 0.6832	X_d = -1.4562 pH + 5.1628	X_d = -0.8538 pH + 3.1833
0.025	X_d = -0.4317 pH + 1.1105	X_d = -0.3807 pH + 1.6985	X_d = -2.073 pH + 7.588	X_d = -1.1817 pH + 4.5484

8.3.1.1.2 Membrane charge density and zeta potential

Figures 8.2, 8.3 and 8.4 correlate the dimensionless X_d of Desal DK, NF270 and NTR7450 with the dimensionless zeta potential (ξ) for NaCl and KCl at three different concentrations, 0.001M, 0.01M and 0.025M. Dimessionless X_d was obtained by dividing X_d on the electrolyte concententrations, i.e. 0.001M, 0.01M and 0.025M, while the dimessionless zeta potential (ξ) is calculated as follow (Hunter 1981):

$$\xi = \frac{e\zeta}{k_B T} \qquad [8.1]$$

where ξ is the dimessionless zeta potential, e is electron charge, k_B is Boltzann constant and T is the absolute temperature.

For Desal DK and NF270, a linear relation is obtained as shown in Figures 8.2 A, 8.2 C, 8.3 A and 8.3 C. On other hand, NTR7450 shows a straight line as shown in Figures 8.4 A and 8.4 C. Several researchers have found that membrane charge density is a function of salt types and concentration, which can be expressed by the Freundlich isotherm (Ariza et al. 2001; Peeters et al. 1999; Artuğ et al. 2007):

$$log|X_d| = s\, logC_F + q \quad [8.2]$$

where C_f is the solution concentration. Equation 8.2 can be written as:

$$X_d = r(C_F)^S \quad [8.3]$$

where r and s are the characteristic adsorption parameters and log r = q.

The plots of log $|X_d|$ against log $|\xi|$ for NaCl and KCl are shown in Figures B and D of Figures 8.2, 8.3 and 8.4, and the values of r and s are shown in Table 8.2. The degree of linearity obtained for NaCl is better than that for KCl.

Table 8.2: Values of r and s of equation $X_d = r(\xi)^S$ for Figures 8.2 B and 8.2 D.

	Desal DK				NF270			
	NaCl		KCl		NaCl		KCl	
Concentration (M)	s	r	s	r	s	r	s	r
0.001	0.94	0.728	0.22	0.25	0.415	338	2.2	0.5
0.01	0.59	0.254	0.68	0.095	-0.26	327	4.23	0.13
0.025	2.3	0.267	2.98	0.172	-0.374	2130	3.68	0.12

8.3.1.2 Na_2SO_4, $MgSO_4$, $CaCl_2$ and $MgCl_2$

Unlike NaCl and KCl, the calculation of X_d for $MgSO_4$ and Na_2SO_4 gave one value for each examined concentration over the whole pH range as the rejection of these two salts was high by Desal DK and NF270. Moreover, the model predicted only one X_d value for $MgCl_2$ and $CaCl_2$ at pH 4, which represented the maximum rejection of these two salts. For NTR7450, NaCl, KCl and Na_2SO_4 were independent of the pH of the solution, while the model could not predict any value of X_d for $MgSO_4$, $CaCl_2$ and $CaCl_2$.The values of X_d for Na_2SO_4, $MgSO_4$, $MgCl_2$ and $CaCl_2$ are presented in Table 8.3.

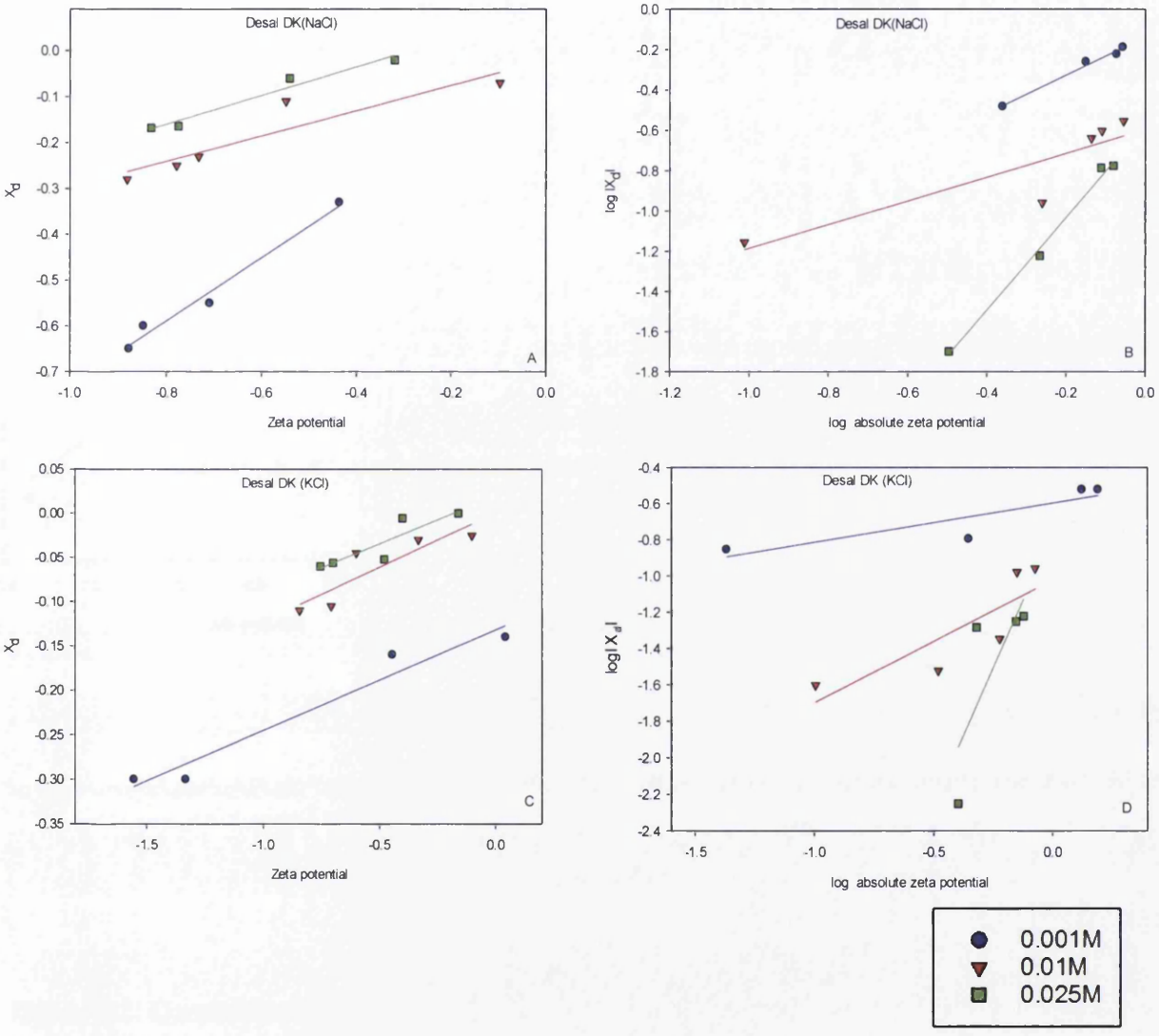

Figure 8.2: Correlations of dimensionless X_d of Desal DK with dimensionless zeta potential for NaCl and KCl at three different concentrations, 0.001M, 0.01M and 0.025M.

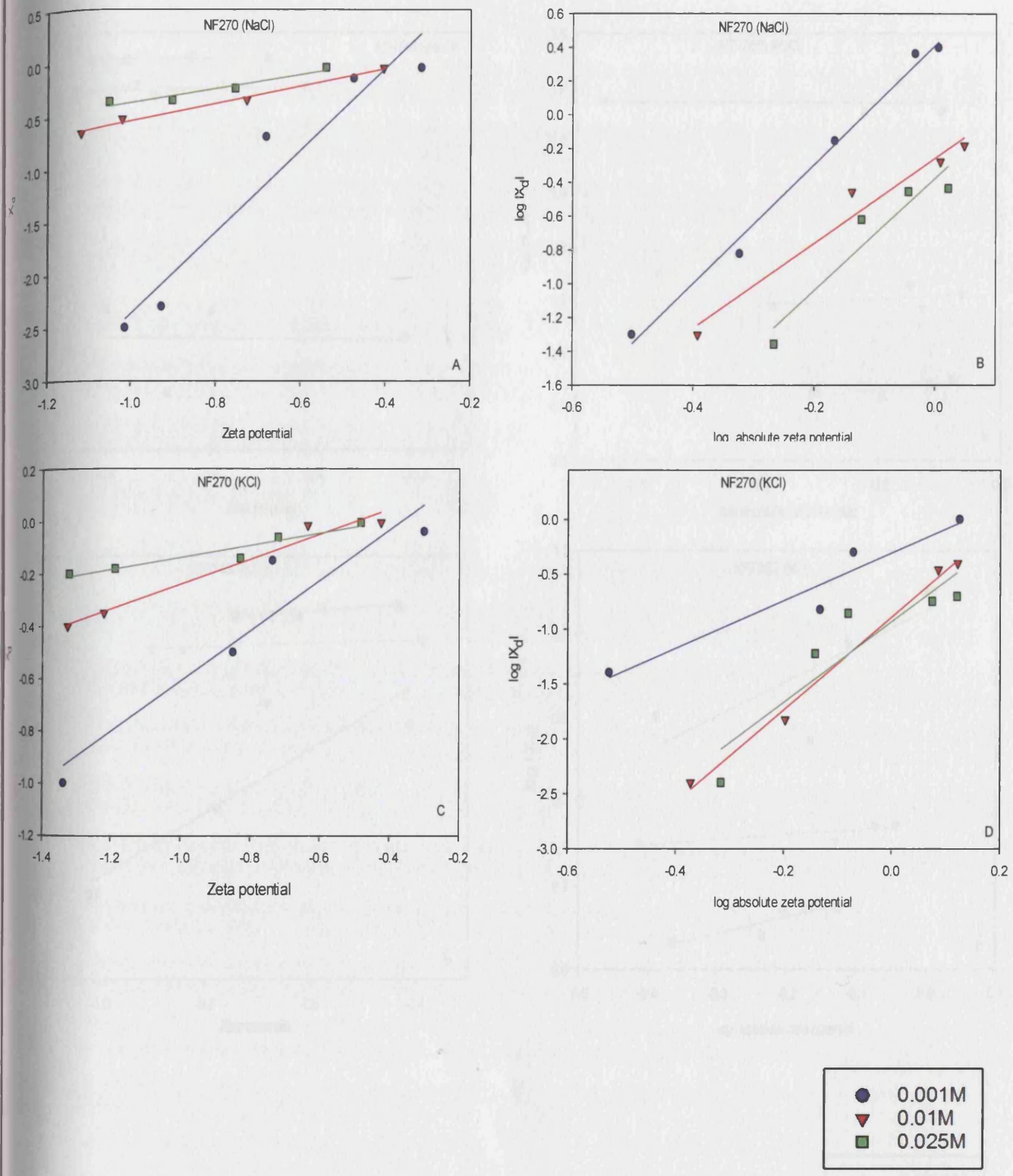

Figure 8.3: Correlations of dimensionless X_d of NF270 with dimensionless zeta potential for NaCl and KCl at three different concentrations, 0.001M, 0.01M and 0.025M.

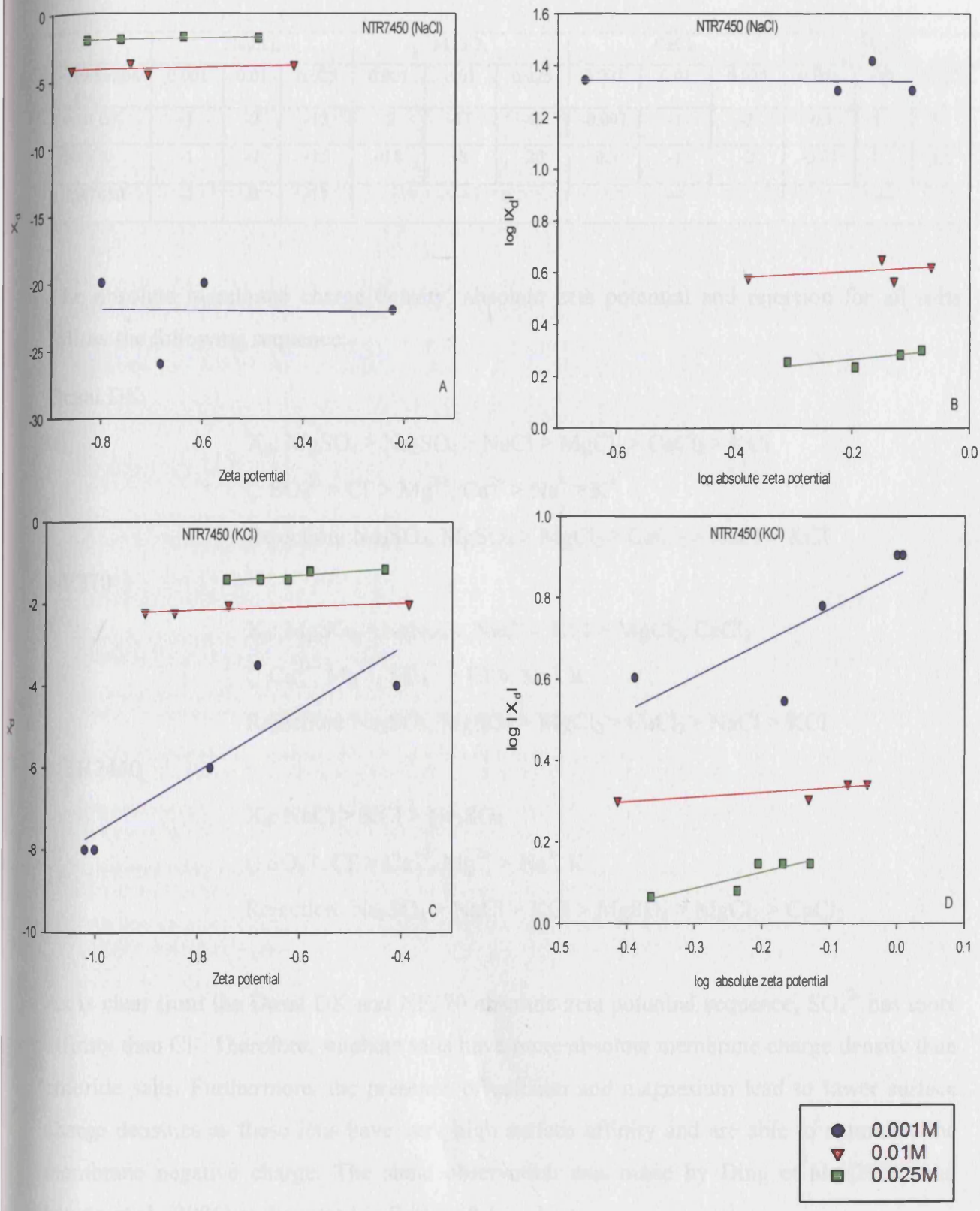

Figure 8.4: Correlations of dimensionless X_d of NTR7450 with dimensionless zeta potential for NaCl and KCl at three different concentrations, 0.001M, 0.01M and 0.025M.

Table 8.3: Values of X_d for Na_2SO_4, $MgSO_4$, $CaCl_2$ and $MgCl_2$.

	Na_2SO_4			$MgSO_4$			$CaCl_2$			$MgCl_2$		
Concentration (M)	0.001	0.01	0.025	0.001	0.01	0.025	0.001	0.01	0.025	0.001	0.01	0.025
Desal DK	-1	-2	-15	-2	-17	-48	-0.001	-1	-2	-0.1	-1	-4
NF270	-1	-7	-15	-0.8	-8	-20	-0.3	-1	-2	-0.03	-1	-2.5
NTR7450	-2	-8	-11	---			---			---		

The absolute membrane charge density, absolute zeta potential and rejection for all salts follow the following sequence:

Desal DK

X_d: $MgSO_4 > Na_2SO_4 > NaCl > MgCl_2 > CaCl_2 > KCl$

ζ: $SO_4^{2-} > Cl^- > Mg^{2+}, Ca^{2+} > Na^+ > K^+$

Rejection: $Na_2SO_4, MgSO_4 > MgCl_2 > CaCl_2 > NaCl > KCl$

NF270

X_d: $MgSO_4 > NaSO_4 > NaCl > KCl > MgCl_2, CaCl_2$

ζ: $Ca^{2+}, Mg^{2+}, SO_4^{2-} > Cl^- > Na^+, K$

Rejection: $Na_2SO_4, MgSO_4 > MgCl_2 > CaCl_2 > NaCl > KCl$

NTR7450

X_d: $NaCl > KCl > Na_2SO_4$

ζ: $SO_4^{-2}, Cl^- > Ca^{+2}, Mg^{2+} > Na^+, K$

Rejection: $Na_2SO_4 > NaCl > KCl > MgSO_4 > MgCl_2 > CaCl_2$

As is clear from the Desal DK and NF270 absolute zeta potential sequence, SO_4^{2-} has more affinity than Cl^-. Therefore, sulphate salts have more absolute membrane charge density than chloride salts. Furthermore, the presence of calcium and magnesium lead to lower surface charge densities as these ions have very high surface affinity and are able to naturalise the membrane negative charge. The same observation was made by Ding et al. (2006) and Morão et al. (2006) as discussed in Section 8.1.

8.3.1.3 Charge density and concentration

Many researchers (Ariza et al. 2001; Peeters et al. 1999; Artuğ et al. 2007) found a linear relation between the membrane charge density and solution concentration (or anion concentration), which can be expressed by the Freundlich isotherm. Molina et al. (1999) found that the values of the surface charge density for the studied membranes depend on concentration and can be described by Langmuir's model for big pore diameters and Freundlich's model for smallest pore diameters. The correlation between log concentration against log $|X_d|$ for NaCl, KCl, Na_2SO_4, $MgSO_4$, $CaCl_2$ and $MgCl_2$ are shown in Figure 8.5 for Desal DK, NF270 and NTR7450. The membrane charge increases in absolute value with increasing concentration.

Table 8.4: Values of r and s of equation $X_d = r(C_F)^S$ for Figure 8.5.

	Desal DK		NF270		NTR7450	
Salts	s	r	s	r	s	r
NaCl	-0.52	0.0093	-0.75	0.0049	-0.76	0.11
KCl	-0.95	0.000283	-0.56	0.0127	-0.314	0.415
Na_2SO_4	0.74	129	0.84	336	-0.28	0.224
$MgSO_4$	0.98	1655	1	800		
$CaCl_2$	2.48	37051	1.4	515		
$MgCl_2$	1.12	212	0.335	3.57		

8.3.2 Membrane charge prediction for mixtures

Membrane charge density for mixtures was calculated using the DSPM model and correlated with pH, zeta potential and individual ions in the mixtures.

8.3.2.1 Na-K mixtures

Figure 8.6 correlates Na percentage with X_d at different pH values for Desal DK, NF270 and NTR7450. The results show that the absolute X_d values increase with increase in the pH. However, the effect of increased pH on X_d for NTR7450 is very little. This can be explained by the fact that NTR7450 is at its ultimate negative charge in the pH range of this study as discussed in the electrokinetic and filtration chapters. This suggests that the adsorption of Na (Figures 5.1, 5.2 and 5.4) and K in mixtures is more than in single salts. However, the

electrokinetic study of mixtures (Figures 5.1, 5.2 and 5.4) and the filtration study (Figures 7.2, 7.5 and 7.8) showed almost similar results for Na-K and single salts.

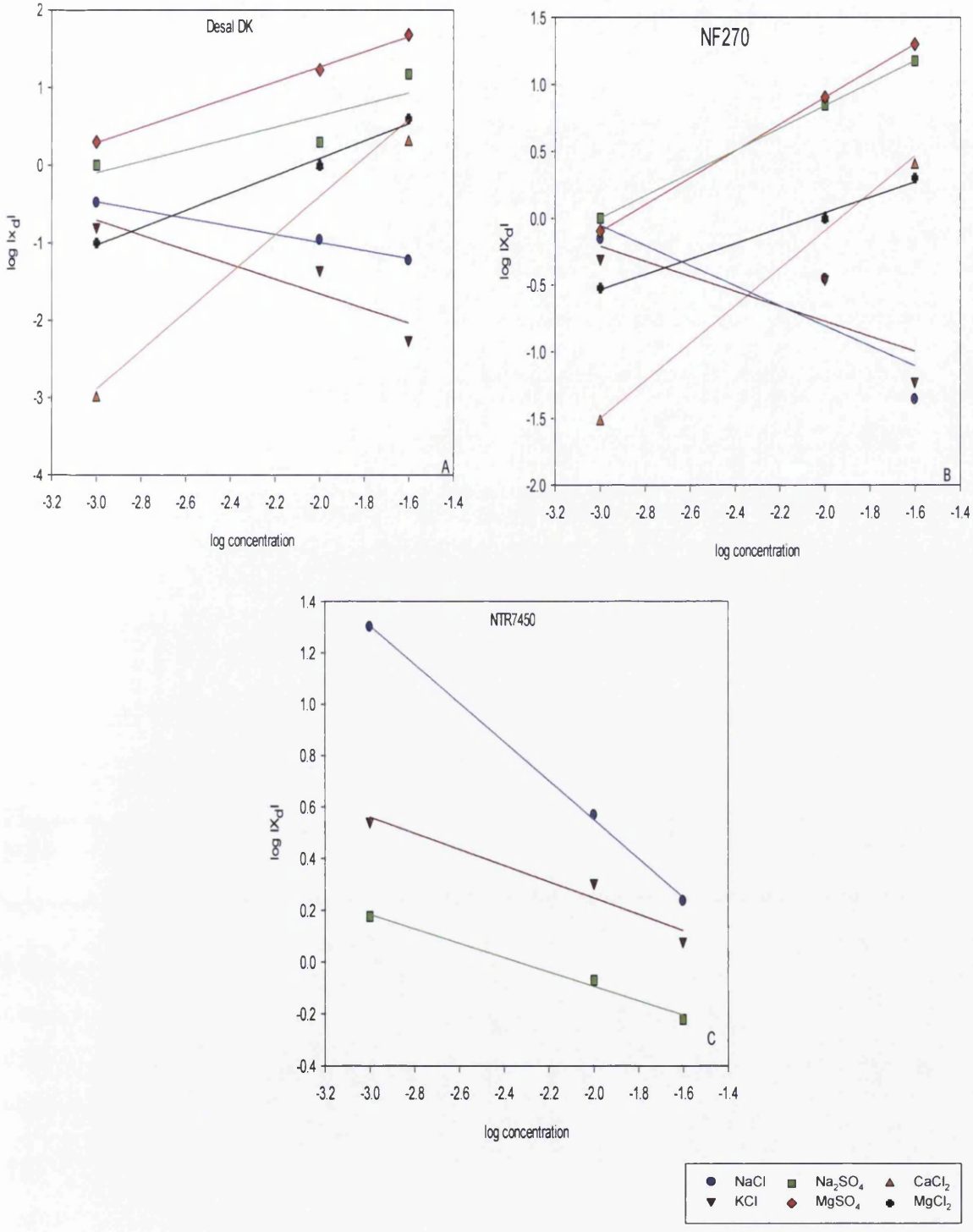

Figure 8.5: Correlation between log concentration against log $|X_d|$ for NaCl, KCl, Na_2SO_4, MgSO4, $CaCl_2$ and $MgCl_2$.

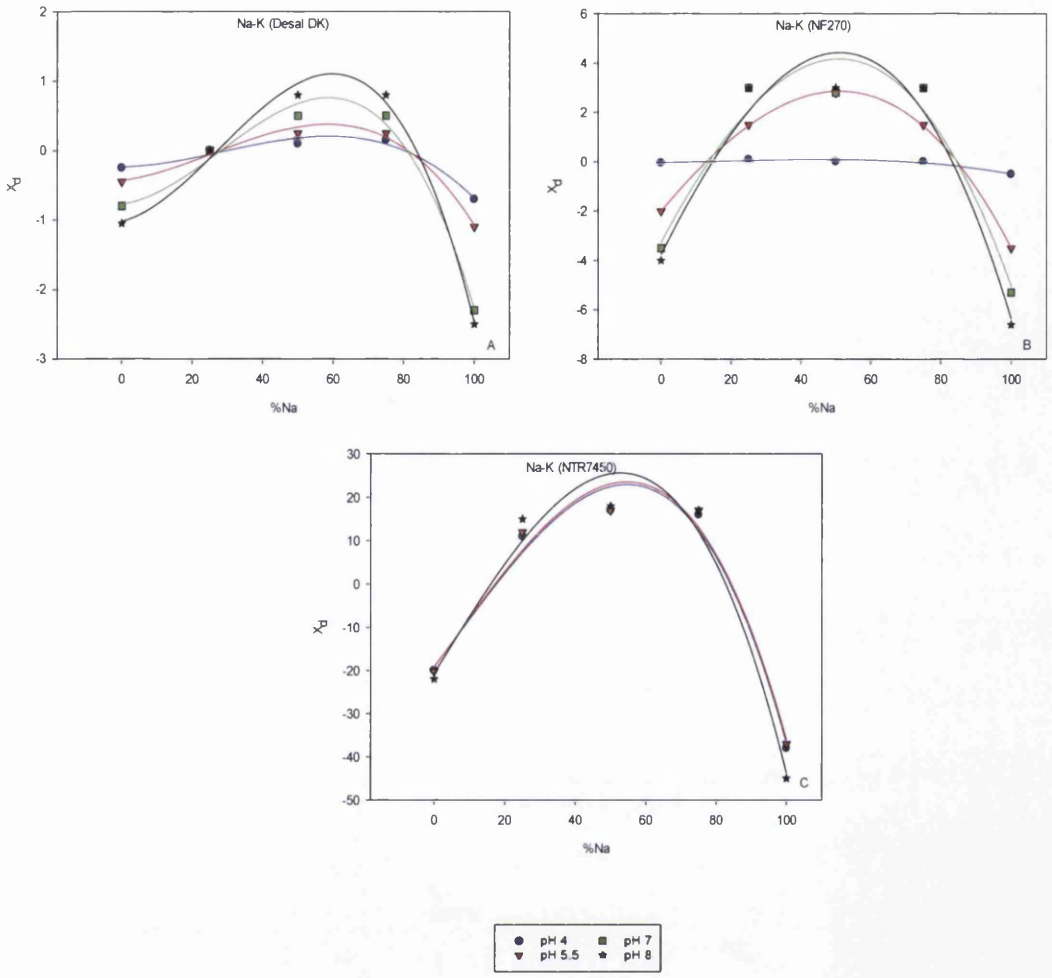

Figure 8.6: Membrane charge density as a function of % Na for Desal DK, NF270 and NTR7450.

Membrane charge density for Na-K mixtures correlated with zeta potential values was obtained from Chapter 5. The results for Desal DK are presented in Figure 8.7, where the dimensionless zeta potential values (ξ) are drawn as a function of dimensionless membrane charge density at different pH values for Desal DK.

The dimensionless membrane charge density was obtained by dividing the calculated membrane charge density by concentration of each ion in the solution, namely Na, K and Cl, and by the ionic strength of the solution. However, dimensionless membrane charge density was calculated only for Na, K and Cl as the ionic strength of these is equal to Cl

concentration, i.e. both of them equal 10 mol/m^3. Linear correlations are obtained where the degree of linearity was the best for Na followed by Cl. Table 8.5 provides the equations of linear lines obtained in Figure 8.7 A.

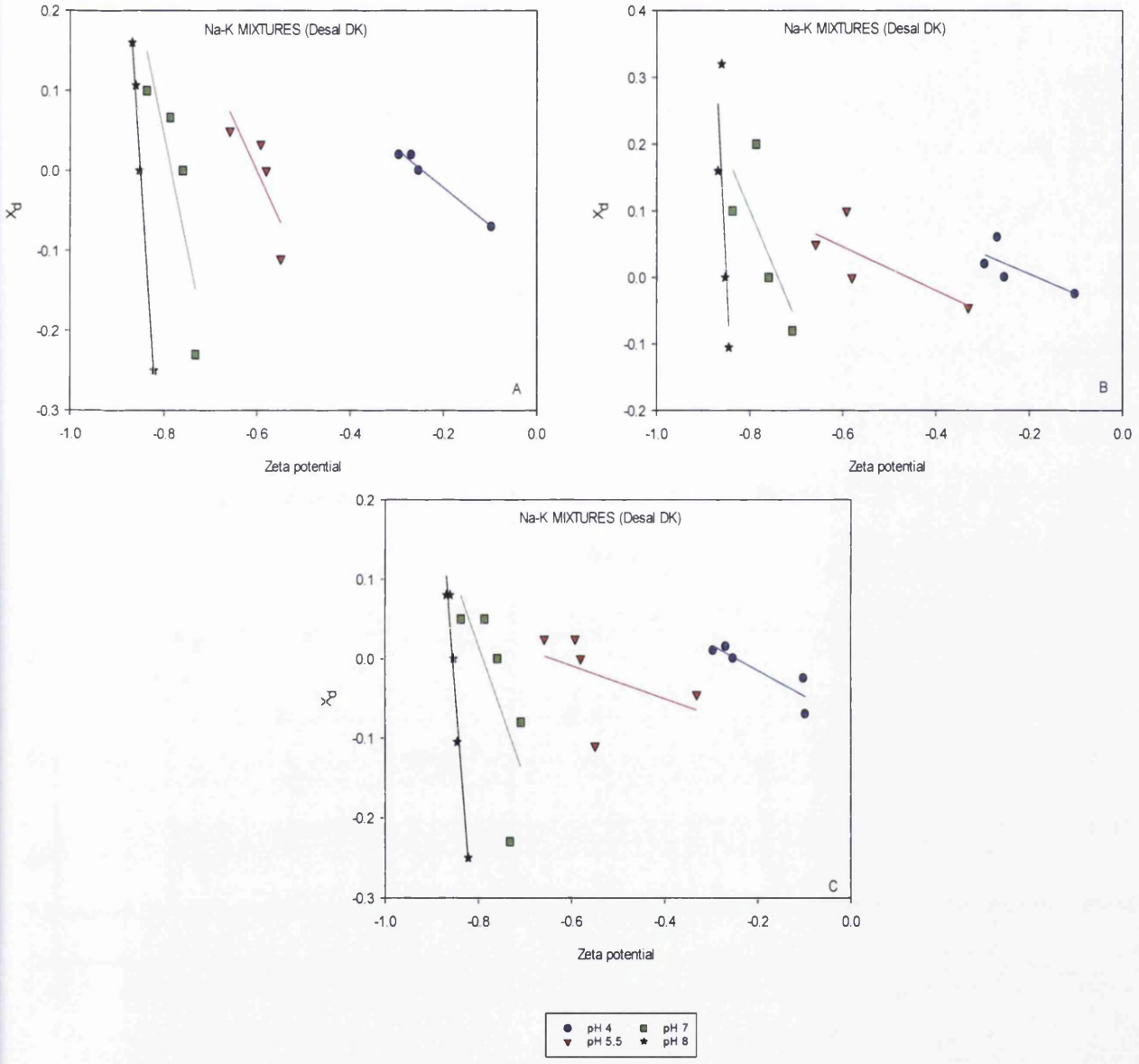

Figure 8.7: Dimensionless membrane charge density as a function of dimensionless zeta potential for Desal DK: (A) X_d calculation based on Na concentration, (B) X_d calculation based on K concentration, and (C) X_d calculation based on Cl concentration.

Table 8.5: Equations correlate dimensionless membrane charge density with dimensionless zeta potential of Na-K mixtures for Desal DK and NF270.

pH	Desal DK	NF270
4	$X_d = -0.4735\,\xi - 0.1157$	$X_d = -10.662\,\xi - 6.0171$
5.5	$X_d = -1.2806\,\xi - 0.7684$	$X_d = -0.0304\,\xi - 0.4101$
7	$X_d = -2.8331\,\xi - 2.2224$	$X_d = -12.21\,\xi + 0.0093$
8	$X_d = -8.8536\,\xi - 7.5297$	$X_d = -9.8112\,\xi + 0.2971$

As in the case of Desal DK, the data homogeneity for NF270 is the best when X_d is calculated based on Na concentration (Figure 8.8A).

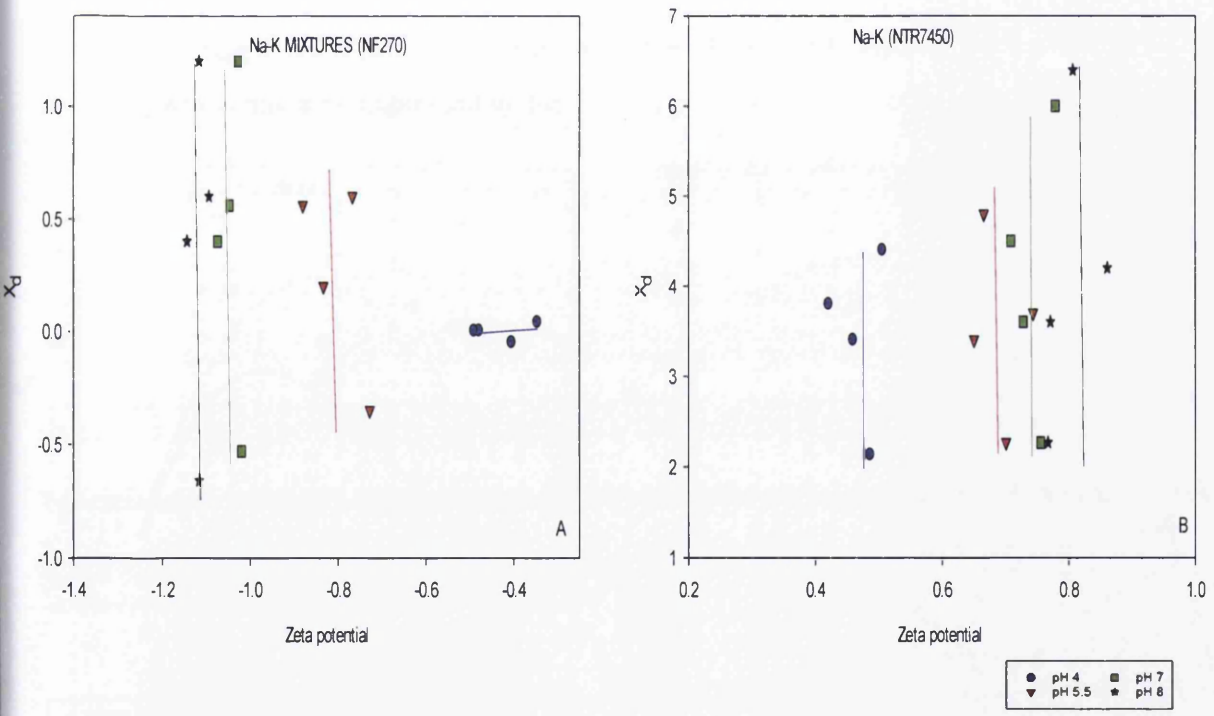

Figure 8.8: Dimensionless membrane charge density calculated based on Na concentration as a function of dimensionless zeta potential for NF270 and NTR7450.

The data for NTR7450 (Figure 8.8 B) show a trend that is opposite to the Desal DK and NF270 data trends. To illustrate, the sets of X_d values at a particular pH for NTR7450

membranes shift to left of the graph with increase in pH, while for Desal DK and NF270, it is vice versa.

8.3.2.2 Na-Ca and Na-Mg mixtures

Introducing Ca and Mg to the solution caused a problem in calculating X_d. Like single salts (see Section 8.3.1.2), X_d can only be calculated at pH near isoelectric point (pH 4), where the rejection for these two ions are maximum. X_d values could be obtained for all Na-Ca mixtures concentration at pH 4 for Desal DK and NF270, however -6 mol m^{-3} was the only X_d value obtained for Na-Ca with NTR7450, which was at 75% Na-25% Ca. In fact, X_d could not be obtained for NTR7450 with $CaCl_2$, $MgCl_2$ and $MgSO_4$ single salts (see Table 8.3). Furthermore, when comparing Ca-Mg, the model did not give any X_d value for all the membranes, which were clear as result of synergetic effect.

Figure 8.9 correlates Na percentage with X_d at pH 4 values for Desal DK, NF270 and NTR7450. The X_d values obtained for Na-Ca mixtures are more than those found with $CaCl_2$ and $MgCl_2$ single salt. This observation was also found with Na-K mixtures (see Section 8.3.2.1), which might be explained by the

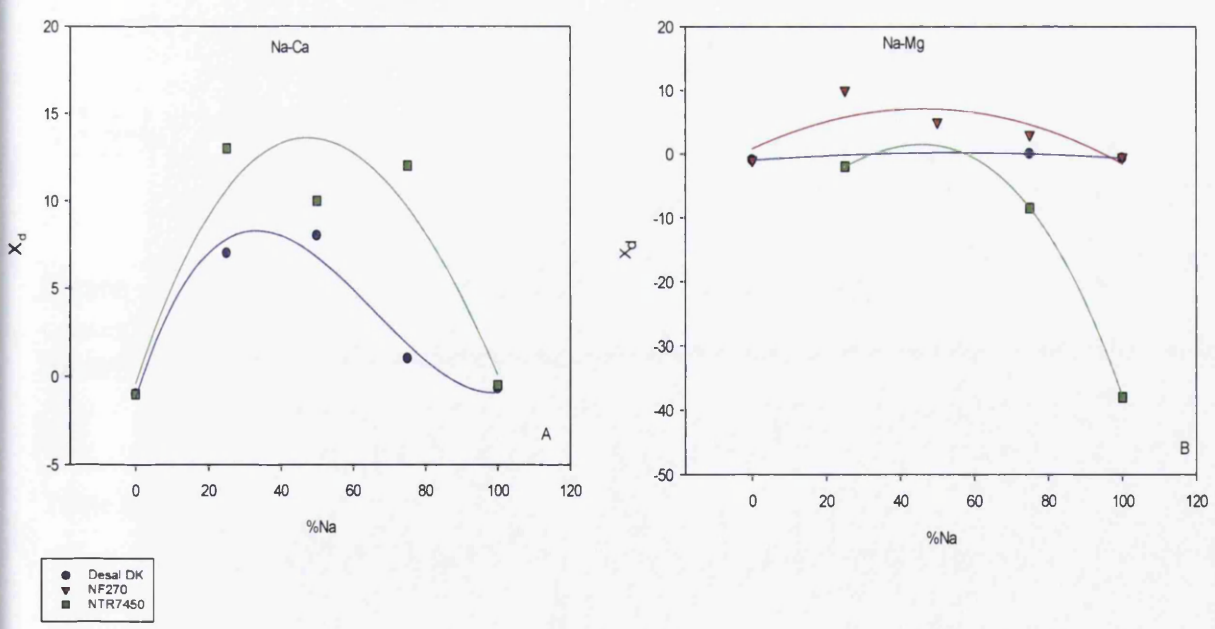

Figure 8.9: Membrane charge density as a function of % Na for Desal DK, NF270 and NTR7450.

increase in the adsorption of Ca and Na in mixtures compared to the single salts. Another explanation for this increase in X_d is as a result of increasing ionic strength. Membrane charge density for Na-Ca mixtures correlated with zeta potential values for Desal DK and NF270, as shown in Figure 8.10 A. The data for Na-Mg showed the same behaviour, but the data could be linearized as shown in Figure 8.10 B. Table 8.6 provides the equations of linear lines obtained in Figure 8.10 B.

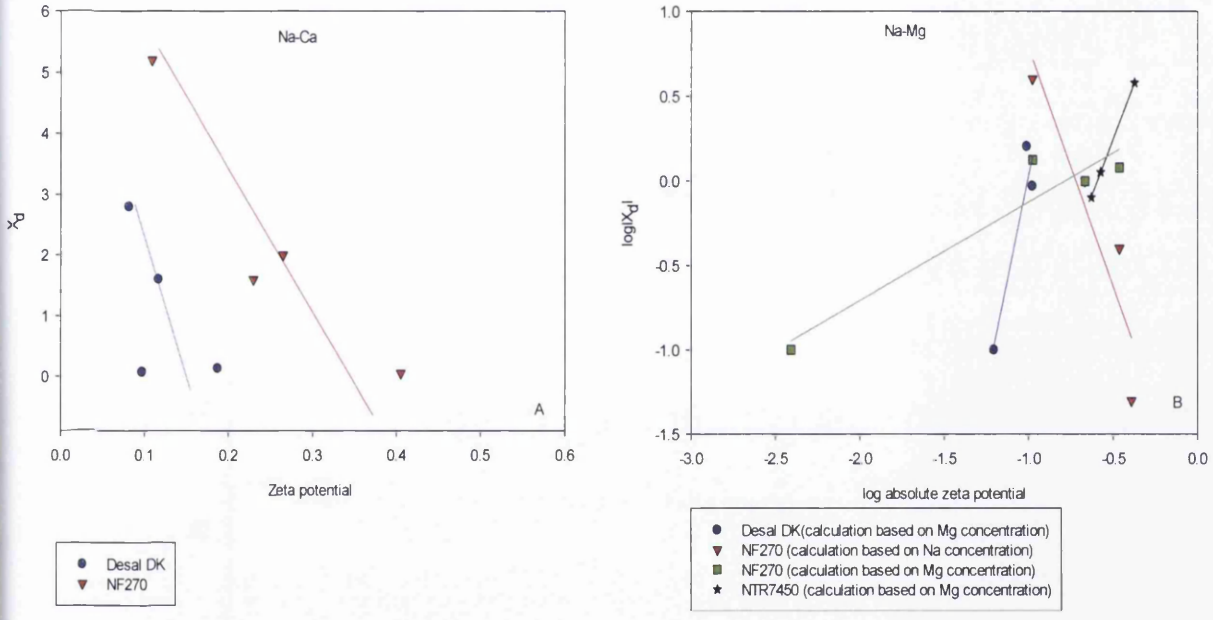

Figure 8.10: (A) Dimensionless membrane charge density calculated based on Na concentration as a function of dimensionless zeta potential for Desal DK and NF270, and (B) linearized correlation of membrane charge density and zeta potential.

Table 8.6: Values of r and s of equation $X_d = r(\xi)^S$ for Figure 8.10 B.

Ion used to calculate dimensionless X_d	Desal DK		NF270		NTR7450	
	s	r	s	r	s	r
Na	---	---	-2.8	9.22×10^{-3}	2.64	37.5
Mg	4.94	95499	0.58	2.9	--	--

8.3.2.3 Cl-SO_4 mixtures

Because the rejection of solutions that contain SO_4 is very high (~99%), only one X_d value could be calculated. Figure 8.11 correlates Cl percentage with X_d values for Desal DK, NF270 and NTR7450. Increasing the percentage of Cl makes the X_d value slightly more positive. However, this is not the case with NTR7450, where the X_d is almost not affected at all by increasing the percentage of Cl and there is a sharp drop in X_d value (X_d value becomes more negative) at 100% Cl.

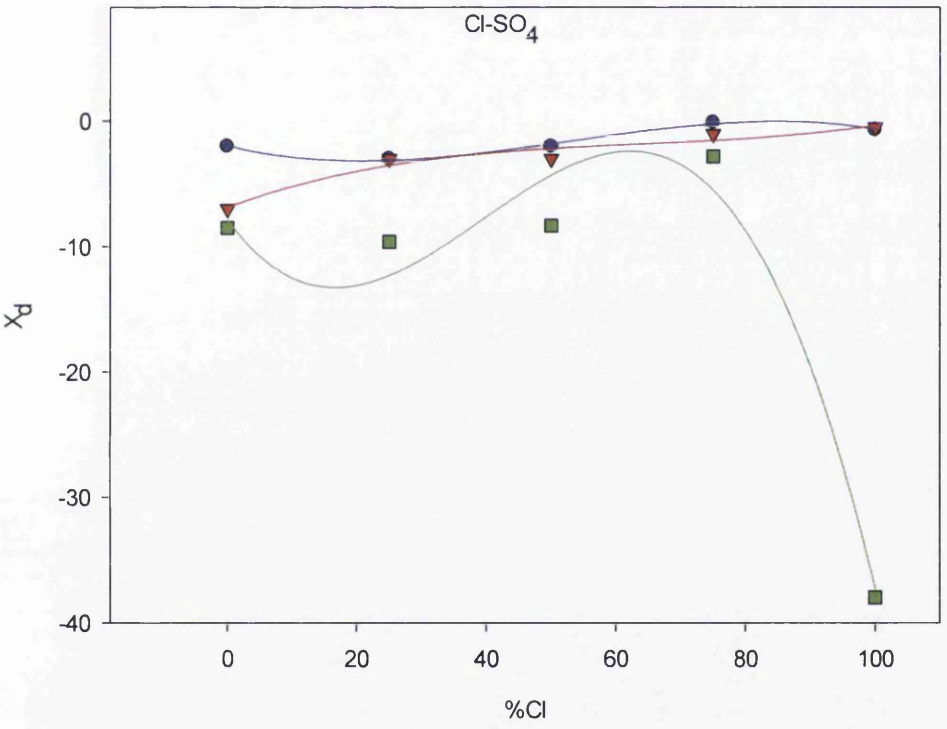

Figure 8.11: Membrane charge density as a function of % Cl for Desal DK, NF270 and NTR7450.

Figure 8.12 correlates membrane charge density for Cl-SO_4 mixtures with zeta potential values for Desal DK, NF270 and NTR7450 as shown in Figure 8.12 B; Table 8.7 provides the equations of linear lines obtained in Figure 8.12 B.

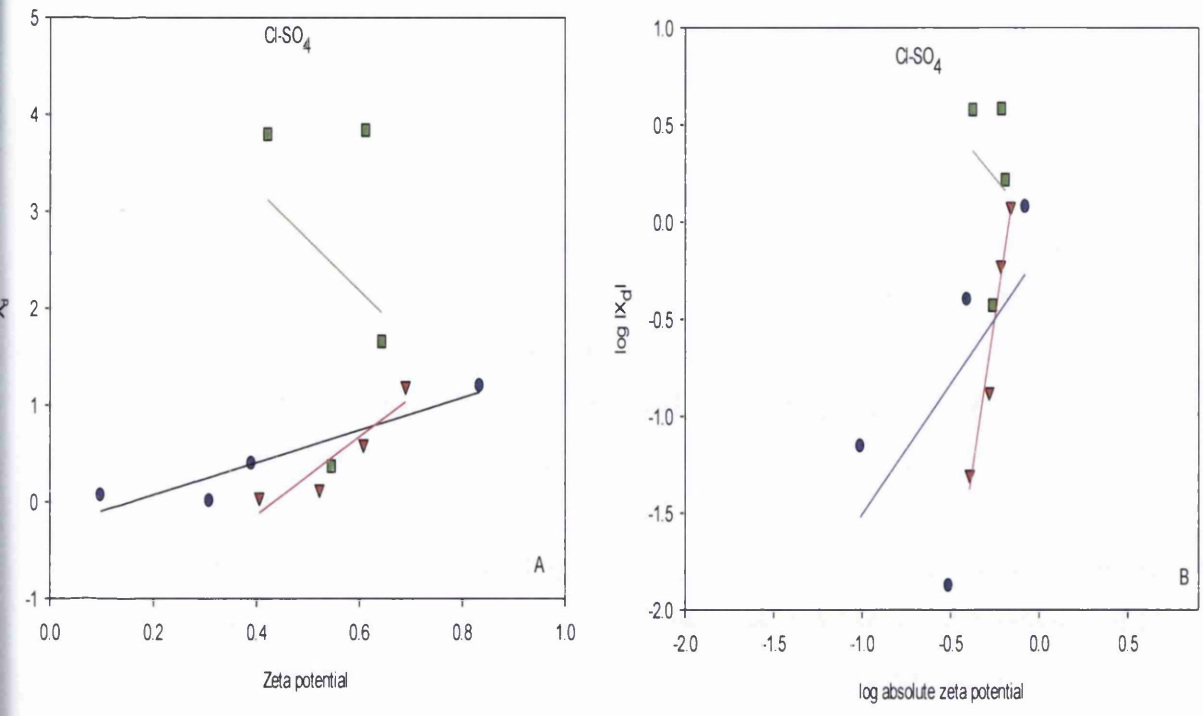

Figure 8.12: (A) Dimensionless membrane charge density calculated based on Cl concentration as a function of dimensionless zeta potential for Desal DK, NF270 and NTR7450, and (B) linearized correlation of membrane charge density and zeta potential.

Table 8.7: Values of r and s of equation $X_d = r(\xi)^S$ for Figure 8.12 B.

Ion used to calculate dimensionless X_d	Desal DK		NF270		NTR7450	
	s	r	s	r	s	r
Cl	1.34	0.69	6.17	11.07	-1.11	0.887

8.4 Conclusion

The experimental rejection data were used in this chapter to calculate the volumetric effective membrane charge density (X_d), which, in turn, was then correlated with pH, zeta potential and concentration for both single salts and mixture salt systems. The results showed that the absolute value of X_d for both single salts and mixtures increase with increase in pH value for Desal DK and NF270 and is almost stable in the case of NTR7450 over the entire pH range. For NaCl and KCl single salts, X_d was calculated for Desal DK, NF270 and NTR7450 over the entire pH range and for all concentrations, namely 0.001M, 0.01M and 0.025. Unlike NaCl and KCl, the calculation of X_d for $MgSO_4$ and Na_2SO_4 gives one value for each examined concentration over the whole pH range as the rejection of these two salts is very high by Desal DK, NF270 and NTR7450. Moreover, the model predicts only one X_d value for $MgCl_2$ and $CaCl_2$ at pH 4 for Desal DK and NF270, which represents the maximum rejection of these two salts. For NTR7450, NaCl, KCl and Na_2SO_4 are independent of the pH of the solution, while the model could not predict any value of X_d for $MgSO_4$, $CaCl_2$ and $CaCl_2$.

Like single salts, the X_d for Desal DK, NF270 and NTR7450 could be calculated for Na and K solutions (Na-K mixtures) over the entire pH range as well as all concentrations and Cl-SO_4 gave one value for each examined concentration over the whole pH range. Introducing Ca and Mg to the solution, i.e. Na-Ca and Na-Mg, caused a problem in calculating X_d. Like single salts, X_d for Desal DK and NF270 can only be calculated at a pH near isoelectric point (pH 4) where the rejection for these two ions are maximum. X_d values could be obtained for all Na-Ca mixtures concentration at pH 4 for Desal DK and NF270, but -6 mol m^{-3} was the only X_d value obtained for Na-Ca with NTR7450, which was at 75% Na-25% Ca. In fact, X_d could not be obtained for NTR7450 with $CaCl_2$, $MgCl_2$ and $MgSO_4$ single salts. Furthermore, when Ca-Mg was compared, the model did not give any X_d value for any of the membranes, which was clear as the result of synergetic effect.

The X_d values obtained for Na-Ca, Na-Mg and Na-K mixtures are more than those found with their single salts. On other hand, NTR7450 showed a sharp drop in X_d value (X_d value became more negative) at 100% Cl in the Cl-SO_4 mixture. This suggests that mixtures behave differently than single salts.

To sum up, it is clear that the presence of Ca and Mg in the feed solution causes a problem in calculating X_d for both single salts and mixtures, especially for NTR7450, which has the lowest charged surface of all the membranes under study here. These observations indicate that the current state-of-the-art model, which uses the extended Nernst–Planck equation and descriptions of equilibrium partitioning that include both the Donnan and dielectric effects, needs to be improved upon. This is essentially an issue with the fundamental descriptions used by the models and illustrates the lack in understanding of separation mechanisms of ionic species, particularly for systems containing multivalent ions where rejection is close to the maximum. While this work is not intended to deliver a step forward in nanofiltration modelling, the work does highlight that there are clearly membrane-solute-solvent interactions occurring that are not accounted for and any advancement in future models should account for the phenomena detailed here.

9.0 Conclusions and Recommendations

9.1 Conclusions

Understanding membrane separation mechanisms is essential to improving the performance of the separation. For example, change of feed solution pH or concentration has an effect on the ionic species rejection and flux. The global objective of this thesis was to investigate the role of membrane charge in the separation of ionic species at the surface of nanofiltration membranes. In order to do that, the first step was to characterize membrane charge and then use this knowledge, along with separation data, to gain insights to the mechanisms that govern the separation process of charged species by NF membranes. Finally, correlations between membrane charge characterization and the separation process were developed. The aim of creating such correlations was to reduce the amount of experimental work (only characterization needed) required to evaluate the separation efficiency of an NF membrane either in a single salt system or salt mixtures, which, in turn, would save time, labour and money.

The literature review presented in Chapter 2 suggests that the most useful technique to study membrane charge is tangential streaming potential (TSP). Therefore, this technique was selected to study the interaction between the membranes' charge and solutions in this study and the zeta potential was obtained. Unfortunately, the membrane charge studies discussed in the literature review used a limited number of salts, concentrations and membranes and most of the filtration was carried out with dead-end or frontal filtration set-ups. Some of these studies used membranes that no longer exist in the industrial market. Furthermore, most studies investigated the single salt system and a quantitative correlation between membrane charge and membrane separation performance was not achieved. Therefore, this thesis is considered a comprehensive study in which four commercial membranes were used with six different salts and mixtures of these salts at different pH and concentrations. Also, a spiral wound NF membrane module was used, which enables studying a large membrane area and using large volumes of solution in order to increase accuracy and mimic industrial separations. In addition to investigating the efficiency of separation by calculating the rejection, this thesis studied the product fluxes, individual ions rejection and proton rejection. The thesis also studied the optimization of zeta potential measurements, contact angle of the membranes, flux of deionized water at different pressures, mass transfer studies and

determination of pore size and dielectric constants for the NTR7450 membrane (most of this characterization information was not previously available).

The results of the electrokinetic study for single salts and mixtures gave full information about the magnitude of charge of each membrane and how this charge interacted with different types of ions. In fact, the divalent ions (cations and anions) were found to have the most ability to alter the membrane surface charge as they have strong affinity to the membrane surface. SO_4^{2-} was found to have the strongest affinity amongst the ions studied and is able to get closer to the surface as compared to the other anions.

The characterization of membranes (see Chapter 3) provides a full description of membrane characteristics obtained from experiments and a comparison is made with literature where available and this information can be used as a guideline for choosing the right membrane for a specific purpose. For example, the NTR7450 membrane was shown to have the largest pore size, but has the highest rejection rate for 0.01M NaCl at natural pH, while its permeability is lower than that of NF270 and higher than that of Desal DK. Therefore, this membrane may be good for Na metal recovery at this pH as the rejection of NaCl is high, but NF270 might be better for the desalination industry as its permeability is the highest among the membranes studied.

The results of the filtration study confirmed that the role of membrane charge is the most important mechanism in the separation of ionic species. The charge effect was clear because the performance of membranes was strongly dependent on pH, concentration and type of salt. In addition, although the ionic radius of ions is much smaller than the pore size of the membranes used, these ions are still highly rejected. Generally, as discussed with electrokinetic data, the divalent ions (cations and anions) have the most influential role to play in the separation performance of NF membranes and were typically more highly rejected than the monovalent ions as they hold more charge. The co-ions that adsorbed more to the membrane surface than the other ions as found in the electrokinetic study are also rejected more.

The UDSPM model was used to calculate the volumetric effective membrane charge density and many useful correlations such as charge density–pH, membrane charge density–zeta potential and membrane charge density–concentration were developed. The model was shown to work well with NaCl, KCl and Na_2SO_4. However, the membrane charge density

could not be calculated in some cases where Ca or Mg was present in the solution. The model did not provide any result with $CaCl_2$, $MgCl_2$ and $MgSO_4$ for NTR7450 and Ca-Mg mixtures for all membranes. This indicates that there are clear areas, particularly for divalent ions, where the current state-of-the-art in fundamental understanding is lacking and this work provides a framework that can be built upon to develop better models for the future. The aim of this work was not based in model development, however the results clearly emphasize that the membrane-solute-solvent interactions occurring at the surface and within the pores of nanofiltration membranes are not fully understood and modifications to the extended Nernst–Planck equation and the current descriptions of equilibrium partitioning are recommended.

To sum up, this thesis provides useful information about the interaction between membrane surface and solution, which helps to improve the fundamental understanding of NF membrane separation. This is not only important for researchers, but also for industries such as desalination and water treatment plants in order to assist production engineers to increase the efficiency of these plants.

9.2 Recommendations

The work presented in this thesis can be further developed by using the following suggestions:

1. Electrokinetic and separation studies can be carried out for sea water and different waste waters and the knowledge obtained in this thesis can be used to explain the findings of these studies.
2. EKA manufacturers and researchers can work together to optimize and standardize the zeta potential measurement procedures and provide the required tools to EKA operators to check the quality of their results.
3. Although tangential streaming potential (TSP) is a useful technique in studying membrane charge, using other techniques in this filed such as force measurements from AFM could further enhance understanding.
4. Similar characterization methods could be investigated for different kinds of membranes and membrane materials such as RO and ceramic membranes, etc. This would facilitate a much broader outlook on separations of membrane charge.
5. Research could be conducted on small commercial plants and the knowledge obtained in this thesis could be used to explain the findings of these studies.

6. Although most of the findings in this thesis can be explained from the knowledge obtained in the literature review, there is some conflict between the various research studies in some areas, especially in membrane selectivity. Therefore, more research is needed in order to improve the theory part of ionic separation.
7. Although charge effects characterization and its role in separation is very important, recent research conducted in this field is limited. Generally, the membrane charge studies found in the literature review were not comprehensive because only a limited number of salts, concentrations and membranes were used.
8. Although UDSPM is a useful tool in calculating membrane charge density and modelling membrane charge in general, the model needs to be improved for Ca and Mg solutions.
9. A computer simulation package could be developed to allow non-specialized engineers to use available NF predictive models for the optimization of existing NF plants.

Appendices

Appendix A1: List of Publications arising from this Work

A1.1 Published Papers from this work

Darren L Oatley, Laia Llenas, Nasser H.M Aljohani, Paul M Williams, Xavier , Miquel Rovira, Joan de Pablo, Investigation of the dielectric properties of nanofiltration membranes, *Desalination*, 2013, 315, 100-106.

Michael L. Gerardo, Nasser H.M. Aljohani, Darren L. Oatley-Radcliffe, Robert W. Lovitt, Moving towards sustainable resources: recovery and fractionation of nutrients from dairy manure digestate using membranes, Water Research, 2015, 80, 80-89.

A1.2 Conference Papers (* denotes presenter)

N.H.Aljohani*, D. L. Oatley, Electrokinetic study of single salt systems, Euromembrane Conference 2012, 23-27 September 2012 (Poster Presentation).

A2 The effect of electrolytes chemistry on zeta potential

The effect of solutions chemistry on zeta potential studied in literature review section 2.2.2.4.1. The electrolytes which have been used in zeta potential include indifferent salts (NaCl &KCl), divalent cations (Ca^{2+}, Mg^{2+}), divalent anions (SO_4^{2-}), humic acids, and anionic and cationic surfactants (Childress & Elimelech 1996). Table A 2.1 provides a summary of the studies that will be discussed in this section include the membranes used, salt solutions, charge study technique and most important findings.

Table A 2.1: Examples of papers studied the effect of electrolytes chemistry on zeta potential.

Salts	Membranes Membrane charge characterization method	Most important findings	References
Na_2SO_4 and KCl (single salts)	NADIR –NF-PES10 (Polyethersulfone)	For Na_2SO_4 1. Selective adsorption of the SO_4 is responsible for increasing rejection rate in the lower concentration range (up to 1x 10^{-3} mol/l) which is corresponds to higher ζ absolute value. 2. At higher concentration (>1x 10^{-3}M) a sign reversal of ζ value take place which indicates the specific adsorption of Na^+. For KCl 3. there is no preferential adsorption of the ions, neither Cl^- nor K^+	(Ernst et al. 2000)

Salts	Membranes Membrane charge characterization method	Most important findings	References
NaCl, Na_2SO4, $CaCl_2$ (single salts)	ASP35(Advanced Membrane Technology), NF45 (Dow) TSP (homemade), transversal streaming potential and Filtration (Dead End)	1. The zeta potentials decreased with increasing salt concentration, whereas the kinetic surface charge densities increased. 2.ζ values from TSP are higher than transversal streaming potential, but having the same isoelectric point.	(Peeters et al. 1999)
NaCl, sodium dodecyl sulphate (SDS), dodecyll trimethylammonium bromide(DTAB) and humic acid (HA)	NF55 (Film Tec Corp, Minneapolis, MN) aromatic TFC TSP(BI-EKA) and Filtration	1. Humic macromolecules readily adsorb to the membrane surface and that the negatively charged functional groups of the humics dominate the membrane surface charge 2. In the presence of SRHA, the NF-55 displays no isoelectric point over the pH range investigated. 3. At low pH, where the membrane and SRHA are oppositely charged, adsorption of SRHA is favourable because of both electrostatic and hydrophobic interactions. 4. At higher pH values, where the SRHA and the membrane are similarly charged, adsorption is likely dominated by hydrophobic interactions. 5. At higher pH the adsorption characteristics of surfactants are governed by the molecular structure of the surfactant molecules (e.g., type of polar head) and the characteristics of the membrane surface (e.g., charge, hydrophobicity).	(Childress & Elimelech 2000)
KCl (SP) and LiCl,NaCl.KCl.KNO_3 (Membrane Potential)	NTR7450 (PES)(Nitto Denko), NF40 Polypiperazine amide(Dow), UTC20 Polypiperazine amide(Toray Industries) and CA30 Cellulose Acetate(Hoechst) Titration , TSP(Homemade) and Membrane Potential	1. For NTR 7450, the zeta potential remained negative over the pH range studied. 2. All other membranes have a positive zeta potential at pH 3.	(Schaep & Vandecasteele 2001)

Salts	Membranes Membrane charge characterization method	Most important findings	References
Phosphate ions (as KH_2PO_4), citrate (as $KH_2C_6H_5O_7$), KCl and $CaCl_2$	SR3 and SR4(Koch), DESAL-5(GE osmonics) All are Polyamide membranes TSP (Homemade) ,Contact angle and FTIR	KCl 1. A higher ζ at alkaline conditions suggests a greater density of carboxylic to amine dissociated groups on the membrane which approved by the ATR-FTIR. $CaCl_2$ 2. Calcium decrease the magnitude of the zeta potential at pH values above IEP at different extent and surface becomes saturated at very low concentrations. In multi-ionic mixtures of low solution concentration, the membrane potential is ruled by counterions with the highest charge number, such as calcium multivalent anion solutions 3. Phosphate ions have no significant effect on the zeta potential; on the other hand, addition of citrate resulted in some changes to the membrane surface charge. However citrate appeared to not influence the membrane charge at higher pH values due to electrostatic repulsion by the negatively charged membrane surface. The charge alteration at low pH may be due to the citrate chemically binding to the positively charged amine groups Mixture of multivalent electrolyte solutions 4. When calcium and multivalent anions were combined, the anions reduced the impact on surface charge by calcium, either by simultaneous/competitive binding or by speciation with the calcium. phosphate and citrate can form soluble charged species with the calcium ions, reducing the net Ca^{2+} concentration and hence the overall effect of calcium on the membrane. The subsequent reduction in Ca^{2+} concentration, brought about by these interactions, lessened the overall effect of calcium on the membrane.	(Rice et al. 2011)
KCl (10 mM) in presence of 1 mM buffer ions : Tris,Acetate, Phosphate,Phthalate,Citrate	Biomax(-)asymmetric polyethersulfone and Biomax (+) both from (Millipore), Omeg (Filtron Technology Corp. (Northborough, MA). transversal streaming potential	1. Multivalent anions (like phosphate and citrate) have little effect on the surface charge of the BiomaxTM membranes since these anions are largely excluded from the double layer. 2. Strong adsorption/ binding of the di- and tri-valent anions to the surface of the positively-charged membrane.	(Burns & Zydney 2000)
NaCl,NH_4Cl, $FeCl_2$,$AlCl_3$, Na_2SO_4 ,$CaCl_2$ Na_2S,Na_3PO_4, $FeSO_4$ and $Al_2(SO_4)_3$	Microfiltration ceramic membrane (Nanjing jiusi high Tec co Ltd china) Electroosmosis	1.The shifting of the IEP of the membrane to a higher pH value in $FeCl_2$, $CaCl_2$and $AlCl_3$solutions shows specific adsorption of the cations, and specific adsorption of the S^{2-} , SO_4^{2-}, $PO4^{3-}$ ions shifts the IEP to a lower pH value. 2.The zeta potential in $FeSO_4$ and $Al_2(SO_4)_3$ solutions were very low, indicating a decrease of charge density on the membrane surface due to the complex co-adsorption of the cations and the anions on the membrane surface. 3. The IEP of the membrane obtained in this paper is different from that reported in some literatures and from alumina particles which may be related to the effects of the preparation process on the membrane surface properties.	(Zhao et al. 2005)

Salts	Membranes Membrane charge characterization method	Most important findings	References
NaCl, Glucose, KCl	NF200(Dow) Polyamide, Desal -5 DL Polyamide(Osmonics) and NTR7450 PES (Hydranautics) TSP (Homemade), Filtration and Contact angle	1.The NF 200 membrane has much more surface charge than the other membranes which maybe because the membrane possesses dissociable carboxylic and amine groups and therefore can exhibit negative or positive surface charge depending on pH. 2. NF 200 membrane has a much stronger negative charge at basic conditions than positive charge at acidic condition.	(Mänttäri et al. 2006)
NaCl,$CaCl_2$, Na_2SO_4,$MgSO_4$,Humic acid ,Surfactants (Cationic, Anionic)	Polyamide RO (TFC), NF(TFC) both from Fluid System (Sandiego), NF70 (TFC) from Film Tec (Minnepolis) and Asymmetric Cellulose from Desalination System(Escondido, CA) TSP(B1-EKA)	1. Divalent cations more readily adsorb to the membrane surface than divalent anions, especially in the higher pH range. 2. Humic acid readily adsorb to the membrane surface and the adsorption is enhanced with increasing molecular weight of the humic macromolecules and with the addition of divalent cations to the solution. 3. Anionic and cationic surfactants readily adsorbed and markedly influence the membrane surface charge at low surfactant concentrations which is attributed to the formation of hemimicelles at the membrane-solution interface. 4. The surface charge origin of cellulose acetate membrane maybe a result of chemical post-treatment with an additive containing acidic functional groups or dissociation of carboxyl groups and the membranes behave as cation exchange membranes at low electrolyte concentration.	(Childress & Elimelech 1996)
NaCl,KCl,Na_2SO_4 and $CaCl_2$	Two kinds of microporous membranes a membrane made of a mixture of alumina-titania and the other membrane covered with an additional titania layer. transversal SP	1. The shifting of the isoelectric point of the membranes shows specific adsorption of calcium and sulphate ions onto the surface. 2. The additional titania layer on the alumina-titania support does not seem to modify the electrokinetic properties of the membrane.	(Szymczyk et al. 1997)

Salts	Membranes Membrane charge characterization method	Most important findings	References
NaCl,KCl, Na_2SO_4,Mg SO_4 and $MgCl_2$	PE–MF membrane (Asahi Kasei ,Japan) transversal streaming potential	1.The sequence of the ratio of ΔE to ΔP from large to small is NaCl > Na_2SO_4 > $MgCl_2$ for a very low salt concentration. 2. The value of ΔE diminishes sharply with an increase of salt concentration and the varying tendency for the solution containing a bivalent cation or anion is faster than that for the solution containing a univalent ion. 3. ΔE is very sensitive to ΔP but not linear if the salt concentration is very low (SP is an effective method to determine the electrical properties at a limited range of salt concentration). 4. The value of SP decreased more rapidly at low salt concentrations and obviously slowly when the salt concentration was over 4.0 mol×m^{-3}. 5. A comparison of the values of SP : KCl is close to NaCl solution; then the value of $MgCl_2$ is about 1/4–1/6 of that of the KCl or NaCl solutions. $MgSO_4$ solution is about 1/2 of that in the Na_2SO_4 solution. Na_2SO_4 solution was about 1/2–1/3 of that in the NaCl solution. The value of SP the MgSO4 solution was about 3/2 of that in $MgCl_2$ solution. 6. the valence of ions have a strong influence on the value of SP of a PE–MF membrane, and that a cation have a stronger influence than an anion.	(Ding et al. 2006)
Tertiary wastewater effluent(actual membrane Feed waters), glutaral-dehyde (a membrane storage agent), atrazine(a pesticide) , Humic acid and $CaCl_2$	TFC-HR , TFC-ULP membrane(Koch Membrane Systems ,Wilmington, MA, USA) TSP(B1-EKA)	1. For tertiary wastewater effluent, adsorption of organic acids in the wastewater effluent may be the cause of the more negative zeta potential in the low pH range and the presence of divalent cations may be the cause of the more positive zeta potential in the high pH range. 2. Glutaraldehyde and atrazine showed little effect on the surface charge of the membranes Unlike sodium meta-bisulfite which caused the membrane to be more negatively charged over 3. When atrazine was combined with humic acid, the atrazine reduced the effect of the humic acid and resulted in a less negative surface charge than when the humic acid was tested alone.	(Deshmukh & Childress 2001)
KCl,$CaCl_2$ and $MgSO_4$	NFT50 TFC RO/NF Polypiperazine amide (Alfa Laval) transversal streaming potential , TSP(Homemade) and Filtration	1. When both divalent cations (Mg^{2+}) and anions (SO_4^{2-}) are present in solution, the effect of the divalent anion is opposite to the effect of the divalent cation. 2. Mg^{2+} adsorbs less than Ca^{2+}, therefore the zeta potential curve is intermediate between the curves obtained for KCl and $CaCl_2$ 3. The increase of the ionic strength decrease the membrane negative charge along the surface produces which is explained by a shielding effect.	(Teixeira et al. 2005).
Four chloride salts KCl,NaCl,$CaCl_2$ and Mg Cl_2, 5potassium salt KNO_3, $KClO_3$, K_2CO_3,, K_2SO_4, $K_2Cr_2O_7$ and Na_2HPO_4	PES (Sartorius AG, Germany) TSP (EKA SurPASS) and FTIR	1. The absolute zeta potentials decreases were in this order: Na+ > Mg2+ ≈ Ca2+ > K+ > at the range of pH=4.0–6.0. 2.the absolute zeta potential decrease in this order: Na+ > K+ > Mg2+ ≈ Ca2+ at the range of pH=6–8. 3. At the range of pH=4.0–8.0 values, PES membranes did not give any isoelectric point, 4. The absolute zeta potential of PES membrane varied almost linearly with solution pH over the range from 4.0 to 8.0 for Cl– anion 5. The absolute zeta potential decrease was in this order: SO_4^{2-}> $Cr_2O_7^{2-}$> CO_3^{2-}> NO^-_3> ClO_3^-> Cl^-	(Salg et al. 2013)

Salts	Membranes Membrane charge characterization method	Most important findings	References
KCl	Degussa P-25 titanium dioxide membrane	1. TSP and FSP measurements were sensitive to solution pH, temperature, fluid pressure and UV irradiation. 2. The pH drifts (difference of initial and final pH) were observed during the TSP measurements of TiO2 membranes.	(Wang & Ku 2006)
	Malvern (Zetasizer 2000, TSP (homemade), transversal streaming potential		
NaCl, Humic Acid	Cellulose acetate ,Composite polyamide RO membranes(Hydranautics,San Diego,USA)	1. Cellulose acetate and composite polyamide acquire a negative surface charge through adsorption of anions from solution. 2. Humic acid adsorb onto membrane surfaces and markedly affect their zeta potential. 3. Chemical substance which introduced during the manufacturing of the membrane can influence the membrane charge.	(Elimelech et al.1994)
	TSP(BI, EKA)		

A3 The Fortran™ code

In order to calculate membrane charge density (X_d) in this thesis (chapter 8), computer codes using the programming language Fortran™ were used. Codes for simple salt and binary systems were provided by Oatley (2004) and Welfoot (2001).

A3.1 The Fortran™ code for single salt

```
PROGRAM MAIN
IMPLICIT DOUBLE PRECISION (A-Z)
INTEGER I, IT1, J, K, SWITCH, NMAX, Z
 PARAMETER (NMAX=2)
DIMENSION D0 (NMAX), RSOL (NMAX), Z(NMAX), CW(NMAX), LAMBDA(NMAX),
    +       PHI (NMAX), KD (NMAX), KC (NMAX), DP (NMAX), DELTAW (NMAX),
    +       C0 (NMAX), TESTFUNC (3)
    COMMON /ALL/    BOLTZC, F, R, TEMP, XD
    COMMON /OTHERS/ C0, DELTAW, PHI, Z, VEL, KC, DP, DX
```

```
*
*---INPUTTING MEMBRANE CHARACTERISTICS
      RP=0.6D-9
*     CHARGE=-1D0
      CBULK=25D0
      XD=-0D0
*
      DPRESS=1.0D6
*
*---ORIENTED SOLVENT LAYER DIELECTRIC
      DIELECL=45D0
*---INPUTING SOLUTE DATA
*
      IT1=3
*
      IF (IT1.EQ.1) THEN
*          (Sodium Chloride NaCl)
           Z (1) =1
           Z (2) =-1
           D0 (1) =1.333D-9
           D0 (2) =2.031D-9
           RSOL (1) =1.840D-10
           RSOL (2) =1.207D-10
           CW (1) =CBULK
           CW (2) =CW (1)
*
       ELSE IF (IT1.EQ.2) THEN
*          (Sodium Sulphate Na2SO4)
           Z (1) =1
           Z (2) =-2
           D0 (1) =1.333D-9
           D0 (2) =1.062D-9
           RSOL (1) =1.840D-10
```

```
      RSOL (2) =2.309D-10
      CW (2) =CBULK
      CW (1) =-(Z (2)/Z (1))*CW (2)
*
    ELSE IF (IT1.EQ.3)THEN
*     (Magnesium Chloride MgCl2)
      Z(1)=2
      Z(2)=-1
      D0(1)=0.705D-9
      D0(2)=2.031D-9
      RSOL(1)=3.479D-10
      RSOL(2)=1.207D-10
      CW(1)=CBULK
      CW(2)=-(Z(1)/Z(2))*CW(1)
*
    ELSE IF (IT1.EQ.4)THEN
*     (Magnesium Sulphate MgSO4)
      Z (1) =2
      Z (2) =-2
      D0 (1) =0.705D-9
      D0 (2) =1.062D-9
      RSOL (1) =3.479D-10
      RSOL (2) =2.309D-10
      CW (1) =CBULK
      CW (2) =CW (1)
*
    ELSE IF (IT1.EQ.5) THEN
*     (Sodium pyruvate)
      Z (1) =1
      Z (2) =-1
      D0 (1) =1.333D-9
      D0 (2) =1.092D-9
      RSOL (1) =1.840D-10
```

```
      RSOL (2) =2.469D-10
      CW (1) =CBULK
      CW (2) =CW (1)
*
    ELSE IF (IT1.EQ.6) THEN
*     (H+ Nanate)
      Z (1) =1
      Z (2) =-1
      D0 (1)=9.31D-9
      D0 (2) =0.698D-9
      RSOL (1) =0.0260D-9
      RSOL (2) =0.351D-9
      CW (1) =CBULK
      CW (2) =CW(1)
    ELSE IF (IT1.EQ.7) THEN
*     (Na Lactate)
      Z (1) =1
      Z (2) =-1
      D0 (1) =1.333D-9
      D0 (2) =1.66D-9
      RSOL (1) =1.840D-10
      RSOL (2) =1.47D-10
      CW (1) =CBULK
      CW (2) =CW (1)
    ELSE IF (IT1.EQ.8) THEN
*     (Cefuroxime)
      Z (1) =1
      Z (2) =-1
      D0 (1) =1.333D-9
      D0 (2) =0.540D-9
      RSOL (1) =1.840D-10
      RSOL (2) =4.530D-10
      CW (1) =CBULK
```

```
        CW (2) =CW (1)
      ELSE IF (IT1.EQ.9) THEN
*       (Calcium chloride CaCl2)
        Z (1) =2
        Z (2) =-1
        D0 (1) =0.791D-9
        D0 (2) =2.031D-9
        RSOL (1) =3.10D-10
        RSOL (2) =1.207D-10
        CW (1) =CBULK
        CW (2) =-(Z (1)/Z (2))*CW (1)
      ELSE IF (IT1.EQ.10) THEN
*       (Potassium chloride KCl)
        Z (1) =1
        Z (2) =-1
        D0 (1) =1.95D-9
        D0 (2) =2.031D-9
        RSOL (1) =1.25D-10
        RSOL (2) =1.207D-10
        CW (1) =CBULK
        CW (2) =CW (1)

      END IF
*
*--INPUTTING CONSTANTS
    PI=DACOS (-1D0)
*---FARADAY [C mol-1]
    F=96487D0
*---GAS [J mol-1 K-1]
    R=8.314D0
*---BOLTZMANN [J K-1]
    BOLTZC=1.38066D-23
*---TEMPERATURE [K]
```

```
    TEMP=298D0
*---ELECTRIC FIELD [C V-1 m-1]
    ELEFIELDC=8.85419D-12
*---ElEMENTAL ELECTRON CHARGE [J V-1]
    CHARGE=1.602177D-19
*---BULK SOLVENT VISCOSITY (@ 298 K) [kg m-1 s-1]
    VISCOS=0.893D-3
*---BULK SOLVENT DIELECTRIC
    DIELECB=80D0
*---MEMBRANE THICKNESS [m]
    DX=1D-6
*
*---CALCULATION OF PORE SIZE DEPENDENT PROPERTIES
*
*---PORE VISCOSITY
    IF (RP.LT.0.28D-9) THEN
      VISCP=10D0*VISCOS
    ELSE
      RATIO=0.28D-9/RP
      VISCP=VISCOS*(1D0+ (18D0*RATIO)-(9D0*RATIO**2))
    END IF
*
*---CALCULATION OF HINDERANCE FACTORS
*  (7TH ORDER NEW VERSION)
    DO I=1, NMAX
      LAMBDA (I) =RSOL (I)/RP
      PHI (I) = (1D0-LAMBDA (I)) **2
*
*---CONSTANTS FOR KD
      KD1=1.0000D0
      KD2=-2.1812D0
      KD3=0.7328D0
      KD4=-0.9065D0
```

```
      KD5=6.7272D0
      KD6=-10.2324D0
      KD7=6.3293D0
      KD8=-1.4692D0
*
      IF (LAMBDA (I).GT.0.98D0) THEN
        KD (I) =0D0
      ELSE
        KD (I) =KD1+KD2*LAMBDA (I) +KD3*LAMBDA (I) **2+KD4*LAMBDA (I)
**3+
     +        KD5*LAMBDA (I) **4+KD6*LAMBDA (I) **5+KD7*LAMBDA (I) **6+
     +        KD8*LAMBDA (I)**7
      END IF
*
*---CONSTANTS FOR KC
      KC1=1.0000D0
      KC2=0.0650D0
      KC3=-1.9370D0
      KC4=8.5211D0
      KC5=-27.3398D0
      KC6=44.4150D0
      KC7=-34.5582D0
      KC8=10.3358D0
*
      KC (I) = (KC1+KC2*LAMBDA (I) +KC3*LAMBDA (I) **2+KC4*LAMBDA (I)
**3+
     +      KC5*LAMBDA (I) **4+KC6*LAMBDA (I) **5+KC7*LAMBDA (I) **6+
     +      KC8*LAMBDA (I) **7)*(2D0-PHI (I))
*
      DP (I) =KD (I)*D0 (I)*VISCOS/VISCP
    END DO
*
*---CALCULATION OF PORE DIELECTRIC CONSTANT
```

```
      IF (RP.LE.0.28D-9) THEN
        DIELECP=DIELECL
      ELSE
        MU=0.28D-9/RP
        FUNC=DIELECB-DIELECL
        DIELECP=DIELECB-2D0*MU*FUNC+FUNC*MU**2
      END IF
*---CALCULATION OF BORN ENERGY TERM
      FUNC2=1D0/DIELECP-1D0/DIELECB
      DO I=1, NMAX
        DELTAW (I) = ((Z (I) **2)*(CHARGE**2)*FUNC2)/
     +          (8D0*PI*ELEFIELDC*RSOL (I))
      END DO
*
*---CALLING FOR THE INLET CONCENTRATION C0 (I) FROM PARTITN
*
      CALL PARTITN (CW, DELTAW, PHI, Z, C0)
*
*---SETTING MAX AND MIN VALUE FOR OUTPUT CONCENTRATION
*
      CP1MIN=1D-6*CW (1)
      CP1MAX=CW (1)
*
      CP1START= (CP1MAX+CP1MIN)/2D0
*
*---SETTING UP THE PRESSURE LOOP
      PRESS=0D6
*     DPRESS=0.1D6
      OPEN (5, FILE='2IONFULL.RES')
      WRITE (5, 10) 0D0, 0D0
*
*---CALCULATION OF REJECTION
      DO I=1, 1
```

```
      PRESS=PRESS+DPRESS
      VEL= (PRESS*RP**2)/ (8D0*DX*VISCP)
      CP1STEP=CP1MAX/5D0
*---INITIAL CP1 GUESS VALUES
      CP1C=CP1START
      CP1N=CP1C+CP1STEP
      CP1S=CP1C-CP1STEP
*---INITIAL TEST FUNCTION
      TEST=10D0
      TESTMIN=2000D0
      K=0
      DOWHILE (TEST.GT.1D-12)
*
*---CALCULATION OF EXIT CONCENTRATION FOR EACH POINT
        CALL ROOT (CP1C, CDX1C)
        CALL ROOT (CP1N, CDX1N)
        CALL ROOT (CP1S, CDX1S)
*
*---CHECKING FOR NEGATIVE CONCENTRATIONS AND CALCULATING
PROFILES
*
        CALL CONC (CP1N, CDX1N, SWITCH)
        IF (SWITCH.EQ.0) THEN
          CALL FULL (CP1N, CDX1N, TESTN)
        ELSE
          TESTN=100D0
          SWITCH=0
        END IF
*
        CALL CONC (CP1S, CDX1S, SWITCH)
        IF (SWITCH.EQ.0) THEN
          CALL FULL (CP1S, CDX1S, TESTS)
        ELSE
```

```
        TESTS=100D0
        SWITCH=0
      END IF
*
      CALL CONC (CP1C, CDX1C, SWITCH)
      IF (SWITCH.EQ.0) THEN
        CALL FULL (CP1C, CDX1C, TESTC)
      ELSE
        TESTC=100D0
        SWITCH=0
      END IF
*---EVALUATING THE MINIMUM TEST FUNCTION
      TESTFUNC (1) =TESTC
      TESTFUNC (2) =TESTN
      TESTFUNC (3) =TESTS
*
      K=1
      DO J=1, 3
        IF (TESTFUNC (J).LT.TESTMIN) THEN
          TESTMIN=TESTFUNC (J)
          K=J
        END IF
      END DO
      IF (K.EQ.1) THEN
        TEST=TESTC
        CP1STEP=CP1STEP/1.1D0
        CP1C=CP1C
        CP1N=CP1C+CP1STEP
        CP1S=CP1C-CP1STEP
      END IF
      IF (K.EQ.2) THEN
        TEST=TESTN
        CP1C=CP1N
```

```
          CP1N=CP1C+CP1STEP
          CP1S=CP1C-CP1STEP
        END IF
        IF (K.EQ.3) THEN
          TEST=TESTS
          CP1C=CP1S
          CP1N=CP1C+CP1STEP
          CP1S=CP1C-CP1STEP
        END IF
*         IF (CP1STEP.LT.1D-50) THEN
*           GO TO 15
*         END IF
        WRITE (*, 11) TEST, I
        IF (CP1STEP.LT.1D-20) THEN
          SSW=1D0
          GOTO 13
          ELSE
          SSW=0D0
        END IF
      END DO
*       CP2C=-(Z (1)*CP1C/Z (2))
*  15   CONTINUE
      REJ1=1D0-CP1C/CW (1)
*       REJ2=1D0-CP2C/CW (2)
      WRITE (*, 10) (PRESS/1D6), REJ1
  13    IF (SSW.LT.0.5D0) THEN
          WRITE (5, 10) (PRESS/1D6), REJ1
        ELSE
          WRITE (5, 10) (PRESS/1D6)
      END IF
  10    FORMAT (1X, T4, F12.3, T18, F12.6, T32, F12.6)
  11    FORMAT (1X, T4, F15.12, T22, I4)
*  10    FORMAT(1X,F12.3,3X,F12.6,3X,F12.6,3X,F12.6,3X,E12.4,3X,F12.6)
```

```
      CP1START=CP1C
    END DO
*     WRITE (5,*)  "
*     WRITE (5, 3704) 'Membrane Pore Radius', RP
*     WRITE (5, 3705) 'Membrane Charge Density', XD
*     WRITE (5, 3705) 'Layer Dielectric Constant', DIELECL
*     WRITE (5, 3705) 'Pore Dielectric Constant', DIELECP
*     WRITE (5, 3704) 'Pore Viscosity', VISCP
*     WRITE (5,*)  "
*     WRITE (5,*) ('OTHER DERIVED VALUES FOR THE CALCULATION')
*     WRITE (5,*)  "
*     WRITE (5, 3702) 'Species',' Chloride',' Sodium'
*     WRITE (5, 3703) 'Feed Conc =', CW (1), CW (2)
*     WRITE (5, 3700) 'Mem Conc. Co', C0 (1), C0 (2)
*     WRITE (5, 3700) 'Lambda =', LAMBDA (1), LAMBDA (2)
*     WRITE (5, 3700) 'Phi =', PHI (1), PHI (2)
*     WRITE (5, 3700) 'KD =', KD (1), KD (2)
*     WRITE (5, 3700) 'KC =', KC (1), KC (2)
*     WRITE (5, 3701) 'DP =', DP (1), DP (2)
*     WRITE (5, 3701) 'BORN =', DELTAW (1), DELTAW (2)
*3700  FORMAT(1X,T4,A12,T18,F12.6,T32,F12.6,T46,F12.6,T60,F12.6)
*3703  FORMAT(1X,T4,A12,T18,F12.3,T32,F12.3,T46,F12.3,T60,F12.3)
*3701  FORMAT(1X,T4,A12,T18,E12.3,T32,E12.3,T46,E12.3,T60,E12.3)
*3702  FORMAT(1X,T4,A12,T18,A12,T32,A12,T46,A12,T60,A12)
*3704 FORMAT (1X, T2, A25, T40, E13.3)
*3705 FORMAT (1X, T2, A25, T40, F13.3)
    CLOSE (5)
    STOP
    END
*
*-----------------------------------------------------------------------
*========================== END OF MAIN PROGRAM
==========================
```

```
*-----------------------------------------------------------------------
*
*---SUBROUTINE PARTITN FOR C0 (I)
      SUBROUTINE PARTITN (CW, DELTAW, PHI, Z, C0)
      IMPLICIT DOUBLE PRECISION (A-Z)
      INTEGER*4 COUNT, I, NMAX, Z
      PARAMETER (NMAX=2)
      DIMENSION C0 (NMAX), CONC (NMAX), CW (NMAX), DELTAW (NMAX),
     +        PHI (NMAX), Z (NMAX)
      COMMON /ALL/    BOLTZC, F, R, TEMP, XD
*
*===== CALCULATION =====
*---Initial values
      PSI=0D0
      TEST=20D0
      COUNT=0
*---Iteration
      DOWHILE (TEST.GT.1D-6)
        PSINEW=PSI
        SUM=0D0
        DO I=1, NMAX
          CONC (I) =CW (I)*PHI (I)*DEXP ((-Z (I)*F*PSINEW)/(R*TEMP))*
     +             DEXP (-DELTAW (I)/ (BOLTZC*TEMP))
          SUM=SUM+ (Z (I)*CONC (I))
        ENDDO
        TESTNEW=SUM+XD
        IF (COUNT.EQ.0) THEN
          IF (TESTNEW.GT.0) THEN
            PSI=PSINEW+0.1D0
            PSIABOVE=PSINEW
            TEST=DABS (TESTNEW)
            COUNT=1
          ENDIF
```

```
    IF (TESTNEW.LT.0) THEN
      PSI=PSINEW-0.1D0
      PSIBELOW=PSINEW
      TEST=DABS (TESTNEW)
      COUNT=2
    ENDIF
  ENDIF
  IF (COUNT.EQ.1) THEN
    IF (TESTNEW.GT.0) THEN
      PSI=PSINEW+0.1D0
      PSIABOVE=PSINEW
      TEST=DABS (TESTNEW)
    ENDIF
    IF (TESTNEW.LT.0) THEN
      PSI=PSINEW-0.1D0
      PSIBELOW=PSINEW
      TEST=DABS (TESTNEW)
      COUNT=3
    ENDIF
  ENDIF
  IF (COUNT.EQ.2) THEN
    IF (TESTNEW.GT.0) THEN
      PSI=PSINEW+0.1D0
      PSIABOVE=PSINEW
      TEST=DABS (TESTNEW)
      COUNT=3
    ENDIF
    IF (TESTNEW.LT.0) THEN
      PSI=PSINEW-0.1D0
      PSIBELOW=PSINEW
      TEST=DABS (TESTNEW)
    ENDIF
  ENDIF
```

```
      IF (COUNT.EQ.3) THEN
        IF (TESTNEW.GT.0) THEN
          PSIABOVE=PSINEW
          TEST=DABS (TESTNEW)
        ENDIF
        IF (TESTNEW.LT.0) THEN
          PSIBELOW=PSINEW
          TEST=DABS (TESTNEW)
        ENDIF
        PSI= (PSIABOVE+PSIBELOW)/2D0
      ENDIF
    ENDDO
*
*===== CONCENTRATION AT PORE ENTRANCE =====
    DO I=1, NMAX
      C0 (I) =CONC (I)
    ENDDO
*
*---RETURN TO MAIN PROGRAM
    RETURN
    END
*
*---SUBROUTINE ROOTS FOR CDXi VALUE
    SUBROUTINE ROOT (CP1, CDX1)
    IMPLICIT DOUBLE PRECISION (A-Z)
    INTEGER*4 I, NMAX, SWITCH, COUNT, Z
    PARAMETER (NMAX=2)
    DIMENSION A (NMAX), C0 (NMAX), DELTAW (NMAX), Z (NMAX),
   +        PHI (NMAX), KC (NMAX), DP (NMAX)
    COMMON /ALL/    BOLTZC, F, R, TEMP, XD
    COMMON /OTHERS/ C0, DELTAW, PHI, Z, VEL, KC, DP, DX
*
*---CP2 VALUE FROM ELECTRONEUTRALITY
```

```
    CP2=-(Z (1)*CP1/Z (2))
*---FUNCTIONS
    DO I=1, NMAX
      A (I) =PHI (I)*DEXP (-DELTAW (I)/ (BOLTZC*TEMP))
    ENDDO
*
*===== CHECK CONCENTRATIONS =====
    SWITCH=0
    IF (CP1.LT.0) THEN
      SWITCH=1
    ENDIF
*
*===== SWITCH =====
    IF (SWITCH.EQ.0) THEN
*===== NEWTON METHOD =====
*---INITIAL GUESS FOR CDX1
      COLD=C0 (1)
      CCOMP=1D0
      COUNT=0
      DOWHILE (CCOMP.GT.1D-6)
*---FUNC FUNCTIONS
      P1=Z (1)*COLD
      P2=Z (2)*A (2)*CP2*((COLD/(CP1*A(1)))**(Z(2)/Z(1)))
      P3=XD
*---DERIVF FUNCTIONS
      S1=Z (1)
      S2=((A(2)*CP2*Z(2)**2)/(Z(1)*CP1*A(1)))*((COLD/(CP1*A(1)))**
     +    ((Z (2)/Z (1))-1))
*
        FUNC=P1+P2+P3
        DERIVF=S1+S2
        CNEW=COLD-(FUNC/DERIVF)
        CCOMP=100D0*DABS ((CNEW-COLD)/CNEW)
```

```
        CRES=COLD
        COLD=CNEW
        COUNT=COUNT+1
        IF (COUNT.GT.1000) THEN
          CRES=-1D0
          CCOMP=1D-9
          PRINT*,'no ROOT!!!'
        END IF
      ENDDO
*---CDXi VALUES
    CDX1=CRES
*
    ELSE
      CRES=-1D0
      CDX1=CRES
    END IF
*--RETURN TO MAIN PROGRAM
    RETURN
    END
*
*---SUBROUTINE CONC TO CHECK FOR NEGATIVE CONCENTRATIONS
    SUBROUTINE CONC (CP1, CDX1, SWITCH)
    IMPLICIT DOUBLE PRECISION (A-Z)
    INTEGER*4 SWITCH
*
*===== SEARCH FOR NEGATIVE CONCENTRATION VALUES =====
    SWITCH=0
    IF (CP1.LT.0D0) THEN
      SWITCH=1
    END IF
    IF (CDX1.LT.0D0) THEN
      SWITCH=1
    END IF
```

```
*---RETURN TO MAIN PROGRAM
      RETURN
      END
*
*---SUBROUTINE FULL TO CALCULATE PROFILE ACROSS MEMBRANE
      SUBROUTINE FULL (CP1, CDX1, TEST)
      IMPLICIT DOUBLE PRECISION (A-Z)
      INTEGER*4 I, NMAX, NSTEP, Z
      PARAMETER (NMAX=2)
      DIMENSION C0 (NMAX), Z (NMAX), KC (NMAX), DP (NMAX),
     +          DELTAW (NMAX), PHI (NMAX)
      COMMON /ALL/    BOLTZC, F, R, TEMP, XD
      COMMON /OTHERS/ C0, DELTAW, PHI, Z, VEL, KC, DP, DX
*
*====== CALCULATION ======
*
      T=TEMP
      NSTEP=500
      OPEN (6, FILE='CONCPROFILE.RES')
      WRITE (6, 12) 0D0, 1D0
*
*---SETTING THE INITIAL CONDITIONS
*
      C1OLD=C0 (1)
      DH=DX/NSTEP
      X=0D0
*
*---FUNCTIONS
      A=Z (1)*VEL*(KC (1)/DP (1)-KC (2)/DP (2))
      B=Z (1)*VEL*(1D0/DP (2)-1D0/DP (1))
      E=VEL*KC (2)/DP (2)
      G=Z (1) **2-Z (1)*Z (2)
      H=Z (2)
```

```
*
*---CALCULATION OF CONCENTRATION GRADIENT
*
    DO I=1, NSTEP
*
*---CALCULATION OF ENERGY POTENTIAL
*
      DSI=(A*C1OLD+B*CP1-E*XD)/(G*C1OLD-H*XD)
*
*---FIRST RUNGA-KUTTA GRADIENT
*
      K1= (VEL/DP (1))*(KC (1)*C1OLD-CP1)-Z (1)*DSI*C1OLD
*
*---SECOND RUNGA-KUTTA GRADIENT
*
      K2= (VEL/DP (1))*(KC (1)*(C1OLD+0.5D0*DH*K1)-CP1)
     +      -Z (1)*DSI*(C1OLD+0.5D0*DH*K1)
*
*---THIRD RUNGA-KUTTA GRADIENT
*
      K3= (VEL/DP (1))*(KC (1)*(C1OLD+0.5D0*DH*K2)-CP1)
     +      -Z (1)*DSI*(C1OLD+0.5D0*DH*K2)
*
*---FOURTH RUNGA-KUTTA GRADIENT
*
      K4= (VEL/DP (1))*(KC (1)*(C1OLD+DH*K3)-CP1)
     +      -Z (1)*DSI*(C1OLD+DH*K3)
*
*---CALCULATION OF NEW CONCENTRATION
*
      C1NEW=C1OLD+DH*(1D0/6D0)*(K1+2D0*K2+2D0*K3+K4)
      C1OLD=C1NEW
*
```

```
*---CALCULATING CONCENTRATION PROFILE THROUGH MEMBRANE
*
*---POSITION INSIDE MEMBRANE
      X=X+DH
      DIST=X/DX
*
*---OUTPUTTING THE DATA
*
      WRITE (6, 12) DIST, C1NEW/C0 (1)
*
    END DO
*---CONVERTING CONCENTRATION
*
    CDX1C=C1NEW
*
*---EVALUATING TEST FUNCTION
*
    T1= (CDX1C-CDX1) **2
    TEST=SQRT (T1)
*
  12 FORMAT (1X, T4, F8.4, T15, F12.6)
    CLOSE (6)
*
*---RETURN TO MAIN PROGRAM
    RETURN
    END
*
```

A3.2 The Fortran™ code for binary salt systems

Program: 3ionFull.for

```
*
*  ---------------------------------------------------------------
*  WRITTEN BY:     DARREN OATLEY
*                  CENTRE FOR COMPLEX FLUIDS PROCESSING
```

```
*               SCHOOL OF ENGINEERING
*               UNIVERSITY OF WALES SWANSEA
*               SINGLETON PARK
*               SWANSEA, SA2 8PP
*  ------------------------------------------------------------
*
*  BACKGROUND OF THE PROGRAM...
*
*  This program is used to predict the rejection of a 3 ion system.
*  Theoretical rejection is predicted as a function of effective
*  pressure using the Full version of the extended Nernst-
*  Planck equation.  The code is written in algebraic terms such that
*  the equilibrium partitioning and transport equations are universal
*  and will accept ions of any given valence.
*
*  ------------------------------------------------------------
*
================================================================
*  ------------------------------------------------------------
*
      PROGRAM MAIN
      IMPLICIT DOUBLE PRECISION (A-Z)
      INTEGER       I, K, SWITCH, NMAX, Z, J
      PARAMETER     (NMAX=3)
      DIMENSION     D0 (NMAX), RSOL (NMAX), Z (NMAX), CW (NMAX), PHI
(NMAX),
     +              LAMBDA (NMAX), KD (NMAX), KC (NMAX), DELTAW (NMAX),
     +              DP (NMAX), C0 (NMAX), TESTFUNC (5)
      COMMON /ALL/    BOLTZC, F, R, TEMP, XD
      COMMON /OTHERS/ C0, DELTAW, PHI, Z, VEL, KC, DP, DX
*
*---INPUTTING SOLUTE DATA
*---Na+, Mg2+, Cl-
```

* D0 (3) =1.33D-9
* D0 (2) =0.72D-9
* D0 (1) =2.03D-9
* RSOL (3) =0.184D-9
* RSOL (2) =0.35D-9
* RSOL (1) =0.12D-9
* Z (3) =1
* Z (2) =2
* Z (1) =-1
* CW (3) =5D0
* CW (2) =5D0
* CW (1) =15D0
*

*---Mg^{2+}, SO_4^{2-}, Na^+
* D0 (1) =0.72D-9
* D0 (2) =1.06D-9
* D0 (3) =1.33D-9
* RSOL (1) =0.35D-9
* RSOL (2) =0.23D-9
* RSOL (3) =0.18D-9
* Z (1) =2
* Z (2) =-2
* Z (3) =1
* CW (1) =0.625D0
* CW (2) =1.25D0
* CW (3) =1.25D0
*

*---Na+, SO_4^{2-}, Cl^-

D0 (1) =1.33D-9
D0 (2) =1.06D-9
D0 (3) =2.03D-9
RSOL (1) =0.184D-9
RSOL (2) =0.23D-9

RSOL (3) =0.12D-9

Z (1) =1

Z (2) =-2

Z (3) =-1

CW (1) =17.5D0

CW (2) =7.5D0

CW (3) =2.5D0

*

*---Na^+, Cefuroxime-, lactate-

* D0 (1) =1.333D-9

* D0 (2) =0.540D-9

* D0 (3) =1.060D-9

* RSOL (1) =0.184D-9

* RSOL (2) =0.453D-9

* RSOL (3)=0.231D-9

* Z (1) =1

* Z (2) =-1

* Z (3) =-1

* CW (2) =4.58D0

* CW (3) =31.82D0

* CW (1) =CW (2) +CW (3)

*

*---Na+,MB Dye+,Cl-

* D0 (1) =1.333D-9

* D0 (2) =0.505D-9

* D0 (3) =2.032D-9

* RSOL (1) =0.184D-9

* RSOL (2) =0.486D-9

* RSOL (3) =0.121D-9

* Z (1) =1

* Z (2) =1

* Z (3) =-1

* CW (1) =4.6D0

```
*     CW (2) =1.1D0
*     CW (3) =CW (1) +CW (2)
*
*---INPUTTING MEMBRANE CHARACTERISTICS
      RP=0.45D-9
      XD=1D0
      DIELECL=31D0
*     CHARGE=-0D0
*     XD=CHARGE*(CW (1) +CW (2) +CW (3))
*
*---INPUTTING CONSTANTS
      PI=DACOS (-1D0)
*---FARADAY [C mol-1]
      F=96487D0
*---GAS [J mol-1 K-1]
      R=8.314D0
*---BOLTZMANN [J K-1]
      BOLTZC=1.38066D-23
*---TEMPERATURE [K]
      TEMP=298D0
*---ELECTRIC FIELD [C V-1 m-1]
      ELEFIELDC=8.85419D-12
*---ElEMENTAL ELECTRON CHARGE [J V-1]
      CHARGE=1.602177D-19
*---BULK SOLVENT VISCOSITY (@ 298 K) [kg m-1 s-1]
      VISCOS=0.893D-3
*---BULK SOLVENT DIELECTRIC
      DIELECB=80D0
*---ORIENTED SOLVENT LAYER DIELECTRIC
*     DIELECL=41D0
*---MEMBRANE THICKNESS [m]
      DX=1D-6
*
```

```
*---CALCULATION OF THE PORE SIZE DEPENDANT PROPERTIES
*
*---POREWISE VISCOSITY
    IF (RP.LE.0.28D-9) THEN
      VISCP=10D0*VISCOS
    ELSE
      RATIO=0.28D-9/RP
      VISCP=VISCOS*(1D0+(18D0*RATIO)-(9D0*(RATIO**2)))
    ENDIF
*---HINDERANCE FACTORS (7TH ORDER VERSION)
    DO I=1, NMAX
      LAMBDA (I) =RSOL (I)/RP
      PHI (I) = (1D0-LAMBDA (I)) **2
*
*---CONSTANTS FOR KD
      KD1=1.0000D0
      KD2=-2.1812D0
      KD3=0.7328D0
      KD4=-0.9065D0
      KD5=6.7272D0
      KD6=-10.2324D0
      KD7=6.3293D0
      KD8=-1.4692D0
*
      IF (LAMBDA (I).GT.0.98D0) THEN
        KD (I) =3D-5
      ELSE
        KD (I) =KD1+KD2*LAMBDA (I) +KD3*LAMBDA (I) **2+KD4*LAMBDA (I)
**3+
   +          KD5*LAMBDA (I) **4+KD6*LAMBDA (I) **5+KD7*LAMBDA (I) **6+
   +          KD8*LAMBDA (I) **7
      END IF
*
```

```
*---CONSTANTS FOR KC
      KC1=1.0000D0
      KC2=0.0650D0
      KC3=-1.9370D0
      KC4=8.5211D0
      KC5=-27.3398D0
      KC6=44.4150D0
      KC7=-34.5582D0
      KC8=10.3358D0
*
      KC (I) = (KC1+KC2*LAMBDA (I) +KC3*LAMBDA (I) **2+KC4*LAMBDA (I)
**3+
     +      KC5*LAMBDA (I) **4+KC6*LAMBDA (I) **5+KC7*LAMBDA (I) **6+
     +      KC8*LAMBDA (I) **7)*(2D0-PHI (I))
*
*
*
      DP (I) =KD (I)*D0 (I)*VISCOS/VISCP
    ENDDO
*---PORE DIELECTRIC CONSTANT
    IF (RP.LE.0.28D-9) THEN
      DIELECP=DIELECL
    ELSE
      MU=0.28D-9/RP
      FUNC=DIELECB-DIELECL
      DIELECP=DIELECB-(2D0*MU*FUNC)+(FUNC*(MU**2))
    ENDIF
*---BORN ENERGY BARRIER
    FUNC2= (1D0/DIELECP)-(1D0/DIELECB)
    DO I=1, NMAX
      DELTAW (I) = (((Z (I) **2)*(CHARGE**2))/
     +      (8D0*PI*ELEFIELDC*RSOL (I)))*FUNC2
    ENDDO
```

```
*
*---CALLING FOR INLET CONCENTRATIONS C0(I) FROM PARTITN
*
    CALL PARTITN (CW, LAMBDA, DELTAW, PHI, Z, C0)
*
*---SETTING MAX AND MIN VALUES FOR OUTPUT CONCENTRATIONS
*
    CP1MIN=1D-6*CW (1)
    CP1MAX=CW (1)
    CP2MIN=1D-6*CW (2)
    CP2MAX=CW (2)
*
    CP1START= (CP1MAX+CP1MIN)/2D0
    CP2START= (CP2MAX+CP2MIN)/2D0
*
*---OPENING OUTPUT FILE
*
    OPEN (5, FILE='3ionFull.res')
*     WRITE (5, 3702) 'MPa','Rej 1','Rej 2','Rej 3'
    WRITE (5, 10)    0D0, 0D0, 0D0, 0D0
*
*---SETTING UP THE PRESSURE LOOP
*
    PRESS=0D5
    DPRESS=0.5D5
*
*---CALCULATION OF REJECTION
*
    DO I=1, 2
      PRESS=PRESS+DPRESS
      VEL= (PRESS*RP**2)/ (8D0*DX*VISCP)
      CP1STEP=CP1MAX/5D0
      CP2STEP=CP2MAX/5D0
```

```
*
*---INITIAL CONCENTRATION GUESSES
*
      CP1C=CP1START
      CP1N=CP1C
      CP1S=CP1C
      CP1E=CP1C+CP1STEP
      CP1W=CP1C-CP1STEP
*
      CP2C=CP2START
      CP2N=CP2C+CP2STEP
      CP2S=CP2C-CP2STEP
      CP2E=CP2C
      CP2W=CP2C
*
*---INITIAL VALUES FOR TEST FUNCTIONS
*
      TEST=10D0
      TESTMIN=2000D0
      K=0
      DOWHILE (TEST.GT.1D-12)
*
*---CALCULATION OF EXIT CONCENTRATIONS CDXi FOR EACH POINT
*
        CALL ROOT (CP1C, CP2C, CDX1C, CDX2C)
        CALL ROOT (CP1N, CP2N, CDX1N, CDX2N)
        CALL ROOT (CP1S, CP2S, CDX1S, CDX2S)
        CALL ROOT (CP1E, CP2E, CDX1E, CDX2E)
        CALL ROOT (CP1W, CP2W, CDX1W, CDX2W)
*
*---CHECKING FOR NEGATIVE CONCENTRATIONS AND CALCULATING
PROFILES
*
```

```
CALL CONC (CP1N, CP2N, CDX1N, CDX2N, SWITCH)
IF (SWITCH.EQ.0) THEN
  CALL FULL (CP1N, CP2N, CDX1N, CDX2N, TESTN)
  ELSE
    TESTN=1000D0
    SWITCH=0
END IF
CALL CONC (CP1S, CP2S, CDX1S, CDX2S, SWITCH)
IF (SWITCH.EQ.0) THEN
  CALL FULL (CP1S, CP2S, CDX1S, CDX2S, TESTS)
  ELSE
    TESTS=1000D0
    SWITCH=0
END IF
CALL CONC (CP1E, CP2E, CDX1E, CDX2E, SWITCH)
IF (SWITCH.EQ.0) THEN
  CALL FULL (CP1E, CP2E, CDX1E, CDX2E, TESTE)
  ELSE
    TESTE=1000D0
    SWITCH=0
END IF
CALL CONC (CP1W, CP2W, CDX1W, CDX2W, SWITCH)
IF (SWITCH.EQ.0) THEN
  CALL FULL (CP1W, CP2W, CDX1W, CDX2W, TESTW)
  ELSE
    TESTW=1000D0
    SWITCH=0
END IF
CALL CONC (CP1C, CP2C, CDX1C, CDX2C, SWITCH)
IF (SWITCH.EQ.0) THEN
  CALL FULL (CP1C, CP2C, CDX1C, CDX2C, TESTC)
  ELSE
    TESTC=1000D0
```

```
          SWITCH=0
        END IF
*
*---EVALUATION OF THE MINIMUM TEST FUNCTION
*
        TESTFUNC (1) =TESTC
        TESTFUNC (2) =TESTN
        TESTFUNC (3) =TESTS
        TESTFUNC (4) =TESTE
        TESTFUNC (5) =TESTW
*
        K=1
        DO J=1, 5
          IF (TESTFUNC (J).LT.TESTMIN) THEN
            TESTMIN=TESTFUNC (J)
            K=J
          END IF
        END DO
*
        IF (K.EQ.1) THEN
          CP1STEP=CP1STEP/1.1D0
          CP2STEP=CP2STEP/1.1D0
          CP1C=CP1C
          CP1N=CP1C
          CP1S=CP1C
          CP1E=CP1C+CP1STEP
          CP1W=CP1C-CP1STEP
*
          CP2C=CP2C
          CP2N=CP2C+CP2STEP
          CP2S=CP2C-CP2STEP
          CP2E=CP2C
          CP2W=CP2C
```

```
      TEST=TESTC
    END IF
    IF(K.EQ.2)THEN
      CP1C=CP1N
      CP1N=CP1C
      CP1S=CP1C
      CP1E=CP1C+CP1STEP
      CP1W=CP1C-CP1STEP
*
      CP2C=CP2N
      CP2N=CP2C+CP2STEP
      CP2S=CP2C-CP2STEP
      CP2E=CP2C
      CP2W=CP2C
      TEST=TESTN
    END IF
    IF (K.EQ.3) THEN
      CP1C=CP1S
      CP1N=CP1C
      CP1S=CP1C
      CP1E=CP1C+CP1STEP
      CP1W=CP1C-CP1STEP
*
      CP2C=CP2S
      CP2N=CP2C+CP2STEP
      CP2S=CP2C-CP2STEP
      CP2E=CP2C
      CP2W=CP2C
      TEST=TESTS
    END IF
    IF(K.EQ.4)THEN
      CP1C=CP1E
      CP1N=CP1C
```

```
          CP1S=CP1C
          CP1E=CP1C+CP1STEP
          CP1W=CP1C-CP1STEP
*
          CP2C=CP2E
          CP2N=CP2C+CP2STEP
          CP2S=CP2C-CP2STEP
          CP2E=CP2C
          CP2W=CP2C
          TEST=TESTE
        END IF
        IF (K.EQ.5) THEN
          CP1C=CP1W
          CP1N=CP1C
          CP1S=CP1C
          CP1E=CP1C+CP1STEP
          CP1W=CP1C-CP1STEP
*
          CP2C=CP2W
          CP2N=CP2C+CP2STEP
          CP2S=CP2C-CP2STEP
          CP2E=CP2C
          CP2W=CP2C
          TEST=TESTW
        END IF
        WRITE (*, 11) TEST, I
        IF (CP1STEP.LT.1D-30) THEN
          GOTO 13
        END IF
      END DO
      CP3C=-(Z (1)*CP1C+Z (2)*CP2C)/Z (3)
      REJ1=1D0-CP1C/CW (1)
      REJ2=1D0-CP2C/CW (2)
```

```
      REJ3=1D0-CP3C/CW (3)
 13    IF (CP1STEP.LT.1D-30) THEN
         WRITE (*, 10) (PRESS/1D6)
         WRITE (5, 10) (PRESS/1D6)
       ELSE
         WRITE (*, 10) (PRESS/1D6), REJ1, REJ2, REJ3
         WRITE (5, 10) (PRESS/1D6), REJ1, REJ2, REJ3
      END IF
 10    FORMAT(1X,T4,F12.3,T18,F12.6,T32,F12.6,T46,F12.6,T60,F12.6)
 11    FORMAT (1X, T4, F16.12, T21, I4)
*      CP1START=CP1C
*      CP2START=CP2C
    END DO
*
*     WRITE (5,*)   "
*     WRITE (5, 3704) 'Membrane Pore Radius', RP
*     WRITE (5, 3705) 'Membrane Charge Density', XD
*     WRITE (5, 3705) 'Layer Dielectric Constant', DIELECL
*     WRITE (5, 3705) 'Pore Dielectric Constant', DIELECP
*     WRITE (5, 3704) 'Pore Viscosity', VISCP
*     WRITE (5,*)   "
*     WRITE (5,*) ('OTHER DERIVED VALUES FOR THE CALCULATION')
*     WRITE (5,*)   "
*     WRITE (5, 3702) 'Species',' ION 1','ION 2','ION 3'
*     WRITE (5, 3703) 'Feed Conc =', CW (1), CW (2), CW (3)
*     WRITE (5, 3700) 'Mem Conc. Co', C0 (1), C0 (2), C0 (3)
*     WRITE (5, 3700) 'Lambda =', LAMBDA (1), LAMBDA (2), LAMBDA (3)
*     WRITE (5, 3700) 'Phi =', PHI (1), PHI (2), PHI (3)
*     WRITE (5, 3700) 'KD =', KD (1), KD (2), KD (3)
*     WRITE (5, 3700) 'KC =', KC (1), KC (2), KC (3)
*     WRITE (5, 3701) 'DP =', DP (1), DP (2), DP (3)
*     WRITE (5, 3701) 'BORN =', DELTAW (1), DELTAW (2), DELTAW (3)
*3700  FORMAT(1X,T4,A12,T18,F12.6,T32,F12.6,T46,F12.6,T60,F12.6)
```

```
*3703  FORMAT(1X,T4,A12,T18,F12.3,T32,F12.3,T46,F12.3,T60,F12.3)
*3701  FORMAT(1X,T4,A12,T18,E12.3,T32,E12.3,T46,E12.3,T60,E12.3)
*3702  FORMAT(1X,T4,A12,T18,A12,T32,A12,T46,A12,T60,A12)
*3704 FORMAT (1X, T2, A25, T40, E13.3)
*3705 FORMAT (1X, T2, A25, T40, F13.3)
      CLOSE (5)
      STOP
      END
*
*  ----------------------------------------------------------------
*  ========================= END OF MAIN PROGRAM
====================
*  ----------------------------------------------------------------
*
*---PARTITIONING SUBROUTINE TO FIND C0(I)
*
      SUBROUTINE PARTITN(CW,LAMBDA,DELTAW,PHI,Z,C0)
      IMPLICIT DOUBLE PRECISION (A-Z)
      INTEGER*4   COUNT, I, NMAX, Z
      PARAMETER   (NMAX=3)
      DIMENSION   C0(1:NMAX),CONC(1:NMAX),CW(1:NMAX),DELTAW(1:NMAX),
     +          PHI (1: NMAX), Z (1: NMAX), LAMBDA (1: NMAX)
      COMMON /ALL/ BOLTZC, F, R, TEMP, XD
*
*===== CALCULATION =====
*---Imitial values
      PSI=0D0
      TEST=20D0
      COUNT=0
*---Iteration
      DOWHILE (TEST.GT.1D-6)
        PSINEW=PSI
        SUM=0D0
```

```
      DO I=1, NMAX
        IF (LAMBDA (I).GE.1D0) THEN
          CONC (I) =0D0
        ELSE
          CONC (I) =CW (I)*PHI (I)*DEXP ((-Z (I)*F*PSINEW)/(R*TEMP))*
     +          DEXP (-DELTAW (I)/ (BOLTZC*TEMP))
        END IF
        SUM=SUM+ (Z (I)*CONC (I))
      ENDDO
      TESTNEW=SUM+XD
      IF (COUNT.EQ.0) THEN
        IF (TESTNEW.GT.0) THEN
          PSI=PSINEW+0.1D0
          PSIABOVE=PSINEW
          TEST=DABS (TESTNEW)
          COUNT=1
        ENDIF
        IF (TESTNEW.LT.0) THEN
          PSI=PSINEW-0.1D0
          PSIBELOW=PSINEW
          TEST=DABS (TESTNEW)
          COUNT=2
        ENDIF
      ENDIF
      IF (COUNT.EQ.1) THEN
        IF (TESTNEW.GT.0) THEN
          PSI=PSINEW+0.1D0
          PSIABOVE=PSINEW
          TEST=DABS (TESTNEW)
        ENDIF
        IF (TESTNEW.LT.0) THEN
          PSI=PSINEW-0.1D0
          PSIBELOW=PSINEW
```

```
        TEST=DABS (TESTNEW)
        COUNT=3
      ENDIF
    ENDIF
    IF (COUNT.EQ.2) THEN
      IF (TESTNEW.GT.0) THEN
        PSI=PSINEW+0.1D0
        PSIABOVE=PSINEW
        TEST=DABS (TESTNEW)
        COUNT=3
      ENDIF
      IF (TESTNEW.LT.0) THEN
        PSI=PSINEW-0.1D0
        PSIBELOW=PSINEW
        TEST=DABS (TESTNEW)
      ENDIF
    ENDIF
    IF (COUNT.EQ.3) THEN
      IF (TESTNEW.GT.0) THEN
        PSIABOVE=PSINEW
        TEST=DABS (TESTNEW)
      ENDIF
      IF (TESTNEW.LT.0) THEN
        PSIBELOW=PSINEW
        TEST=DABS (TESTNEW)
      ENDIF
      PSI= (PSIABOVE+PSIBELOW)/2D0
    ENDIF
  ENDDO
*
*---CONCENTRATION AT PORE ENTRANCE
  DO I=1, NMAX
    C0 (I) =CONC (I)
```

```
    ENDDO
*
*---RETURN TO MAIN PROGRAM
    RETURN
    END
*
*
*---SUBROUTINE ROOT FOR CDXi VALUES
*
    SUBROUTINE ROOT (CP1, CP2, CDX1, CDX2)
    IMPLICIT DOUBLE PRECISION (A-Z)
    INTEGER*4      I, NMAX, SWITCH, COUNT, Z
    PARAMETER      (NMAX=3)
    DIMENSION      A (NMAX), C0 (NMAX), DELTAW (NMAX), Z (NMAX), DP
(NMAX),
   +               PHI (NMAX), KC (NMAX)
    COMMON /ALL/    BOLTZC, F, R, TEMP, XD
    COMMON /OTHERS/ C0, DELTAW, PHI, Z, VEL, KC, DP, DX
*
*---CP3 VALUE FROM ELECTRONEUTRALITY
    CP3=-(Z (1)*CP1+Z (2)*CP2)/Z (3)
*---FUNCTIONS
    DO I=1, NMAX
      A (I) =PHI (I)*DEXP (-DELTAW (I)/ (BOLTZC*TEMP))
    ENDDO
*
*---CHECK CONCENTRATIONS
    SWITCH=0
    IF (CP1.LT.0) THEN
      SWITCH=1
    ENDIF
    IF (CP2.LT.0) THEN
      SWITCH=1
```

```
      ENDIF
      IF (CP3.LT.0) THEN
        SWITCH=1
      ENDIF
*
*---SWITCH
      IF (SWITCH.EQ.0) THEN
*---NEWTON METHOD
*---INITIAL GUESS FOR CDX1
        COLD=C0 (1)
        CCOMP=1D0
        COUNT=0
        DOWHILE (CCOMP.GT.1D-6)
*---FUNC FUNCTIONS
        P1=Z (1)*COLD
        P2=Z (2)*A (2)*CP2*((COLD/ (CP1*A (1))) ** (Z (2)/Z (1)))
        P3=Z (3)*A (3)*CP3*((COLD/ (CP1*A (1))) ** (Z (3)/Z (1)))
        P4=XD
*---DERIVF FUNCTIONS
        S1=Z (1)
        S2=((A(2)*CP2*Z(2)**2)/(Z(1)*CP1*A(1)))*((COLD/(CP1*A(1)))**
     +     ((Z (2)/Z (1))-1))
        S3=((A(3)*CP3*Z(3)**2)/(Z(1)*CP1*A(1)))*((COLD/(CP1*A(1)))**
     +     ((Z (3)/Z (1))-1))
*
          FUNC=P1+P2+P3+P4
          DERIVF=S1+S2+S3
          CNEW=COLD-(FUNC/DERIVF)
          CCOMP=100D0*DABS ((CNEW-COLD)/CNEW)
          CRES=COLD
          COLD=CNEW
          COUNT=COUNT+1
          IF (COUNT.GT.1000) THEN
```

```
          CRES=-1D0
          CCOMP=1D-9
          PRINT*,'no ROOT!!!'
        ENDIF
      ENDDO
*---CDXi VALUES
    CDX1=CRES
    CDX2=A (2)*CP2*((CDX1/ (A (1)*CP1)) ** (Z (2)/Z (1)))
*
    ELSE
      CRES=-1D0
      CDX1=CRES
      CDX2=CRES
    ENDIF
*---RETURN TO MAIN PROGRAM
    RETURN
    END
*
*---SUBROUTINE CONC TO SEARCH FOR NEGATIVE VALUES
*
    SUBROUTINE CONC (CP1, CP2, CDX1, CDX2, SWITCH)
    IMPLICIT DOUBLE PRECISION (A-Z)
    INTEGER*4 SWITCH
*
*===== SEARCH FOR NEGATIVE CONCENTRATION VALUES =====
    SWITCH=0
    IF (CP1.LT.0D0) THEN
      SWITCH=1
    ENDIF
    IF (CP2.LT.0D0) THEN
      SWITCH=1
    ENDIF
    IF (CDX1.LT.0D0) THEN
```

```
      SWITCH=1
    ENDIF
    IF (CDX2.LT.0D0) THEN
      SWITCH=1
    ENDIF
*---RETURN TO MAIN PROGRAM
    RETURN
    END
*
*---SUBROUTINE LINEAR TO CALCULATE CONCENTRATION PROFILES
*
    SUBROUTINE FULL (CP1, CP2, CDX1, CDX2, TEST)
    IMPLICIT DOUBLE PRECISION (A-Z)
    INTEGER*4      NMAX, NSTEP, Z
    PARAMETER      (NMAX=3)
    DIMENSION      C0 (NMAX), Z (NMAX), KC (NMAX), DP (NMAX),
   +               DELTAW (NMAX), PHI (NMAX)
    COMMON /ALL/   BOLTZC, F, R, TEMP, XD
    COMMON /OTHERS/ C0, DELTAW, PHI, Z, VEL, KC, DP, DX
*
*===== CALCULATION =====
*
    T=TEMP
    NSTEP=500
    OPEN (6, FILE='CONCPROFILE.RES')
    WRITE (6, 12) 0D0, 1D0
*
*---SETTING THE INITIAL CONDITIONS
*
    C1OLD=C0 (1)
    C2OLD=C0 (2)
    DH=DX/NSTEP
    X=0D0
```

```
*
*---FUNCTIONS
      A=Z (1)*VEL*(KC (1)/DP (1)-KC (3)/DP (3))
      B=Z (2)*VEL*(KC (2)/DP (2)-KC (3)/DP (3))
      G=Z (1)*VEL*(1/DP (3)-1/DP (1))
      H=Z (2)*VEL*(1/DP (3)-1/DP (2))
      L=VEL*KC (3)/DP (3)
      M= (F/(R*T))*((Z (1) **2)-Z (1)*Z (3))
      N1= (F/(R*T))*((Z (2) **2)-Z (2)*Z (3))
      Q= (F/(R*T))*Z (3)
*
*---CALCULATION OF THE CONCENTRATION GRADIENT
*
      DO I=1, NSTEP
*
*---CALCULATION OF CHARGE FUNCTION (DSI/DX)
*
         DSIDX= (A*C1OLD+B*C2OLD+G*CP1+H*CP2-L*XD)/
     +        (M*C1OLD+N1*C2OLD-Q*XD)
*
*---FIRST RUNGA-KUTTA GRADIENT
*
         K11= (VEL/DP (1))*(KC (1)*C1OLD-CP1)
     +        -C1OLD*Z (1)*(F/(R*T))*DSIDX
         K12= (VEL/DP (2))*(KC (2)*C2OLD-CP2)
     +        -C2OLD*Z (2)*(F/(R*T))*DSIDX
*
*---SECOND RUNGA-KUTTA GRADIENT
*
         K21= (VEL/DP (1))*(KC (1)*(C1OLD+0.5D0*DH*K11)-CP1)
     +        - (C1OLD+0.5D0*DH*K11)*Z (1)*(F/(R*T))*DSIDX
         K22= (VEL/DP (2))*(KC (2)*(C2OLD+0.5D0*DH*K12)-CP2)
     +        - (C2OLD+0.5D0*DH*K12)*Z (2)*(F/(R*T))*DSIDX
```

```
*
*---THIRD RUNGA-KUTTA GRADIENT
*
      K31= (VEL/DP (1))*(KC (1)*(C1OLD+0.5D0*DH*K21)-CP1)
     +      - (C1OLD+0.5D0*DH*K21)*Z (1)*(F/(R*T))*DSIDX
      K32= (VEL/DP (2))*(KC (2)*(C2OLD+0.5D0*DH*K22)-CP2)
     +      - (C2OLD+0.5D0*DH*K22)*Z (2)*(F/(R*T))*DSIDX
*
*---FOURTH RUNGA-KUTTA GRADIENT
*
      K41= (VEL/DP (1))*(KC (1)*(C1OLD+DH*K31)-CP1)
     +      - (C1OLD+DH*K31)*Z (1)*(F/(R*T))*DSIDX
      K42= (VEL/DP (2))*(KC (2)*(C2OLD+DH*K32)-CP2)
     +      - (C2OLD+DH*K32)*Z (2)*(F/(R*T))*DSIDX
*
*---CALCULATION OF NEW CONCENTRATION
*
      C1NEW=C1OLD+ (1D0/6D0)*(K11+2*K21+2*K31+K41)*DH
      C2NEW=C2OLD+ (1D0/6D0)*(K12+2*K22+2*K32+K42)*DH
      C1OLD=C1NEW
      C2OLD=C2NEW
*
*---CALCULATING CONCENTRATION PROFILE
*
      X=X+DH
      DIST=X/DX
      WRITE (6, 12) DIST, C2NEW/C0 (2)
*
*---THE INTEGRAL IS COMPLETE
*
    END DO
*
*---RE-ORGANISING THE CONCENTRATION FOR OUTPUT
```

```
*
    CDX1C=C1NEW
    CDX2C=C2NEW
*
*---EVALUATING TEST FUNCTION
*
    T1= (CDX1C-CDX1) **2
    T2= (CDX2C-CDX2) **2
    TEST=SQRT (T1+T2)
*
  12 FORMATS (1X, T4, F8.4, T15, F12.6)
    CLOSE (6)
*
*---RETURN TO MAIN PROGRAM
    RETURN
    END
*  ------------------------------------------------------------
*  ========================= END OF SUBROUTINES
=====================
*  ------------------------------------------------------------
```

References

Afonso, M.D., 2006. Surface charge on loose nanofiltration membranes. *Desalination*, 191(1-3), pp.262–272.

Aljohani, N., 2007. *Study of Some Chemical Additives as Antiscale/Anti-corrosion Agents In Water Treatment Plants*. Al-Azhar University.

Almalek, S., 2012. *SYNTHESIS AND CHARACTERIZATION OF POLYETHERSULFONE MEMBRANE USING DIFFERENT ADDITIVES*. Swansea University.

Al-Zoubi, H., Hilal, N., Darwish, N. a., & Mohammad, A. W. (2007). Rejection and modelling of sulphate and potassium salts by nanofiltration membranes: neural network and Spiegler-Kedem model. *Desalination*, *206*(1-3), 42–60.

Argelaguet, L.L., 2011. *Experimental and modelling study of nanofiltration focused on seawater desalination*. universitat politècnica de catalunya.

Ariza, M.J. & Benavente, J., 2001. Streaming potential along the surface of polysulfone membranes : a comparative study between two different experimental systems and determination of electrokinetic and adsorption parameters. *Journal of Membrane Science*, 190, pp.119–132.

Ariza, M.J., Cañas, A. & Benavente, J., 2001. Electrokinetic and electrochemical characterizations of porous membranes. *Colloids and Surfaces A: Physicochemical and Engineering Aspects*, 189(1-3), pp.247–256.

Artug, G., 2007. *Modelling and simulation of Nanofiltration membranes*. Available at: http://tejat.de/~lessappeal/Gamze/Diss/diss.pdf [Accessed October 9, 2014].

Artuğ, G., Roosmasari, I., Richau, K., & Hapke, J., 2007. A Comprehensive Characterization of Commercial Nanofiltration Membranes. *Separation Science and Technology*, *42*(13), 2947–2986.

Ben Amar, N., Saidani, H., Palmeri, J., & Deratani, A., 2009. Effect of temperature on the rejection of neutral and charged solutes by Desal 5 DK nanofiltration membrane. *Desalination*, *246*(1-3), 294–303.

Bandini, S., Drei, J. & Vezzani, D., 2005. The role of pH and concentration on the ion rejection in polyamide nanofiltration membranes. *Journal of Membrane Science*, 264(1-2), pp.65–74.

Bandini, S. & Mazzoni, C., 2005. Modelling the amphoteric behaviour of polyamide nanofiltration membranes. *Desalination*, 184(1-3), pp.327–336.

Bargeman, G., Westerink, J. B., Guerra Miguez, O., & Wessling, M., 2014. The effect of NaCl and glucose concentration on retentions for nanofiltration membranes processing concentrated solutions. *Separation and Purification Technology*, *134*, 46–57.

Bellona, C. & Drewes, J.E., 2005. The role of membrane surface charge and solute physico-chemical properties in the rejection of organic acids by NF membranes. *Journal of Membrane Science*, 249, pp.227–234.

Born, M., 1920. Volumen and hydratationswärme der ionen. *Z. Physik. Chem*, 1, p.45.

Boussu, K., Van der Bruggen, B., Volodin, a, Snauwaert, J., Van Haesendonck, C., & Vandecasteele, C. , 2005. Roughness and hydrophobicity studies of nanofiltration membranes using different modes of AFM. *Journal of Colloid and Interface Science*, *286*(2), 632–8.

Bowen, W., Welfoot, J. & Williams, P.M., 2002. A linearised transport model for nanofiltration: development and assessment. *AIChE J*, 48, p.760.

Bowen, W.R. & Clark, R.A., 1984. Electro-osmosis at microporous membranes and the determination of zeta-potential. *Journal of colloid and interface science*, 97(2), pp.401–409.

Bowen, W.R., Doneva, T. A & Stoton, J.A.G., 2002. The use of atomic force microscopy to quantify membrane surface electrical properties. *Colloids and Surfaces A: Physicochemical and Engineering Aspects*, 201(1-3), pp.73–83.

Bowen, W.R. & Mohammad, A.W., 1998a. CHARACTERIZATION AND PREDICTION OF GENERAL ASSESSMENT. *Trans IChemE*, 76(November).

Bowen, W.R. & Mohammad, A.W., 1998b. Diafiltration by Nanofiltration: Prediction and Optimisation. *AIChE Journal*, 44, p.1799.

Bowen, W.R., Mohammad, A.W. & Hilal, N., 1997. Characterisation of nanofiltration membranes for predictive purposes — use of salts, uncharged solutes and atomic force microscopy. *Journal of Membrane Science*, 126(1), pp.91–105.

Bowen, W.R. & Welfoot, J.S., 2002. Modelling the performance of membrane nanofiltration—critical assessment and model development. *Chemical Engineering Science*, 57(7), pp.1121–1137.

Brant, J. A & Childress, A.E., 2002a. Assessing short-range membrane – colloid interactions using surface energetics. *Journal of Membrane Science*, 203, pp.257–273.

Brant, J. A. & Childress, A.E., 2004. Colloidal adhesion to hydrophilic membrane surfaces. *Journal of Membrane Science*, 241(October 2003), pp.235–248.

Brant, J. A. & Childress, A.E., 2002b. Membrane–Colloid Interactions: Comparison of Extended DLVO Predictions with AFM Force Measurements. *Environmental Engineering Science*, 19(6), pp.413–427.

Brant, J., Johnson, K. & Childress, A.E., 2006. Examining the electrochemical properties of a nanofiltration membrane with atomic force microscopy. *Journal of Membrane Science*, 276(1-2), pp.286–294.

Bukšek, H., Luxbacher, T. & Petrinić, I., 2010. Zeta potential determination of polymeric materials using two differently designed measuring cells of an electrokinetic analyzer. *Acta chimica Slovenica*, 57(3), pp.700–6.

Burghoff, H., Lee, K.L. & Pusch, W., 1980. Characterisation of transport across cellulose-acetate membranes in the presence of strong solute-membrane interactions. *J. App. Ploy. Sci*, 25, p.323.

Burns, D.B. & Zydney, A.L., 2000. Buffer effects on the zeta potential of ultrafiltration membranes. *Journal of Membrane Science*, 172(September 1999), pp.39–48.

Chakkrit, U., 2010. *ACID FROM FERMENTATION BROTH BY*. Suranaree University of Technology. Available at: http://sutir.sut.ac.th:8080/sutir/bitstream/123456789/3719/2/Fulltext.pdf.

Chemteach, C., Determination of Calcium Ion Concentration. Available at: http://www.chemteach.ac.nz/investigations/documents/calcium.pdf.

Childress, A.E. & Elimelech, M., 1996. Effect of solution chemistry on the surface charge of polymeric reverse osmosis and nanofiltration membranes. *Journal of Membrane Science*, 119(2), pp.253–268.

Childress, A.E. & Elimelech, M., 2000. Relating Nanofiltration Membrane Performance to Membrane Charge (Electrokinetic) Characteristics. *Environmental Science & Technology*, 34(17), pp.3710–3716.

Chiu, T.Y. & James, A. E., 2007. Electrokinetic characterisation techniques on asymmetric microfiltration membranes. *Colloids and Surfaces A: Physicochemical and Engineering Aspects*, 301(1-3), pp.281–288.

Cho, D., Lee, S. & Frey, M.W., 2012. Characterizing zeta potential of functional nanofibers in a microfluidic device. *Journal of colloid and interface science*, 372(1), pp.252–60.

Chun, M., Cho, H.I. & Song, I.K., 2002. Electrokinetic behavior of membrane zeta potential during the filtration of colloidal suspensions. , 148, pp.363–367.

Chun, M.-S., Lee, S.Y. & Yang, S.M., 2003. Estimation of zeta potential by electrokinetic analysis of ionic fluid flows through a divergent microchannel. *Journal of Colloid and Interface Science*, 266(1), pp.120–126.

Chun, M.-S.S. & Park, W.C., 2004. Time evolution of electrokinetic flow-induced streaming potential and flux in dead-end and cross-flow filtration of colloids through nanopores. *Journal of Membrane Science*, 243(1-2), pp.417–424.

Datta, S., Conlisk, A., Kanani, D., Zydney, A., Fissell, W. & Roy, S., 2010. Characterizing the surface charge of synthetic nanomembranes by the streaming potential method. *Journal of Colloid and Interface Science*, 348, pp.85–95.

Department of Chemistry, C.U., No Title. Available at: http://www.outreach.canterbury.ac.nz/chemistry/documents/chloride_mohr.pdf.

Deshrnukh, S.S. & Childress, A.E., 2001. Zeta potential of commercial RO membranes : influence of source water type and chemistry. , 4.

Dickson, J., 1988. Fundamental aspects of reverse osmosis. *In Reverse Osmosis Technology, Ed. B. S. Parekh.*

Dina, M., Hagmeyer, G. & Gimbel, R., 2001. Streaming potential measurements to assess the variation of nanofiltration membranes surface charge with the concentration of salt solutions. *Separation and Purification Technology*, 23, pp.529–541.

Ding, N., Wang, X.-L. & Wang, J., 2006. Electrokinetic phenomena of a polyethylene microfiltration membrane in single salt solutions of NaCl, KCl, MgCl2, Na2SO4, and MgSO4. *Desalination*, 192(1-3), pp.18–24.

DOW, C., 2012. NF270 Specifications. Available at: http://www.dow.com.

Dresner, L. & Johnson, J.S., 1980. *Hyperfiltration (Reverse Osmosis) in Principles of Desalination* 2nd editio., Academic Press.

Dupavillon, J.L. & Gillanders, B.M., 2009. Impacts of seawater desalination on the giant Australian cuttlefish Sepia apama in the upper Spencer Gulf, South Australia. *Marine Environmental Research*, 67(4-5), pp.207–218.

Durham, R.J., Sleigh, R.W. & Hourigan, J.A., 2003. Nanofiltration for recovery of spent ion exchange brines. In *International Membrane Science and Technology Conference*. UNESCO Centre for Membrane Science and Technology, University of New South Wales, pp. 2–7.

Edward, T., Gilbert, K. & Wittenberg, M. D., 2014. Essential Equations for Anaesthesia, Morse equation and osmotic pressure . Cambridge University Press, pp. 145-146.

Egueh, A. N. D., Lakard, B., Fievet, P., Lakard, S. & Buron, C., 2010. Charge properties of membranes modified by multilayer polyelectrolyte adsorption. *Journal of Colloid and Interface Science*, *344*, 221–227.

Elimelech, M., Chen, W. H. & Waypa, J. J. ,1994. Measuring the zeta (electrokinetic) potential of reverse osmosis membranes by a streaming potential analyzer. *Desalination*, *95*, 269–286.

Ernst, M., Bismarck, A., Springer, J. & Jekel, M., 2000. Zeta-potential and rejection rates of a polyethersulfone nanofiltration membrane in single salt solutions. *Journal of Membrane Science*, *165*(2), 251–259.

Escoda, A., Fievet, P., Lakard, S., Szymczyk, A. & Déon, S., 2010. Influence of salts on the rejection of polyethyleneglycol by an NF organic membrane: Pore swelling and salting-out effects. *Journal of Membrane Science*, *347*(1-2), 174–182.

Fievet, P., Szymczyk, A., Magnenet, C. & Sbaï, M., 2006a. Characterisation of microporous tubular membranes by tangential streaming potential. *Desalination*, *200*(1-3), 183–185.

Fievet, P., Sbaï, M., Szymczyk, A. & Vidonne., A., 2003. Determining the ζ-potential of plane membranes from tangential streaming potential measurements: effect of the membrane body conductance. *Journal of Membrane Science*, *226*(1-2), 227–236.

Fievet, P., Szymczyk, a., Aoubiza, B. & Pagetti, J., 2000. Evaluation of three methods for the characterisation of the membrane-solution interface: Streaming potential, membrane potential and electrolyte conductivity inside pores. *Journal of Membrane Science*, *168*, 87–100.

Fievet, P., Szymczyk, A. & Sbaï, M., 2006b. Tangential streaming potential as a tool in the characterisation of microporous membranes. *Desalination*, 199(1-3), pp.18–19.

GE, W., 2014. GE Osmonics membranes. Available at: http://www.lenntech.com/products/membrane/osmonics/osmonics.htm [Accessed October 29, 2014].

GeoCities Chlorate Site, Simple Chloride Titration. Available at: http://oxidizing.typhoonguitars.com/chlorate/cl_titr.html [Accessed March 4, 2015].

Ghosh, P., Electrostatic Double Layer Force : Part II. , pp.1–18., National Programme on Technology Enhanced Learning (NPTEL), India. Available at:nptel.ac.in/courses/103103033/modules 3/lecture 3.pdf

HACH, DR/2000 Spectrophotometer | Hach USA - Downloads - Obsolete | Hach. Available at: http://www.hach.com/dr-2000-spectrophotometer/product-downloads?id=7640439022 .

Hagmeyer, G. & Gimbel, R., 1999. Modelling the rejection of nanofiltration membranes using zeta potential measurements. *Separation and Purification Technology*, 15(1), pp.19–30.

Hagmeyer, G. & Gimbel, R., 1998. Modelling the salt rejection of nanofiltration membranes for ternary ion mixtures and for single salts at different pH values. *Desalination*, 117, pp.247–256.

Han, M.J., Baroña, G.N.B. & Jung, B., 2011. Effect of surface charge on hydrophilically modified poly(vinylidene fluoride) membrane for microfiltration. *Desalination*, 270(1-3), pp.76–83.

Herbig, R., Arki, P., Tomandl, G., & Bräunig, R. E., 2003. Comparison of electrokinetic properties of ceramic powders and membranes. *Separation and Purification Technology*, *32*(1-3), 363–369.

Hilal, N., Al-Zoubi, H., Mohammad, A. W., & Darwish, N. A., 2005. Nanofiltration of highly concentrated salt solutions up to seawater salinity. *Desalination*, *184*(1-3), 315–326.

Huisman, I.H., Prádanos, P. & Hernández, A., 2000. Electrokinetic characterisation of ultrafiltration membranes by streaming potential , electroviscous effect , and salt retention. , 178, pp.55–64.

Huisman, I.H. & Tra, G., 1999. Determining the zeta potential of ultrafiltration membranes using their salt retention. , 157, pp.261–268.

Hunter, R.J., 1981. *Zeta Potential in Colloid Science*, London ; New York : Academic Press, 1981.

Hurwitz, G., Guillen, G.R. & Hoek, E.M.V., 2010. Probing polyamide membrane surface charge, zeta potential, wettability, and hydrophilicity with contact angle measurements. *Journal of Membrane Science*, 349(1-2), pp.349–357.

Hussain, A.A., Nataraj, S.K., Abashar, M.E.E, Al-Mutaz, I.S. & Aminabhavi, T.M., 2008. Prediction of physical properties of nanofiltration membranes using experiment and theoretical models. *Journal of Membrane Science*, 310, pp.321–336.

Ikeda, K., Nakano, T., Ito, H., Kubota, T., & Yamamoto, S., 1988. New composite charged reverse osmosis membrane. *Desalination*, *68*(2-3), 109–119.

Kim, K. J., Fane, A. G., Nystrom, M.& Pihlajamaki, A., 1997. Chemical and electrical characterization of virgin and protein-fouled polycarbonate track-etched membranes by FTIR and streaming-potential measurements. *Journal of Membrane Science*, *134*, 199–208.

Krishna, R. & Wesselingh, J.A., 1997. The Maxwell-Stefan approach to mass transfer. *Chem. Eng. Sci.*, 52, p.861.

Kukizaki, M., 2009. Relation between salt rejection and electrokinetic properties on Shirasu porous glass (SPG) membranes with nano-order uniform pores. *Separation and Purification Technology*, 69(1), pp.87–96.

Lanteri, Y., Fievet, P., Déon, S., Sauvade, P., Ballout, W., & Szymczyk, A., 2012. Electrokinetic characterization of hollow fibers by streaming current, streaming potential and electric conductance. *Journal of Membrane Science*, *411-412*, 193–200.

Levesque, M., 1928. Les lois de la transmission de chaleur par convection. *Annales Mines*, 13, p.201.

Luo, J. & Wan, Y., 2013a. Desalination of effluents with highly concentrated salt by nanofiltration: From laboratory to pilot-plant. *Desalination*, 315, pp.91–99.

Luo, J. & Wan, Y., 2013b. Effects of pH and salt on nanofiltration—a critical review. *Journal of Membrane Science*, 438, pp.18–28.

Luxbacher, T., 2006. Electrokinetic characterization of flat sheet membranes by streaming current measurement. *Desalination*, 199(1-3), pp.376–377.

Malvern Instruments Ltd, 2012. A basic guide to particle characterization. *Inform White Paper*, pp.1 – 26. Available at:http://golik.co.il/Data/ABasicGuidtoParticleCharacterization(2)_1962085150.pdf.

Mänttäri, M., Pihlajamäki, A. & Nyström, M., 2006. Effect of pH on hydrophilicity and charge and their effect on the filtration efficiency of NF membranes at different pH. *Journal of Membrane Science*, 280(1-2), pp.311–320.

Mart, A. & Mart, F., 2003. Zeta potential of membranes as a function of pH Optimization of isoelectric point evaluation. *Journal of Membrane Science*, 213, pp.225–230.

Mart, F. & Mart, A., 2002. Streaming potential through and on ultrafiltration membranes Influence of salt retention. , 206, pp.431–441.

Matsumoto, H., Koyama, Y. & Tanioka, A, 2003. Pore-surface characterization of amphoteric charged membranes by means of zeta potential measurements. *Colloids and Surfaces A: Physicochemical and Engineering Aspects*, 222(1-3), pp.165–173.

Mazzoni, C. & Bandini, S., 2006. On nanofiltration Desal-5 DK performances with calcium chloride–water solutions. *Separation and Purification Technology*, 52(2), pp.232–240.

Mazzoni, C., Bruni, L. & Bandini, S., 2007. Nanofiltration: Role of the Electrolyte and pH on Desal DK Performances †. *Industrial & Engineering Chemistry Research*, 46(8), pp.2254–2262.

Merdaw, A. A., Sharif, A. O. & Derwish, G. A. W., 2010. Water permeability in polymeric membranes, Part I. *Desalination*, 260(1-3), pp.180–192.

Möckel, D., Staude, E. & Dal-Cin, M., 1998. Tangential flow streaming potential measurements: hydrodynamic cell characterization and zeta potentials of carboxylated polysulfone membranes. *Journal of Membrane Science*, 145, pp.211–222.

Mohammad, A.W., 1998. *Predictive models for nanofiltration membrane processes / Abdul Wahab Mohammad.* University of Wales Swansea.

Mohammad, A.W. & Takriff, M.S., 2003. Predicting flux and rejection of multicomponent salts mixture in nanofiltration membranes. *Desalination*, 157(May), pp.105–111.

Molina, C., Victoria, L., Arenas, A., & Ibáñez, J. A., 1999. Streaming potential and surface charge density of microporous membranes with pore diameter in the range of thickness. *Journal of Membrane Science*, *163*, 239–255.

Morão, A.I.C., Brites Alves, A.M. & Afonso, M.D., 2006. Concentration of clavulanic acid broths: Influence of the membrane surface charge density on NF operation. *Journal of Membrane Science*, 281, pp.417–428.

Moritz, T., Benfer, S., Árki, P., & Tomandl, G. , 2001. Influence of the surface charge on the permeate flux in the dead-end filtration with ceramic membranes. *Separation and Purification Technology*, *25*(1-3), 501–508.

Mueller, N. C., Van der Bruggen, B., Keuter, V., Luis, P., Melin, T., Pronk, W., ... Nowack, B., 2012. Nanofiltration and nanostructured membranes-Should they be considered nanotechnology or not? *Journal of Hazardous Materials*, *211-212*, 275–280.

Mulder, M., 1996. *Basic Principles of Membrane Technology*, Dordrecht: Springer Netherlands. Available at: http://link.springer.com/10.1007/978-94-009-1766-8 [Accessed January 7, 2015].

Mullet, M., Fievet, P., Reggiani, J. C., & Pagetti, J. (1997). Surface electrochemical properties of mixed oxide ceramic membranes " Zeta-potential and surface charge density. *Journal of Membrane Science*, *123*, 255–265.

Nakao, S. & Kimura, 1981. Analysis of solutes rejection in ultrafiltration. *J. Chem. Eng. Japan*, 14, p.32.

Narong, P. & James, A. E., 2006. Sodium chloride rejection by a UF ceramic membrane in relation to its surface electrical properties. *Separation and Purification Technology*, 49(2), pp.122–129.

Ng, K. C., Thu, K., Oh, S. J., Ang, L., Shahzad, W. M., & Bin Ismail, A., 2015. Recent developments in thermally-driven seawater desalination: Energy efficiency improvement by hybridization of the MED and AD cycles. *Desalination*, *356*, 255–270.

Norberg, D., Hong, S., Taylor, J., & Zhao, Y., 2007. Surface characterization and performance evaluation of commercial fouling resistant low-pressure RO membranes. *Desalination*, *202*(1-3), 45–52.

Nystrom, M., Pihlajamaki, A., Bowen, W. R., & Mukhtar, H., 1996. Evaluation of electroosmosis and streaming potential for measurement of electric charges of polymeric membranes, *116*, 149–159.

Oatley, D.L., 2004. *Characterisation and prediction of membrane separation performance : an industrial assessment / Darren Lee Oatley.*

Oatley, D.L., L. Llenas, R. Perez, P.M. Williams, X. Martínez-Lladó, and M. Rovira (2012), Review of the dielectric properties of nanofiltration membranes and verification of the single oriented solvent layer approximation, Adv. Col. Int. Sci., 173, 1-11

Opong, W.& Zydney, A.L., 1991. Diffusive and convective protein transport through asymmetric membranes. *AIChE Journal*, 37, p.1497.

Paar, A., Anton Paar EKA. Available at: http://www.asi-team.com/asi team/brookhaven/BI EKA.pdf .

Park, S.O. & East, M., 2012. User training- Dynamic Light Scattering Achieving reliable Nano particle sizing. Available at: http://149.171.168.221/partcat/wp-content/uploads/Malvern-Zetasizer-LS.pdf.

Peeters, J.M.M., Mulder, M.H.V. & Strathmann, H., 1999. Streaming potential measurements as a characterization method for nanofiltration membranes. *Colloids and Surfaces A: Physicochemical and Engineering Aspects*, 150(1-3), pp.247–259.

Petriniæ, I., Pušiæ, T. & Mijatoviæ, I., 2007. Characterization of Polymeric Nanofiltration Membranes. *Kem.Ind*, 56(11), pp.561–567.

Rautenbach, R. & Albrecht, R., 1994. *Membrane Processes*, John Wiley.

Religa, P., Kowalik, A. & Gierycz, P., 2011. Effect of membrane properties on chromium(III) recirculation from concentrate salt mixture solution by nanofiltration. *Desalination*, 274(1-3), pp.164–170.

Rice, G. Barber, A.R., O'Connor, A.J., Pihlajamaki, A., Nystrom, M., Stevens, G.W.& Kentish, S.E., 2011. The influence of dairy salts on nanofiltration membrane charge. *Journal of Food Engineering*, 107, pp.164–172.

Ricq, L., Pierre, A., Bayle, S., & Reggiani, J.C. , 1997. Electrokinetic characterization of polyethersulfone UF membranes. *Desalination*, *109*(3), 253–261.

Ricq, L., Pierre, A., Reggiani, J.-C., Pagetti, J.& Foissy, A. (1998). Use of electrophoretic mobility and streaming potential measurements to characterize electrokinetic properties of ultrafiltration

and microfiltration membranes. *Colloids and Surfaces A: Physicochemical and Engineering Aspects*, *138*(2-3), 301–308.

Ricq, L. & Pagetti, J., 1999. Inorganic membrane selectivity to ions in relation with streaming potential. *Journal of Membrane Science*, 155(1), pp.9–18.

Sabir, A. K., Bhuiyan, L.B. & Outhwaite, C.W., 1998. Influence of ion size and valence on classical ionic criticality. *Molecular Physics*, 93(January), pp.405–409.

Salg, S., Salgı, U. & Soyer, N., 2013. Streaming Potential Measurements of Polyethersulfone Ultrafiltration Membranes to Determine Salt Effects on Membrane Zeta Potential. *International Journal of Electrochemical Science*, 8, pp.4073–4084.

Saline Corporation, water conversion, *Lab Analysis Manual.*

San Digo Miramar, C., Using the AA240 Spectrometer. Available at: http://faculty.sdmiramar.edu/fgarces/labmatters/instruments/aa/AAS_Operation/index.html [Accessed March 4, 2015].

Sbaï, M., Fievet, P., Szymczyk, A., Aoubiza, B., Vidonne., A. & Foissy, A., 2003. Streaming potential, electroviscous effect, pore conductivity and membrane potential for the determination of the surface potential of a ceramic ultrafiltration membrane. *Journal of Membrane Science*, *215*(1-2), 1–9.

Schaep, j., Vandecasteele, C., Wahab Mohammad, A.& Richard Bowen, W., 2001. Modelling the retention of ionic components for different nanofiltration membranes. *Separation and Purification Technology*, 23, pp.169–179.

Schaep, J. & Vandecasteele, C., 2001. Evaluating the charge of nanofiltration membranes. *Journal of Membrane Science*, 188(February), pp.129–136.

Schlögl, R., 1966. Membrane permeation in system far from equilibrium, Berichte der Bunsengesellschaft. *Physik. Chem*, 70, p.400.

Somicon, L., 2014. Somicon LTD. Available at: http://www.somicon.com/ [Accessed October 29, 2014].

Systems, P. Sizing, Electrophoretic Light Scattering | Particle Sizing Systems. *Particle sizing Systems Santa Barbara, California, USA; http://www.colorado.edu/ceae/environmental/ryan/research/pdfs/pss-zls-manual.pdf (Stand: 11.2006)*. Available at: http://pssnicomp.com/definitions/electrophoretic-light-scattering/ [Accessed March 1, 2015].

Systems, P. Sizing, 2006. *Nicomp 380 ZLS User Manual*, Available at: http://www.colorado.edu/ceae/environmental/ryan/research/pdfs/pss-zls-manual.pdf (Stand: 11.2006).

Szoke, S., Patzay, G. & Weiser, L., 2002. Characteristics of thin-film nanofiltration membranes at various. *Desalination*, 151, pp.123–129.

Szymczyk, A., Fievet, P., Reggiani, J. C. & Pagetti, J.,1998. Characterisation of surface properties of ceramic membranes by streaming and membrane potentials. *Journal of Membrane Science, 146*(2), 277–284.

Szymczyk, A., Pierre, A., Reggiani, J.C. & Pagetti, J., 1997. Characterisation of the electrokinetic properties of plane inorganic membranes using streaming potential measurements. *Journal of Membrane Science*, 134(1), pp.59–66.

Szymczyk, A., Fievet, P., Mullet, M., Reggiani, J. C. & Pagetti, J. , 1998a. Comparison of two electrokinetic methods - Electroosmosis and streaming potential - To determine the zeta-potential of plane ceramic membranes. *Journal of Membrane Science, 143*, 189–195.

Szymczyk, A., Fievet, P., Mullet, M., Reggiani, J. C.& Pagetti, J., 1998b. Study of eletrokinetic properties of plate ceramic membranes by electroosmosis and streaming potential. *Desalination, 119*, 309–314.

Szymczyk, A., Fatin-Rouge, N. & Fievet, P., 2007. Tangential streaming potential as a tool in modeling of ion transport through nanoporous membranes. *Journal of colloid and interface science*, 309(2), pp.245–52.

Tanninen, J. & Nyström, M., 2002. Separation of ions in acidic conditions using NF. *Desalination*, 147, pp.295–299.

Tay, J.-H., Liu, J. & Sun, D.D., 2002. Effect of solution physico-chemistry on the charge property of nanofiltration membranes. *Water research*, 36(3), pp.585–98.

Teixeira, M., Rosa, M. & Nystrom, M., 2005. The role of membrane charge on nanofiltration performance. *Journal of Membrane Science*, 265(1-2), pp.160–166.

Tra, C., Pihlajama, A., Huisman, I. H. & Tra, G., 1998. Determining the zeta-potential of ceramic micro filtration membranes using the electroviscous effect. *Journal of Membrane Science, 147*, 187–194.

Van der Bruggen, B. V., 2009. Influence of Solute - Membrane Affinity on Rejection of Uncharged Organic Solutes by Nanofiltration Membranes. *Environmental Science & Technology, 43*(7), 2400–2406.

Wang, M., Wu, L.-G., Zheng, X.-C., Mo, J.-X. & Gao, C.J., 2006. Surface modification of phenolphthalein poly(ether sulfone) ultrafiltration membranes by blending with acrylonitrile-based copolymer containing ionic groups for imparting surface electrical properties. *Journal of Colloid and Interface Science, 300*(1), 286–92.

Wang, W. & Ku, Y., 2006. Effects of solution pH and UV irradiation on the streaming potential of the titanium dioxide membranes. *Journal of Membrane Science*, 282, pp.342–350.

Welfoot, J.S., 2001. *Predictive modelling of membrane nanofiltration*. Swansea university.

Wilbert, M., Delagah, S. & Pellegrino, J., 1999. Variance of streaming potential measurements. *Journal of Membrane Science*, 161(1-2), pp.247–261.

Williams, S., 2015. *Recovery of small organics from natural sources using membrane technology.* Swansea university.

Xu, Y., Wang, M., Ma, Z. & Gao, C., 2011. Electrochemical impedance spectroscopy analysis of sulfonated polyethersulfone nanofiltration membrane. Desalination, 271(1-3), pp.29–33.

Xu, Y. & Lebrun, R. E., 1999. Investigation of the solute separation by charged nano filtration membrane : effect of pH , ionic strength and solute type. *Journal of Membrane Science*, *158*, 93–104.

Yang, J., Bellmann, C., Grundke, K., Michel, S., Kostiuk, L. & Kwok, D., 2003. Characterization of porous membranes by zeta-potential under an ac electric field: analytical treatment of time-dependent electroosmostic flow. *Journal of Membrane Science*, *225*(1-2), 155–164.

Yaroshchuk, A. & Luxbacher, T., 2010. Interpretation of electrokinetic measurements with porous films: role of electric conductance and streaming current within porous structure. *Langmuir : the ACS journal of surfaces and colloids*, 26(13), pp.10882–9.

Yaroshchuk, A. & Ribitsch, V., 2002. Role of Channel Wall Conductance in the Determination of ζ-Potential from Electrokinetic Measurements. *Langmuir*, 18(6), pp.2036–2038.

Zhao, Y., Xing, W., Xu, N., & Wong, F.S., 2005. Effects of inorganic electrolytes on zeta potentials of ceramic microfiltration membranes. *Separation and Purification Technology*, *42*(2), 117–121.